C51.17/12:988/4

Tech Notes

APRIL 1988

PB88-925904

NTIS

U.S. DEPARTMENT OF COMMERCE
National Technical Information Service
Center for the Utilization of Federal Technology

ALSO DESCRIBES 90 FEDERAL TECHNICAL INFORMATION CENTERS

NOW! Work Directly with Government Labs and Engineering Facilities

"The Directory should be popular in research and business libraries"

—Reference Book Bulletin
American Libraries Association

Find them easily in the Directory of Federal Laboratory & Technology Resources. This valuable directory will guide you to hundreds of Federal agencies, laboratories, and engineering centers willing to share their expertise, equipment, facilities, and special services to aid your research and engineering efforts. Detailed summaries of these unique resources are arranged in 32 subject-oriented areas for easy reference. Descriptions of 90 Technical Information Centers are included.

These centers offer information services and expertise in areas such as fuels, cold regions, concrete, fisheries, toxicology, pesticides, plastics, and much more.

The NAME, ADDRESS, PHONE NUMBER OF A PERSONAL CONTACT IS LISTED FOR EACH RESOURCE!

Help is available in 32 technical areas including:

Aeronautics (31)* • Agriculture & Food (120) • Biological Sciences (68) • Building Technology (20) • Computer Technology (15) • Electrotechnology (43) • Energy (77) • Engineering (86) • Environmental Sciences (67) • Manufacturing (19) • Materials (61) • Medicine (112) • Nuclear (128) • Ocean Sciences & Technology (36) • Physical Sciences (110) • Transportation (14) • Plus others

*number of summaries

Four handy indexes make it easy to locate the resource you need.

1. Subject Term Index
Identifies resources in your technical interest areas.

2. State Index
Find all the resources in your State.

3. Resource Name Index
Look up any resource by name of laboratory or program.

4. Agency Index
Lists resources by agency and State.

All listed resources offer unique capabilities (not readily duplicated in the private sector) to encourage greater use of Federal technology.

To increase your awareness of hundreds of Federal Technology Resources available to work with you on your projects, order your DIRECTORY now!

ASK FOR:
PB88-100011/AAW

DIRECTORY OF FEDERAL LABORATORY AND TECHNOLOGY RESOURCES

CALL: (703) 487-4650

WRITE:

NTIS Springfield, VA 22161

Enclose check to NTIS for $36 plus $3 for shipping and handling or
Charge to: NTIS Deposit Account, American Express, VISA, or MasterCard.
Please furnish card number, expiration date, signature, and complete mailing address.

Tech Notes

Highlighting Selected U.S. Government Technology & Resources

APRIL 1988

Contents

Agriculture & Food 241

Computers 243

Electrotechnology 250

Energy 270

Engineering 276

Environmental Science & Technology 292

Manufacturing, Machinery & Tools 294

Materials 304

Medicine & Biology 318

Natural Resources Technology & Engineering 322

Physical Sciences 324

Transportation & Components 338

PENNSYLVANIA STATE UNIVERSITY
APR 11 1988
DOCUMENTS COLLECTION

Published monthly by the National Technical Information Service (NTIS), Tech Notes bring together individual one to two page fact sheets prepared by Federal agencies, their laboratories, or contractors. These fact sheets highlight current Federal technology determined to have commercial or practical application. Topics cover new processes, materials, techniques, software, instrumentation, and resources.

Some of the current sources are the Department of the Navy, Department of the Army, NASA, Department of Energy, Environmental Protection Agency, Department of the Interior, and the Department of Agriculture.

Special assistance is provided by the Federal Laboratory Consortium.

Change of address or questions concerning subscriptions should be sent to:
Subscriptions Department
National Technical Information Service
Springfield, VA 22161
(703) 487-4630

Suggestions, comments, or questions concerning Tech Notes should be directed to:
Tech Notes Editor
Room 300B F
National Technical Information Service
Springfield, VA 22161
(703) 487-4805

U.S. Depository Copy

How to Use Tech Notes

Every Tech Notes fact sheet lists a source for additional information. The source of this information may be a special support package from the originating agency, a personal contact, a licensing opportunity, or a backup report available from NTIS.

Each fact sheet also is perforated to allow for easy removal for those subscribers who may wish to keep a special fact sheet file or route to others in their organization

Sources of Further Backup Information

Below are two representative examples of how each Tech Note fact sheet provides you with a source of further information. In most cases, this information is provided directly by the agency or its laboratory. However, there are cases where NTIS is the source for backup documentation. In these cases, use the order form at the end.

Examples:

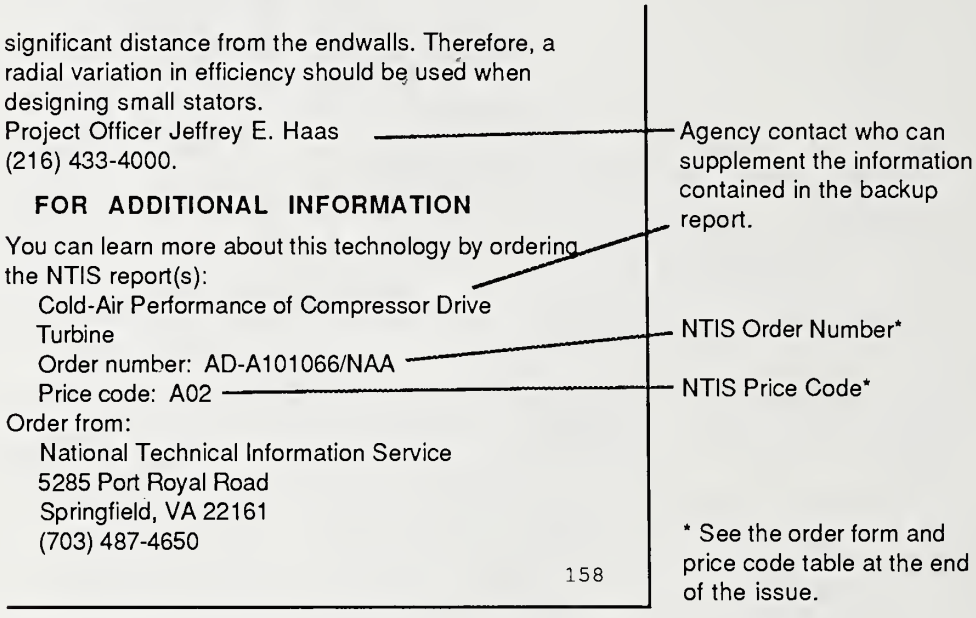
significant distance from the endwalls. Therefore, a radial variation in efficiency should be used when designing small stators.
Project Officer Jeffrey E. Haas
(216) 433-4000.
FOR ADDITIONAL INFORMATION
You can learn more about this technology by ordering the NTIS report(s):
Cold-Air Performance of Compressor Drive Turbine
Order number: AD-A101066/NAA
Price code: A02
Order from:
National Technical Information Service
5285 Port Royal Road
Springfield, VA 22161
(703) 487-4650
158
Agency contact who can supplement the information contained in the backup report.
NTIS Order Number*
NTIS Price Code*
* See the order form and price code table at the end of the issue.

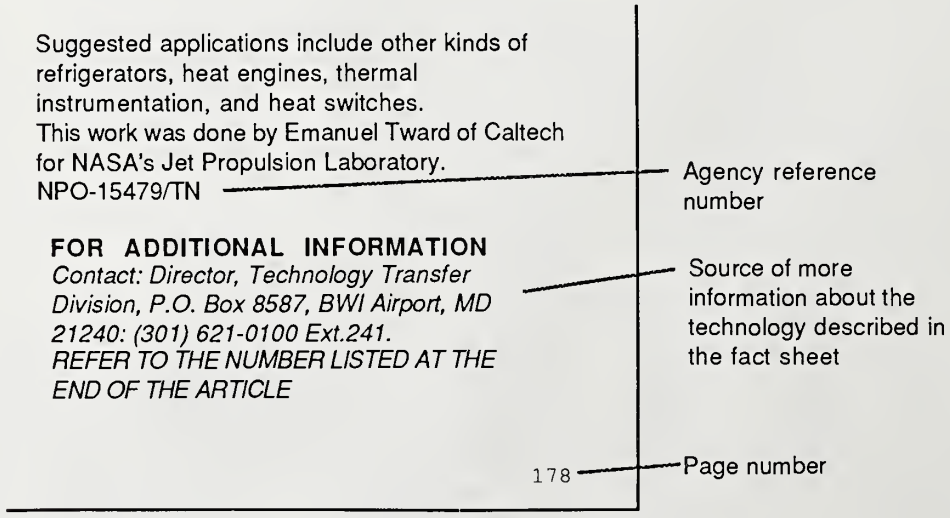
Suggested applications include other kinds of refrigerators, heat engines, thermal instrumentation, and heat switches.
This work was done by Emanuel Tward of Caltech for NASA's Jet Propulsion Laboratory.
NPO-15479/TN
FOR ADDITIONAL INFORMATION
Contact: Director, Technology Transfer Division, P.O. Box 8587, BWI Airport, MD 21240: (301) 621-0100 Ext.241.
REFER TO THE NUMBER LISTED AT THE END OF THE ARTICLE
178
Agency reference number
Source of more information about the technology described in the fact sheet
Page number

Tech Notes Title List for April 1988

Agriculture & Food

241 Upgrading Fats and Oils With Enzymes

242 Uses for Starch from Surplus Corn

Computers

243 Knowledge-Acquisition Tool for Expert System — Digital flight-control systems will be monitored by a computer program that can evaluate and recommend. (Licensing Opportunity)

244 Minimum-Time Control for Robotic Manipulators — An existence theorem is proved for nonlinear systems.

245 Digital Control for Remote Manipulators — Multiple microprocessors enable large separations between controllers and manipulators.

246 Interface for Color-Video Monitor — A wide range for video signals can be accommodated.

247 Self-Stabilizing Storage Loops for Magnetic-Bubble Memories — Adjacent, sinusoidal loops provide defect-tolerant, self-stabilizing structures.

248 Central Processor Acts as High-Speed DMA Controller — Maximum transfer rates are achieved with a reduction in cost and complexity. (Licensing Opportunity)

Software

249 Program for Development of Artificial Intelligence — CLIPS surpasses other programs in its category.

Electrotechnology

250 Microcircuit Reliability Assessment Program Diskette Version

251 Non-Operation Reliability Databook — Compiles Field and Test Data for an Assortment of Electrical and Electromechanical Parts

252 Electrical Grounding in Cold Regions

253 Electromagnetics Laboratory Accredition Program

255 Diode Structure for Microwave and Infrared Applications — Microwave signals can be switched or modulated optically.

256 Predicting False Lock in Phase-Locked Loops — Methods are derived for calculating false-lock frequency errors.

257 Optical Design and Signal Processing for Edge Detection — The number of edge-detection computations is reduced by a factor of 100.

258 Binary-Symmetry Detection — Transmission errors for zeros and ones are tabulated separately.

259 Ultrasonic Ranging System with Increased Resolution — The master-oscillator frequency is increased.

260 Analysis of a Four-Reflector S/X-Band Antenna — Physical optics accounts for the near field, cross polarization, and higher-order modes.

261 Diffraction Analysis of Antennas with Mesh Surfaces — A strip-aperture model replaces a wire-grip model.

262 High-Voltage Switch Containing (DI)^2 Devices — Series switching diodes are triggered on by passing above the threshold voltage.

263 Improved Flux-Gate Magnetometer — A simplified circuit drives heading indicator and senses the magnetic field of the Earth. (Licensing Opportunity)

264 Waveguide-Hort-to-Waveguide Transition Assembly — A microstrip-to-waveguide transition is integrated with a waveguide-horn antenna element.

265 Imaging Radar Polarimeter — Radar measures the full polarization tensor of each element in the scene in one sweep.

Testing & Instrumentation

266 Adjustable, Audible Continuity Tester for Delicate Circuits — The unit is adjustable to resistances up to 35 ohms.

267 Testing Instrument for Flight-Simulator Displays — Many devices for many diverse functions are combined in one equipment item. (Licensing Opportunity)

268 Measuring Microwave Emissivities — A Dicke radiometer and a cryoload are combined in emissivity determinations of mesh antennas. (Licensing Opportunity)

Other Items of Interest

339 Engine-Monitoring Algorithm — Allowances are made for erroneous sensor readings.

Energy

270 Cogeneration from Biofuels — A Technical Guidebook.

272 Parameter Estimation Study of Heat Loss from Underground Steam Pipelines

273 Summary and Evaluation of Field Performance Data on Unitary Heat Pumps

274 Hanging Windmills from Cables — A relatively inexpensive structure would enable the raising and lowering of windmills. (Licensing Opportunity)

271 System-Assurance Analysis for Nuclear Powerplants — Rocket-Launch reliability techniques could be adapted to benefit powerplants.

Testing & Instrumentation

275 Cooling-Energy Measurements of Unoccupied Single-Family Houses with Attics Containing Radiant Barriers

Engineering

276 Finite Element Analysis in Reliability Studies

277 In Situ Repair of Deteriorated Concrete in Hydraulic Structures — An evaluation.

278 Analyzing Wakes from Hovering-Helicopter Rotor Blades — An Analytical method and computer program yield realistic results quickly. (Licensing Opportunity)

279 Calculations of Wall Effects on Propeller Noise — Reverberations affect sound levels in wind tunnels.

Engineering (Cont.)

280 Design of Fiber Composites for Structural Durability — Hygrothermomechanical effects can be analyzed by computers.

281 High-Differential-Pressure Heat Exchanger — All critical joints are full-penetration welds inspectable with x-rays. (Licensing Opportunity)

282 Preliminary-Design Software for Composite Structures — An easy-to-use program enables fast analysis and evaluation of rough designs.

283 Stiffening Heat-Exchanger Tubes Against Vibrations — Midsection clamps reduce the harmful effects of crossflow.

284 Structural Dynamics of Filament-Wound Booster Rockets — A mathematical model agrees closely with measurements.

285 Thermally Insulating Support for Cryogenic Tanks — A passive alternate-load-path support scheme keeps weight low while conserving cryogenic liquid. (Licensing Opportunity)

286 Wedge Joints for Trusses — Structures could be assembled rapidly with simple hand tools. (Licensing Opportunity)

Software

287 Computer Program for Flow in a Combustor — This program simulates subsonic, swirling, reacting, turbulent flow abut a bluff body.

Testing & Instrumentation

288 Color-Video Thermal Maps — Temperatures appear in time-varying color.

289 Gamma-Ray Fuel Gauges for Airplanes — An accurate system overcomes problems of capacitance gauges.

290 Measuring and Plotting Surface Contour Deviations — An electromechanical apparatus provides along-track and across-track displacement information to a plotter.

291 Microscopic Gas-Flow Controller — Small flows at low pressures would be monitored and throttled. (Licensing Opportunity)

Other Items of Interest

338 Computing Aerodynamics of Propfans — The cost and duration of wind-tunnel tests could be reduced.

340 Generating Coordinates for Aerodynamical Calculations — A mathematical method represents an aircraft surface as grids of variable spacing. (Licensing Opportunity)

Environmental Science & Technology

292 Fog Chamber Advances Air Pollution Studies

Software

293 BASIC Programming in Water and Wastewater Analysis — A collection of programs speeds routine calculations.

Manufacturing, Machinery, & Tools

294 An Improved Method for Simulating Radiographs

295 Flexible Part Fixturing Device (Licensing Opportunity)

296 Higher-Quality Weld Joints for Tube Sections — Less material in weld inserts results in better fusion.

297 Lead Scales for X-Radiographs — Indentions are made by typing on lead tape.

298 Linear Anomaly in Welded 2219-T87 Aluminum Alloy — Microdensitometry can be used to distinguish between cracks and harmless anomalies in radiographs.

299 Making Double-Bevel End Cuts on Tubes — A fixture for a power saw saves time, eliminates waste, and ensures precision.

300 Pressure-Localizing Inserts for Bagging Laminations — These devices can compress composite laminates to conform to tight inside corners of the molds. (Licensing Opportunity)

301 Preset Electrodes for Electrical-Discharge Machining — Time-consuming loading and setting are eliminated. (Licensing Opportunity)

302 Single-Axis Acoustic Levitator with Rotation Control — Rotation-control equipment is simplified.

Testing & Instrumentation

303 Assessing the Reliability of NDE — A computer program assesses the ability of inspection techniques to find structural flaws.

Other Items of Interest

244 Minimum-Time Control for Robotic Manipulators — An existence theorem is proved for nonlinear systems.

245 Digital Control for Remote Manipulators — Multiple microprocessors enable large separations between controllers and manipulators.

Materials

304 Rapidly Solidified Magnesium-Base and Titanium-Base Alloys

305 Development of a Primer/Topcoat and Flexible Primer for Aluminum

306 Nickel Aluminides-New Superalloys for the Future (Licensing Opportunity)

307 ZZX-4200 High-Temperature Thermal Insulation Structures (Licensing Opportunity)

308 Amorphous Insulator Films with Controllable Properties — These films have potential for optical, electronic, magnetic, and mechanical applications.

309 Bismaleimide Copolymer Matrix Resins — Bismaleimide copolymers yield strong graphite composites. (Licensing Opportunity)

310 Determining Directions of Ultrasound in Solids — Ultrasound shadows are cast by grooves.

311 Fatigue Lives of Materials Cut be Lasers — Laser machining may help to balance high-speed rotating machinery.

312 Fluidized-Bed Cleaning of Silicon Particles — Metallic impurities are removed by acids.

313 Mixing Valve for Protein-Crystal Growth — A multi-chamber unit combines reactants as necessary. (Licensing Opportunity)
314 Protective Coatings for Spacecraft Polymers — Thin films of metal-oxide/polymer are applied by ion-beam sputtering. (Licensing Opportunity)
315 Radiation Resistances fo Dielectric Liquids — Although data are sparse for some liquids, polyphenyls appear to be particularly stable.
316 Thermomechanical Properties Indicate Degree of Epoxy Cure — The glass-transition temperature and the density increase as the reaction proceeds.
317 Tribological Properties of Structural Ceramics — Studies of wear and lubrication promote longer component lives.

Other Items of Interest

298 Linear Anomaly in Welded 2219-T87 Aluminum Alloy — Microdensitometry can be used to distinguish between cracks and harmless anomalies in radiographs.

Medicine & Biology

318 Baron Studies in Bone Hardening
319 Dual-Energy X-Radiography with Gadolinium Filter — The image resolution would be increased, and the cost would be reduced.

Testing & Instrumentation

320 High Selectivity-Sensitivity Determination of PAH-DNA Adducts and Metabolites Using Fluorescence Line Narrowing Spectrometry
321 Bacterium, Listeria Monocytogenes, Now can be Detected Accurately

Natural Resources Technology & Engineering

322 Ventilated Cutting Drum Reduces Longwall Dust

Software

323 Estimating Geophysical Parameters from Gravity Data — Features of planets are extracted from Doppler spacecraft-tracking measurements

Physical Sciences

324 Ternary Rare Earth-Lanthanide Sulfide
325 Approximate Simulation of Turbulence — Computed spectra resemble van Karman spectra of frequencies of interest.
326 Coating a Hydrogran-Maser Chamber with CF_4 — Sprayed gas forms a smooth frozen surface.
327 Experiments in Boundary-Layer Turbulence — Motion in the layer is highly three-dimensional.
328 Growing II/VI Semiconductors with Double Decantation — A concept for growing single crystals combines sheet solidification with controlled cooling.

Testing & Instrumentation

329 Low-Level Particle Beam Monitor and Current Meter
330 Micropolarimeter for High Performance Liquid Chromatography (Licensing Opportunity)
331 Concentrating Trace Gases at Low Pressures — An open adsorption tube enables the measurement of gases at parts-per-trillion-by-volume concentrations. (Licensing Opportunity)
332 High-Rydberg Xenon Submillimeter-Wave Detector — The use of reactive alkali metals is avoided. (Licensing Opportunity)
333 Measuring Contact Thermal Conductances at Low Temperatures — An apparatus applies controlled force to metal samples at controlled heat flows. (Licensing Opportunity)
334 Fiber-Optic Temperature Sensor — A remote thermometer should be small, lightweight, and immune to electrical noise.
335 Measuring Electrostatic Discharge — A variety of materials can be tested together under controlled conditions. (Licensing Opportunity)
336 Measuring Gases with Laser-Induced Fluorescence — The temperature, density, and pressure are measured simultaneously in supersonic, turbulent flow. (Licensing Opportunity)
337 Measuring Viscosities of Gases at Atmospheric Pressure — A thermal mass flowmeter provides a capillary section for differential-pressure measurement. (Licensing Opportunity)

Other Items of Interest

320 High Selectivity-Sensitivity Determination of PAH-DNA Adducts and Metabolites Using Fluorescence Line Narrowing Spectrometry

Transportation & Components

338 Computing Aerodynamics of Propfans — The cost and duration of wind-tunnel tests could be reduced.
339 Engine-Monitoring Algorithm — Allowances are made for erroneous sensor readings.
340 Generating Coordinates for Aerodynamical Calculations — A mathematical method represents an aircraft surface as grids of variable spacing. (Licensing Opportunity)

Agriculture & Food

241 Upgrading Fats and Oils With Enzymes

242 Uses for Starch from Surplus Corn

United States Department of Agriculture

Research Technology
Agricultural Research Service

Upgrading Fats and Oils With Enzymes

There's a way to convert used or low-quality fats and oils into fatty acids and glycerol—important industrial ingredients for a host of products such as cosmetics, drugs, inks, lubricants, and tires.

It's a process called hydrolysis, and ARS scientists are patenting ways to improve it.

Current heat-processing hydrolysis methods require huge steel vessels and costly heating equipment, and they risk polluting the environment. The product may still smell so bad that secondary deodorizing is a must. And despite all this effort, the product's impurities may limit its use to soapmaking.

But new, cold methods put the enzyme lipase to work as a catalyst to produce a product that is odor free and considerably purer. With one such cold method, the fats slowly move through a lipase-impregnated membrane, ending up in a mixing chamber.

An ARS scientist has patented a way to hurry the process along by lowering the pressure in the mixing chamber. The fat or oil moves through the catalyst-laden membrane more quickly, and the catalyst stays in place, contrary to expectations that it would be dislodged by the flow.

The patented system is easier to control and operate. Reaction activity is higher, translating into faster processing.

For Additional Information:

Inquiries concerning rights for commercial use of this invention should be addressed to

Office of Federal Patent Licensing
Center for the Utilization of Federal Technology
Room 13R, NTIS
Springfield, VA 22161
(703) 487-4738

Refer to Patent Application 7-050,451

For technical information, contact Frank Taylor, USDA-ARS Engineering Science Research, Eastern Regional Research Center, 600 East Mermaid Lane, Philadelphia, PA 19118. *Patent Application "Re-actions Between Immiscible Fluids."*

United States Department of Agriculture

Research Technology
Agricultural Research Service

Uses for Starch From Surplus Corn

Cornstarch could become a pesticide for crop-eating insects. This is just one of the intriguing new uses of cornstarch that scientists are exploring for farm, home, and industry, according to Dr. William M. Doane of USDA's Agricultural Research Service. "Finding new uses for cornstarch will add to its value and create new markets to help reduce the nation's 137-million-ton corn surplus."

Agency researchers have patents pending or have applied for patents on a number of ways to process and use cornstarch. Doane said new products using cornstarch could include slow-release pesticides and many other slow-release products, biodegradable plastic films, soil stabilizers to prevent erosion, seed coatings to improve germination, and a dip for citrus seedling roots to help the survival of a tiny worm showing promise as a biological pest control. Lab and field tests are being done at Peoria and an agency laboratory in Ankeny, Iowa, to see if the bacterium Bacillus thuringiensis and a virus from the alfalfa looper moth encapsulated in cornstarch can control corn borers.

Doane said some companies are already interested in the new process, in which the bacteria and viruses are added in water to pregelatinized cornstarch. The mixture is stirred until it forms a gel. After the gel stands for half an hour, it is ready to be dried and crumbled into granules.

Peoria scientists also applied for a patent on a new way to regulate the release of a variety of liquids and solids encapsulated in starch. "The number of timed-release products with commercial potential is limited mainly by one's imagination," he said.

The technique is based on varying the proportions of amylose and amylopectin, two starch components in the encapsulation mix. "Amylose polymers are linear and form tight molecular bonds," Doane explains. "Amylopectin polymers are branched and form looser bonds. The more amylose in the cornstarch mix, the more slowly the encapsulated substance is released, whether it's a medicine or a pesticide or something else."

FOR ADDITIONAL INFORMATION: Contact: William M. Doane, research chemist, Plant Polymer Research Unit, Northern Regional Research Center, Agricultural Research Service, USDA, Peoria, IL 61604; (309) 685-4011, Ext. 556.

Computers

243 Knowledge-Acquisition Tool for Expert System — Digital flight-control systems will be monitored by a computer program that can evaluate and recommend. (Licensing Opportunity)

244 Minimum-Time Control for Robotic Manipulators — An existence theorem is proved for nonlinear systems.

245 Digital Control for Remote Manipulators — Multiple microprocessors enable large separations between controllers and manipulators.

246 Interface for Color-Video Monitor — A wide range for video signals can be accommodated.

247 Self-Stabilizing Storage Loops for Magnetic-Bubble Memories — Adjacent, sinusoidal loops provide defect-tolerant, self-stabilizing structures.

248 Central Processor Acts as High-Speed DMA Controller — Maximum transfer rates are achieved with a reduction in cost and complexity. (Licensing Opportunity)

Software

249 Program for Development of Artificial Intelligence — CLIPS surpasses other programs in its category.

250 Microcircuit Reliability Assessment Program Diskette Version

NASA Tech Brief
National Aeronautics and Space Administration

Licensing Opportunity

Knowledge-Acquisition Tool for Expert System

Digital flight-control systems will be monitored by a computer program that can evaluate and recommend.

According to a report, flight-systems engineers for advanced, high-performance aircraft will soon use a knowledge-acquisition tool (computer program) for an expert-system flight-status monitor that supplies interpretative data. An expert system is an artificial-intelligence (AI) system in which the knowledge of one or more human experts has been put into a computer. The interpretative function is especially important in time-critical, high-stress situations because it can facilitate problem identification and corrective strategy. Conditions can be evaluated and recommendations can be made by ground-based engineers who will have essential knowledge for the analysis and monitoring of the performances of advanced aircraft systems.

Monitoring techniques available today supply system-status and -failure indications, but do not provide the interpretation function that is becoming increasingly necessary for advanced avionics and digital flight-control systems. Among the goals of development of the expert-system flight-status monitor is a hierarchical set of flight-monitoring capabilities. In this set, levels one and two represent the degree of flight-monitoring automation currently available. The third-level goal of expert interpretation includes the capability of putting information together and providing knowledge. Level three is expected to be operational within one year.

As a semi-intelligent "editor", the knowledge-acquisition tool is a computer program that enables easy access to the knowledge base of the expert system and that provides aid and direction in creating, modifying, and maintaining that base. Additionally, the onboard system maintains, corrects, and puts information into the expert system. Through help screens and online documentation, the knowledge-acquisition component of the expert-system flight-status monitor provides a coherent source of information. The subsequent use of the expert system reflects the logically consistent and complete knowledge base generated by the knowledge-acquisition tool.

The expert-system flight-status monitor processes the telemetry-downlink failure and status words, using a ground-based symbolic processor. The failure words are processed through a rule-based model of the failure-management system of the aircraft to arrive at an independent assessment of the state of the vehicle flight-control system. (For this purpose, a rule is a compact and manageable unit of knowledge that is reducible to an if/then expression.)

If the expert system detects any failures, the second level of rules is invoked to produce a high-level evaluation of the overall status of the aircraft. Any detected failure will be compared to the status-indicator words by the failure-management system of the aircraft. Rules yet to be developed are expected to resolve discrepancies between the onboard system and the expert system. Conditions that can adversely affect the safety of flight will cause cautions and warnings to be issued to the systems engineer, who will then be able to query the expert system for an explanation or to request a more detailed description of the aircraft state. The expert system will also be able to display messages or emergency procedures when necessary.

A structured, yet flexible, method enables easy modification of the knowledge base of the expert system. Because knowledge must be changed frequently, it cannot be hard-wired into the system. Instead, a means of forcing consistency in the rule base is established while the representation is deliberately kept simple and uniform enough to facilitate reading and manipulation of the knowledge base.

Some of the rules used by the knowledge-acquisition tool are in the form of traditional if/then (production) rules; others are defined in unusual formats to facilitate the definition of the knowledge base and to increase the execution speed of the inference mechanism in the expert system. In consideration of power and computational expense, production rules are eliminated whenever possible by partitioning the total system knowledge base into multiple knowledge bases that can be processed sequentially.

Using consistency and partitioning, the knowledge-acquisition tool provides a means of entering aircraft rules in an orderly manner. Consistency in rule entry is achieved by limiting the vocabulary through the use of certain basic words and previously defined clauses. The basic words are used to identify bits in the telemetry stream. Basic words, which are also considered to be rules, are either failure indications, status indications, or cross-channel-assessment indications. Unlike failure indications and status indications, cross-channel indications provide assessments of the computers that generate them.

The knowledge-acquisition tool is in current use on an advanced high-performance aircraft at the NASA Ames Dryden Flight Research Facility. As a side benefit, the tool provides automatic text generation of aircraft-system rules, creating systems-level documentation.

This work was done by James D. Disbrow, Eugene L. Duke, and Victoria A. Regenie of **Ames Research Center**. *Further information may be found in NASA TM-86802 [N86-16944/NSP], "Development of a Knowledge Acquisition Tool for an Expert System Flight Status Monitor."*

Copies may be purchased from the National Technical Information Service, Springfield, Virginia 22161, [A02]

Inquiries concerning rights for the commercial use of this invention should be addressed to the Patent Counsel, Ames Research Center
Refer to ARC-11706 /TN

Ames Research Ctr.
Moffett Field, CA 94035
Technology Utilization Officer: Laurance Milov
Mail Code 223-3
(415) 694-6370
Patent Counsel:
Darrell G. Brekke
Mail Code 200-11
(415) 694-5104

FOR ADDITIONAL INFORMATION: *Contact: Director, Technology Transfer Division, P.O. Box 8757, BWI Airport, MD. 21240; (301) 621-0100 Ext. 241*
REFER TO THE NUMBER LISTED AT THE END OF THE ARTICLE

NASA Tech Brief
National Aeronautics and Space Administration

Minimum-Time Control for Robotic Manipulators

An existence theorem is proved for nonlinear systems.

A report discusses the mathematical requirements for the existence of a solution to the minimum-time control problem for a robotic manipulator that obeys nonlinear equations of motion. In essence, the problem is how to specify the sequence of manipulator-joint torques (within the allowable limits on those quantities) to move the manipulator from one particular position and orientation to another.

The authors begin by reviewing linear systems, for which the existence conditions for minimum-time control have been derived previously. Each such optimal control sequence is unique and is of the "bang-bang" type; that is, it involves the application of full torque to start or alter the motion, zero torque during each segment of the motion, and full torque to stop the motion.

Nonlinear systems are more likely to be encountered in practice and require more conditions for the existence of minimum-time solutions. The derivation begins with a statement of Fillipov's theorem, according to which the three conditions for minimum-time control are the following:

1. The trajectories generated by the admissible controls do not finitely escape during the interval to be minimized.
2. The final state is reachable in finite time using the admissible controls.
3. In the abstract control space, the control dynamics are convex over all admissible controls.

The third condition is satisfied in most of the applications envisioned by the authors. The second condition is not generally easy to satisfy; however, the reachability condition can be calculated for a nonlinear system that is feedback-equivalent to a linear system by calculating the condition for the equivalent linear system. The first condition can be checked using a Lyapunov-function approach. By constructing the energy Lyapunov function, the condition is shown always satisfied. Hence, for the robotic manipulators, the minimum-time control exists provided the available torque is large enough to overcome the gravity, thus satisfying the reachability condition. In the absence of gravity — for example, in space applications — the minimum-time control always exists.

This work was done by John T. Wen of Caltech for **NASA's Jet Propulsion Laboratory** *and Alan Desrochers of Rensselaer Polytechnic Institute. To obtain a copy of the report, "Existence of the Time Optimal Control for Robotic Manipulators," NPO-16919 /TN*

FOR ADDITIONAL INFORMATION: *Contact: Director, Technology Transfer Division, P.O. Box 8757, BWI Airport, MD. 21240; (301) 621-0100 Ext. 241*
REFER TO THE NUMBER LISTED AT THE END OF THE ARTICLE

NASA Tech Brief
National Aeronautics and Space Administration
NASA's Jet Propulsion Laboratory, Pasadena, California

Digital Control for Remote Manipulators

Multiple microprocessors enable large separations between controllers and manipulators.

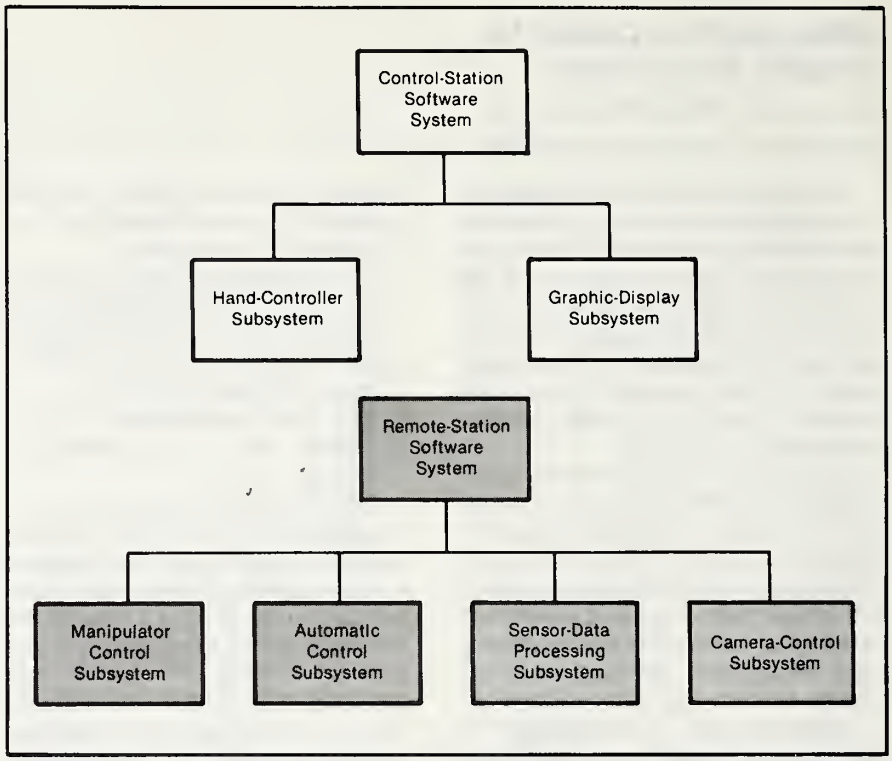

Software for the Controller is distributed between the master and the slave locations. It is organized into modules, as indicated by the blocks. Hardware and software for the system, still under development, have been demonstrated in a laboratory model.

A controller for a remote manipulator requires no direct mechanical connection between the slave arm and the master arm moved by the human operator. The controller employs two-way digital data transmission rather than a mechanical linkage between the master and the slave. The manipulator can therefore be a considerable distance from the operator — perhaps thousands of kilometers away.

The microprocessor-based controller sends commands to the slave according to the operator's hand and arm movements; it returns signals to the master to give the operator visual and kinesthetic feedback. The master and slave arms need not be kinematically and dynamically identical: the master arm can be designed to suit the needs of the operator and the control station, whereas the slave arm can be designed to suit the remote environment. Microprocessors at the master and slave locations make the necessary transformations of positions, orientations, forces, and torques to adapt the two units to each other. The microprocessors are modular and expandable and control such auxiliary functions as television cameras and displays.

Four central-processing units (CPU's) are used so that the large computation burden can be handled in real time. Each CPU includes a 32000-series microprocessor; 128 kbytes of random-access memory; floating-point, timing-control, interrupt-control, and memory-management units; serial and parallel ports; and an expansion connector. Two CPU's are grouped together on a multibus chassis at each location. Each CPU pair can thus readily share information and memory space for coordinating robot control and sensor-data display.

In a demonstration model of the controller, the master manipulator is a general-purpose, 6-degree-of-freedom, back-drivable joystick. A dedicated 32016 microprocessor translates the joint-angle potentiometer values of the master into position instructions for transmission to the slave. The microprocessor accepts data on the orientation, position, forces, and torques at the remote end effector and combines the data to back-drive six torque motors on the master. It thus conveys to the operator a sense of the inertia of the remote manipulator and a feel for the compliance of objects in the remote workspace.

An 8086B microprocessor on the end effector reads and normalizes sensor data for transmission to the control station. This microprocessor also controls the servomechanism that closes the robot hand as instructed by the control station.

The controller software is organized in a modular structure that increases versatility and reliability and makes duplication of programs unnecessary (see figure). The software modularity also makes software-error detection and correction easier and faster.

This work was done by Antal K. Bejczy and Ronald S. Dotson of Caltech for **NASA's Jet Propulsion Laboratory.**
NPO-16879 /TN

FOR ADDITIONAL INFORMATION: *Contact: Director, Technology Transfer Division, P.O. Box 8757, BWI Airport, MD 21240; (301) 621-0100 Ext. 241*
REFER TO THE NUMBER LISTED AT THE END OF THIS ARTICLE

NASA Tech Brief
National Aeronautics and Space Administration
Goddard Space Flight Center, Greenbelt, Maryland

Interface for Color-Video Monitor

A wide range of video signals can be accommodated.

A commercially produced color-video monitor is modified by the addition of an interface circuit to accommodate a wider-than-usual range of scanning rates and resolutions. The monitor displays a properly adjusted picture as long as the input video signal conforms to one of several industry standards and has a horizontal-synchronization frequency of 15.0 to 37.5 kHz, a vertical-synchronization frequency of 43 to 65 Hz, a horizontal resolution up to 1,280 elements, and a vertical resolution up to 1,024 elements. With little or no intervention by the operator and without having to be turned off for adjustments, the interface adapts the monitor within 1 second to changes in rates or resolutions, as long as those parameters remain within the specified ranges.

The interface design relies on the fact that standard video signals having the same vertical- and horizontal-synchronization frequencies usually require similar aspect ratios and other monitor settings. The interface adjusts the monitor identically for video signals for which those frequencies are sufficiently close.

The vertical- and horizontal-synchronization pulses are taken from a sampling point in the monitor after these pulses have been separated from the incoming video signal. The interface measures the two pulse frequencies and processes them, according to a transfer function, into eight outputs that adjust the width, height, centering, geometric distortion, and other characteristics of the picture (see Figure 1).

The transfer function is contained in electronic memory in the form of two "lookup" tables that specify the outputs for input frequencies in various combinations of nonoverlapping ranges. Table 1 contains the adjustment records, which are defined by the operator during the initial calibration. Table 2 contains fixed calibration values that are used when Table 1 does not contain an entry for a particular video signal. An important feature is that the contents of Table 1 are maintained in nonvolatile memory.

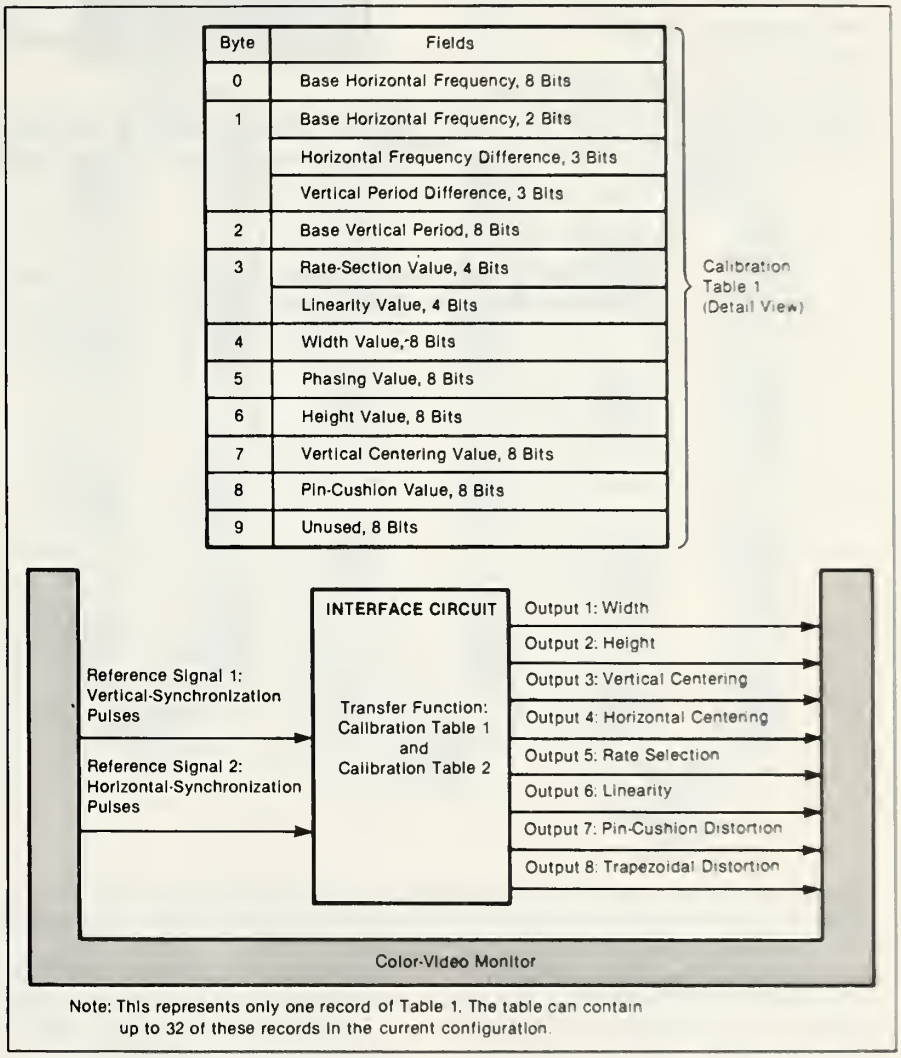

Figure 1. **The Interface Circuit** measures the frequencies of the horizontal- and vertical-synchronizing pulses. When these frequencies fall within a combination of preset ranges, the interface generates an associated preset combination of eight picture-adjusting signals.

The interface repeatedly measures the two pulse frequencies. A match is found when each frequency lies within the range specified in a particular adjustment record, and the two most recent consecutive readings of the frequencies differ by no more than one count. When a match is found, the values in the adjustment record are used to control the monitor. When a match is not found, the interface uses arbitrary values from Table 2 that keep the monitor in a safe operating condition and that might accidentally provide a correctly adjusted picture with some input video signals.

The adjustment records are made during an initial calibration, which is conducted with the help of a computer connected to the monitor (see Figure 2). A video generator is set to one of the anticipated combinations of signal parameters. For each combination, the interface is allowed to adjust the monitor from Table 2. The operator then makes fine adjustments manually for the best picture. The optimized adjustment values, along with the horizontal and vertical frequency range for that combination, is then stored in Table 1. The procedure is repeated for each different combination.

This work was done by Eric Rodriguez of **Goddard Space Flight Center**.

GSC-13076 /TN

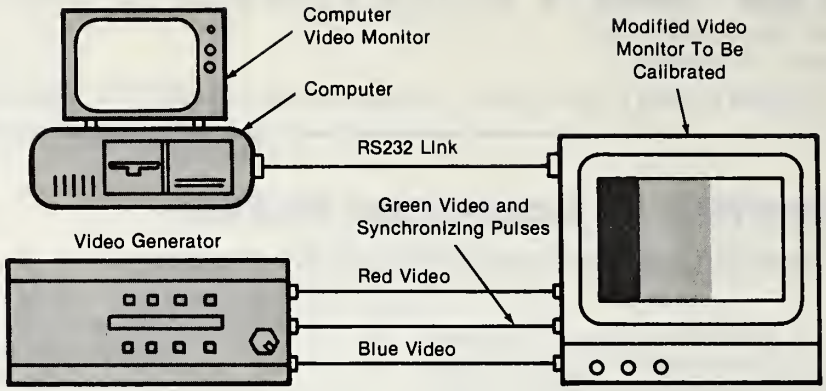

Figure 2. The **Video Monitor Is "Trained"** by a computer that helps to control the calibration procedure and inserts the values in the calibration tables.

FOR ADDITIONAL INFORMATION: *Contact: Director, Technology Transfer Division, P.O. Box 8757, BWI Airport, MD 21240; (301) 621-0100 Ext. 241*

REFER TO THE NUMBER LISTED AT THE END OF THIS ARTICLE

NASA Tech Brief
National Aeronautics and Space Administration

Self-Stabilizing Storage Loops for Magnetic-Bubble Memories

Adjacent, sinusoidal loops provide defect-tolerant, self-stabilizing structures.

Langley Research Center, Hampton, Virginia

In a self-structured magnetic-bubble memory (SSBM) device, in which magnetic bubbles are placed at small separations and strongly interact, it is necessary to provide position-stabilizing forces on all bubbles so that both propagation and stopping of propagation do not disrupt bubble positions and order. The SSBM device requires slippage (propagation) of columns of bubbles past one another with small spacings. The closeness results in strong repulsive forces between the bubbles, tending to disrupt the bubble positions. With the standard propagation-aperture positions shown in Figure 1, the bubble-propagation positions never form a hexagonal configuration, which tends to be self-stabilizing. Also, the propagation positions are never directly opposed, in which situation they would also be balanced but metastable. In addition, the repulsive forces on the bubbles tend to push the columns apart.

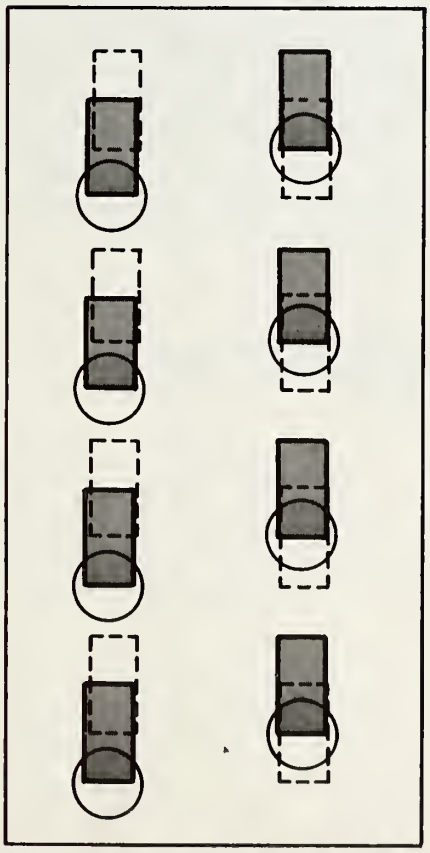

Figure 1. **Magnetic Bubbles Are Never at Regular Hexagonal Spacings** in the rest position with a conventional aperture.

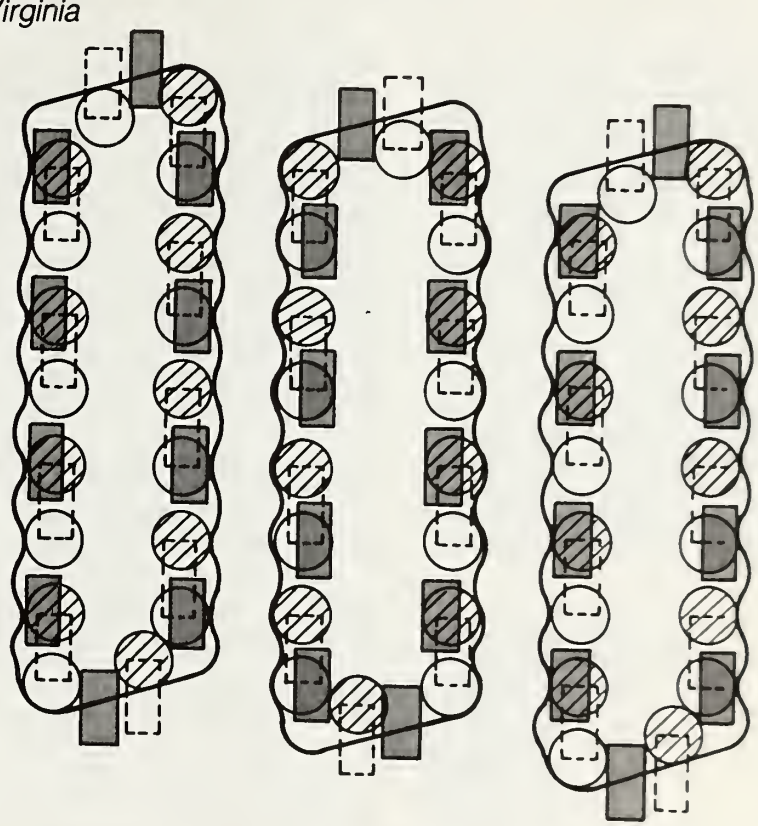

Figure 2. **Counterrotating, Properly Phased Storage Loops** provide additional stability by maintaining hexagonal relative positioning between adjacent columns in adjacent loops.

In an SSBM-device design in which propagation fields are provided by dual-aperture conductors, there are no magnetic features on the surface of the garnet film to position bubbles, as there would be in conventional devices. Therefore, bubble-position and order stability must be provided in the absence of these magnetic features and in the presence of the potentially large destabilizing forces of the close bubbles.

A new technology consists of three components that provide self-stabilizing structures. First, the apertures are positioned so that bubbles propagate alternately into hexagonally related positions (longitudinally stable) and directly opposed positions (longitudinally metastable); the addition of straight barriers by ion milling or implantation of the garnet adds transverse stability but still leaves the longitudinally metastable positions. Second, the modification of the barrier to a sinusoidal shape provides "energy wells" in the longitudinal direction at the opposed positions and eliminates the metastability. Third, the positioning and phasing of counterrotating storage loops, as shown in Figure 2, provide stable hexagonal support between the adjacent loops.

Test devices with bubbles 7 to 8 μm in diameter have been fabricated and tested. Storage loops with 25-μm periodicity were successfully operated at frequencies up to 2.5 MHz, with demonstrated tolerance for fabrication defects in a major-loop/minor-loop design. Defect-tolerant, self-stabilizing behavior was obtained, in that even deliberate defects in the propagation conductors did not upset the behavior.

This work was done by Gary L. Nelson of Sperry Corp. for **Langley Research Center**. *Further information may be found in NASA CR-172554 [N85-22525], "Feasibility of Self-Structured Current Accessed Bubble Devices in Spacecraft Recording Systems."*

Copies may be purchased from the National Technical Information Service, Springfield, Virginia 22161, [A13]

LAR-13625 /TN

FOR ADDITIONAL INFORMATION: *Contact: Director, Technology Transfer Division, P.O. Box 8757, BWI Airport, MD. 21240; (301) 621-0100 Ext. 241*
REFER TO THE NUMBER LISTED AT THE END OF THE ARTICLE

NASA Tech Brief
National Aeronautics and Space Administration

Licensing Opportunity

Central Processor Acts as High-Speed DMA Controller

Maximum transfer rates are achieved with a reduction in cost and complexity.

Langley Research Center, Hampton, Virginia

A computer-system architecture enables the system host central processor (CP) to make high-speed, direct-memory-access (DMA) data transfers without the cost and complexity of adding a dedicated DMA controller. Typically, to obtain maximum rates of data transfer, a dedicated DMA controller is used. In a typical non-DMA transfer, the CP performs at least two bus cycles to move the data word and another bus cycle to read the status word (which indicates that another data word is ready to be transferred). As a result, the transfer rate is far lower than that provided by a DMA-type transfer. The new design is a hybrid of these two former methods that eliminates the disadvantages of both.

With the new system, the CP is used as the DMA controller, obviating the need for a dedicated DMA controller; yet the maximum transfer rates are equivalent to those obtained with a dedicated DMA controller. The CP has access to the memory, as in a conventional configuration. The CP address bus addresses the memory, and the read/write (R/W) line controls the direction of data flow both at the RAM and through the bidirectional buffers. The buffer is enabled and the memory transaction occurs through the activation of the CP data strobe.

Similarly, the CP has direct access to peripheral devices. Again, the bidirectional data-bus buffers are enabled and directed by the CP R/W line, and data flow to and from the peripheral device. The transaction at the peripheral device is a normal read or write as controlled by R/W, address, select, and data strobe. Thus, the CP has access to the peripheral device for initialization or for use in the non-DMA mode.

A bidirectional bus buffer is inserted into the data bus between the CP and the local bus. This arrangement enables data to flow directly between the peripheral device and the memory, while the CP supplies the necessary addresses and control signals. This is conveniently done with a MOVE and autoincrement instruction.

The concept is fairly general in nature, and applications should be widespread. This system may be useful wherever a dedicated DMA controller is desired because of required data-transfer rates but is impractical because of cost and complexity or where it is not necessary to perform DMA transfers and concurrently use the CP for other tasks. A typical application would be where it is desirable to absorb incoming data at a rate that is greater than the CP could otherwise handle. The CP would place the data by DMA into its local memory for later use, enabling the system to connect to high-speed external equipment that otherwise would require the addition of a dedicated DMA controller.

This work was done by Matthew S. Blaha of The Charles Stark Draper Laboratory, Inc. for **Langley Research Center**.

Inquiries concerning rights for the commercial use of this invention should be addressed to the Patent Counsel. Langley Research Center Refer to LAR-13497./TN

Langley Research Ctr.
Hampton, VA 23665
Technology Utilization Officer: John Samos
Mail Stop 139A
(804) 865-3281
Patent Counsel:
George F. Helfrich
Mail Code 279
(804) 865-3725

FOR ADDITIONAL INFORMATION: *Contact: Director, Technology Transfer Division, P.O. Box 8757, BWI Airport, MD. 21240; (301) 621-0100 Ext. 241*
REFER TO THE NUMBER LISTED AT THE END OF THE ARTICLE

NASA Tech Brief
National Aeronautics and Space Administration

Program for Development of Artificial Intelligence

CLIPS surpasses other programs in its category.

The C Language Integrated Production System (CLIPS) computer program is a shell for developing expert systems. It was designed to enable research, development, and delivery of artificial intelligence on conventional computers. The primary design goals for CLIPS were portability, efficiency, and functionality. For these reasons, the program was written in C. CLIPS meets or out-performs most microcomputer- and minicomputer-based artificial-intelligence tools.

CLIPS is a forward-chaining-rule-based language. The program contains an inference engine and a language syntax that provide a framework for the construction of an expert system. CLIPS is based on the Rete algorithm, which enables very efficient pattern matching. The collection of conditions, and, the actions to be taken if the conditions are met, is constructed into a rule network. As facts are asserted either prior to or during a session, CLIPS pattern-matches the number of fields. Wild cards and variables are supported for both single and multiple fields. CLIPS syntax allows the inclusion of externally defined functions (outside functions written in a language other than CLIPS). CLIPS itself can be embedded in a program in such a way that the expert system is available as a simple subroutine call.

CLIPS is written in C for interactive execution and has been implemented on an IBM PC computer operating under DOS with a central-memory requirement of approximately 256K of 8-bit bytes. It should run on any computer system that supports a full (Kernighan and Ritchie) C compiler. CLIPS was developed in 1986.

This program was written by Gary Riley, Chris Culbert, and Frank Lopez of **Johnson Space Center**.

MSC-21208 /TN

FOR ADDITIONAL INFORMATION *CONTACT:*

COSMIC®
112 Barrow Hall
University of Georgia
Athens, GA 30602
(404) 542-3265

FOR ADDITIONAL INFORMATION: *Contact: Director, Technology Transfer Division, P.O. Box 8757, BWI Airport, MD. 21240; (301) 621-0100 Ext. 241*
REFER TO THE NUMBER LISTED AT THE END OF THE ARTICLE

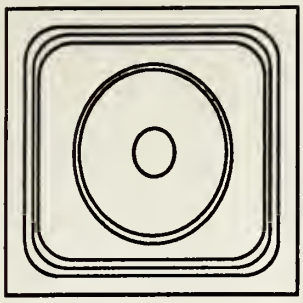

U.S. Air Force
Reliability Analysis Center (RAC)
Rome Air Development Center, Griffiss Air Force Base, NY 13441

Microcircuit Reliability Assessment Program Diskette Version

The Reliability Analysis Center is currently offering a version of Microcircuit Reliability Assessment Program, MRAP, on diskette. The diskette version for MRAP is intended to complement the hardcopy version, and is offered to subscribers as a supplement.

MRAP is a list of integrated circuits, compiled by the Microelectronics Reliability Division of RADC, which have been assigned a Mil- Slash Number and a Qualified Parts List status.

The package contains the data used to generate the current version of MRAP in a database which is accompanied by a Data Access program. The Data Access program allows the user to retrieve MRAP data by specifying a search criteria consisting of any combination of the contained information.

The diskette version will be updated quarterly, as is the hardcopy, and distributed to subscribers along with the hardcopy versions.

The package is designed to operate on an IBM PC/XT, PC/AT or equivalent, operating under DOS 2.10 or later. Hardware requirements are 384K of RAM and a Fixed Disk. The data file, which is compatible with Ashton-Tate's dBase III Plus format, requires 750K of disk space while the access program requires 250K.

The cost for the hardcopy subscription to MRAP/SRAP, Microcircuit / Semiconductor Reliability Assessment Program, is $125.00 per year for United States subscribers and $165.00 per year for the combination hardcopy/diskette version (MRAP only). Non-United States subscribers add $10.00 to either subscription rate.

IBM, PC, XT and AT are trademarks of IBM Corporation. Ashton-Tate and dBase III Plus are trademarks of Ashton-Tate Corporation

Electrotechnology

251 Non-Operation Reliability Databook — Compiles Field and Test Data for an Assortment of Electrical and Electromechanical Parts

252 Electrical Grounding in Cold Regions

253 Electromagnetics Laboratory Accredition Program

255 Diode Structure for Microwave and Infrared Applications — Microwave signals can be switched or modulated optically.

256 Predicting False Lock in Phase-Locked Loops — Methods are derived for calculating false-lock frequency errors.

257 Optical Design and Signal Processing for Edge Detection — The number of edge-detection computations is reduced by a factor of 100.

258 Binary-Symmetry Detection — Transmission errors for zeros and ones are tabulated separately.

259 Ultrasonic Ranging System with Increased Resolution — The master-oscillator frequency is increased.

260 Analysis of a Four-Reflector S/X-Band Antenna — Physical optics accounts for the near field, cross polarization, and higher-order modes.

261 Diffraction Analysis of Antennas with Mesh Surfaces — A strip-aperture model replaces a wire-grip model.

262 High-Voltage Switch Containing $(DI)^2$ Devices — Series switching diodes are triggered on by passing above the threshold voltage.

263 Improved Flux-Gate Magnetometer — A simplified circuit drives heading indicator and senses the magnetic field of the Earth. (Licensing Opportunity)

264 Waveguide-Horn-to-Waveguide Transition Assembly — A microstrip-to-waveguide transition is integrated with a waveguide-horn antenna element.

265 Imaging Radar Polarimeter — Radar measures the full polarization tensor of each element in the scene in one sweep.

Testing & Instrumentation

266 Adjustable, Audible Continuity Tester for Delicate Circuits — The unit is adjustable to resistances up to 35 ohms.

267 Testing Instrument for Flight-Simulator Displays — Many devices for many diverse functions are combined in one equipment item. (Licensing Opportunity)

268 Measuring Microwave Emissivities — A Dicke radiometer and a cryoload are combined in emissivity determinations of mesh antennas. (Licensing Opportunity)

Other Items of Interest

339 Engine-Monitoring Algorithm — Allowances are made for erroneous sensor readings.

U.S. Air Force
Reliability Analysis Center (RAC)
Rome Air Development Center, Griffiss Air Force Base, NY 13441

Non-Operating Reliability Databook

Compiles Field and Test Data for an Assortment of Electrical and Electromechanical Parts

After numerous delays, the RAC has produced a databook devoted to the nonoperating use condition. NON OP-1 entitled "Nonoperating Reliability Databook" is a compilation of nonoperating field and test data for an assortment of electrical and electromechanical parts. The data presented has been collected by the Reliability Analysis Center (RAC) from government and nongovernment sources and resides in RAC databases.

NONOP-1 provides summarized and unsummarized data on a variety of part types. Records are grouped into various logical sub-categories to allow quick comparisons between related part types. Summary data tables provide field failure rates for the merged data records along with their respective predicted failure rate values. As an example, the following figure from NON OP-1 illustrates merged failure rates observed for various MIL-HDBK-217 groups of transistors.

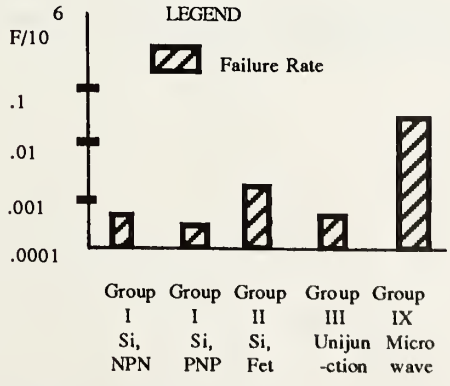

Also presented in the book are predicted failure rates derived from RAC's Nonoperating Reliability Prediction System (RAC-NRPS) which is based on RADC's Technical Report, Impact of Nonoperating Periods on Equipment Reliability, RADC-TR-85-91. The following figure illustrates how this predicted value compares with the observed value for MIL-HDBK-217 Group I, II and IX transistors.

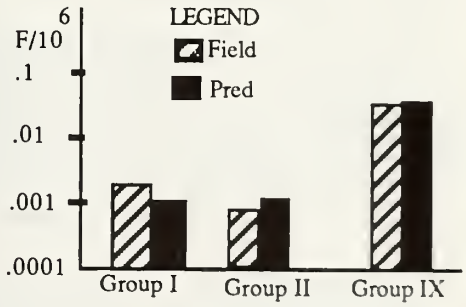

A component failure rate section for miscellaneous components which are not currently represented by reliability prediction models and a section outlining the effects of periodically testing nonoperating systems are also presented. This book is intended to complement documents such as RADC-TR-85-91 or MIL-HDBK-217. **Users are cautioned that any data presented herein may not be used in lieu of contractually cited references.**

US Army Corps of Engineers
Cold Regions Research & Engineering Laboratory
Hanover, NH 03755

Electrical Grounding in Cold Regions

Electrical grounding for temporary and permanent installations in cold regions is complicated by the existence of frozen soil. This is because the electrical resistivity of frozen soil can be several orders of magnitude higher than unfrozen soil. The contact resistance between the grounding electrodes and the soil, which is usually negligible under unfrozen conditions, can become significant if a veneer of ice forms on the electrode, and it is difficult to drive grounding rods into frozen soil.

The Cold Regions Research & Engineering Laboratory prepared a digest to describe the factors to consider when planning a grounding system for permanent and temporary installations in regions of seasonal frost and permafrost. They found that the chance of finding and developing a low-resistance grounding site decreases greatly when moving towards polar regions from the zone of seasonal frost to the discontinuous and continuous permafrost zones. Large seasonal variations in the resistance to ground can be expected in areas of frozen ground. Grounding may not be difficult during the summer but will likely become a problem when the surface layer freezes.

The search for suitable grounding sites can be aided by geophysical methods that locate low-resistivity (usually unfrozen) earth. A knowledge of an area's topography, vegetation, and surface and ground-water sources can provide good information for locating thawed zones and conductive soils for a grounding site. Multiple-rod grounding arrays or horizontal grounding configurations can be used to achieve a lower Rg than with a single grounding rod.

FOR ADDITIONAL INFORMATION: A copy of this report is available from NTIS, Springfield, VA 22161; (703) 487-4600.

NTIS order number: AD-A181405/2/NAC

Price code: A02

To discuss this effort further, contact Ms. Karen Henry, USA Cold Regions Research and Engineering Laboratory, Hanover, NH 03755-1290.

NBS technology update

National Bureau of Standards
U.S. Department of Commerce
Gaithersburg, MD 20899

Electromagnetics Laboratory Accreditation Program

The electromagnetics laboratory accreditation program managed by NBS under the National Voluntary Laboratory Accreditation Program (NVLAP) has been expanded to meet requests from participating labs, manufacturers, and the U.S. Naval Air Systems Command. Test methods have been added to help labs improve the quality of testing on products that must meet Federal Communications Commission (FCC) approval and to assure the performance of electronic devices for weapons systems. The expanded program includes test methods for radio frequency devices including receivers (FCC Part 15); industrial, scientific and medical devices (FCC Part 18); radio transmitters (FCC Part 90); and a military standard (MIL STD-462) to measure electromagnetic interference characteristics. The electromagnetics program was initially limited to test methods for computing devices (FCC Part 15J), and for telephone equipment compatibility (FCC Part 68).

FOR ADDITIONAL INFORMATION: Contact:
National Voluntary Laboratory Accreditation
A 31 Administration Building
National Bureau of Standards
Gaithersburg, MD 20899
(301) 975-4016

NASA Tech Brief
National Aeronautics and Space Administration

Diode Structure for Microwave and Infrared Applications

Microwave signals can be switched or modulated optically.

Goddard Space Flight Center, Greenbelt, Maryland

A planar diode with a transparent cathode can be made in GaAs, Si, and InSb versions. Depending on the specific configuration and material, such a diode could be used for the optical modulation of a microwave signal or as an infrared detector.

The fabrication of the GaAs version (see figure) begins with the etching of a hole about 10 μm deep into a semi-insulating, Cr-doped substrate having a resistivity of 5 $\times$ 10^8 Ω-cm. An n^+ layer about 15 μm thick is grown by vapor-phase epitaxy, filling the etched hole. The wafer is then chemically polished, leaving the n^+-filled pocket. An n-type GaAs epitaxial layer is grown on the n^+. A mesa of n is etched completely inside the n^+ region to form an n/n^+ region.

Au/Ge is evaporated onto the device to form an ohmic contact. The Au/Ge window is etched to open up the area for the transparent cathode, which consists of Ni/Au or Au electroplated to two skin depths at the illuminating wavelength of interest. Lift-off is used to delineate the transparent cathode and the ohmic contact to the cathode.

Similar techniques are used to fabricate InSb version. Because InSb is used primarily in the infrared region, the cathode is made of Si, which is transparent to infrared.

In the Si version, single-crystal n-type Si is grown on a sapphire substrate, and native oxide is available for masking. Photoresist methods are used to open up the oxide to the diffusion of As. A layer of P-doped silicon is then grown over the n^+ pocket. The ohmic contact, cathode, and cathode contact are formed by methods similar to those for the GaAs device.

These processes yield Schottky-barrier

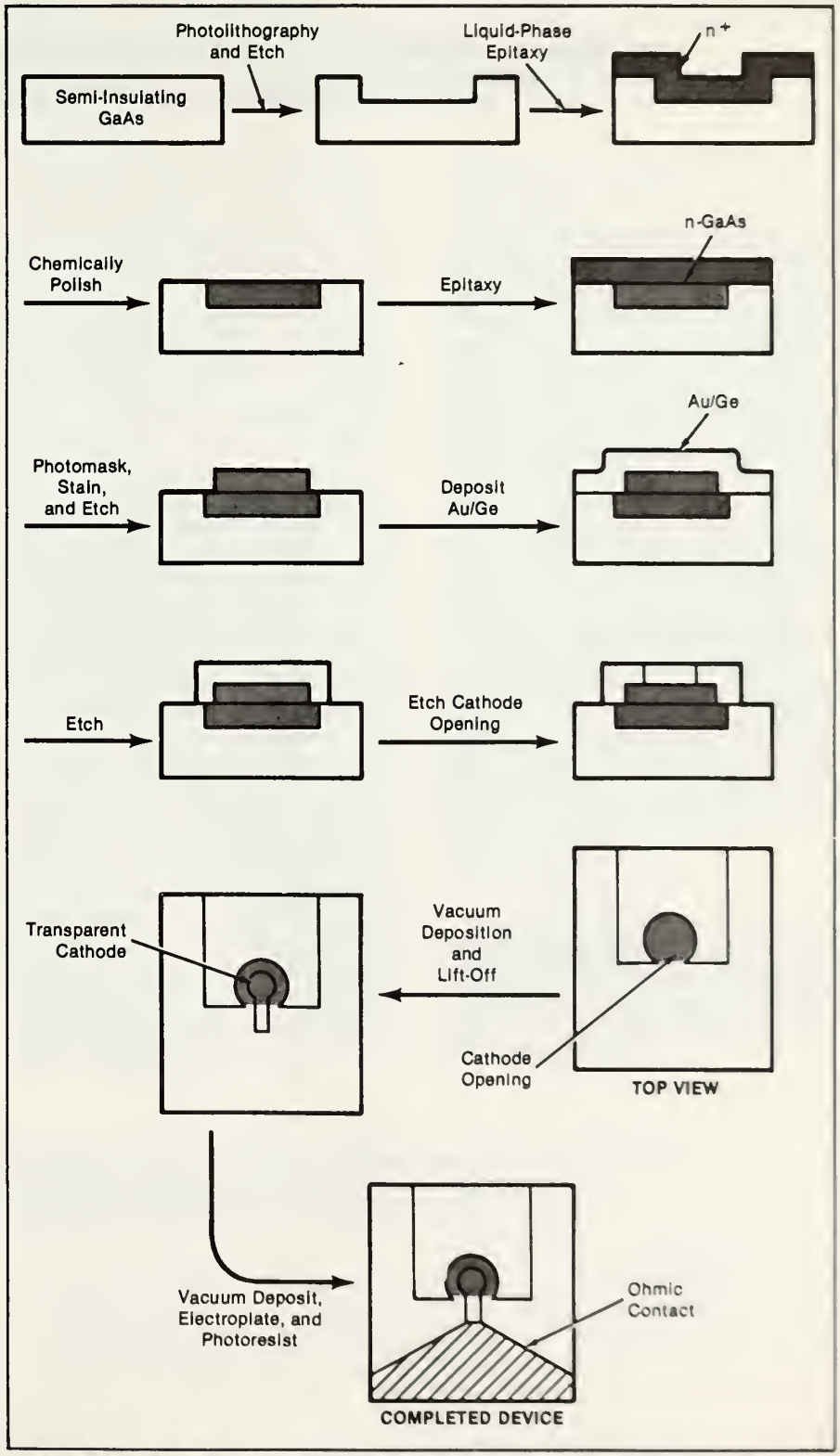

A **Transparent Cathode** is fabricated on a GaAs diode so that the diode can be illuminated to generate and control the short-circuit current.

diodes. When such a diode is operated with reverse bias and no illumination, the space-charge region is depleted of carriers, and the diode acts as an insulator. If placed in a waveguide while operating in this mode, it would thus allow a microwave signal to pass through. However if the diode is illuminated through the transparent cathode, electron/hole pairs generated by the impinging photons increase the short-circuit current: this causes the diode to present a short circuit to the incident microwave, which is thus prevented from traveling further along the waveguide.

The light can be turned on or off or it can be modulated to switch or modulate the microwave signal at high speeds. Because of the lower mobilities of charge carriers in Si, the Si version is used at microwave frequencies lower than those of the GaAs version. The InSb device is used mainly for the detection of infrared.

This work was done by George Alcorn, Charles Leinteran, and Bing Chiang of **Goddard Space Flight Center.**

GSC-12962 /TN

FOR ADDITIONAL INFORMATION: *Contact: Director, Technology Transfer Division, P.O. Box 8757, BWI Airport, MD. 21240; (301) 621-0100 Ext. 241*

REFER TO THE NUMBER LISTED AT THE END OF THE ARTICLE

NASA Tech Brief
National Aeronautics and Space Administration

Predicting False Lock in Phase-Locked Loops

Methods are derived for calculating false-lock frequency errors.

A theoretical paper discusses advances in the mathematical analysis of phase-locked loops. It presents new results in the prediction of false locking; that is, locking to a frequency other than the intended one. The paper should be of interest to users of phase-lock circuits and to researchers seeking ways to detect or avoid false lock.

The analysis is based on a classical model of a phase-locked loop. An input signal proportional to $\sin(\omega_i t)$, where ω_i is angular frequency and t is time, and a voltage-controlled oscillator signal proportional to $\cos(\omega_V t - \psi)$ with unknown phase factor ψ are fed to a mixer. The mixer output passes through a filter, the response of which is characterized by

$$F(S) = \frac{S^M + a_{M-1}S^{M-1} + \ldots + a_0}{S^N + b_{N-1}S^{N-1} + \ldots + b_0}$$

where S is the Laplace-transform complex-frequency variable and the a_i and b_i are constants. The filter output is the control voltage for the oscillator.

The nonlinear differential equation governing the evolution of the unknown phase factor ψ is

$$\left[\frac{d^N}{dt^N} + b_{N-1}\frac{d^{N-1}}{dt^{N-1}} + \ldots + b_0\right] \times \left[\omega_i - \omega_0 - \frac{d\psi}{dt}\right] = \delta\left[\frac{d^M}{dt^M} + a_{M-1}\frac{d^{M-1}}{dt^{M-1}} + \ldots + a_0\right] \times \sin(\omega_i t + \psi)$$

where ω_0 is the oscillator angular frequency at zero control voltage, δ is a closed-loop gain factor, and $\omega_f = \omega_i - \omega_V$; that is, ω_f is the negative of the false-lock angular-frequency error.

The differential equation is written in state-vector form, with ψ and its derivatives constituting the components of the vector. To find the false lock, the derivative of the state vector is postulated to be periodic, repeating at intervals $T = 2\pi/\omega_f$.

The equation is solved with the help of a perturbation expansion in which δ serves as the smallness parameter. Starting from the previous observation that only discrete false-lock frequencies are possible and from the assumption that false lock occurs for all values of δ near zero, a necessary condition for false lock is derived, which is expressed as a relationship among the multipliers of the perturbation equation.

For the first variation in the perturbation expansion of a system with $F(S) = (S + a)/(S + b)$, the necessary condition yields series expansions for the periodic state vector and for ω_f^{-1}. Another algorithm for calculating ω_f^{-1} involves a system of nonlinear algebraic equations derived from the necessary condition and the dynamic-loop equations. These equations are solved numerically by the Newton-Raphson technique, with the Jacobian computed by a finite-difference scheme. This algorithm produces results that are limited only by the precision of the computer on which it is executed.

The paper gives computational results for a system with $a = 5$, $b = 1$, and $\omega_i - \omega_0 = 35$ rad/s. For example, at a loop gain of $\delta = 10$, the perturbation method yields $\omega_f = 29.05173$ rad/s to second order in δ, and 27.02784 rad/s to fourth order in δ. At the same value of loop gain, the algebraic method yields $\omega_f = 25.5071$ rad/s.

This work was done by Bill Reed of **Marshall Space Flight Center** *and John L. Stensby of the University of Alabama. To obtain a copy of the report, "New Results on the PLL False Lock Phenomenon," MFS-27110/TN*

FOR ADDITIONAL INFORMATION: *Contact: Director, Technology Transfer Division, P.O. Box 8757, BWI Airport, MD. 21240; (301) 621-0100 Ext. 241*
REFER TO THE NUMBER LISTED AT THE END OF THE ARTICLE

NASA Tech Brief
National Aeronautics and Space Administration

Optical Design and Signal Processing for Edge Detection

The number of edge-detection computations is reduced by a factor of 100.

Langley Research Center, Hampton, Virginia

As in human vision, most current approaches to machine vision include edge detection as an initial processing step. The optimal edge-detection response for machine vision closely approximates the spatial response of human vision and is given by the difference-of-Gaussian (DOG) function.

Spatial filtering in the computer requires large (up to 31-by-31) filter masks to approximate the DOG function satisfactorily. This technique offers a design approach to approximate this function closely with only a 3-by-3 element mask, thereby reducing the number of required computations by as much as a factor of 100. This is accomplished by properly combining optical design, including lens apodization, with the signal-processing algorithm as depicted in Figure 1. Figure 2 demonstrates that the resultant response $\tau(x,y)$ closely approximates the DOG-function response.

The desired response can be obtained either by parallel processing of signals from a large number of neighboring photosensor elements (i.e., a large mask) or, with a minimal amount of processing, by appropriately shaping the spatial-frequency response of the objective lens. Various combinations of optical design and signal processing algorithms can be used. For example, to increase sensitivity, it may become necessary to increase the lens aperture diameter beyond the diameter (and hence beyond the cutoff frequency) that provides the best realizable spatial response. It would then be advantageous to defocus the optical system.

The importance of this concept lies in the realization that the optical design and the signal-processing algorithm can be combined to approximate closely the optimal edge-detection response with a minimal amount of processing. The processing can be done either in the computer or in the focal plane of the sensor-array image-gathering system. If the processing is done in the focal plane, then the dynamic range required for analog-to-digital conversion and the amount of data that must be transmitted are both substantially reduced.

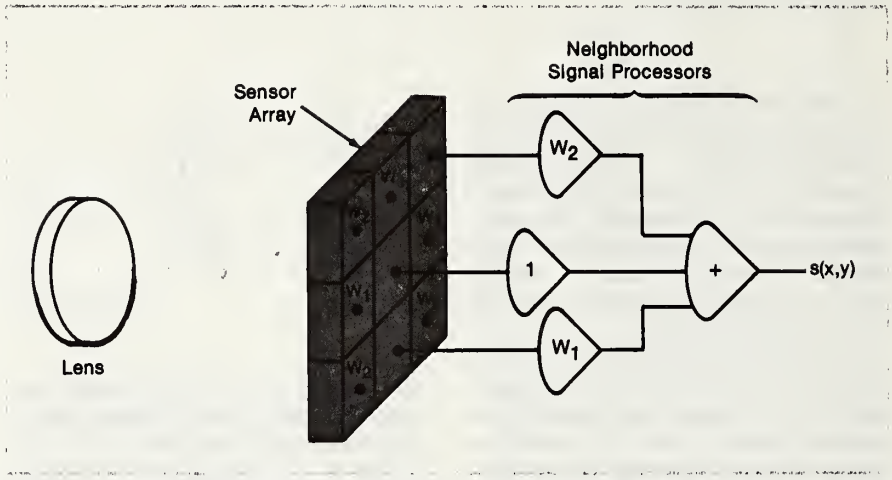

Figure 1. Properly combining the optical design with a **3-by-3 Element Mask** reduces the number of required computations by a factor of as much as 100.

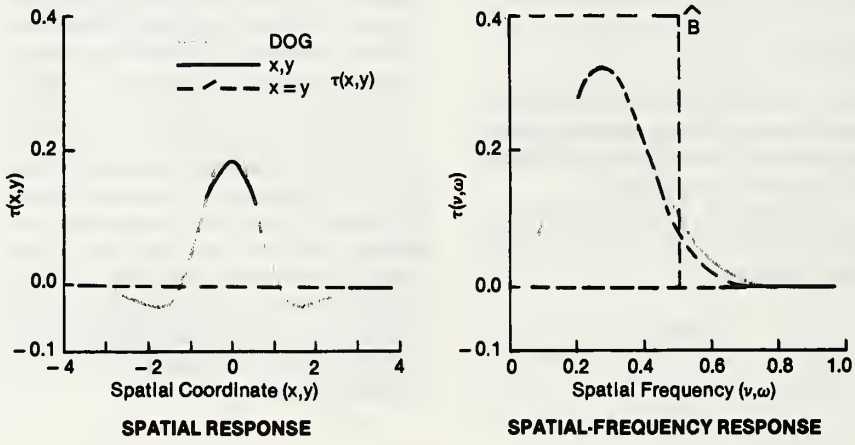

Figure 2. These **Spatial and Spatial-Frequency Responses** are obtained in the system of Figure 1 by the combination of the optical design and the signal-processing algorithm. These curves closely approximate difference-of-Gaussian-function response.

This work was done by Friedrich O. Huck of **Langley Research Center** *and Kathryn Stacy of Computer Sciences Corp. LAR-13416 /TN*

FOR ADDITIONAL INFORMATION: *Contact: Director, Technology Transfer Division, P.O. Box 8757, BWI Airport, MD. 21240; (301) 621-0100 Ext. 241*
REFER TO THE NUMBER LISTED AT THE END OF THE ARTICLE

NASA Tech Brief
National Aeronautics and Space Administration

Binary-Symmetry Detection

Transmission errors for zeros and ones are tabulated separately.

Goddard Space Flight Center, Greenbelt, Maryland

When dealing with a digital binary data-transmission system, a priori assumption is made of the existence of a binary symmetrical channel for most calculations. The prediction and computation of the probabilistic bit-error performance of a given system is based on this assumption and on the postulate of equal probability for the transmitted logical ones and zeroes. The present bit-error measurements provided by commercially available test sets simply lump or totalize all errors, masking a wealth of information about the performance of a system

The probability of error in digital transmission systems can be calculated by $P_e = (1/2)\,erfc\,[(E_b/N_o)^{1/2}]$, (where E_b is the energy per bit, and N_o is the noise energy during a bit period) for a memoryless uncoded channel in the presence of additive white Gaussian noise, with the corollary assumption that the channel is binary symmetrical. The errors that result when binary data are sent through the noisy channel are in fact logical transpositions (inversions) of the transmitted logical elements sent. For example, each transposition with an equal probability of occurrence for the well-behaved, model channel is depicted by the binary-symmetry model.

The judicious examination of the detected errors and whether the logical ones were transposed into zeroes and, conversely, the zeroes transposed into ones can reveal the nature of the system impairment. It follows that any binary asymmetry thus detected can be correlated to equipment imbalances or inabilities to match the channel.

The binary-symmetry detector employs the psuedo-random data pattern used as a test message coming through the channel, which message is then modulo-2 added to the locally generated and synchronized version of the test data pattern in much the same manner found in the manufactured test sets of today. In the early Nascom test-set version, the errors thus detected were correlated by exclusive-or gating with the bit-delayed version of the pattern to resolve the ambiguity of the error (see Figure 1). Steering flip-flops are then used to route the detected ones or transposed zeroes to a separate counter from the zeroes or transposed ones. A binary symmetrical channel will show nearly a 50-percent ones to 50-percent zeroes correspondence. The degree of the asymmetry represents imbalances due to either the modulation, transmission, or demodulation processes of the system when perturbed by noise.

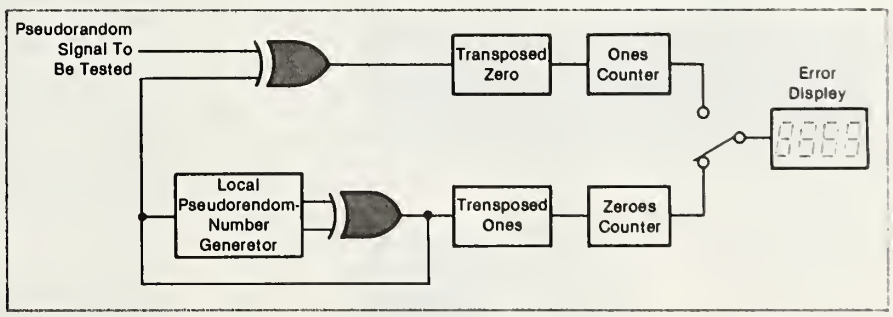

Figure 1. An **Early Test Set** correlated errors by exclusive-or gating with the bit-delayed version of the test signal.

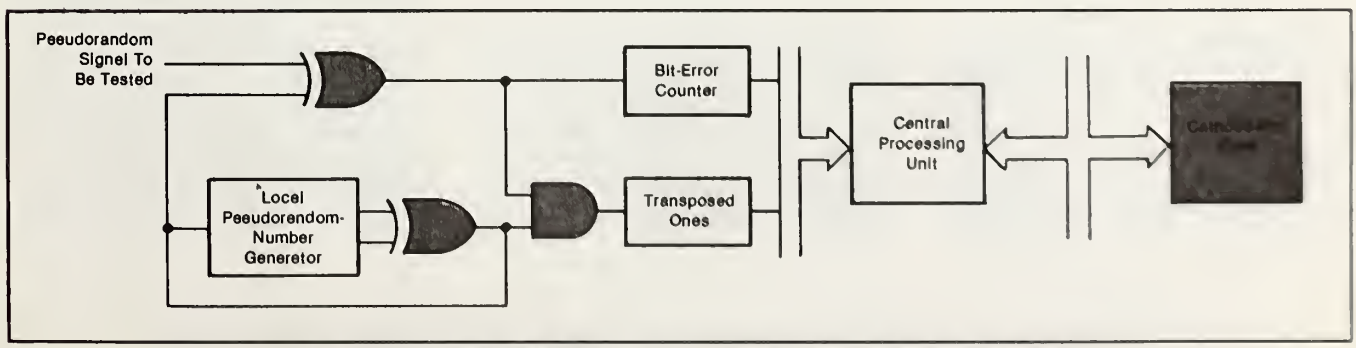

Figure 2. A **Bit-Error-Rate Tester** of the new type includes the symmetry feature.

The advent of microprocessors has made this binary-symmetry detection easier to depict by graphing the asymmetry on a cathode-ray tube. This measurement is normally made such that a dynamic channel performance can be viewed without disturbing the basic bit-error performance computation.

Asymmetry-anomaly-characterization and -detection circuits are not commercially available in off-the-shelf test sets. A typical bit-error-rate tester (BERT, as they are commonly denoted) was built by Nascom with symmetry-detection circuitry as depicted in Figure 2. The new test-set model 610, developed by the NASA Communications Division under contract with Astrotronics, Inc., includes all features found in commerciallv available BERT's, plus the symmetry feature. Moreover, the symmetry detection is displayed on the self-contained 5-in. (12.7-cm) cathode-ray tube. The display scrolls the channel symmetry as a function of test time. It is envisioned that this method be included as a feature in all commercial test sets to aid in the troubleshooting of digital binary transmission systems.

This work was done by Hiram Lopez of **Goddard Space Flight Center**.
GSC-12985 /TN

FOR ADDITIONAL INFORMATION: *Contact: Director, Technology Transfer Division, P.O. Box 8757, BWI Airport, MD. 21240; (301) 621-0100 Ext. 241*
REFER TO THE NUMBER LISTED AT THE END OF THE ARTICLE

NASA Tech Brief
National Aeronautics and Space Administration

Ultrasonic Ranging System With Increased Resolution

The master-oscillator frequency is increased.

Lyndon B. Johnson Space Center, Houston. Texas

An ultrasonic range-measuring system (see figure) with 0.1-in. (2.5-mm) resolution provides a continuous digital display of four distance readings, each updated four times per second. The four rangefinder modules in the system are modified versions of the rangefinders used for automatic focusing in a commercial series of cameras. The ultrasonic pulses emitted by the system are innocuous to both people and equipment.

Each rangefinder module includes a capacitive transducer that both emits and detects ultrasonic pulses. The distance from the transducer to the target is determined by counting the number of cycles of an oscillator that occur between the emission of a pulse and the detection of its echo. The resolution of the rangefinder was increased by increasing the oscillator frequency so that each cycle corresponds to a range increment of 0.1 in. (2.5 mm) rather than the original 0.1 ft (30.5 mm). The basic characteristics of the measuring circuits as manufactured would permit the improvement of resolution to about 0.01 in. (0.25 mm) by increasing the oscillator frequency further. Temperature compensation could be applied to the oscillator circuit to make the range measurements independent of the variation of the speed of sound with temperature.

Synchronizing circuits gate the operation of the rangefinder transducers so that each transducer channel responds only to its own emitted pulses. The transducers are mounted in machined enclosures to protect them from physical damage and to narrow their beams to prevent the inadvertent returns of signals from other objects near the intended beam.

The system was developed to speed payload installation in the Space Shuttle. Installed on the payload-handling mechanism, it provides continuous remote monitoring of the payload position without contact with either the payload or the vehicle. Previously, cargo installation was a slow, iterative process requiring repeated small movements alternating with manual position measurements. In addition to use in other cargo-handling situations, the system could provide economical solutions to such distance-measurement problems as those posed by a boat approaching a dock, a truck backing toward a loading platform, runway-clearance readout for the tail of an airplane with a high angle of attack, or a burglar alarm.

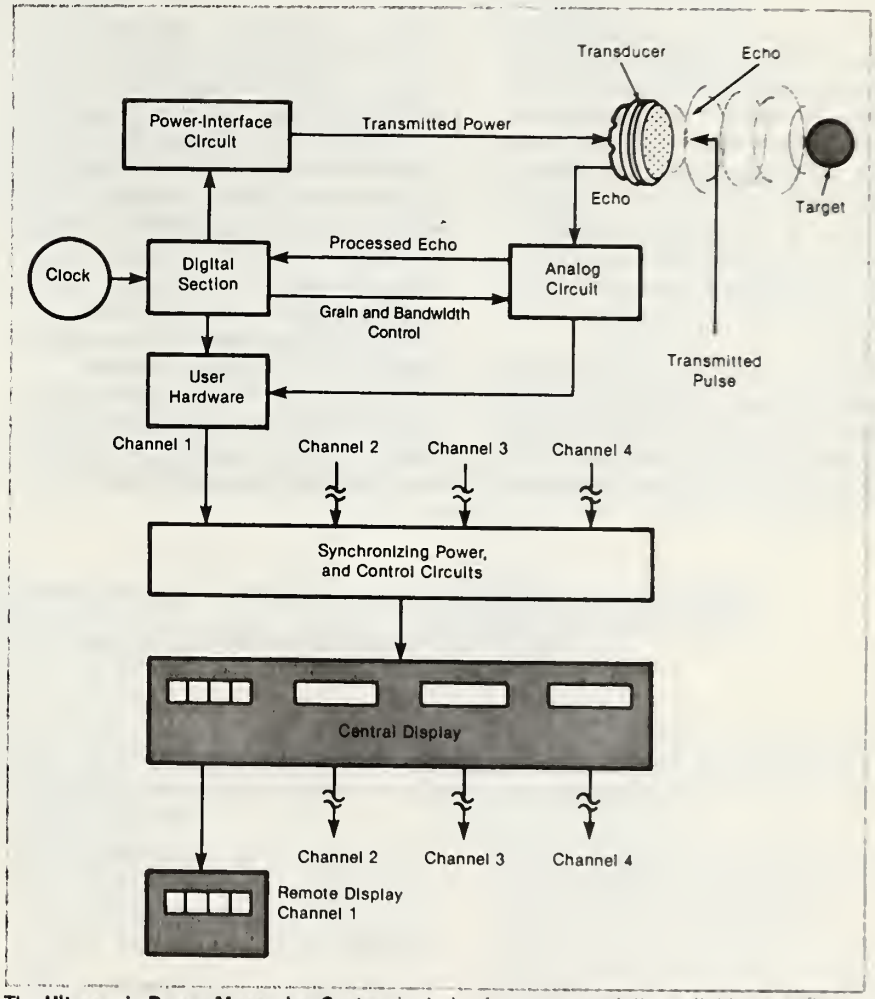

The Ultrasonic Range-Measuring System includes four commercially available rangefinder modules that have been modified to provide higher range resolution and an increased measurement-repetition rate.

This work was done by William E. Meyer and William G. Johnson of Rockwell International Corp. for **Johnson Space Center** *MSC-21090/TN*

FOR ADDITIONAL INFORMATION: *Contact: Director, Technology Transfer Division, P.O. Box 8757, BWI Airport, MD. 21240; (301) 621-0100 Ext. 241*
REFER TO THE NUMBER LISTED AT THE END OF THE ARTICLE

NASA Tech Brief
National Aeronautics and Space Administration

Analysis of a Four-Reflector S/X-Band Antenna

Physical optics accounts for the near field, cross polarization, and higher-order modes.

A report presents a physical-optics analysis of the four-reflector, 64-m antennas of the Deep Space Network. The excellent agreement of the results with the measured properties (e.g., gain, beam shape, and beam offset angle) of the actual antennas is taken as an independent validation of the algebra and computer code used. This appears to be the first time such a complete and rigorous analysis has been performed on such a complex antenna system.

Because the analysis is thorough and detailed, the report also has instructional value as an example for designers of large microwave dishes with subreflectors and involving reflector surfaces with hyperboloidal, paraboloidal, ellipsoidal, and more complex shapes. The analysis accounts fully for all near-field, cross-polarization, and higher-order-mode-generation effects caused by various asymmetries in the antenna structure and operation. The analysis procedure could be useful in ground-station-antenna design efforts, including the design of high-efficiency shaped reflectors and beam waveguide feeds, and in microwave metrology (holography) applied to the measurements of large reflector surfaces.

The analysis of the four-element, 64-m design proceeds element by element. The far-field diffraction patterns of the feed-horn, ellipsoidal reflector, dichroic mirror, and asymmetric subreflector are computed in turn by physical-optics integrations, using the results from each element as input for the next element. Finally, the far-field diffraction pattern of the symmetric main reflector is computed. The near-field diffraction patterns are calculated from the far fields with the help of a spherical-wave expansion.

In view of the success with the 64-m system, the analysis will be extended to designs that upgrade the antennas to 70-m diameter.

This work was done by Alan G. Cha of Caltech for **NASA's Jet Propulsion Laboratory**. *To obtain a copy of the report, "Physical Optics Analysis of Four-Reflector Antenna," NPO-16839/TN*

FOR ADDITIONAL INFORMATION: *Contact: Director, Technology Transfer Division, P.O. Box 8757, BWI Airport, MD. 21240; (301) 621-0100 Ext. 241*
REFER TO THE NUMBER LISTED AT THE END OF THE ARTICLE

NASA Tech Brief
National Aeronautics and Space Administration

Diffraction Analysis of Antennas With Mesh Surfaces

A strip-aperture model replaces a wire-grid model.

NASA's Jet Propulsion Laboratory, Pasadena, California

The application of large reflector antennas for satellite communications, such as the third-generation Land Mobile Satellite system concept and ground terminals, has resulted in the use of mesh surfaces, because of their light weight, reduced wind effects, and unfurlability. An accurate performance analysis of these mesh reflectors for various applications demands that the effects of the mesh be properly accounted for in the vector diffraction analysis. This is done by modifying the solid-surface physical-optics-induced current as shown in the block diagram of Figure 1.

The far-field radiation pattern of an antenna with a mesh reflector is calculated more accurately with a new strip-aperture model than with a wire-grid model of the reflector surface. The strip-aperture model is more adaptable than the wire-grid model to a variety of practical configurations and is decidedly superior for reflectors in which the mesh-cell width exceeds the mesh thickness. Unlike the wire-grid model, the strip-aperture model satisfies the reciprocity theorem (relating to the interchangeability of sources and receptors of the electromagnetic field).

The new model (see Figure 2) is applied where the mesh cells are no larger than about a tenth of a wavelength. This small cell size permits the use of the simplifying approximation that the reflector-surface current induced by the electromagnetic field is present even in the apertures. The approximation is particularly useful in calculating the far field.

Instead of treating the surface-current problem in the full spatial complexity of the mesh, the effect of the apertures is incorporated into the equations for an equivalent current pattern induced on a smooth reflector surface. A matrix of transmission and reflection coefficients is used to calculate the effect of the apertures on the surface current. To obtain the coefficients, the strip-aperture model is applied in the following way:

- Each point on the reflector surface is treated as an infinitesimal part of a plane tangent to the reflector at that point.
- The incident electromagnetic field is approximated by a plane-wave incident upon the plane along a direction from the antenna feedhorn to that point.
- The local strip-aperture structure is repeated periodically over the entire plane.

Because of the periodic nature of the mesh, the effect of the surface current on the scattering of the electromagnetic field is expressible in terms of spatial harmonics (aperture modes). Because the apertures are small compared to the wavelength, only a few of the aperture modes need to be calculated to obtain an accurate result.

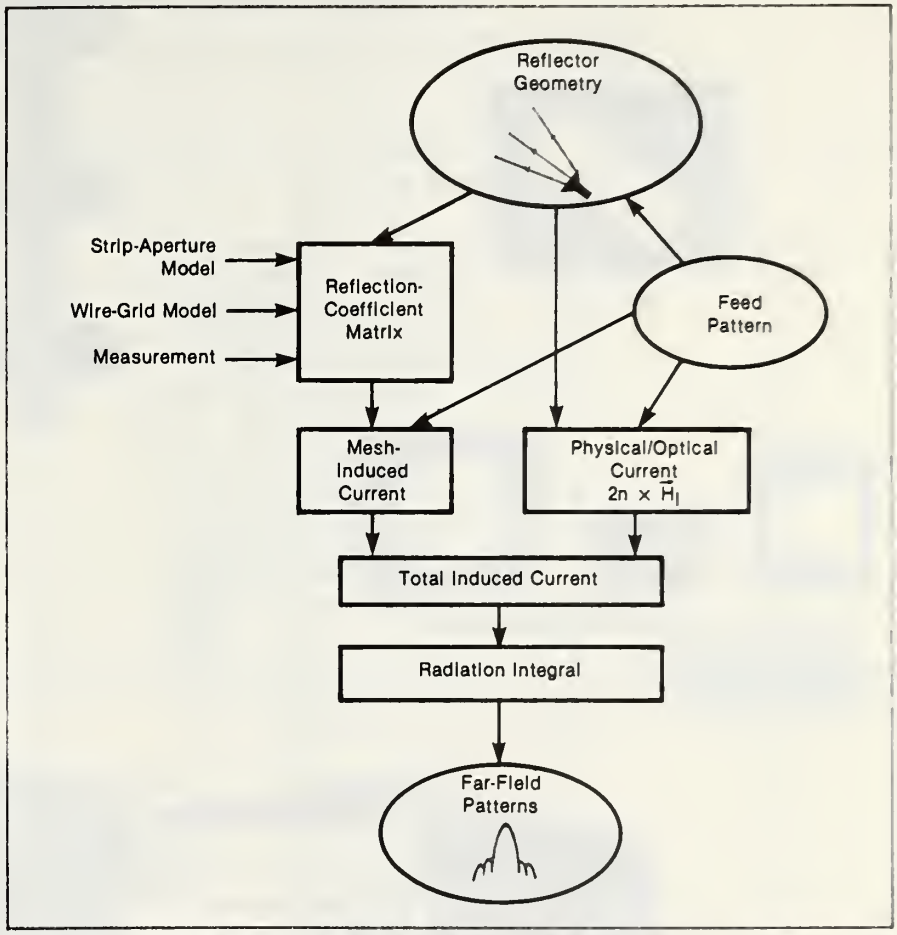

Figure 1. The Computation of the Far-Field Radiation Pattern requires the modification of the current previously assumed to be induced on a solid antenna surface, to account for the effects of the mesh.

Like the wire-grid model, the strip-aperture model can be used to study the performances of many mesh-reflector antennas. In addition, the strip-aperture model can be applied to reflector surfaces perforated with circular holes. Effects that can be investigated include the generation of cross-polarized fields, gain as a function of cell size, the reduction of directivity by surface power dissipation, and other far-field phenomena that are affected by the spatially varying, vector nature of the surface current.

This work was done by Yahya Rahmat-Samii of Caltech for **NASA's Jet Propulsion Laboratory**. *NPO-16474/7N*

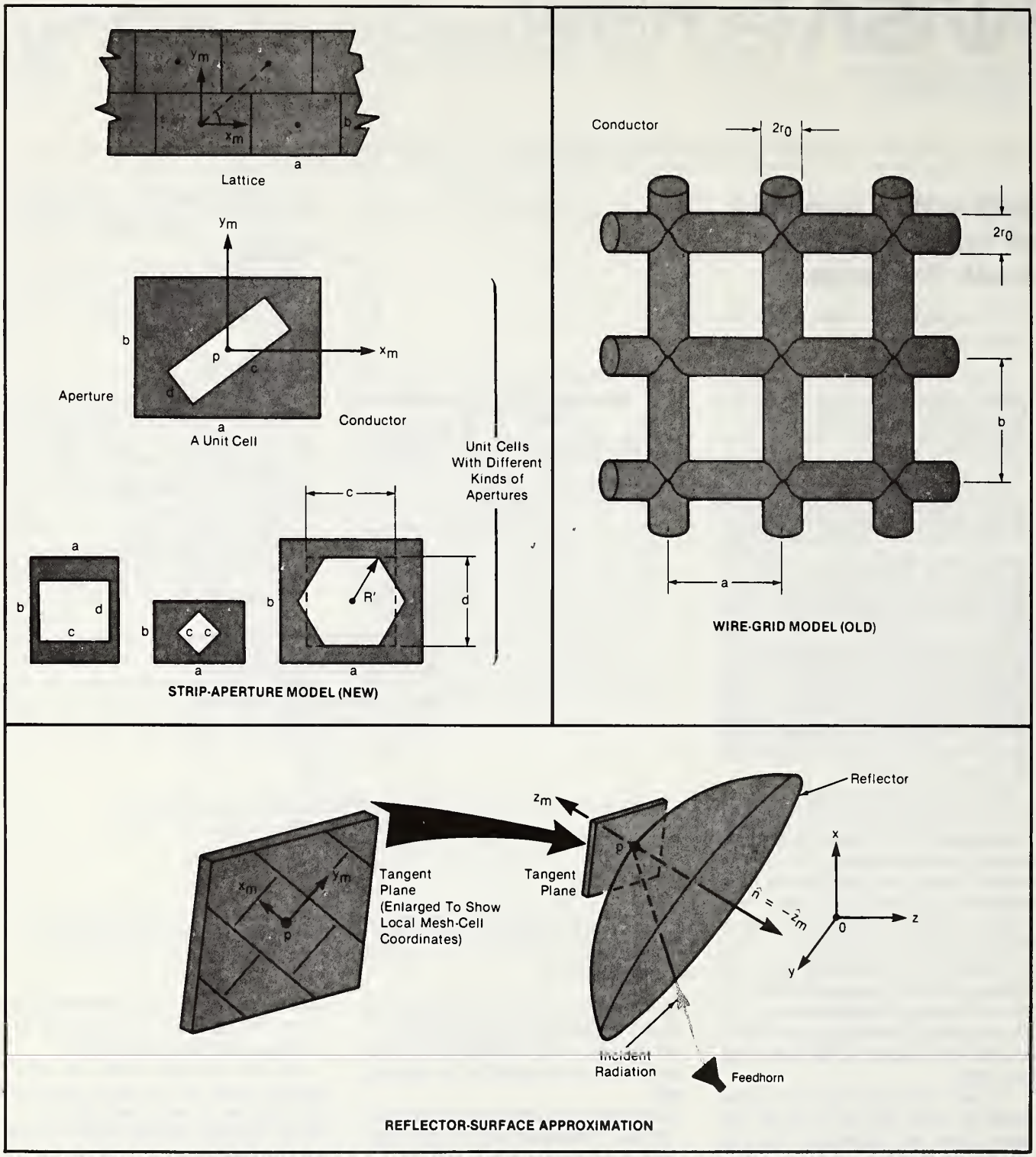

Figure 2. The **Strip-Aperture Model** (top left) of a mesh antenna reflector surface is used in place of the older, wire-grid, model (top right). The strip-aperture model is more easily adapted to a variety of mesh configurations and gives more accurate results for some practical antennas. The reflector surface (bottom) is approximated locally by a tangent plane over which the local aperture structure extends periodically.

FOR ADDITIONAL INFORMATION: *Contact: Director, Technology Transfer Division, P.O. Box 8757, BWI Airport, MD. 21240; (301) 621-0100 Ext. 241*

REFER TO THE NUMBER LISTED AT THE END OF THE ARTICLE

NASA Tech Brief
National Aeronautics and Space Administration

High-Voltage Switch Containing $(DI)^2$ Devices

Series switching diodes are triggered on by passing above the threshold voltage.

Lewis Research Center, Cleveland, Ohio

A high-voltage switch is made by connecting a multitude of deep-impurity, double-injection [$(DI)^2$] devices in series with each other and with another, triggerable high-voltage device such as a thyristor (see figure). The triggerable device can be operated near ground potential to avoid insulation problems in the triggering circuit.

In operation, a high voltage from a pulse-forming network or other source would be applied across the high-voltage switch. This voltage would be near, but less than, the combined threshold voltages of the $(DI)^2$ devices, so that the current flowing through these devices would be small. Equal voltage sharing among the $(DI)^2$ devices and the thyristor can be assured through a resistive network in parallel with the high-voltage devices. Triggering the thyristor on causes the voltage across each of the $(DI)^2$ devices to increase to the threshold value, causing them to switch to the high-current, low-voltage mode; the entire string of devices switches to the on condition, sending a high-current pulse through the load.

Because there is no way to turn the switch off, it will continue to conduct current as long as a sufficient voltage is maintained by the voltage source. This is the conventional mode of operation of thyristor circuits.

The advantages of this type of high-voltage switch over conventional high-voltage thyristor strings are the following:

- Since only one of the devices in the series string requires a triggering signal, the difficulties inherent in sending trigger signals to those devices that are at high potentials relative to ground can be avoided.
- Because the switching of one device in a series string automatically causes other devices in the string to switch, it is unnecessary to apply trigger signals simultaneously to each device in the string, and a high degree of switch reliability is obtained.
- $(DI)^2$ devices are, at least in principle, easy to fabricate because they do not require high-voltage p/n junctions. As a result, they are expected to be less costly to fabricate than voltage thyristors.
- $(DI)^2$ devices can be made as lateral devices on a semiconductor wafer; this would avoid the difficulties associated with double-sided diffusions and metallization required with high-voltage thyristors. It would even be possible to connect several $(DI)^2$ devices in series on a single wafer instead of separating them for individual packages as is required for high-voltage thyristors.
- Other investigators have reported that silicon $(DI)^2$ devices are capable of operating at higher temperatures (over 400 °C) than those permissible for thyristor operation (125 °C). This characteristic would permit the use of $(DI)^2$ switches in certain high-temperature applications, where conventional silicon devices can-

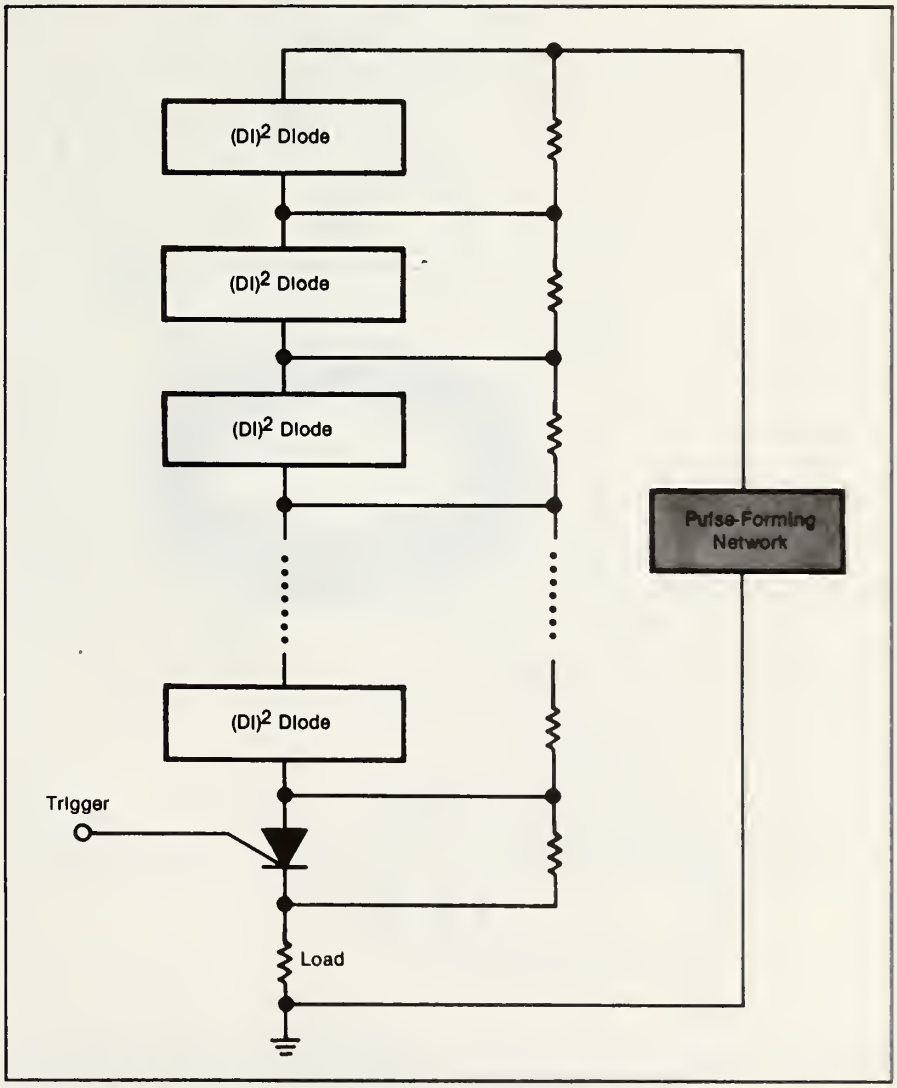

A High-Voltage Switch is made by cascading deep-impurity, double-injection [$(DI)^2$] devices in series with the load and a thyristor.

not be used.

- Other investigators have reported that silicon $(DI)^2$ devices continue to operate normally after exposure to high doses of nuclear radiation (in excess of 100 megarads total dose). This characteristic would permit the use of $(DI)^2$ switches in applications involving nuclear fission or fusion reactors and in military or space applications.

This work was done by Maurice H. Hanes and Richard J. Fiedor of Westinghouse Electric Corp. for **Lewis Research Center**. *Further information may be found in: NASA TM-86957 [N85-20246/NSP], [A02]*

"A New Very High Voltage Semiconductor Switch" and NASA CR-174936 [N86-30073/NSP], [A06]

Copies may be purchased from the National Technical Information Service, Springfield, Virginia 22161,

LEW-14390 /TN

FOR ADDITIONAL INFORMATION: *Contact: Director, Technology Transfer Division, P.O. Box 8757, BWI Airport, MD. 21240; (301) 621-0100 Ext. 241*

REFER TO THE NUMBER LISTED AT THE END OF THE ARTICLE

NASA Tech Brief
National Aeronautics and Space Administration

Licensing Opportunity

Improved Flux-Gate Magnetometer

A simplified circuit drives heading indicator and senses the magnetic field of the Earth.

Langley Research Center, Hampton, Virginia

An unusually simple flux-gate magnetometer (see figure), which will supply a digital readout of the magnetic heading of a vehicle, has been developed to drive a heading indicator, or to supply heading information to an autopilot or to other navigational instruments. An important feature is that the core is driven into saturation in one direction only by the alternating drive voltage, which swings from zero to one polarity and back rather than from positive to negative and back as in other systems. Since only one core saturation occurs during each cycle of the driving frequency, the resulting signal from the sensing winding is predominantly at the same frequency as that of the driving voltage rather than at its second harmonic.

The square-wave voltage from the oscillator (a commercially available integrated circuit) is applied to the driving winding of the core by the core driver, which is simply a power amplifier that produces sufficient current to saturate the core and isolates the core winding from the oscillator so that the square wave from the oscillator is not distorted by the loading effect of the core winding. The demodulator is a bilateral switch — a commercially available integrated switching circuit that clamps the output of the sensing winding to ground during half of each cycle of drive voltage.

A current-limiting resistor, R_L, is placed in series with the sensing winding so that only a small current need be switched by the demodulator. Since the signal voltage from the sensing winding has predominantly the same frequency as that of the driving voltage, the demodulator may be controlled by the oscillator voltage without need for a frequency doubler. The damping resistor, R_D, is connected in parallel with the sensing winding, and its value is adjusted to damp out most of the transient oscillations of the signal pulses without materially reducing the amplitude of the original pulse.

The frequency of the oscillator may be increased in order to reduce the "dead time" between pulses and to increase the energy content of the signal. Appreciable time is required in conventional systems for the core magnetization to traverse from one saturation region to the other when the polarity of the magnetizing current is reversed. Since the core in this system is saturated in only one direction, the core may be driven at a much higher frequency, increasing the energy content of the signal considerably over that obtained when operating in the conventional second-harmonic mode.

In the demodulator, the square wave from the oscillator is used to close an electronic switch, clamping the signal output of the sensing coil to ground during that portion of the cycle in which the core is saturated. In this case it removes the positive pulses, leaving a series of negative pulses, which, when processed by the low-pass filter consisting of R_F and C, are converted into a dc signal of negative polarity, the amplitude of which is proportional to the amplitude of the pulses and, consequently, to the intensity of the external magnetic field parallel to the centerline of the sensing

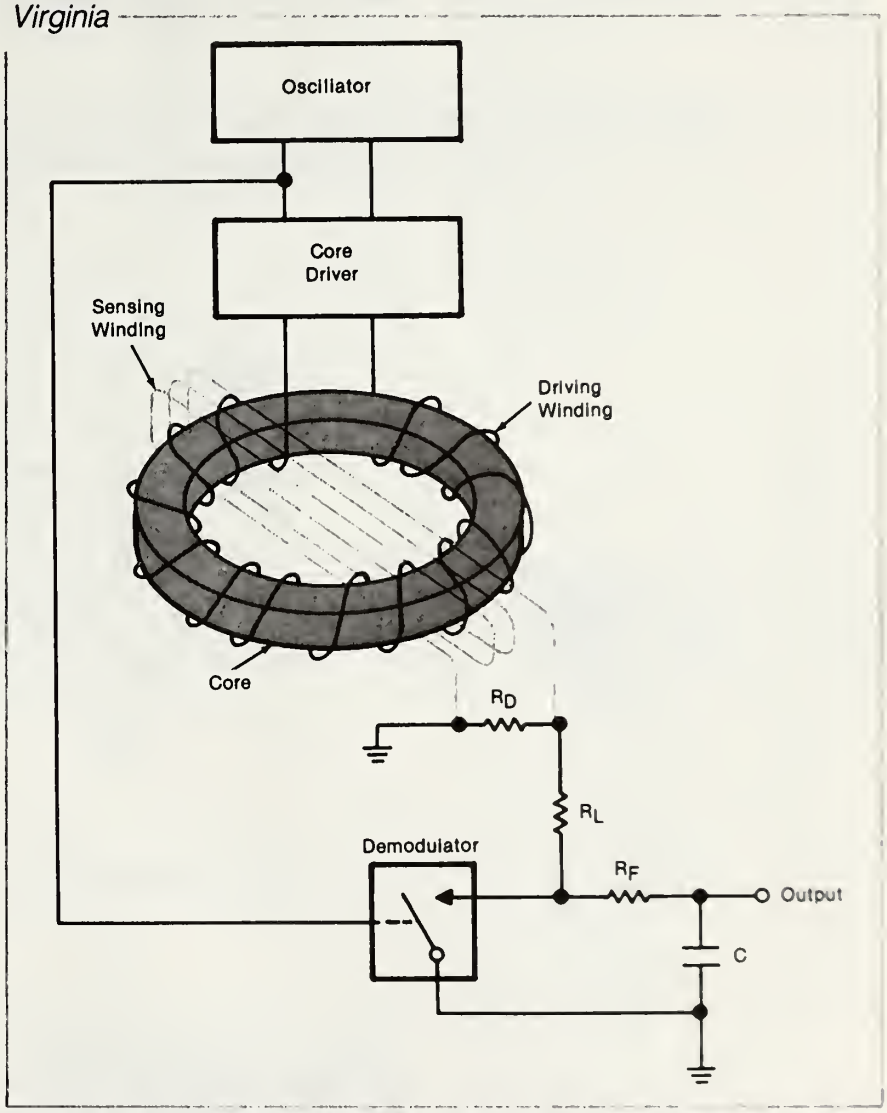

The **Simplified Flux-Gate Magnetometer** is made in part of commercially available integrated circuits.

coil. If the magnetometer core assembly were rotated 180°, negative pulses rather than positive pulses would be removed from the signal, resulting in a positive dc signal.

In order to implement an electronic compass, one can use two orthogonally mounted magnetometers that share the same oscillator but have separate core drivers. Similarly, a single core with a pair of orthogonally mounted sensing coils could be used to achieve the same purpose. When this circuit is equipped with the appropriate northerly turning-error compensation system and with a single-chip microcomputer to perform the necessary computations, it offers a heading reference equivalent to that of conventional combination of a magnetic compass and a directional gyroscope at great savings in weight, cost, and maintenance.

This work was done by H. Douglas Garner of **Langley Research Center**.

This invention is owned by NASA, and a patent application has been filed. Inquiries concerning nonexclusive or exclusive license for its commercial development should be addressed to the Patent Counsel, Langley Research Center Refer to LAR-13560 /TN

Langley Research Ctr.
Hampton, VA 23665
Technology Utilization Officer: John Samos
Mail Stop 139A
(804) 865-3281
Patent Counsel:
George F. Helfrich
Mail Code 279
(804) 865-3725

FOR ADDITIONAL INFORMATION: *Contact: Director, Technology Transfer Division, P.O. Box 8757, BWI Airport, MD. 21240; (301) 621-0100 Ext. 241*
REFER TO THE NUMBER LISTED AT THE END OF THE ARTICLE

NASA Tech Brief
National Aeronautics and Space Administration

Waveguide-Horn-to-Waveguide Transition Assembly

A microstrip-to-waveguide transition is integrated with a waveguide-horn antenna element.

Lyndon B. Johnson Space Center, Houston, Texas

The integration of a microstrip-to-waveguide transition and a waveguide-horn antenna element overcomes two major problems of previous systems: (1) the need to assemble two subassemblies during manufacture and (2) the need for a mechanical design that overcomes the inherent structural weaknesses associated with joining two subassemblies. The new horn/transition antenna element also allows for an end launch into the waveguide for easier mechanical and electrical connections. The antenna element operates by coupling electromagnetic energy from the environment through the horn to the connector at the other end via the microstrip-to-waveguide transition.

The transition assembly (see figure) includes an inner printed circuit positioned between the halves of an appropriately shaped split metal block. When the block halves and the printed circuit are assembled, one end of the block forms a waveguide-horn antenna element. The other end of the assembly can be joined to a microstrip or coaxial transmission line, depending on the type of connector used.

This work was done by Shayla E. Davidson of **Johnson Space Center** *and Roland W. Shaw, Jeffery K. Kovitz, George W. Raffoul, and Larry A. Johnson of Lockheed Corp. No further documentation is available.*
MSC-21146/TN

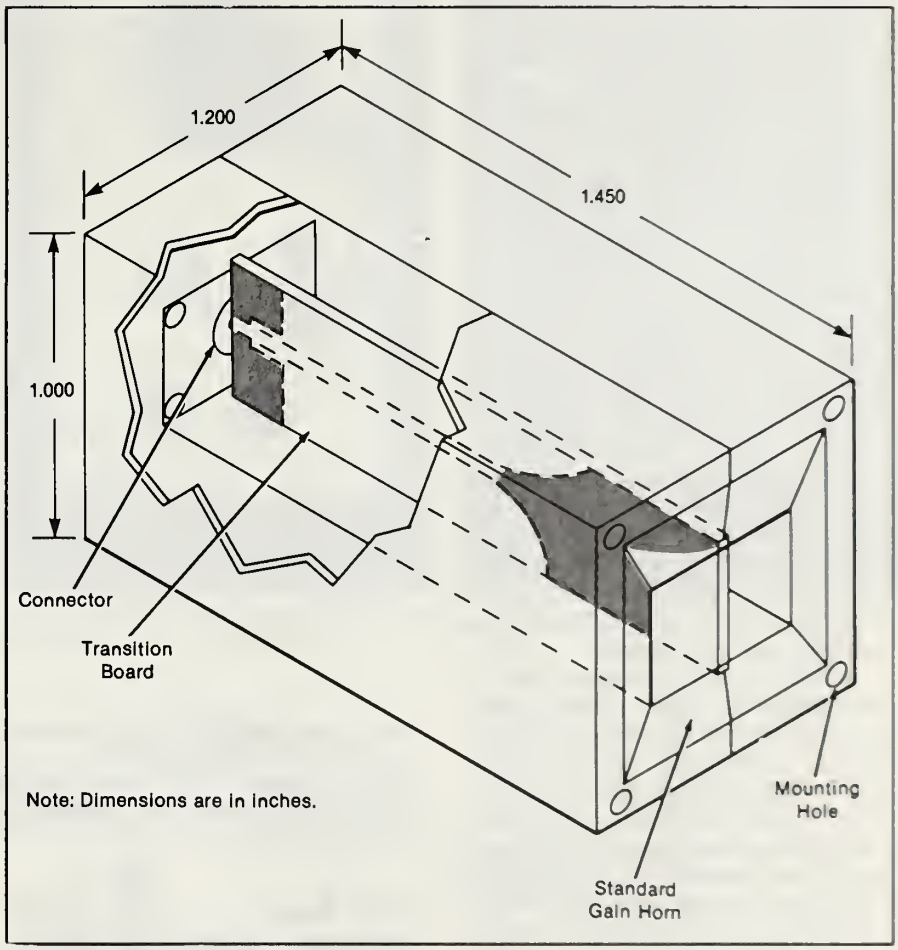

The **Integrated Waveguide-Horn/Microstrip-to-Waveguide Transition Assembly** couples electromagnetic energy through the horn and transition board to the connector.

FOR ADDITIONAL INFORMATION: *Contact: Director, Technology Transfer Division, P.O. Box 8757, BWI Airport, MD. 21240; (301) 621-0100 Ext. 241*
REFER TO THE NUMBER LISTED AT THE END OF THE ARTICLE

NASA Tech Brief
National Aeronautics and Space Administration
NASA's Jet Propulsion Laboratory, Pasadena, California

Imaging Radar Polarimeter

Radar measures the full polarization tensor of each element in the scene in one sweep.

By alternately transmitting horizontally and vertically polarized pulses (see figure) and recording the backscatter received in both polarizations in one pass over the terrain, an imaging-radar polarimeter collects all the information necessary to compute the full polarization tensor of each scene element. The antenna on a conventional imaging radar transmits and receives only one polarization component, making it impossible to obtain the full polarizaiton data in one pass.

The new system comprises a dual-polarized antenna, a single transmitter, and a four-channel receiver and digital recorder installed in an aircraft, plus a digital processor on the ground. This system produces radar-backscatter images corresponding to 10- by 10-km regions on the ground. A resolution of 10 m in the across-track direction is achieved by transmitting a pulse of 18-MHz bandwidth. In the along-track direction, a resolution of 3 m, one look (12 m, four looks) is obtained by the synthetic-aperture technique.

With the new radar, the signals recorded from orthogonal linearly polarized antennas are combined in a computer after the flight to synthesize any desired combination of transmitted and received polarizations. The data recorded on a single flight can be processed to provide multiple images, each representing the backscattered energy from the scene for a different combination of observational polarizations. A study of the polarization images can indicate the optimum choice of polarization representation for the observation of particular classes of objects and can provide insight into the dominant scattering mechanisms for each kind of object, thus improving the ability to identify correctly objects seen in the radar images.

The scattering matrix, S, contains the polarization information about the scene element in question. If a radar signal is transmitted with a polarization vector $\mathbf{C}_t$ and the target return is received with the antenna set to a polarization vector $\mathbf{C}_r$, then the voltage, V, at the receiver terminal is given by

$$V \propto C_{rx}(S_{xx}C_{tx} + S_{xy}C_{ty}) + C_{ry}(S_{yx}C_{tx} + S_{yy}C_{ty})$$

where x and y denote the horizontal and vertical components, respectively. If, for example, the signal is transmitted with horizontal polarization ($C_{tx} = 1, C_{ty} = 0$) and received with vertical polarization ($C_{rx} = 0$, $C_{ry} = 1$), then the received signal is proportional to S_{yx}. Similarly, the other elements of the scattering matrix are found by transmitting and receiving in various combinations of horizontal and vertical polarization.

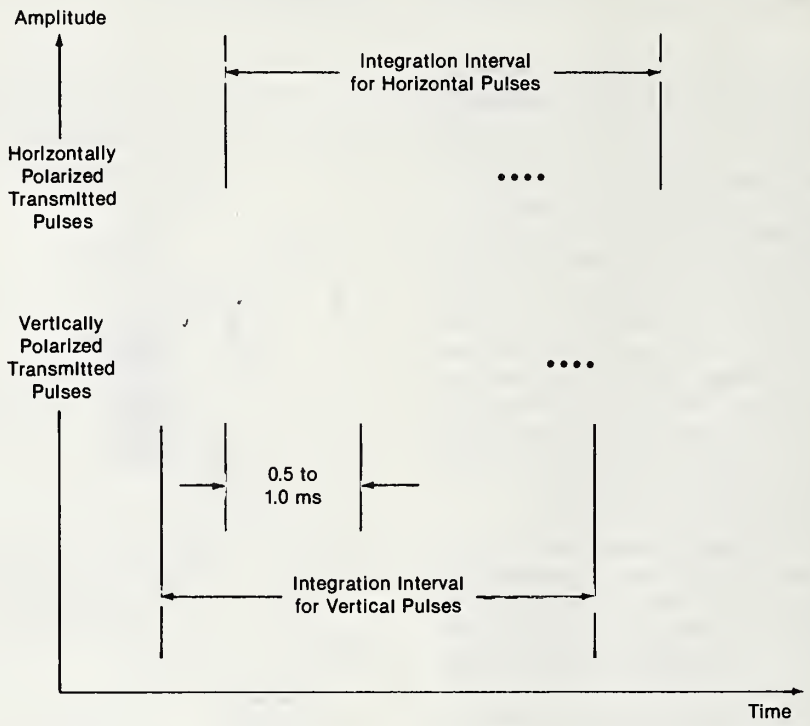

The Imaging Radar Polarimeter alternately transmits horizontally and vertically polarized pulses at intervals of 0.5 to 1.0 ms. A synthetic aperture is formed by coherent integration over approximately 1,500 pulses of each transmitted polarization. Four separate integrations are done, one for each possible combination of horizontal and vertical transmitted and received polarizations.

This work was done by Howard A. Zebker, Daniel N. Held, and Walter E. Brown of Caltech for **NASA's Jet Propulsion Laboratory**. *NPO-16875 /TN*

FOR ADDITIONAL INFORMATION: *Contact: Director, Technology Transfer Division, P.O. Box 8757, BWI Airport, MD. 21240; (301) 621-0100 Ext. 241*
REFER TO THE NUMBER LISTED AT THE END OF THE ARTICLE

NASA Tech Brief
National Aeronautics and Space Administration
Goddard Space Flight Center, Greenbelt, Maryland

Adjustable, Audible Continuity Tester for Delicate Circuits

The unit is adjustable to resistances up to 35 ohms.

An adjustable, audible electrical-continuity tester gives an audible indication, making it unnecessary for the user to look directly at the instrument to observe a meter reading. The user's eyes can be kept on the circuit board being tested; there is therefore little risk that the user would let the tester probes slip from the terminals under test and cause false indications or damage the circuit or components.

In addition, the current and voltage of the tester are strictly limited. It can apply no more than 0.6 volts dc and no more than 3 mA through the probes. It can therefore be used safely on circuit boards in which semiconductor components have been installed, and on complementary metal oxide/semiconductor integrated circuits, which are highly susceptible to damage during testing.

The tester is compact (see Figure 1), and its circuit is simple (see Figure 2). It can

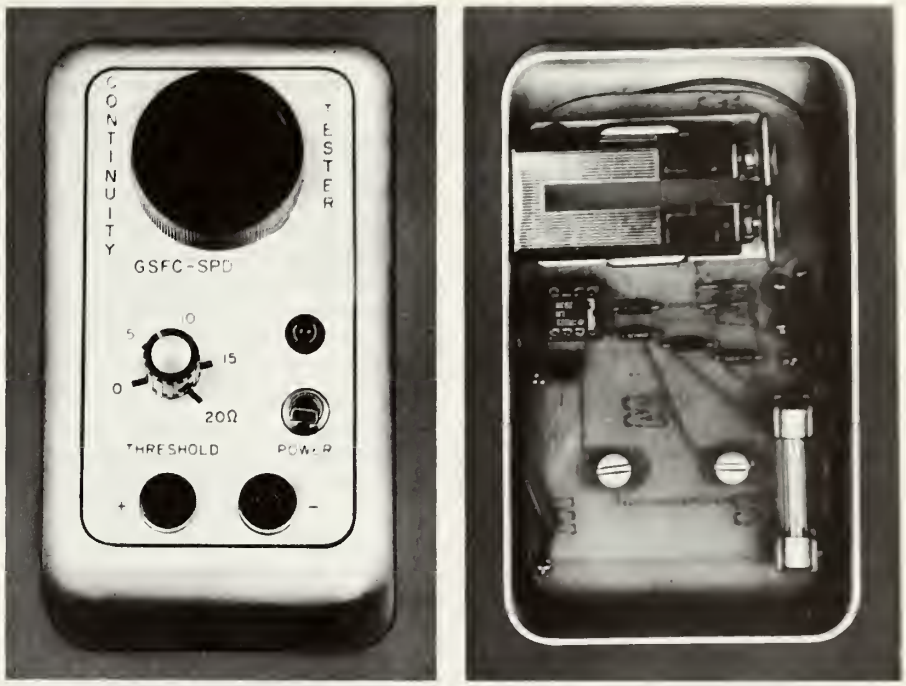

Figure 1. The **Continuity Tester** is mounted on a small circuit board in a compact enclosure.

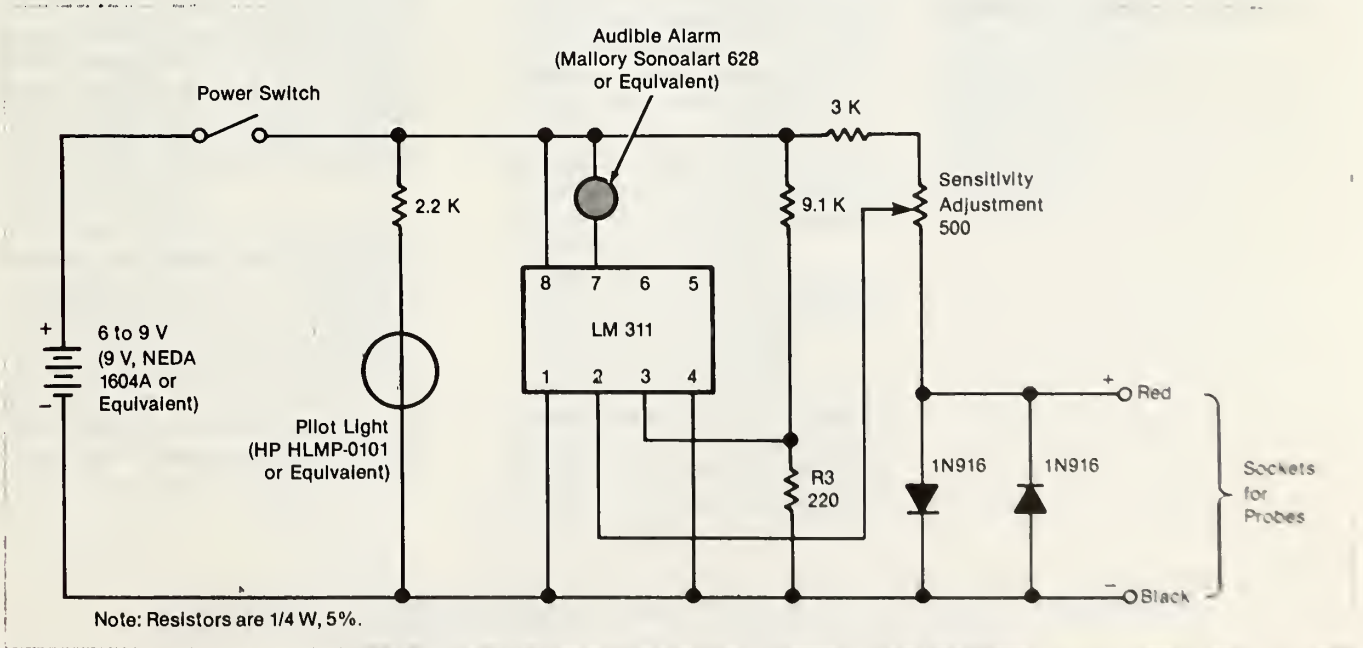

Figure 2. The **Tester Circuit** consists of only a few components. The 500-Ω potentiometer sets the threshold (maximum) resistance that will trigger the alarm. The circuit is housed in a compact enclosure on a small circuit board.

be built from inexpensive standard components available from retail outlets.

The tester can be adjusted to indicate continuity below any resistance value up to 35 ohms. For example, if the user sets the tester to 30 ohms, the unit will emit an audible tone whenever the resistance between the probes is 30 ohms or less; if, for example, the resistance is 30.2 ohms, the unit will remain silent.

This work was done by William B. McAlister of **Goddard Space Flight Center**. *No further documentation is available.*
GSC-13102 /TN

FOR ADDITIONAL INFORMATION: *Contact: Director, Technology Transfer Division, P.O. Box 8757, BWI Airport, MD 21240; (301) 621-0100 Ext. 241*
REFER TO THE NUMBER LISTED AT THE END OF THIS ARTICLE

NASA Tech Brief
National Aeronautics and Space Administration
Ames Research Center, Moffett Field, California

Licensing Opportunity

Testing Instrument for Flight-Simulator Displays

Many devices for many diverse functions are combined in one equipment item.

Displays for flight-training simulators are rapidly aligned with the aid of an integrated optical instrument. Calibrations and tests such as aligning the boresight of a display with respect to the user's eyes, checking and adjusting the display horizon, checking image sharpness, measuring the illuminance of displayed scenes, and measuring the distance of the optical focus of a scene can be performed with a single unit.

The instrument is intended for simulators in which a pilot sits in a cockpit as in an airplane and looks at a display that represents, in both color and perspective, the scene that would surround the plane. Lenses and other optical elements between the pilot and a cathode-ray-tube (CRT) display make the scene appear realistically distant.

Previously, many pieces of equipment had to be used for calibrations and tests. Each instrument had to be carefully positioned at the design eyepoint (DEP) — the locus of points at which a pilot's eyes are likely to be during simulator flight for looking out of cockpit windows and watching the instrument panel. The difficulty was compounded because flight-training simulators usually had more than just one scene display; most had at least four, and it was necessary to reposition each test device for each display. Clearly, this was a time-consuming procedure and prone to measurement error.

The new instrument, in contrast, combines all measurement devices in a single, compact, integrated unit. It requires just one initial setup. It employs a laser instead of an incoherent light source and thus produces a narrow, collimated beam for greater measurement accuracy. To improve accuracy further, it uses only one moving part, a double right prism, to position the laser beam.

The key components of the instrument are as follows:

1. A low-power helium/neon laser
2. A glass, double right prism mounted on a rotatable base with a thumb-lock knob — Angular accuracy up to 0.25° is possible. The center of rotation is positioned at the DEP in the cockpit or laboratory so that only the prism need be rotated to project the laser beam in various directions across the horizontal meridian. The prism serves as a beam splitter that enables the observer to look safely along the laser beam to evaluate the display-system optical performance, as indicated by the displacement, reflection, and refraction of the beam.
3. An aperture plate — Small-diameter apertures are located between the laser and the double right prism so that the beam size can be varied.
4. A y-z-adjustable microscope stage — This support stage permits the aperture plate to be moved precisely in the y (horizontal, perpendicular to the laser beam) and z (vertical) directions to center the aperture over the laser beam. The stage also holds a variety of clear and frosted lenses, which may be used to spread the laser beam.
5. A neutral-density wedge filter — Located between the laser and the aperture plate, this filter can be slid to any position in a slot to increase or decrease the beam intensity.
6. A viewing eyepiece — The eyepiece lens has a relatively large exit pupil of 0.87 in. (2.2 cm) in diameter. It has a spring-loaded tie-down strap.
7. A telescope objective lens — Used with the eyepiece lens, the telescope objective is 2 in. (5.1 cm) in diameter and has an effective focal length of about 11 in. (27.9 cm). It is focused by an adjusting screw.
8. An illuminometer — This battery-powered device rests on an aluminum bracket that permits its photosensitive head to be rotated into position in place of the human observer's eye behind the eyepiece.
9. A base — A plate made of rigid aluminum with threaded holes and lightening holes supports the instrument components.
10. Legs — Four collapsible metal legs allow the unit to be placed securely on a horizontal or tilted surface.
11. A dioptometer — This is an optical rangefinder similar to the eyepiece in size and shape. It is mounted in place of the eyepiece and used to find the effective optical distance of the scene from the design eyepoint.

This work was done by Richard F. Haines of **Ames Research Center.**

Inquiries concerning rights for the commercial use of this invention should be addressed to the Patent Counsel, Ames Research Center Refer to ARC-11504 /TN

Ames Research Ctr.
Moffett Field, CA 94035
Technology Utilization Officer: Laurance Milov
Mail Code 223-3
(415) 694-6370
Patent Counsel:
Darrell G. Brekke
Mail Code 200-11
(415) 694-5104

FOR ADDITIONAL INFORMATION: *Contact: Director, Technology Transfer Division, P.O. Box 8757, BWI Airport, MD. 21240; (301) 621-0100 Ext. 241*
REFER TO THE NUMBER LISTED AT THE END OF THE ARTICLE

NASA Tech Brief
National Aeronautics and Space Administration
Langley Research Center, Hampton, Virginia

Licensing Opportunity

Measuring Microwave Emissivities

A Dicke radiometer and a cryoload are combined in emissivity determinations of mesh antennas.

Surface emissivity, important to know in the temperature range anticipated for space use, is difficult to measure for mesh antennas. A newly developed measuring apparatus and procedure present a solution to this problem and thus fill a technological void in the accurate determination of surface emissivities at microwave frequencies.

The apparatus, which is capable of measuring independently the electromagnetic emissivity and/or intrinsic losses of surfaces, comprises a radiometer, a horn antenna, a test section, and a cryogenically cooled matched load (cryoload). In the system shown in Figure 1, the radiometer is of the Dicke type with pulsed noise-injection feedback that has proven to be stable over very long periods of time. The cryoload is filled with liquid nitrogen. A paraboloidal reflector is desirable in order to avoid phase-front distortions. A flat-plate reflector is easier to install in most cases but needs critical adjustment within the system.

Derived from Plank's radiation law, the value of the surface emissivity of the mesh sample, in the microwave region up to 100 GHz, is given by

$$\varepsilon = (T_{B2} - T_{B1})/(T_{M2} - T_{M1})$$

where T_B is the radiometer brightness temperature, T_M is the physical temperature of the mesh sample, and 1 and 2 denote different temperature levels.

An example of the results of the measurement of a mesh-membrane sample is shown in Figure 2. T_B and T_M are shown in relation to one another and to the temperature changes that were produced by heater elements. Using this test apparatus and the above equation, the emissivity of the mesh sample was determined to be 0.01855. The intrinsic loss was 0.0811 dB. These measurements were conducted at 2.65 GHz with a radiometer integration time of 22 seconds and a brightness-temperature resolution of 0.02K.

This work was done by Hans-Juergen C. Blume of **Langley Research Center.**

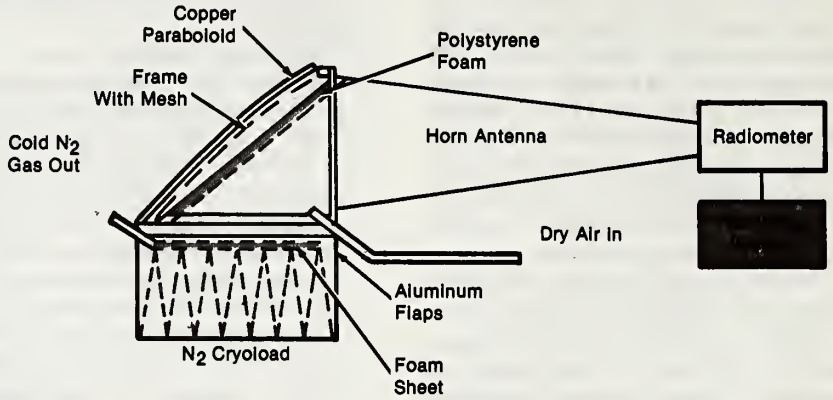

Figure 1. An **Ultrasensitive, Stable Radiometer** is used to measure very small emissivities with temperature changes with high resolution.

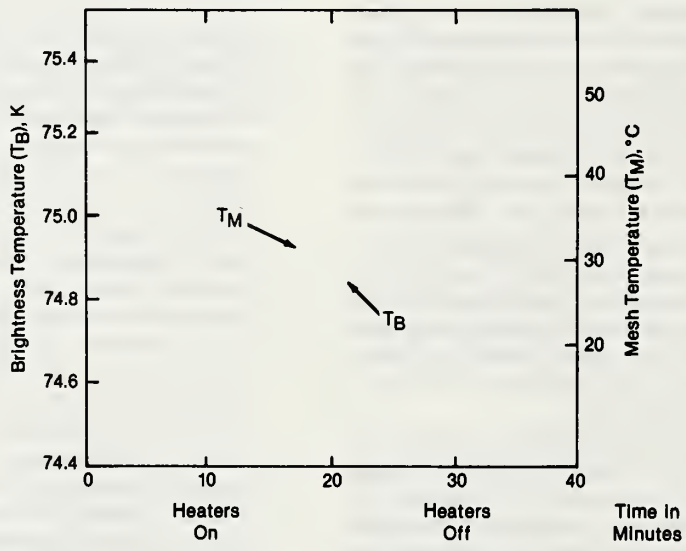

Figure 2. The **Temperatures of a Mesh Antenna** are used to calculate the surface emissivity in the microwave frequency range.

This invention is owned by NASA, and a patent application has been filed. Inquiries concerning nonexclusive or exclusive license for its commercial development should be addressed to the Patent Counsel, Langley Research Center
Refer to LAR-13455 /TN

Langley Research Ctr.
Hampton, VA 23665
Technology Utilization Officer: John Samos
Mail Stop 139A
(804) 865-3281

Patent Counsel: George F. Helfrich
Mail Code 279
(804) 865-3725

FOR ADDITIONAL INFORMATION: *Contact: Director, Technology Transfer Division, P.O. Box 8757, BWI Airport, MD. 21240; (301) 621-0100 Ext. 241*
REFER TO THE NUMBER LISTED AT THE END OF THE ARTICLE

Energy

270 Cogeneration from Biofuels — A Technical Guidebook.

272 Parameter Estimation Study of Heat Loss from Underground Steam Pipelines

273 Summary and Evaluation of Field Performance Data on Unitary Heat Pumps

274 Hanging Windmills from Cables — A relatively inexpensive structure would enable the raising and lowering of windmills. (Licensing Opportunity)

271 System-Assurance Analysis for Nuclear Powerplants — Rocket-Launch reliability techniques could be adapted to benefit powerplants.

Testing & Instrumentation

275 Cooling-Energy Measurements of Unoccupied Single-Family Houses with Attics Containing Radiant Barriers

Cogeneration from Biofuels

A Technical Guidebook

Cogeneration, the simultaneous production of more than one form of useful energy, has long been used by industry as a means of producing both thermal and electric energy to meet on-site process requirements. Biomass feedstocks such as wood are currently used as the fuel in many cogeneration systems, yet there are substantial opportunities for expanding the use of these feedstocks in the southeastern region of the U. S. The extensive quantity and diversity of biomass resources in the Southeast provide an excellent opportunity to reduce the use of fossil fuels.

A guidebook focuses primarily on issues related to the use of biomass fuels for cogeneration in the Southeast. It is targeted toward those plant managers and engineers who could use a biomass fueled system but are not knowledgeable or aware of the potential or applications of biomass fuel for cogeneration. The guidebook emphasizes a systems level understanding and is not intended to be a detailed "nuts and bolts" handbook. Detailed technical information is limited to biomass fuel characteristics, an area where engineers' standard reference documents may be inadequate.

The guidebook is organized into nine chapters, each of which deals with a particular aspect of the application of biomass fuels to cogeneration. The successful design of a biomass fueled cogeneration facility involves a study of complex interactions between economic, fuel, and technical issues. Chapter 2 provides a framework within which the decision-maker can operate to develop a successful design. The steps that must be taken to decide which technologies to use are outlined, and a design checklist is included to assist in planning.

Chapter 3 addresses fuel procurement, a subject area which is often the number one concern of decision-makers in considering a biofueled system. The characteristics of biomass fuels are also summarized, including wood, agricultural residues, manure and municipal waste. In Chapter 4, fuel handling and storage considerations are addressed. Since biomass is a bulky fuel, handling and storage tend to be the second greatest concern of decision-makers regarding the use of biofuels (after fuel procurement). Chapter 5 covers the side spectrum of technologies that can be used to convert biomass into thermal and electric energy in cogeneration systems. Systems considerations are addressed in Chapter 6, such as assessing energy loads and their relationship to cogeneration system design. One of the key criteria for a viable cogeneration system is the presence of a substantial year-round thermal energy requirement or demand.

Chapter 7 covers the establishment of the Public Utility Regulatory Policies Act (PURPA), which was enacted in 1978 to provide benefits and incentives for cogeneration. Under this Act, there is significant support and economic incentive for the installation of biomass fueled cogeneration facilities. Environmental issues are covered in Chapter 8, with most attention paid to fuel use issues rather than fuel production issues. There are significant environmental advantages to burning biomass fuels instead of fossil fuels, particularly coal. Biomass fuels contain insignificant amounts of sulfur and thus, a whole area of pollution control for sulfur emissions is eliminated.

Chapter 9 deals with the economic and financial aspects of a biomass fueled cogeneration system. Costs of various fuels and equipment are discussed. An overview is also provided on the impact of the new 1986 tax law on biofueled cogeneration systems. With a 10 percent biomass energy tax credit in 1987, and accelerated 5-year depreciation for biofueled cogeneration, the new tax law seems to have enhanced the attractiveness of these systems as an investment, relative to other types of investments. As a result, 1987 might be a particularly good year to install a biofueled cogeneration system. Finally, methods of financing are outlined and the calculation of economic return is addressed.

FOR ADDITIONAL INFORMATION: A copy of the report is available from NTIS, Springfield, VA 22161; (703) 487-4600.

NTIS order number: DE87-007871/NAC

Price code: A06

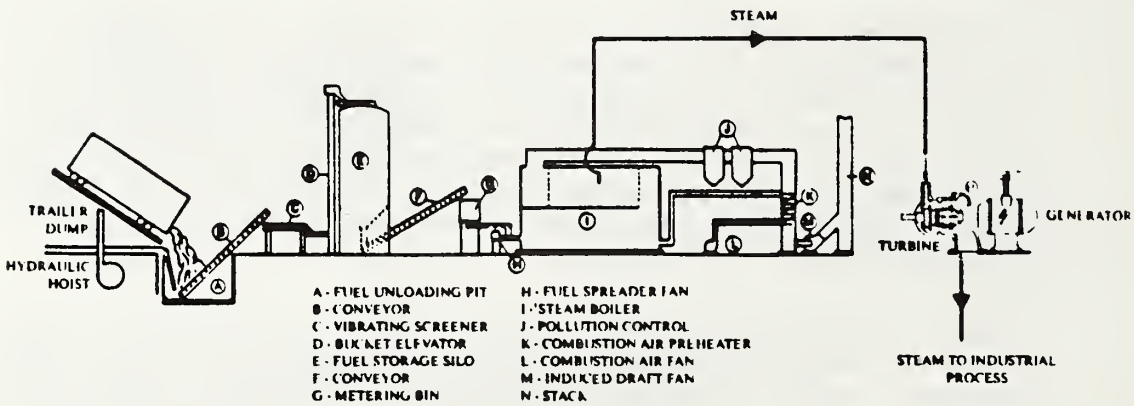

Figure 1-2
SCHEMATIC OF A TYPICAL BIOMASS COGENERATION SYSTEM

NASA Tech Brief
National Aeronautics and Space Administration

System-Assurance Analysis for Nuclear Powerplants

Rocket-launch reliability techniques could be adapted to benefit powerplants.

John F. Kennedy Space Center, Florida

A system-assurance-analysis (SAA) methodology developed for aerospace launch-support systems has been proposed for nuclear powerplants. Launch-support systems and nuclear powerplants are similar in complexity and share common reliability and safety goals. This similarity prompted a study that showed that it would be feasible and practical to apply SAA methodology to nuclear powerplants.

SAA methodology is simply the combination of well-known safety and reliability analytical techniques with new management methods to identify, track, and resolve critical items and hazards (see figure). The SAA examines systems, subsystems, components, control functions, integrated systems, and human/machine operations.

SAA started early in the design-engineering process becomes the foundation for an expanded analysis as design progresses. Tracking of the results of the analysis continues after design is complete and operations and test procedures are defined — in fact, tracking continues as long as the system operates. Future modifications in the system will be analyzed and integrated into the information system for presentation to management.

When a given design is complete, the reviewing agency examines the acceptance rationale for the remaining critical items and residual hazards and evaluates the risks involved. The SAA thus gives management a focal point at which problems can be assessed.

For this methodology to be most useful and attractive to the nuclear-power industry, it should be an integral part of the design and licensing process, not just an

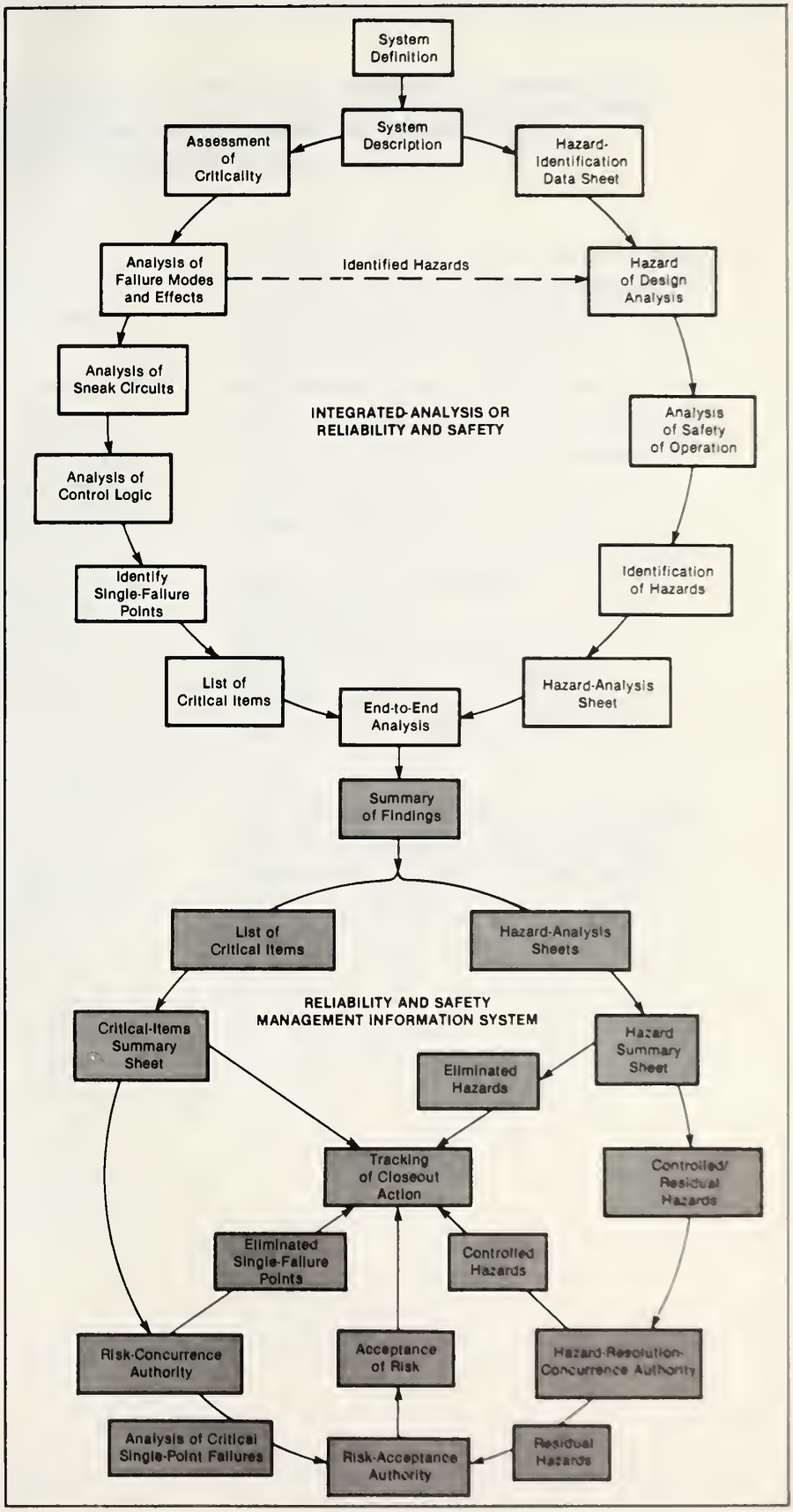

The SAA Methodology is essentially a combination of analytical techniques related to safety and reliability with an information system that assists managers in making decisions that affect safety and reliability.

additional requirement. A further consideration is that SAA methodology differs somewhat from the present direction of Nuclear Regulatory Agency policy, which relies on safety goals with numerical guidelines. Although SAA methodology does consider the probability of failure in the single-failure-point assessment, this is only one of the many items examined to determine whether a single failure point is an acceptable risk. Other items include design safety margins, qualification testing, mandatory inspections, training and certification requirements, and operating procedures.

This work was done by Donald W. Page of **Kennedy Space Center**. *To obtain copies of the reports, "Application of NASA Kennedy Space Center System Assurance Analysis Methodology to Nuclear Power Plant Systems Designs," and "System Assurance Analysis Application Handbook," KSC-11306/TN*

FOR ADDITIONAL INFORMATION: *Contact: Director, Technology Transfer Division, P.O. Box 8757, BWI Airport, MD. 21240; (301) 621-0100 Ext. 241*

REFER TO THE NUMBER LISTED AT THE END OF THE ARTICLE

Department of Energy

Technology Application

Oak Ridge National Laboratory

PARAMETER ESTIMATION STUDY OF HEAT LOSS FROM UNDERGROUND STEAM PIPELINES

Central heating plants frequently distribute energy by sending steam through buried pipelines. Heat loss occurs during the use of these pipelines. Knowledge of the extent of such losses is needed for several reasons, such as determining if maintenance needs to be done on a section of pipeline. The objective of this study was to derive a simple procedure for accurately estimating the heat loss from a section of buried pipeline.

The method examined at ORNL was to estimate the heat loss using shallow temperature measurements. However, temperature measurements near the ground can vary considerably in time periods as small as two hours. For this reason, new transient and quasi-steady-state solutions were developed. Subsurface temperature measurements obtained from the ORNL steam system were used to estimate pipe heat loss and depth. The data were analyzed in several ways. For example, parameters were estimated at each axial position of the pipe, and the data were used to obtain a single set of parameters in a sequential manner that showed the effects of including measurements of each location. The work is important because it holds the promise of providing simpler, more rapid field tests for estimating heat loss from buried pipes.

Additional information:

Office of Technology Applications
Information Service
Martin Marietta Energy Systems, Inc.
P.O. Box X
Oak Ridge, TN 37831
Telephone: (615) 574-4192; FTS 624-4192

J. V. Beck and M. A. Karnitz, *Parameter Estimation Study of Heat Losses from Underground Steam Pipelines*, ORNL/TM-9928, Oak Ridge National Laboratory (June 1986).

Department of Energy

Technology Application

Oak Ridge National Laboratory

SUMMARY AND EVALUATION OF FIELD PERFORMANCE DATA ON UNITARY HEAT PUMPS

Accurate data on the performance of installed heat pumps is very difficult to obtain. Installed heat pumps perform differently based on climatic conditions, occupancy patterns, and installation procedures. Methods are available for estimating heat pump performance, but it is not clear that the analytical methods and field test data currently available are enough to satisfy user needs. Thus, the status of existing data on heat pump field performance had to be established and compared with user needs, and additional areas of study and work had to be identified.

Over 100 individuals in over 90 organizations were contacted. Thirty-eight programs involving over 700 heat pumps (of which 90% were residential air-to-air units) were identified. The programs were categorized by three levels based on the type of measurements obtained: level 1—energy input only; level 2—input and output; and level 3—input, output, and dynamic losses. Generally, level 3 programs involved more careful control and measurement of climatic, installation, and operational test conditions than levels 1 and 2, and the method of output measurement (normally duct enthalpy) was more accurate than for level 2, although determination of cooling load continued to be a problem.

Overall, the data base on heat pump field performance is large but uneven in terms of completeness and quality. Energy input data are abundant and frequently reliable, but the results are seldom either statistically valid or easily generalized. A considerable amount of heating seasonal performance factor (and much less seasonal energy efficiency ratio) data is also available. Certain comparisons of these experimental performance factors to predictions based on the ARI 240-81 rating method have indicated good apparent agreement (within $\pm$ 10%). However, questions remain both as to the general applicability of ARI 240-81 and to the specific methods used in normalizing the test data. Relatively little detailed data on dynamic losses are available and even less comparison with analysis.

Additional information:

National Technical Information Service
U.S. Department of Commerce
5285 Port Royal Road
Springfield, MD 22161

J. C. Burke, K. F. Fitzgerald, and L. Frantzis (Arthur D. Little, Inc.), *Summary and Evaluation of Field Performance Data on Unitary Heat Pumps*, ORNL/Sub/85-00219/1, Oak Ridge National Laboratory (April 1986).

NASA Tech Brief
National Aeronautics and Space Administration

Licensing Opportunity

Hanging Windmills From Cables

A relatively inexpensive structure would enable the raising and lowering of windmills.

Langley Research Center, Hampton, Virginia

Windmills would be supported, according to a new concept, by hanging them from cables. There are two primary reasons why this concept may have practical applications. First, it would be possible to raise and lower windmills easily for maintenance and to lower them to avoid excessive windspeeds. Second, because much of the supporting structure would consist of tension members, the structure may be relatively inexpensive. In addition, it may be practical to hang windmills in canyons or other natural wind tunnels where tower structures would be impractical.

The concept is illustrated in the figure. The airframe consists of a fuselage and an empennage. The windmill turns a shaft that drives an electrical generator. The device is aerodynamically stable so that it will rotate in yaw to maintain the windmill in a downwind position as the wind direction changes.

The device is suspended by three cables, two of which are attached to the horizontal stabilizer and the third to the fuselage. The suspension cables are attached to a common point on a "clothesline" cable so that the device swings as a pendulum. The "clothesline" cable spans the space between two poles, trees, or other strong, rigid structures, which may be strengthened by guy wires. A tether cable from the ground is attached to the device to carry the aerodynamic drag force. The electrical cables may be brought down to the ground by attaching them to the tether cable.

In a geographical area where the average wind velocity is at least 20 ft/s (6.1 m/s), one such device with a 14-ft (4.3-m) rotor diameter and a 25-percent energy-conversion factor could produce a significant amount of the power required by a typical household. It may be feasible for an array of several devices or multirotor devices to supply power for a small factory or village. An array of several devices could be suspended from a multidevice rig. The devices could be positioned at different heights above the ground to reduce downwind interference effects. The devices could even be lowered to change the pitch of the rotor blades for maximum efficiency when the average wind velocity changes.

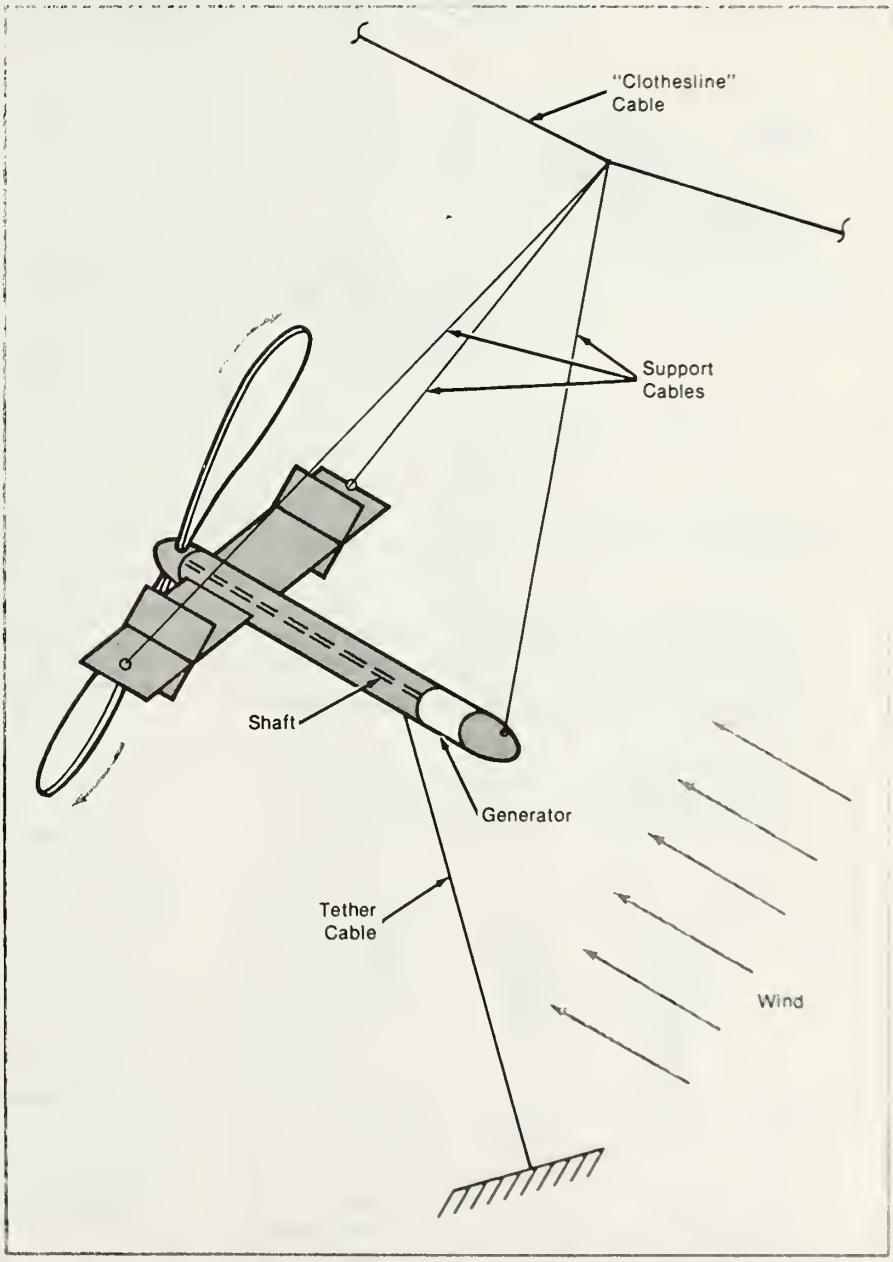

A Simple, Lightweight Windmill and Generator can be raised, lowered, and suspended in an optimal position.

This work was done by Moses G Farmer of **Langley Research Center**. *No further documentation is available.*

Inquiries concerning rights for the commercial use of this invention should be addressed to the Patent Counsel, Langley Research Center.
Refer to LAR-13434/TN

Langley Research Ctr.
Hampton, VA 23665
Technology Utilization Officer: John Samos
Mail Stop 139A
(804) 865-3281
Patent Counsel:
George F. Helfrich
Mail Code 279
(804) 865-3725

FOR ADDITIONAL INFORMATION: *Contact: Director, Technology Transfer Division, P.O. Box 8757, BWI Airport, MD. 21240; (301) 621-0100 Ext. 241*
REFER TO THE NUMBER LISTED AT THE END OF THE ARTICLE

Department of Energy

Technology Application

Oak Ridge National Laboratory

COOLING-ENERGY MEASUREMENTS OF UNOCCUPIED SINGLE-FAMILY HOUSES WITH ATTICS CONTAINING RADIANT BARRIERS

Tests have been conducted at Oak Ridge National Laboratory to determine the magnitude of both cooling and heating energy savings brought about by installing radiant barriers in attics of single-family houses. The initial work was done using the radiant barriers in combination with R-19 fiberglass-batt ceiling insulation. The purpose of the radiant barrier is to reduce the radiant heat transfer component on the fiberglass attic insulation. Later studies have focused on the amount of cooling energy savings attributed to the installation of radiant barriers in combination with both R-11 and R-30 ceiling insulation.

The site used for the radiant barrier experiments was the Karns House Research Facility. This facility consists of three unoccupied ranch-style houses located between Knoxville and Oak Ridge, Tennessee. Radiant barriers were installed in two different ways. One method was to lay the radiant barrier horizontally on top of the attic insulation. The other method was to attach the radiant barrier to the underside of the roof trusses. Figure 1 illustrates the two methods. The third house was left untouched (as a control house). Each test, including calibration runs, lasted from 2 to 3 weeks.

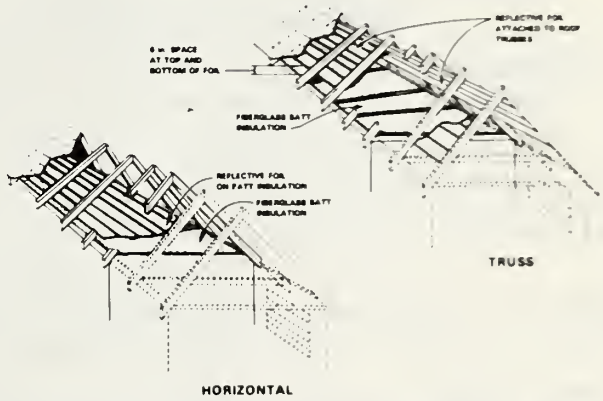

Fig. 1. Two methods for installing radiant barriers.

The results of the testing are illustrated in Fig. 2. They show that radiant barriers in attics have the potential to save HVAC cooling and

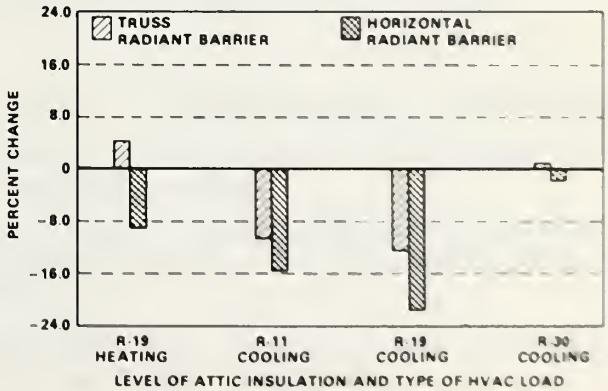

Fig. 2. Summary of radiant barrier effects on Karns House loads. Changes are relative to the same attic R-value with no barrier.

heating energy. Horizontal barriers always performed better than truss radiant barriers. The test results also show that the radiant barrier worked well with R-11 and R-19 insulation but had little effect when used with R-30 ceiling insulation.

Additional information:

National Technical Information Service
U.S. Department of Commerce
5285 Port Royal Road
Springfield, VA 22161

W. P. Levins and M. A. Karnitz, *Cooling Energy Measurements of Unoccupied Single-Family Houses with Attics Containing Radiant Barriers*, ORNL/CON-200, Oak Ridge National Laboratory (July 1986).

W. P. Levins and M. A. Karnitz, *Heating Energy Measurements of Unoccupied Single-Family Houses with Attics Containing Radiant Barriers*, ORNL/CON-213, Oak Ridge National Laboratory (January 1987).

W. P. Levins and M. A. Karnitz, *Cooling Energy Measurements of Single-Family Houses with Attics Containing Radiant Barriers in Combination with R-11 and R-30 Ceiling Insulation*, ORNL/CON-226, Oak Ridge National Laboratory (May 1987).

Engineering

276 Finite Element Analysis in Reliability Studies

277 In Situ Repair of Deteriorated Concrete in Hydraulic Structures — An evaluation.

278 Analyzing Wakes from Hovering-Helicopter Rotor Blades — An Analytical method and computer program yield realistic results quickly. (Licensing Opportunity)

279 Calculations of Wall Effects on Propeller Noise — Reverberations affect sound levels in wind tunnels.

280 Design of Fiber Composites for Structural Durability — Hygrothermomechanical effects can be analyzed by computers.

281 High-Differential-Pressure Heat Exchanger — All critical joints are full-penetration welds inspectable with x-rays. (Licensing Opportunity)

282 Preliminary-Design Software for Composite Structures — An easy-to-use program enables fast analysis and evaluation of rough designs.

283 Stiffening Heat-Exchanger Tubes Against Vibrations — Midsection clamps reduce the harmful effects of crossflow.

284 Structural Dynamics of Filament-Wound Booster Rockets — A mathematical model agrees closely with measurements.

285 Thermally Insulating Support for Cryogenic Tanks — A passive alternate-load-path support scheme keeps weight low while conserving cryogenic liquid. (Licensing Opportunity)

286 Wedge Joints for Trusses — Structures could be assembled rapidly with simple hand tools. (Licensing Opportunity)

Software

287 Computer Program for Flow in a Combustor — This program simulates subsonic, swirling, reacting, turbulent flow abut a bluff body.

Testing & Instrumentation

288 Color-Video Thermal Maps — Temperatures appear in time-varying color.

289 Gamma-Ray Fuel Gauges for Airplanes — An accurate system overcomes problems of capacitance gauges.

290 Measuring and Plotting Surface Contour Deviations — An electromechanical apparatus provides along-track and across-track displacement information to a plotter.

291 Microscopic Gas-Flow Controller — Small flows at low pressures would be monitored and throttled. (Licensing Opportunity)

Other Items of Interest

338 Computing Aerodynamics of Propfans — The cost and duration of wind-tunnel tests could be reduced.

340 Generating Coordinates for Aerodynamical Calculations — A mathematical method represents an aircraft surface as grids of variable spacing. (Licensing Opportunity)

U.S. Air Force
Reliability Analysis Center (RAC)
Rome Air Development Center, Griffiss Air Force Base, NY 13441

Finite Element Analysis in Reliability Studies

With increasing emphasis being put on product reliability, computer aided engineering (CAE) in the form of finite element analysis is playing an ever increasing role. The expansion of CAE as a major contributor toward reliability has been further promoted through the evolution of better PC based finite element analysis packages. With better PC based tools such as MSC/PAL-II, MSC/CAL and NISA, more engineers are now able to take advantage of the power which, only a few years ago, was the exclusive domain of mini and main frame users.

Finite element analysis is an automated tool used to establish the thermal and structural response of a product to imposed operational stimuli. The use of this technique has wide spread application in electronics, aerospace and most other industrial manufacturing areas. The technique relies on partitioning of a continuous structure into a network of nodal points. Interconnecting stresses are computed for each element within the network for any given load. As the grid pattern becomes finer, the finite element solution converges towards the exact solution.

Finite element analysis is a useful tool for design evaluations and optimization of complex structures where an exact analytical solution may not be available or highly impractical using traditional methods. The finite element approach identifies stress concentration areas and the corresponding stress levels. More importantly, it provides a tool to perform design tradeoffs for different materials, dimensions or design configurations.

RAC engineers have used finite element analysis for many different programs. Applications for finite element analysis with the reliability discipline are to (1) evaluate design integrity, (2) optimize design for particular reliability constraints and (3) serve as input to fatigue analysis, stress/strength interference or probabilistic mechanical design.

Applications of finite element analysis being addressed by RAC engineers include:

- Thermal and structural stresses on mating concentric rings revealing part failure due to the initial preload for an ambient interference fit condition. The analysis provided failure verification information and identified dimensional and stress parameters for future design reliability.
- Thermal analysis determined response characteristics of electrical and electromechanical components within the high temperature environment of an aircraft turbine engine.
- Fatigue analysis determined part failure causes in an industrial application. This analysis addressed reliability for customer safety.

For more information concerning the use of finite element analysis in reliability studies, contact Mr. Richard Sadlon of the RAC at (315) 336-2359.

US Army Fact Sheet

In Situ Repair of Deteriorated Concrete in Hydraulic Structures

An Evaluation

According to the results of a survey initiated in 1982 by the U.S. Army Corps of Engineers, the three most common types of deficiencies encountered in concrete hydraulic structures were (a) cracking, (b) seepage, and (c) spalling. These three general categories of deficiencies accounted for 77% of the 10,096 deficiencies identified during a review of available inspection reports for the Corps' civil works structures. Concrete cracking was the deficiency most often observed, accounting for 38% of the total. In situ repair procedures may not be readily applicable in the repair of seepage deficiencies; however, the problems normally resulting from deterioration due to cracking and spalling do seem to be suited to in situ repair procedures.

A literature survey, private discussions, and responses to mail and telephone inquiries have disclosed a wide range of repair methods and materials currently available for the in situ repair of cracked and spalled concrete. Crack repair methods include pressure injection, routing and sealing, stitching, addition of reinforcement, drilling and grouting, flexible sealing, grouting, drypack mortar, crack arrest, polymer impregnation, and overlays and surface treatments. Methods for repairing spalled concrete include coatings, concrete replacement, grinding, jacketing, shotcreting, prepacked concrete, and thin-bonded or unbonded overlays. Repair materials include bituminous materials, portland-cement concrete, mortar and grouts, epoxies, expandable mortars, grouts and concretes, linseed oil, latex-modified concrete, and polymer-concrete materials.

From an evaluation of the repair techniques and materials identified, five procedures (three crack repair techniques and two techniques for repairing spalled concrete) were identified as being the most applicable for in situ repair of concrete hydraulic structures. The selected techniques include pressure injection, polymer impregnation, and addition of reinforcement. In conjunction with these repair procedures, thin reinforced overlays and shotcrete can be used to repair spalled concrete surfaces as well as to resurface a cracked structure after it has been repaired.

FOR ADDITIONAL INFORMATION: A copy of the report is available from NTIS, Springfield, VA 22161; (703) 487-4600.

NTIS order number: AD-A182297/2/NAC

Price code: A05

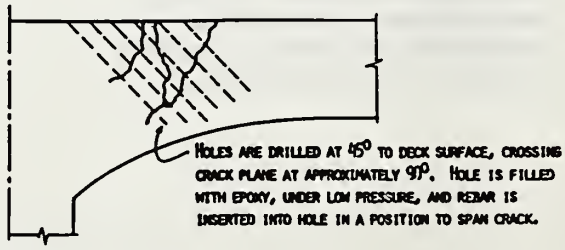
HOLES ARE DRILLED AT 45° TO DECK SURFACE, CROSSING CRACK PLANE AT APPROXIMATELY 90°. HOLE IS FILLED WITH EPOXY, UNDER LOW PRESSURE, AND REBAR IS INSERTED INTO HOLE IN A POSITION TO SPAN CRACK.

Repair of crack by post reinforcement

NASA Tech Brief
National Aeronautics and Space Administration

Licensing Opportunity

Analyzing Wakes From Hovering-Helicopter Rotor Blades

An analytical method and computer program yield realistic results quickly.

Ames Research Center, Moffett Field, California

A new method for analyzing the free wake of a hovering-helicopter rotor produces more reliable results and requires less computer time than do previous methods. The new method copes with wake instabilities — both physical and numerical — that afflict the usual time-stepping analysis methods.

The new method is based on the newly recognized fact that among the solutions of the wake-airflow equations for a hovering-helicopter rotor is one that appears steady when it is viewed in a coordinate frame that rotates with the blades. Although steady, this solution is unstable; that is, it is disrupted when subjected to temporal disturbances. Nevertheless, this solution allows prediction of some average performance characteristics of the rotor.

The steady wake solution must satisfy equilibrium conditions in the rotating frame: a principal one of these conditions is that the sum of velocity contributions from all effects must be such that the wake is not convected to a new size, shape, or location. For the free-tip vortex, the net velocity at each point must be locally tangent to the vortex filament.

In the analysis, the tip vortex is represented by new basic curved vortex elements developed in another aerodynamic research project. The curved elements are more efficient and more accurate than the traditionally-used straight-line elements. The new solution method is naturally compatible with the curved-vortex-element method, since both use many of the same geometric properties.

The velocity components are analyzed in crossflow planes normal to the curved vortex filament in the rotating coordinate plane. These planes are located at the wake collocation points through which the curved vortex elements pass (see figure). The steady solution is reached when, at every crossflow plane, the crossflow velocity is zero; that is, when the local resultant velocity is tangent to the filament.

The method involves the determination of influence-coefficient matrices. Given an initial configuration, the effects of small displacements on the collocation points on the rest of the wake are determined. The matrices are constructed from these effects and used to predict how the collocation points should be displaced to null the crossflow velocities. The calculation is implemented with the help of a special mathematical-relaxation procedure. Only a few steps are required to obtain converged solutions.

The computer time for a solution depends roughly on the square of the number of free-wake points. The traditional time-stepping method, in contrast, depends on the cube of the number of points and therefore is much more time consuming.

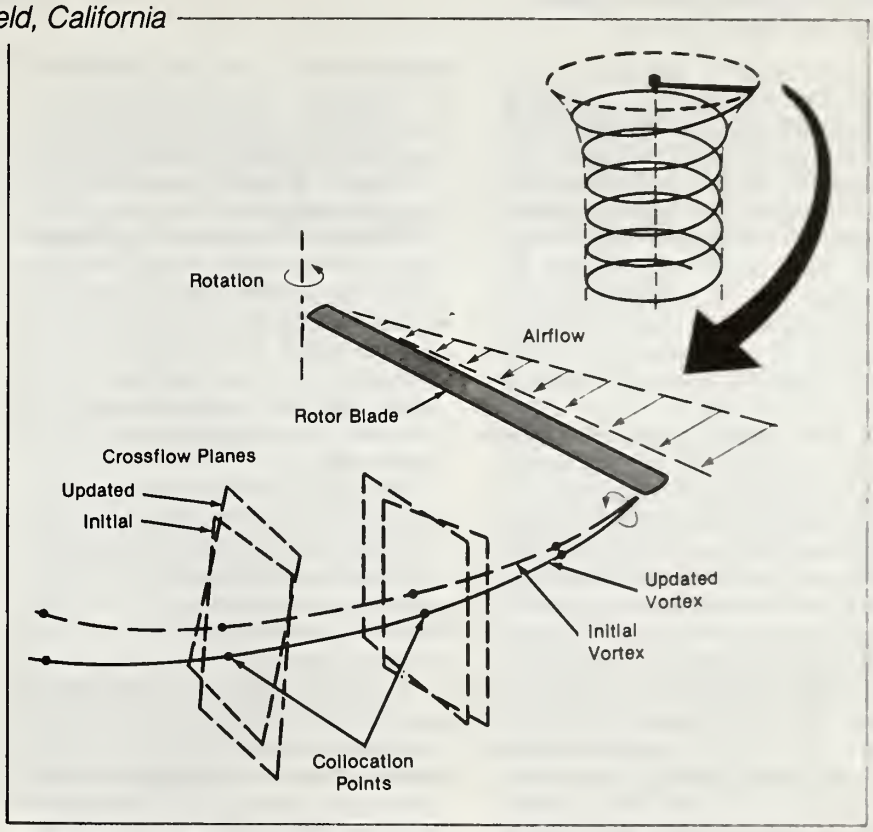

The **Tip-Vortex Position,** in coordinates moving with the rotor blade, is updated in a relaxation procedure. The wake-airflow solution is reached when the updates converge to a steady wake shape.

This work was done by D. B. Bliss, D. A Wachspress, T. R. Quackenbush, and A. J. Bilanin of Continuum Dynamics, Inc., for **Ames Research Center.**

Inquiries concerning rights for the commercial use of this invention should be addressed to the Patent Counsel, Ames Research Center
Refer to ARC-11675/TN

Ames Research Ctr.
Moffett Field, CA 94035
Technology Utilization Officer: Laurance Milov
Mail Code 223-3
(415) 694-6370
Patent Counsel:
Darrell G. Brekke
Mail Code 200-11
(415) 694-5104

NASA Tech Brief
National Aeronautics and Space Administration

Calculations of Wall Effects on Propeller Noise

Reverberations affect sound levels in wind tunnels.

A report describes calculations of the acoustic field of a propeller in a wind tunnel that has walls of various degrees of softness. The understanding provided by this and related studies is necessary for the correct interpretation of wind-tunnel measurements of the noise generated by high-speed, highly loaded, multiple-blade turbopropellers: such measurements are becoming increasingly important because considerations of fuel economy have renewed interest in propeller-driven airplanes.

The mathematical model of the propeller and wind tunnel is a set of acoustical dipoles on a disk that rotates on the axis of a duct of circular cross section. Although a typical wind tunnel has a rectangular cross section, the circular model involves less calculation, and the results should be qualitatively similar to those of a rectangular model. The convected-wave equation for the acoustic field is written in cylindrical coordinates in steady-state, nondimensional form, scaled by the reference values of the air density, speed of sound, mean flow speed, wind-tunnel radius, propeller radius, number of blades, and rotational speed. The wind-tunnel boundary layer is ignored in this analysis.

The duct-wall boundary condition is characterized by an acoustical impedance or admittance. The hard-wall (purely reflecting) boundary condition is represented by zero admittance and a zero perpendicular pressure gradient, while a soft-wall (partly reflecting, partly absorbing) boundary condition is represented by a finite admittance and a perpendicular pressure gradient related to the continuity of the air-particle displacement. The soft-wall boundary conditions are manipulated to investigate the relative effectiveness of various wall linings in creating an acoustic field more nearly representative of the open atmosphere.

The wave equation was integrated numerically by the finite-element method, using a number of different combinations of the acoustic impedance and the scaling parameters. For comparison, the acoustic field of the same propeller in free space was also computed.

The calculations show that at flow speeds much less than that of sound, the wall must be lined with acoustical absorbers to make the free-field and ducted-propeller models agree in acoustic-pressure levels and directionality. The best agreement would occur where the ratio of wall radius to propeller radius is large and the measurements are made away from the walls.

At a flow speed half that of sound, the acoustic-pressure magnitude and directivity along the duct wall near the propeller are similar for a hard wall and for a variety of soft walls. However, the hard-wall results may be fortuitous, and additional studies are needed.

Upstream or downstream from the propeller, soft wall liners having suitable admittances can suppress the usual duct acoustic modes. In this case, the duct and free-field acoustic characteristics can agree over greater sideline distances. At high flow speeds, different upstream and downstream wall admittances are necessary for the equal suppression of duct modes on both sides of the propeller.

This work was done by Kenneth J. Baumeister of **Lewis Research Center** *and Walter Eversman of the University of Missouri. Further information may be found in NASA TM-87333 [N86-29630/NSP], "Modeling the Effects of Wind Tunnel Wall Absorption on the Acoustic Radiation Characteristics of Propellers."*

Copies may be purchased from the National Technical Information Service, Springfield, Virginia 22161. [A02]

LEW-14516/TN

FOR ADDITIONAL INFORMATION: *Contact: Director, Technology Transfer Division, P.O. Box 8757, BWI Airport, MD. 21240; (301) 621-0100 Ext. 241*
REFER TO THE NUMBER LISTED AT THE END OF THE ARTICLE

NASA Tech Brief
National Aeronautics and Space Administration

Design of Fiber Composites for Structural Durability

Hygrothermomechanical effects can be analyzed by computers.

A computational methodology has been developed and is available at NASA Lewis Research Center to design and analyze fiber-composite structures subjected to complex hygrothermomechanical environments. This methodology includes composite mechanics and advanced finite-element structural-analysis methods. Methodology can be applied to such problems as the progressive fracture of a composite material, the design of a composite material for cycle fatigue combined with hot and wet conditions, and general composite-laminate configurations.

A major concern in the fiber-composite community has been the prediction, or even a reasonable approximation, of the structural durability of fiber-composite structures in service environments. Fiber-composite structures need to be designed to resist such service conditions as mechanical load (static, cyclic, or impact), heat, moisture, and combinations of these; i.e., hygrothermomechanical (HTM) conditions.

The general procedure for designing a fiber-composite part that will be exposed to HTM environments begins with the use of empirical data to select laminate configurations for the part, followed by the validation of these data through the preliminary design phase. Subsequently, a variety of tests are conducted in the specified HTM environments. The results of these tests are then used to reconfigure the laminates to meet the design requirements in these HTM environments. This procedure, though successful, is cumbersome because it is costly, time consuming, and needs to be repeated for each new design. It can be circumvented to a large extent by a methodology for predicting the structural durabilities and, therefore, the service lives of fiber composites in HTM environments. The computational methodology developed accurately predicts the HTM effects on fiber-composite stiffness and strength and, therefore, can be used to design fiber-composite structural components for structural durability.

This computational methodology has evolved over the past seven years. It began with the development of an integrated theory for predicting the hygrothermal effects on fiber composites and has culminated in three major computer programs: (1) CODSTRAN (Composite Durability Structural Analysis), (2) INHYD (Intraply Hybrid-Composite Design), and (3) ICAN (Integrated Composite Analyzer). These programs collectively provide analyses required for the design of structures durable in HTM service environments.

This work was done by Christos C. Chamis of **Lewis Research Center**. *Further information may be found in NASA TM-87045 [N85-27978/NSP] "Designing for Fiber Composite Structural Durability in Hygrothermomechanical Environments."*

Copies may be purchased from the National Technical Information Service, Springfield, Virginia 22161, [A09]

LEW-14385 /TN

FOR ADDITIONAL INFORMATION: *Contact: Director, Technology Transfer Division, P.O. Box 8757, BWI Airport, MD. 21240; (301) 621-0100 Ext. 241*

REFER TO THE NUMBER LISTED AT THE END OF THE ARTICLE

NASA Tech Brief
National Aeronautics and Space Administration

Licensing Opportunity

High-Differential-Pressure Heat Exchanger

All critical joints are full-penetration welds inspectable with x rays.

NASA's Jet Propulsion Laboratory, Pasadena, California

A heat exchanger accommodates a large pressure difference between the heat-transfer fluids. It is designed so that all its welded joints can be inspected with x rays to ensure leak-free operation over many years. Joints between the fluids and between each fluid and the environment are radiographically inspectable.

The low-pressure medium can be a liquid; for example, a molten metal or salt. The high-pressure medium can be a gas. The heat-exchanger design can be used in Stirling-cycle engines, including those in proposed nuclear and solar powerplants.

The heat-exchange tubes through which the pressurized gas flows are butt-welded to the tube sheets from inside the tubes (see figure). Nipples machined on the tube sheets help to position the tubes for welding. After welding, the tube-to-sheet joints are inspected radiographically. The tube-to-sheet joints are the only ones at boundaries between the two fluids: all other joints are at boundaries between one of the fluids and the environment.

If the tube welds are found to be satisfactory, stuffers are inserted in the tubes These tubelike structures slow the flow of gas through the tubes to a speed optimum for heat transfer. This minimizes the number of tubes required. The gas manifolds are then welded to the tube sheets, and the outer cylindrical heat-exchanger body is welded to the sheets on the faces opposite the manifolds (see figure). A ring or a flange or both may have to be welded to close the liquid side. These welds are then subjected to x-ray inspection.

This work was done by Edward C. Hylin of Rockwell International Corp. for **NASA's Jet Propulsion Laboratory.**

Inquiries concerning rights for the commercial use of this invention should be addressed to the Patent Counsel, NASA's JPL Refer to NPO-16947/TN

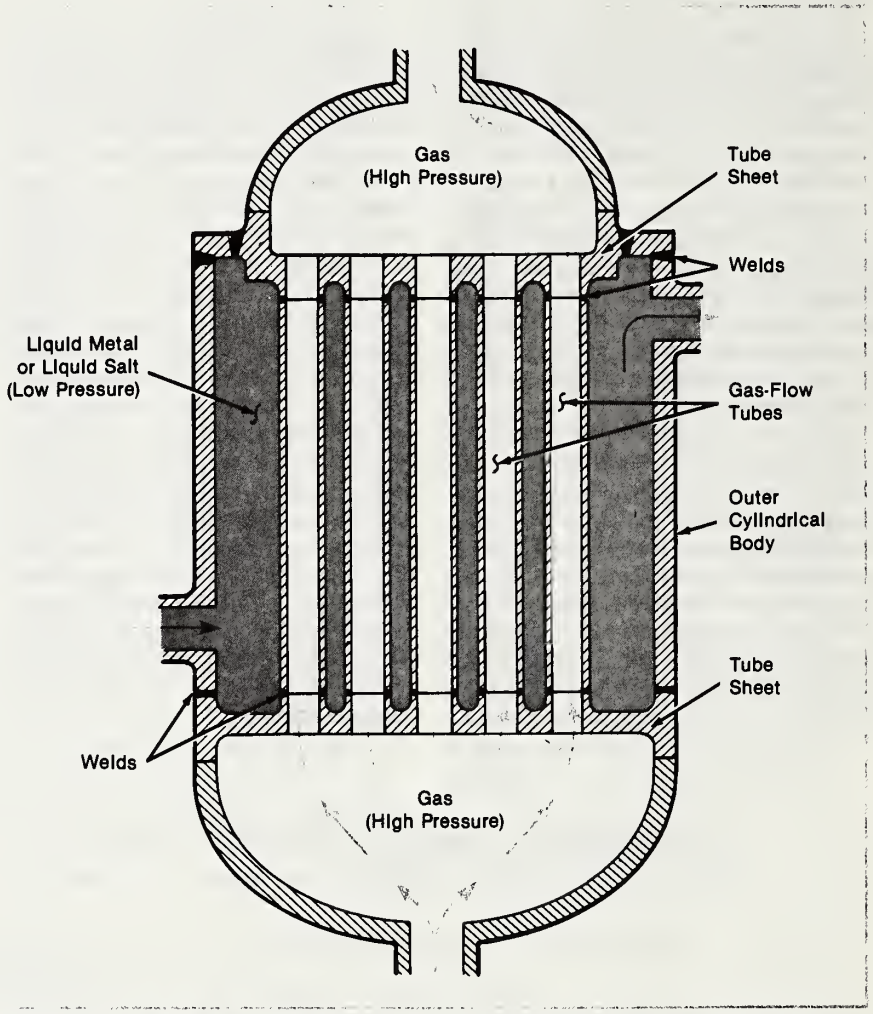

Gas In Tubes Exchanges Heat With Liquid in the spaces between the tubes. The gas is at a pressure of about 150 atm (15 MPa), while the liquid pressure is about 2 atm (0.2 MPa).

Jet Propulsion Lab.
4800 Oak Grove Drive
Pasadena CA 91109

Technology Utilization Mgr.: Norman L. Chalfin
Mail Stop 156-211
(818) 354-2240

NASA Resident Technology Utilization Officer: Gordon S. Chapman
Mail Stop 180-801
(818) 354-4849

Patent Counsel:
Paul F. McCaul
Mail Code 180-801
(818) 354-2734

NASA Tech Brief
National Aeronautics and Space Administration

Preliminary-Design Software for Composite Structures

An easy-to-use program enables fast analysis and evaluation of rough designs.

A report describes an interactive program for the preliminary approximate stress analysis of structures made of fiber-reinforced composite materials. The program, intended for a personal computer, helps the designer select or confirm the sizes of composite structural members. It is useful in evaluating conceptual designs.

Called COMPSIZE, the program uses classical lamination theory to predict an effective elastic modulus for a laminate of arbitrary material and ply orientation. It then uses the elastic modulus in a family of subroutines that incorporate the familiar basic methods of the structural analysis of isotropic materials. Other subroutines calculate the coefficient of thermal expansion of the laminate and the ply-by-ply strains within the laminate.

The procedure is simple and convenient for the user. Its approximate results can later be refined by more detailed and precise methods as the design progresses.

COMPSIZE is written in Basic, a language that proved to be more than adequate for providing an easy-to-use format and for setting up solutions to the equations. It is designed so that a user can initiate the program and solve a problem even without reading the user manual. Its main menu lists 15 major types of problems for selection by the user. Examples include the estimation of the properties of a composite material, axial tension or compression without buckling, shear induced by bending, and section area and moment of inertia. Several of the major problems have submenus of up to five further specialized problems.

For each problem, input and output units are specified. After the solution of a problem, COMPSIZE asks the user whether the results should be printed and whether any additional problems are to be solved.

This work was done by Charles N. Eastlake of Embry-Riddle University for **Marshall Space Flight Center**. *To obtain a copy of the report, "Preliminary Design Methods for Fiber Reinforced Composite Structures Employing a Personal Computer,"*
MFS-27153/TN

FOR ADDITIONAL INFORMATION: *Contact: Director, Technology Transfer Division, P.O. Box 8757, BWI Airport, MD. 21240; (301) 621-0100 Ext. 241*
REFER TO THE NUMBER LISTED AT THE END OF THE ARTICLE

NASA Tech Brief
National Aeronautics and Space Administration

Stiffening Heat-Exchanger Tubes Against Vibrations

Midsection clamps reduce the harmful effects of crossflow.

Marshall Space Flight Center, Alabama

Arrays of parallel tubes in a strong crossflow can be protected from excessive vibration by simple braces. When the velocity of transverse fluid flow rises to a high level, tube arrays (in nuclear-reactor heat exchangers and in rocket-engine fuel injectors, for example) can vibrate unstably.

An effective solution is to brace the tubes in bundles of four near their midpoints (see figure). The stiffness and, therefore, the natural vibrational frequency of the tubes is thereby increased. The tubes are less likely to resonate in response to high crossflow velocities.

This work was done by G. V. R. Rao of Rockwell International Corp. for **Marshall Space Flight Center**. *No further documentation is available.*
MFS-19907/TN

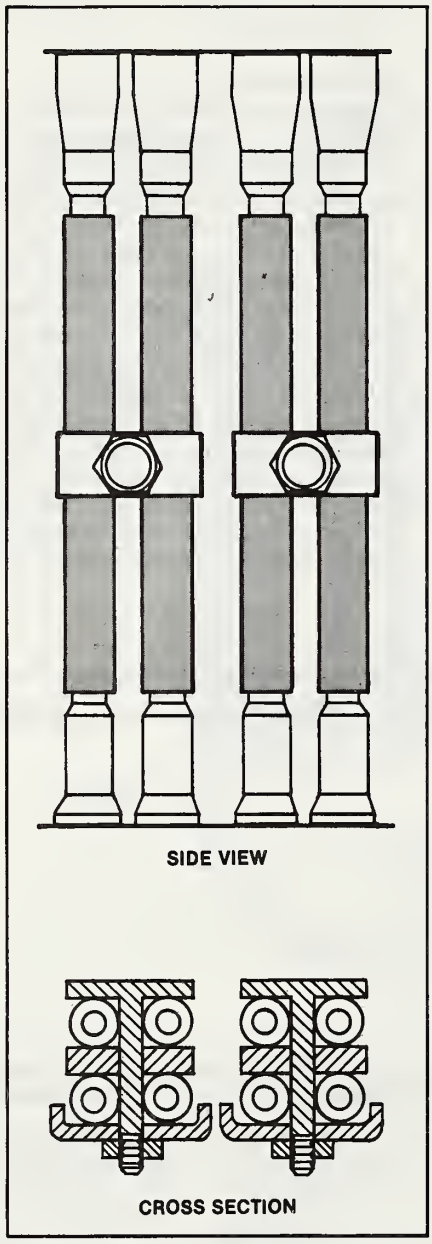

A **Clamp Bolts Onto Four Tubes**, increasing their stiffness and natural frequency. Unstable vibrations are thereby suppressed.

FOR ADDITIONAL INFORMATION: *Contact: Director, Technology Transfer Division, P.O. Box 8757, BWI Airport, MD. 21240; (301) 621-0100 Ext. 241*
REFER TO THE NUMBER LISTED AT THE END OF THE ARTICLE

NASA Tech Brief
National Aeronautics and Space Administration

Structural Dynamics of Filament-Wound Booster Rockets

A mathematical model agrees closely with measurements.

A report summarizes a program of measurements and calculations of vibrations in filament-wound composite models of the Space Shuttle solid-rocket boosters. The vibrational behavior predicted by a finite-element computer model of the structural dynamics correlates well with data from tests on full- and quarter-scale models.

The quarter-scale booster case includes five cylindrical composite segments, formed by winding graphite filaments in ±29° helixes alternating with 90° hoop layers. There are 15 layers, including a glass-cloth layer at the inner surface. The case is intended as a replacement for a heavier steel version.

The computer model was developed with the NASTRAN general-purpose structural-analysis computer code. It employs a grid spacing nearly identical to that of full-scale cases. The segments are modeled with quadrilateral membrane and bending elements having orthotropic material properties. Joints and other metal parts are modeled with triangular and quadratic elements. Bar elements are used to represent stiffener rings and stringers in the forward and aft skirts and to provide most of the ring bending stiffnesses at tang and clevis joints. The model takes into account both the stiffening and the vibrating-mass effects of the propellant content and the decrease thereof after lift-off.

The early versions of the mathematical model correlated poorly with test data: stiffness discrepancies ranged from 10 to 25 percent. However, load and deflection data from full-scale equipment showed that the tang and clevis joints between case segments have low stiffnesses at the interfaces between steel parts and the composite material. When the mathematical-model joints were modified to match the measured joint stiffness, excellent correlations with vibration-mode shapes and frequencies resulted.

This work was done by F. M. Bugg of **Marshall Space Flight Center**. *To obtain a copy of the report, "Structural Dynamics of Filament Wound Space Shuttle Booster Rockets,"*

MFS-28155/TN

FOR ADDITIONAL INFORMATION: *Contact: Director, Technology Transfer Division, P.O. Box 8757, BWI Airport, MD. 21240; (301) 621-0100 Ext. 241*
REFER TO THE NUMBER LISTED AT THE END OF THE ARTICLE

NASA Tech Brief
National Aeronautics and Space Administration

Licensing Opportunity

Thermally Insulating Support for Cryogenic Tanks

A passive alternate-load-path support scheme keeps weight low while conserving cryogenic liquid.

Ames Research Center, Moffett Field, California

A method of supporting the inner vessel of a large Dewar container minimizes heat conductance and weight but ensures high strength and impact resistance. The support method also accommodates thermal expansion and contraction of the vessel while introducing minimal stresses in the structure.

The inner vessel, which may contain liquid helium at 4 K, for example, hangs from three pairs of struts extending from the outer vessel (see figure). A strut consists of two concentric tubes in series with end fittings. The outer tube, made of a fiberglass-reinforced epoxy, is the stronger but has a higher thermal conductivity. The inner thin wall tube is made of low conductance graphite-reinforced epoxy.

The outer tube connects solidly to the outer vessel (the warm end) and connects in series to the inner tube to the inner vessel (the cold end). When a low thrust is transmitted through the strut, both tubes carry the full load in series. However, when the load increases to a large value in tension or in compression, the conical surface of the stem on the inner tube reaches a stop and bypasses the load arround the thin wall inner tube. When the load drops, the stem returns to its original position, and the inner tube again takes up the full load.

The struts are free to swivel at the outer-vessel pins and at the paired joints at the inner vessel. As the diameter of the inner vessel changes with temperature and pressure, the angle between the struts in each pair grows or shrinks slightly to adjust to the new dimensions.

The support method was developed for cryogenic tanks on spacecraft. It allows a tank to withstand the loads imposed on it during launching and maneuvering but keeps heat gain extremely low when the craft is in orbit or on earth. It is expected to reduce thermal conductance by a factor of 10 or more and weight by a factor of 2 in a 3-year-lifetime, superfluid-helium Dewar container. Struts have been fatigue tested up to 500,000 cycles and subjected to tension and compression tests and simulated temperature change tests and have met their design goals. Possible terrestrial applications include transportation of cryogenic liquids. The struts might also be used to support large supercooled magnets that are designed for earthquake loads.

This work was done by Richard T. Parmley of Lockheed Missiles & Space Co., Inc., for **Ames Research Center.** *Further information may be found in NASA CR-177325 [N85-17020/NSP], "Passive Orbital Disconnect Strut (PODS III) Structural Test Program."*

Copies may be purchased from the National Technical Information Service, Springfield, Virginia 2216[1] [A06]

Inquiries concerning rights for the commercial use of this invention should be addressed to the Patent Counsel, Ames Research Center
Refer to ARC-11608/TN

Ames Research Ctr.
Moffett Field, CA 94035
Technology Utilization Officer: Laurance Milov
Mail Code 223-3
(415) 694-6370
Patent Counsel: Darrell G. Brekke
Mail Code 200-11
(415) 694-5104

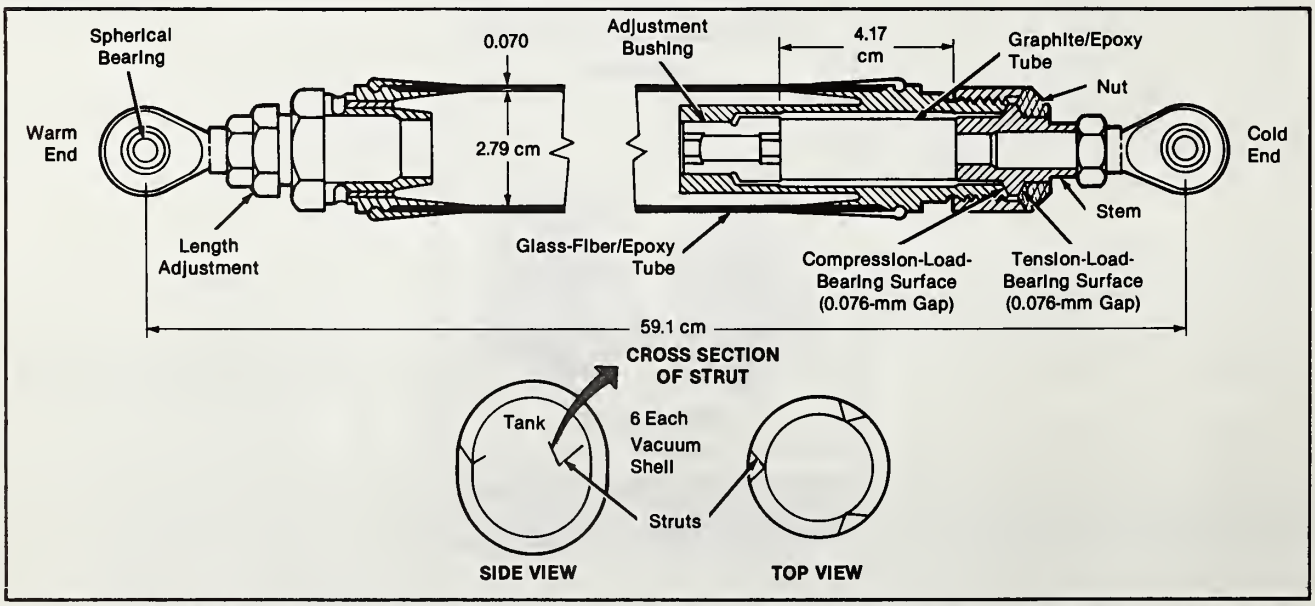

The **Inner Vessel Hangs From Struts** in the outer vessel. The thin wall graphite/epoxy tube is protected from high loads by close tolerance stops.

NASA Tech Brief
National Aeronautics and Space Administration
Lyndon B. Johnson Space Center, Houston, Texas

Licensing Opportunity

Wedge Joints for Trusses

Structures could be assembled rapidly with simple hand tools.

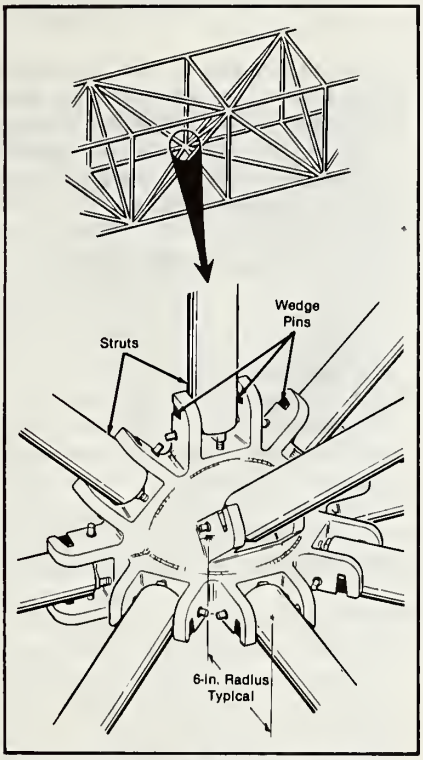

Figure 1. **A Lightweight Structure** would be assembled from tubular struts joined at nodes by wedge pins that fit into mating slots.

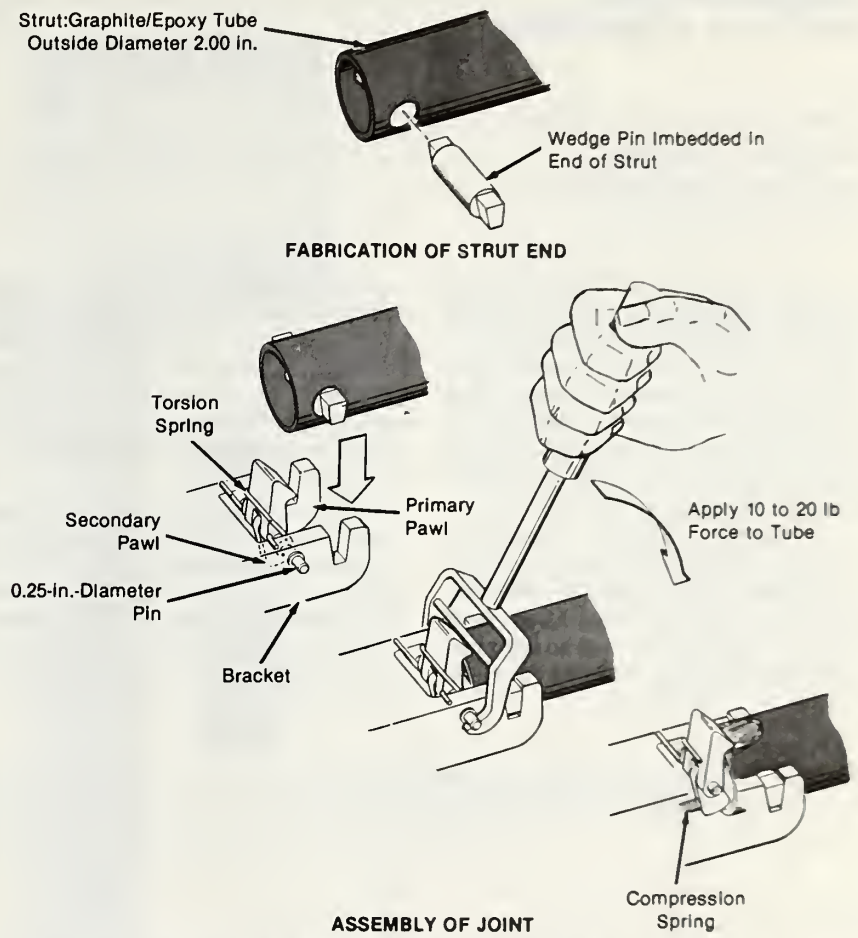

Figure 2. This **Joint Would Be Assembled Rapidly** by seating the wedge pin in the V-shaped slots and deforming the end of the strut until the primary pawl engages it.

Proposed locking wedge joints would enable the rapid assembly of lightweight beams, towers, scaffolds, and other truss-type structures. At each joint, a wedge pin integral with a tubular strut would be held securely in V-shaped slots in a bracket on a node (see Figure 1).

Wedge pins would be installed at the ends of each tubular strut during manufacture. If the strut is to be made of graphite/epoxy composite, as suggested at the left of Figure 2, the pins can be installed before curing the epoxy. After the cure, the wedge faces can be machined to close tolerances for correct strut length, alignment, and seating in the V-shaped slots.

The assembly of a joint would begin with the insertion of the wedge pin into the matching V-shaped slots (also shown in Figure 2). With the help of a specially shaped tool, the assembler would push on (and slightly deform) the end of the strut, forcing the wedge securely into the slots. A spring-loaded primary pawl would then engage the end of the strut to hold it in place. A spring-loaded secondary pawl would intrude a short distance into the inside of the hollow strut to provide additional wedging force and redundant locking.

The wedging action should contribute to the precision of the joints, thereby helping to correct truss misalignments. The wedging force applied by the pawls should assure lifetime wedging with no joint looseness.

This work was done by Kenneth E. Wood of Rockwell International Corp. for **Johnson Space Center.**

Inquiries concerning rights for the commercial use of this invention should be addressed to the Patent Counsel, Johnson Space Center. Refer to MSC-21072 /TN

Lyndon B. Johnson Space Center
Houston, TX 77058
Technology Utilization Officer: Dean C. Glenn
Mail Code EA4
(713) 483-3809

Patent Counsel: Edward K. Fein
Mail Code AL3
(713) 483-4871

FOR ADDITIONAL INFORMATION: *Contact: Director, Technology Transfer Division, P.O. Box 8757, BWI Airport, MD. 21240; (301) 621-0100 Ext. 241*
REFER TO THE NUMBER LISTED AT THE END OF THE ARTICLE

NASA Tech Brief
National Aeronautics and Space Administration

Computer Program for Flow in a Combustor

This program simulates subsonic, swirling, reacting, turbulent flow about a bluff body.

A new version of the TEACH computer program has been developed specifically for use in the analysis of the subsonic, swirling, reacting, turbulent flow in a cylindrical bluff-body research combustor. This combustor design is widely used as a research tool for the mathematical modeling of gas turbines and for the development of diagnostic instrumentation.

The flow field of interest is developed in the open-ended, cylindrical chamber downstream of the base of the bluff body that houses the fuel injector. Such flows can be described by the fully-elliptic, steady-state equations of motion. This version of TEACH solves these equations using an improved finite-difference procedure, the B rounded skew upwind differencing (BSUD) method. The axisymmetric pressure distribution is estimated by means of a new algorithm, the pressure-implicit split-operation (PISO) predictor/corrector technique.

Sections of the computer program have been reorganized in an attempt to minimize the changes necessary to install the program in different computer systems. The input format has been extensively revised to permit more flexibility in setting up and running cases. Additional options include the analysis of two-dimensional planar flow and the selection of the more-conventional hybrid differencing scheme.

This program was written by Louis M. Chiappetta of United Technologies Corp. for **Lewis Research Center**.
LEW-14271 /TN

FOR ADDITIONAL INFORMATION
CONTACT:

COSMIC®
112 Barrow Hall
University of Georgia
Athens, GA 30602
(404) 542-3265

FOR ADDITIONAL INFORMATION: *Contact: Director, Technology Transfer Division, P.O. Box 8757, BWI Airport, MD. 21240; (301) 621-0100 Ext. 241*
REFER TO THE NUMBER LISTED AT THE END OF THE ARTICLE

NASA Tech Brief
National Aeronautics and Space Administration

Color-Video Thermal Maps

Temperatures appear in time-varying color.

Marshall Space Flight Center, Alabama

A computer-simulation method produces a color-video representation of the temperatures in a combustion-chamber wall. Until now, simulators have been limited to modeling temperature behavior at individual points. The new method displays the two-dimensional or three-dimensional temperature variation — that is, across a plane or volume of the coolant channel.

The colors in the display represent specific temperature ranges (see figure). The colors change to show the changes in temperature with flow, pressure, heat flux, and other factors during startup, steady-state operation, and shutdown. The data are used to determine whether the fatigue and structural limits of the combustor design are adequate.

The simulator solves for the temperature by the finite-difference method, making a timewise step-by-step evaluation of the fuel flow, heat flux, and cooling conditions. It converts its digital temperature data to a color-graphic map, changing it either in real time or in slow motion.

This work was done by W. R. Wagner, C. A. Laren, and W. T. Tonis of Rockwell International Corp. for **Marshall Space Flight Center.**

MFS-29223/TN

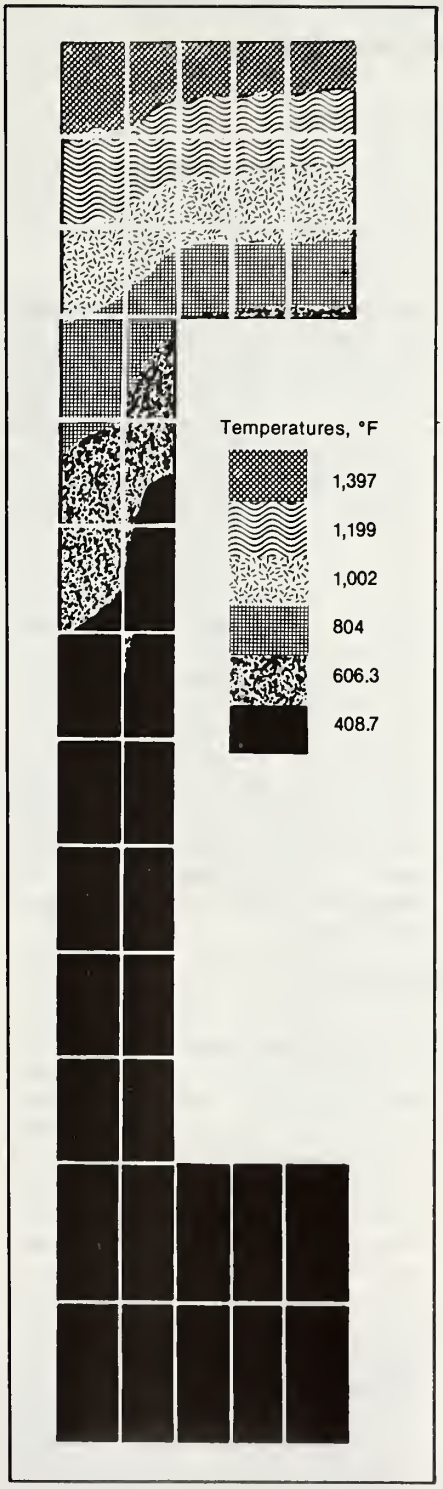

Colors (Depicted Here by Textures) Show Temperatures in a cross section of a coolant channel in the wall of a combustor. Many such cross sections are combined to give a three-dimensional view of temperatures in the channel.

FOR ADDITIONAL INFORMATION: *Contact: Director, Technology Transfer Division, P.O. Box 8757, BWI Airport, MD. 21240; (301) 621-0100 Ext. 241*
REFER TO THE NUMBER LISTED AT THE END OF THE ARTICLE

NASA Tech Brief
National Aeronautics and Space Administration

Gamma-Ray Fuel Gauges for Airplanes

An accurate system overcomes problems of capacitance gauges.

Langley Research Center, Hampton, Virginia

Capacitance fuel gauges have served as the basis for fuel-quantity-indicating systems in aircraft for decades. However, there have been persistent reports by the airlines that these gauges often give faulty indications because of microbial growth and other contaminants in the fuel tanks. A feasibility study has been conducted on the use of attenuation of gamma rays to measure the quantities of fuel in the tanks. Studies with a weak Am^{241} 59.5-keV radiation source indicate that it is possible to monitor continuously the fuel quantity in the tanks to an accuracy of better than 1 percent. These measurements also indicate that there are easily measurable differences in the physical properties and resultant attenuation characteristics of JP-4, JP-5, and Jet A fuels.

The operation of a nuclear gauge is based on the attenuation of gamma rays passing through matter. As a result of interaction of gamma rays with the atoms in the test medium, the number of unaffected primary photons arriving at the detector is a function of the path length in the test medium. Such a gauge will be more sensitive if the attenuation coefficient is large for the incident photons. This dictates the choice of sources of low photon energy (less than 100 keV). Two candidate sources that meet the requirements of low photon energy, long source life, and well-resolved photon spectrum are Am^{241} (458 years) and Cd^{109} (453 days).

Since the exact compositions of aviation fuels are seldom known, it was not possible to calculate their attenuation coefficients for Am^{241} and Cd^{109} gamma rays. Therefore, the attenuation coefficients were measured experimentally for water, JP-4, JP-5, Jet A, and leaded and unleaded automobile gasoline. The nominal radioactive source strengths readily available were of the order of 10 microcuries (Am^{241}) and 100 microcuries (Cd^{109}). They provided good counting statistics for all test fluids over a period of 10 minutes. Measurements were made with and without the source in each case to subtract out the counts due to cosmic rays and other background radiation sources.

After the attenuation coefficients of the test fluids were measured, the wing-tank geometry for a Boeing 737 aircraft was selected for the computer model to test the sensitivity of attenuation of low-energy photons as the basis for fuel-gauging systems aboard aircraft. For purposes of the model, the fuel tank was divided into 14 compartments. Each of the 14 compartments in the fuel tank was approximated by a rectangular box. Any similar wing tank can be modeled by this technique by simply adjusting the number of compartments and the dimensions of each rectangular box. Once the tank geometry was defined, the computer program stepped through fixed percentages of tank capacity. For each amount of fuel, the fuel level was computed assuming a level fuel surface. With the fuel level known, the path length between each source/detector pair occupied by fuel or air was determined. From these path lengths, the number of counts was determined.

The results show that the counting rate is constant at all 14 stations when the tank is full. A 1-percent reduction in tank fuel content causes a large jump (about 57 percent) in the counting rate at the wing-tip detector. As fuel is expended, the counting rates change first in those compartments near the wing tip. After approximately 35 percent of the fuel has been expended, the compartment nearest the tip is empty and shows no further change in the counting rate. When the tank is nearly empty, the counting rates in the outer-station detectors have stabilized, but the counting rates at the stations near the fuselage are changing rapidly.

It is apparent that a suitably designed nuclear gauge should enable continuous monitoring of the fuel-tank contents to an accuracy of better than 1 percent. The nuclear gauge is not expected to be susceptible to the fouling/corrosion problems experienced by the conventional capacitance gauges since both the source and radiation detector are sealed. Any algae or microbial growth on the source and detector windows can be easily removed during scheduled periodic maintenance checks of the gauging system. An added advantage of the nuclear gauge is its inherent capability to detect water buildup in the tank. Also, it is a self-calibrating system with a high degree of cross-checking capability, rendering the system independent of any changes in the background count rate with altitude.

It should be noted that despite the large flux of low-energy photons obtainable with a Cd^{109} source, an Am^{241} source would be more economical since it would be safer to handle and/or shield because of its lower energy. In fact, Am^{241}-based densitometers are currently in use aboard some aircraft, and licensing requirements for Am^{241}-based fuel-quality-measurement systems should be no different from what they are for these aircraft. It is estimated that a complete system, including a microprocessor and associated display devices, can be assembled at a cost of less than $10,000 per fuel tank.

This work was done by Jag J. Singh and Danny R. Sprinkle of **Langley Research Center**, *Gerald H. Mall of Computer Sciences Corporation, and Hoshang Chegini of Old Dominion University. Further information may be found in NASA TM-87706 [N86-28385/NSP], "Feasibility of a Nuclear Gauge for Fuel Quantity Measurement Aboard Aircraft."*

Copies may be purchased from the National Technical Information Service, Springfield, Virginia 22161 [A02]
LAR-13604 /TN

FOR ADDITIONAL INFORMATION: *Contact: Director, Technology Transfer Division, P.O. Box 8757, BWI Airport, MD. 21240; (301) 621-0100 Ext. 241*
REFER TO THE NUMBER LISTED AT THE END OF THE ARTICLE

NASA Tech Brief
National Aeronautics and Space Administration

Measuring and Plotting Surface-Contour Deviations

An electromechanical apparatus provides along-track and across-track displacement information to a plotter.

Lyndon B. Johnson Space Center, Houston, Texas

A hand-held device measures the deviation of the contour of a surface from a desired contour and provides an output to an x-y plotter. A carriage on the device is rolled along a track that represents the desired contour, while a spring-loaded stylus on the device deflects perpendicularly to the track to follow the surface (see Figure 1).

The stylus is connected by a pivot-arm mechanism to a linear-voltage displacement transducer (see Figure 2). Displacements of the stylus as it follows the contour are thus transformed into an electrical signal that is applied to the y-axis input of the plotter.

Two nylon rollers ride on the track, which is 5 ft (1.5 m) long and made of aluminum. The track is maintained at a 0.75-in. (1.9-cm) offset from the desired surface. The track is equipped with pads

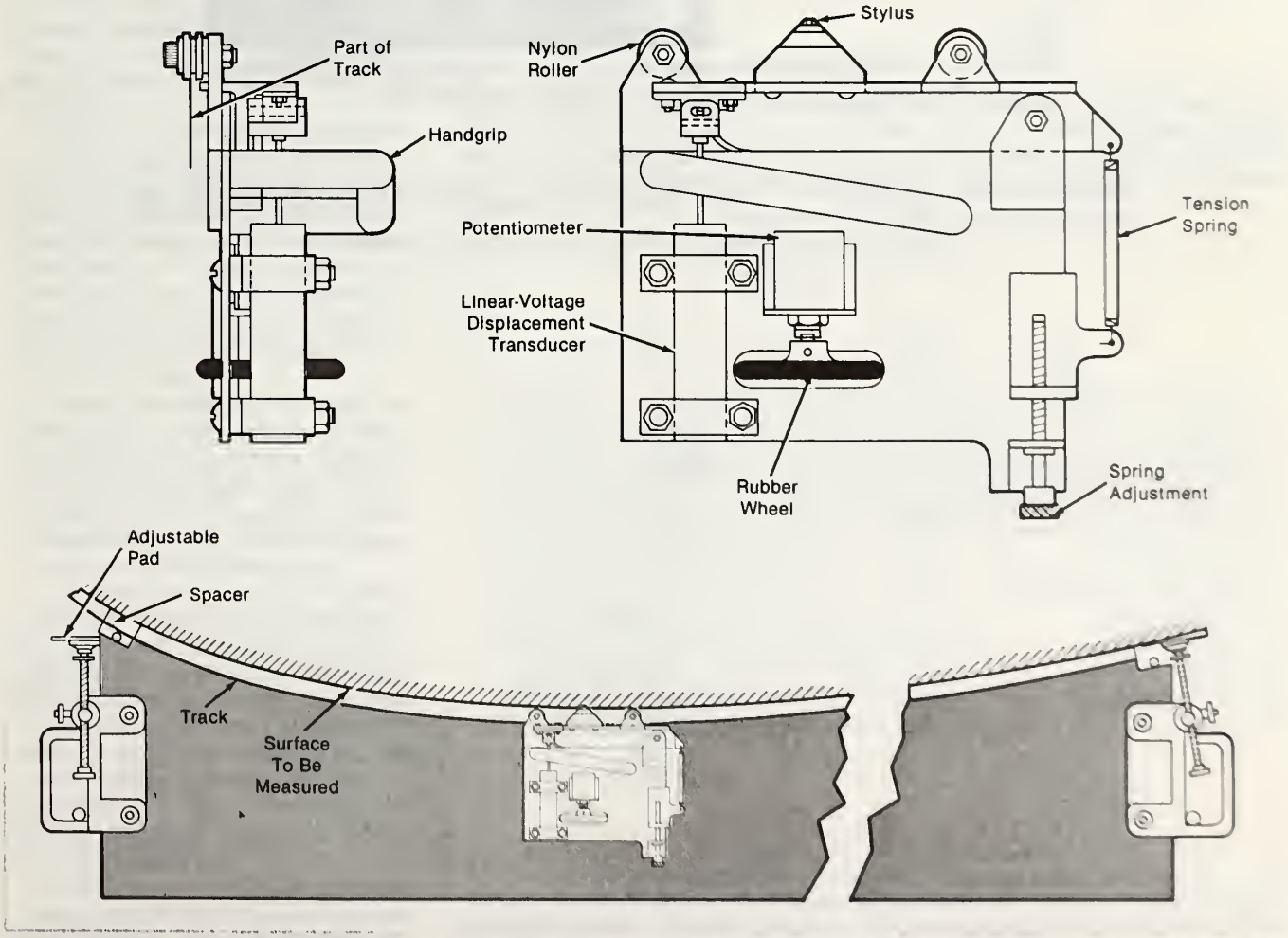

Figure 2. The **Carriage of the Measuring Device** holds a transducer that measures the cross-track displacement of the surface from the desired contour, and a multiple-turn potentiometer that measures the position along the track.

and handholds for manual placement and adjustment. The carriage also has a handgrip so that the operator can move it easily.

A rubber wheel protrudes through a cut-out in the device carriage and bears against the side of the track. As the operator moves the carriage on the track, the wheel turns a potentiometer shaft. The potentiometer resistance thus changes continuously as the stylus moves along the contour, providing a signal for the x input of the x-y plotter. The wheel and the two rollers provide three-point support for the carriage.

This work was done by Lino A. Aragon, Thomas Shuck, and Leroy K. Crockett of Rockwell International Corp. for **Johnson Space Center**.

MSC-21163/TN

Figure 1. An **Operator Moves the Carriage** of the contour-measuring device on a beamlike track. A stylus on the carriage traces the contour of the surface above it.

FOR ADDITIONAL INFORMATION: *Contact: Director, Technology Transfer Division, P.O. Box 8757, BWI Airport, MD. 21240; (301) 621-0100 Ext. 241*

REFER TO THE NUMBER LISTED AT THE END OF THE ARTICLE

NASA Tech Brief
National Aeronautics and Space Administration
Ames Research Center, Moffett Field, California

Licensing Opportunity

Microscopic Gas-Flow Controller

Small flows at low pressures would be monitored and throttled.

A proposed flow-controlling and -measuring device would be made by batch solid-state microelectronic-fabrication techniques. The device would contain an ultrasensitive silicon capacitive pressure transducer, gas-flow channels etched in a silicon wafer, and integrated microvalves. The device is to be used to control and monitor low gas flows at low pressures; for example, in reactive-ion etching equipment or chemical-vapor deposition equipment in the semiconductor industry.

The flow-control and -measuring concept is illustrated by an electrical analog in Figure 1. Gas flows from a pressurized source through a parallel set of narrow channels, each of which provides a known resistance to the flow. The main flow is through channel 1, characterized by flow resistance R_1.

Additional small flow increments are obtained by opening the valves in one or more of the parallel flow channels. This enables fine adjustments of the total flow. The flow resistances in the n parallel channels are in multiple powers of 2 times the flow resistance of channel 2 so that the flow increments can be chosen in small uniform steps over a range of $2^n - 1$ times the smallest step.

The flow is measured in terms of the pressure drop along channel 3, represented in Figure 2 by the flow resistance R_3. R_3 should not exceed R_1 so that the incremental flows through the parallel channels will provide an adequate range of adjustment of the overall flow.

The device consists of the working parts in an integrated silicon wafer sandwiched between two pieces of glass or two other silicon wafers. The silicon could be attached to the glass by electrostatic bonding. The channels would be made by applying anisotropic etchants to the silicon surface. Such etchants can be controlled to produce channels of the precise dimensions needed for the desired flow resistances.

One of the electrodes of the capacitive pressure sensor is a thin layer of metal on the glass plate. The other electrode is a

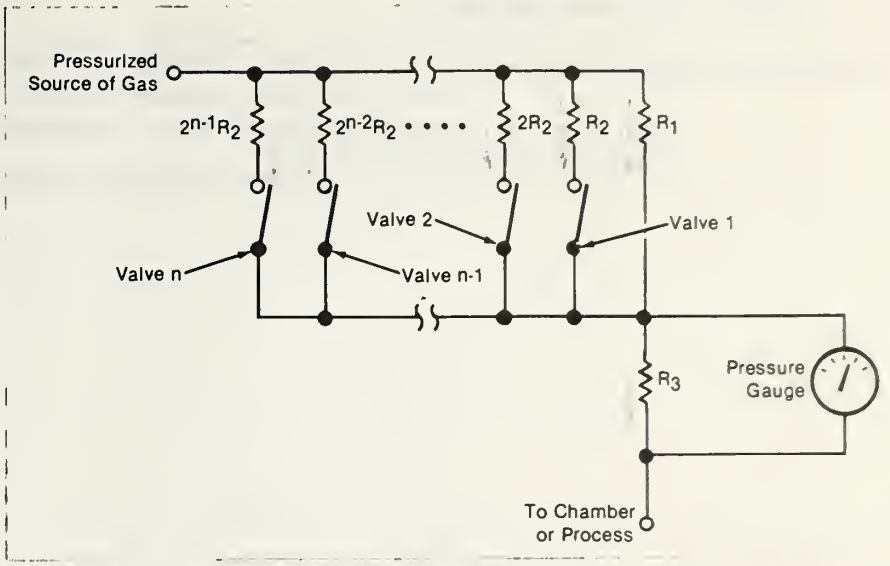

Figure 1. **Gas Flows Through Narrow Passages** of known flow resistance. Different flow resistances are switched in or out to alter the flow. The flow configuration is depicted in the manner of an electrical circuit because the gas flow and pressure are analogous to electrical current and voltage, respectively. The opening of a valve is represented by the closing of a switch and vice versa.

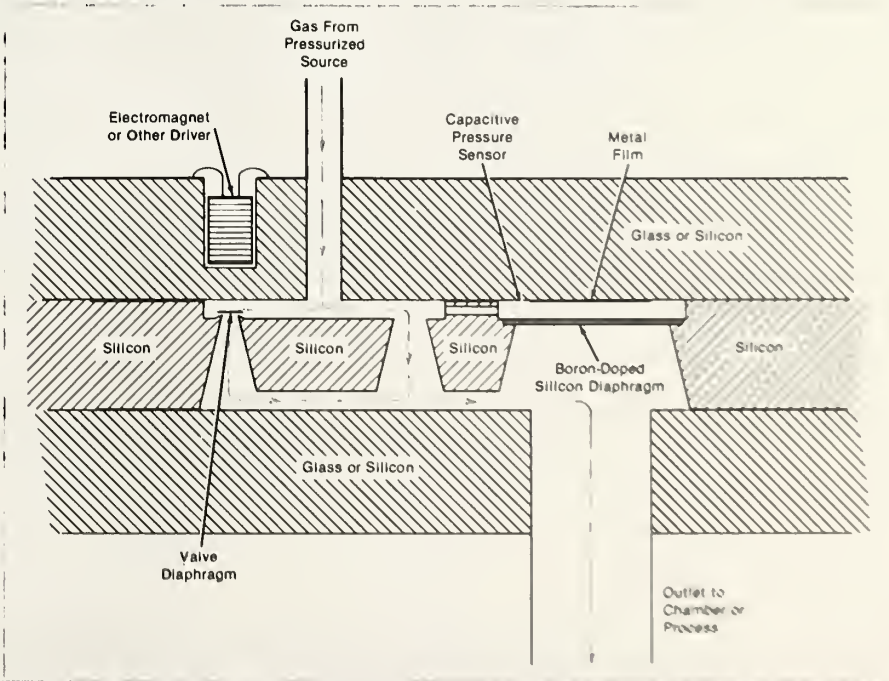

Figure 2. **Narrow Channels** would be etched in a silicon wafer to obtain the flow resistances depicted in Figure 1. For clarity, only one of the parallel channels and its switching valve are shown here.

thin, boron-doped silicon diaphragm that deflects in response to the pressure difference along R_3. The deflection causes a change in capacitance, which is measured by an external circuit.

Each valve includes a slightly raised valve seat covered by a thin undercut diaphragm of polysilicon or other material. The valve diaphragm and seat are formed in a monolithic batch process as part of the wafer-fabrication sequence. The diaphragm can be coated with nickel or another magnetic material to allow magnetic drive as shown, lifting the diaphragm away from the valve seat. Alternatively, electrostatic drive could be used. The process is compatible with the integration of circuitry on the structure for flow sensing and control.

This work was done by Kensall D. Wise of the University of Michigan for **Ames Research Center.**

Inquiries concerning rights for the commercial use of this invention should be addressed to the Patent Counsel, Ames Research Center
Refer to ARC-11704 /TN

Ames Research Ctr.
Moffett Field, CA 94035
Technology Utilization Officer: Laurance Milov
Mail Code 223-3
(415) 694-6370
Patent Counsel:
Darrell G. Brekke
Mail Code 200-11
(415) 694-5104

FOR ADDITIONAL INFORMATION: *Contact: Director, Technology Transfer Division, P.O. Box 8757, BWI Airport, MD. 21240; (301) 621-0100 Ext. 241*
REFER TO THE NUMBER LISTED AT THE END OF THE ARTICLE

Environmental Science & Technology

292 Fog Chamber Advances Air Pollution Studies

Software

293 BASIC Programming in Water and Wastewater Analysis — A collection of programs speeds routine calculations.

Lawrence Berkeley Laboratory

Fog Chamber Advances Air Pollution Studies

Experiments conducted in a fog chamber show that soot covered with a thin film of water catalyzes the formation of sulfate, a major constituent of acid rain, say scientists with the Lawrence Berkeley Laboratory's Atmospheric Aerosol Research Group. The Group recently developed the fog chamber to study the physics and chemistry of air pollutants.

"This is the first laboratory evidence supporting a hypothesis we formulated based on many collaborative field studies of highly polluted areas worldwide," says Group leader Tihomir Novakov.

This is also the first time a chamber of this type has been used to simulate the real-world atmosphere in order to study combustion-derived air pollution.

Sulfate formation in the chamber depends on three ingredients: liquid water, ammonia, and soot particles from the burning of sulfur-containing fuel. Sulfur dioxide released during the combustion process is converted to sulfate in an oxidation type of chemical reaction.

Novakov also plans to use the fog chamber to study the effects of acid rain and fog on biological systems. "One of our future directions will be an interfacing with biologists," he says. "We can expose cells to atmospheric systems created in the laboratory and find out what kind of damage results."

For example, the chamber will allow simulation of atmospheric conditions where vegetation loss is occurring and thereby enable the researchers to figure out which pollutants are responsible.

For Additional Information:

Mr. Robert Morris
Office of Research and Technology Application
50A-4112
Lawrence Berkeley Laboratory
Berkeley, CA 94720
Telephone (415) 486-6502

NASA Tech Brief
National Aeronautics and Space Administration

Computer Software

BASIC Programming in Water and Wastewater Analysis

A collection of programs speeds routine calculations.

This collection of computer programs has been assembled for use in water-analysis laboratories. A number of calculations are necessary for many types of routine chemical analysis, especially in a laboratory that has few or no automated analyzers. In this case, a personal or small business computer can be a valuable tool. The necessary formulas for calculations can be found in the appropriate manual for the specified analysis (USEPA, 1983) (APHA, 1981).

Quality-control calculations are necessary in a laboratory to assure an acceptable degree of accuracy and precision in a given analysis. The first program calculates quality-control parameters used in routine water analysis. These are percent recovery (of spikes) and the industrial statistic (of replicates) (USEPA, 1979).

Curve fitting must be done to calculate unknowns from a number of standards of different concentrations. The second program calculates the line (or curve) of best fit for the standard concentrations and absorbances entered. It provides the slope (M) and the Y-intercept (B), the equation of the line, and the correlation coefficient. A plot of the points is provided to aid the user in the choice among a straight line, log curve, or power curve.

Once the choice is made, the M, B, and correlation coefficient are recalculated using the necessary log conversions, when the second least-squares routine is run. The transformed points can be plotted to show whether they produce a fairly linear relationship. Once the satisfactory relationship is established, the unknowns can be calculated by entering absorbance values. This program also contains a subroutine for the calculation of the quality-control parameters so that the control checks can be made without leaving the program.

The third program calculates the specific conductance from the conductivity measurement and the temperature at which the measurement is taken. This then corrects the conductivity to 25 °C, giving the specific conductance.

The fourth program calculates any one of four types of residue measured in water. The appropriate residue calculation is specified, and weights and volumes are entered to yield the results.

The fifth, sixth, and seventh programs calculate the results of titrations commonly performed on water samples. Normalities and volumes are entered to yield the results.

The eighth program converts measurements, made with a dissolved-oxygen meter that does not compensate for salinity, to the actual dissolved-oxygen concentration using oxygen-saturation values for fresh and salt water. The measured value, salinity, and temperature are entered to yield the actual oxygen concentration.

The ninth and tenth programs perform calculations of two other common titrimetric analyses. Again, normality and volumes are entered to yield the results.

The eleventh program calculates the oil and grease residue from a water sample. To yield the results, the samples are extracted, and the weights are entered.

The last two programs use spectrophotometric measurements of absorbance at different wavelengths and residue measurements. These are used to calculate the concentrations of chlorophyll *a* and phaeophytin *a* in phytoplankton and periphyton and the biomass and autotrophic index of periphyton. Absorbances and weights are entered to yield the results.

The programs included in this collection were written for a Hewlett-Packard 2647F in H-P BASIC. All but the plotting routines can be easily translated for other computers that use the appropriate BASIC language. In the case of the plotting routines, the graphics for another manufacturer's computer will be addressed differently.

This program was written by Thomas Dreschel of Bionetics Corp. for **Kennedy Space Center.** *KSC-11298 /TN*

FOR ADDITIONAL INFORMATION *CONTACT:*

COSMIC®
112 Barrow Hall
University of Georgia
Athens, GA 30602
(404) 542-3265

Manufacturing, Machinery, & Tools

294 An Improved Method for Simulating Radiographs

295 Flexible Part Fixturing Device (Licensing Opportunity)

296 Higher-Quality Weld Joints for Tube Sections — Less material in weld inserts results in better fusion.

297 Lead Scales for X-Radiographs — Indentions are made by typing on lead tape.

298 Linear Anomaly in Welded 2219-T87 Aluminum Alloy — Microdensitometry can be used to distinguish between cracks and harmless anomalies in radiographs.

299 Making Double-Bevel End Cuts on Tubes — A fixture for a power saw saves time, eliminates waste, and ensures precision.

300 Pressure-Localizing Inserts for Bagging Laminations — These devices can compress composite laminates to conform to tight inside corners of the molds. (Licensing Opportunity)

301 Preset Electrodes for Electrical-Discharge Machining — Time-consuming loading and setting are eliminated. (Licensing Opportunity)

302 Single-Axis Acoustic Levitator with Rotation Control — Rotation-control equipment is simplified.

Testing & Instrumentation

303 Assessing the Reliability of NDE — A computer program assesses the ability of inspection techniques to find structural flaws.

Other Items of Interest

244 Minimum-Time Control for Robotic Manipulators — An existence theorem is proved for nonlinear systems.

245 Digital Control for Remote Manipulators — Multiple microprocessors enable large separations between controllers and manipulators.

An Improved Method for Simulating Radiographs

Parameters involved in generating actual radiographs and what can and cannot be modeled were examined. Using the spectral distribution of the radiation source and the mass absorption curve for the material comprising the part to be modeled, research determined the actual amount of radiation that would pass through a part and reach the film. This method increases confidence in the results of the simulation and enables the modeling of parts made of multiple materials. Simulation can account for the physical properties of the materials that comprise the part to be radiographed and the characteristics of the radiation source. Called simulated radiographs, these pictures have a number of potential uses: they can allow mechanical systems to be designed for future nondestructive evaluation, aid in radiation source positioning, and aid in the evaluation of actual radiographs. Using current software, the research could simulate radiographs that have a number of potential uses.

First, and foremost, they can be used during the design phase of complex mechanical systems-systems that are usually designed, prototyped, and even produced without concern for future nondestructive examination. When a radiograph of some component of the assembled system is required, a useful image often cannot be obtained, because the component of interest has been surrounded by other components that act as a mask. This results in the disassembling of the system. Considering the time and effort required to disassemble the system and the possibility that components will be ruined in the process, this is a very undesirable situation. However, by generating a simulated radiograph of the assembly, a designer could determine that a particular component will not be visible in a radiograph before the component is even manufactured. With this knowledge, the design could be altered to allow for future nondestructive examination.

Second, simulated radiographs can be used to evaluate actual radiographs. This is possible because the model of the part in the solid modeler is guaranteed to have no flaws. Third, simulated radiographs can be useful in the area of source positioning. A technician can reduce the number of actual radiographs that would have to be generated by using simulated radiographs to get a rough estimate of the proper source placement.

Finally, simulated radiographs can be used to subtract unwanted features from an actual radiograph. Unwanted features in a radiograph are often so numerous that the feature of interest is difficult to see. This problem could be reduced by using simulated radiographs and an image-processing system. With considerable improvements to current software, simulated radiographs might also be used to estimate exposure times and film and enhancing screen requirements. While it is not clear that the expense of running the simulation is less than the expense of generating an actual

radiograph, the ability to simulate radiographs can be a very useful tool-especially during the design process with its tremendous potential for cost savings.

FOR ADDITIONAL INFORMATION: A copy of the report is available from NTIS, Springfield, VA 22161; (703) 487-4600.

NTIS order number: DE87-006588/NAC

Price code: A02

To discuss this effort further, contact G. W. Laguna, Lawrence Livermore National Laboratory, U.S. DOE, University of California, Livermore, CA 94550.

NBS technology update

Licensing Opportunities

National Bureau of Standards
U.S. Department of Commerce
Gaithersburg, MD 20899

Flexible Part Fixturing Device

Two researchers from the NBS Center for Manufacturing Engineering have received a patent for a computer-controlled vise that can be configured automatically to grip a wide range of parts in a precise, known orientation for machining in a numerically controlled machine tool. The vise can automatically adjust the position of a workpiece in three dimensions, including its tilt along two axes. The vise can have interchangeable jaws for holding oddly shaped workpieces, and can be loaded and unloaded by a robot, making the device suitable for unattended operation in an automated machine shop producing small batches of many different parts. The programmable vise has been tested in the NBS Automated Manufacturing Research Facility.

FOR ADDITIONAL INFORMATION: The patent is assigned to the government, and may be licensed through the National Technical Information Service, Office of Federal Patent Licensing, Box 1423, Springfield, VA 22151; (703) 48704732. Refer to PAT-APPL-6-747486. A patent (4,685,661) has been issued.

NASA Tech Brief
National Aeronautics and
Space Administration

Higher-Quality Weld Joints for Tube Sections

Less material in weld inserts results in better fusion.

Marshall Space Flight Center, Alabama

A redesigned insert for joining tubes by welding improves the quality of the weld. Like its predecessor, the insert is a ring with a T-shaped cross section. In the new insert, however, the leg of the T is shorter so that it does not protrude into the tube cavity.

Occasionally, the old version was not fully consumed in the welding process because of its length. It therefore did not fuse completely with the tube sections. The new, short-leg insert is more easily consumed and decreases the chances of poor fusion on the inside wall. Its shorter leg also facilitates the detection of defects because the unconsumed edges of the tube become apparent during radiographic inspection.

A further advantage of the new insert is that it exhibits a small sag or dropthrough, if it has been properly welded. Dropthrough indicates full weld penetration, total consumption of the insert, and adequate fusion on the inside wall.

This work was done by John T. Olszewski of Rockwell International Corp. for **Marshall Space Flight Center**. *No further documentation is available.*
MFS-29190/TN

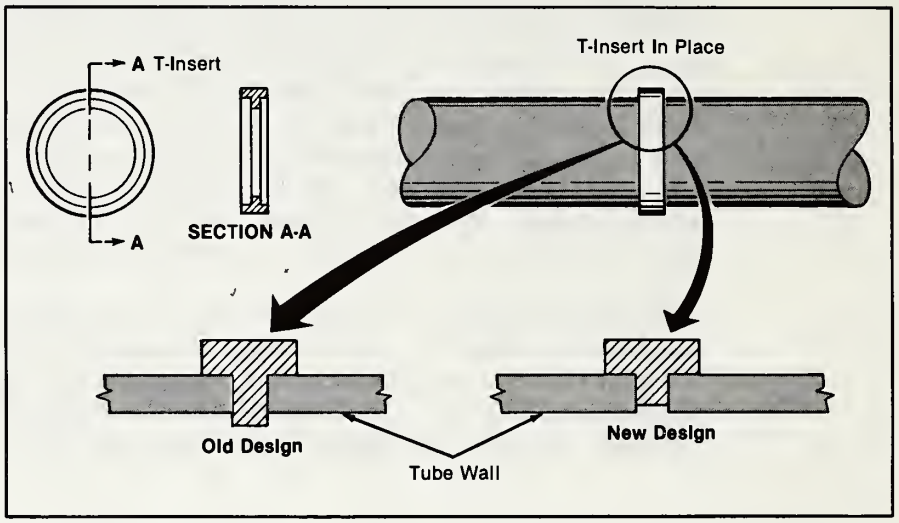

The New Welding Insert Does Not Protrude into the tube channel, whereas the old insert, with its longer-legged T-section, protruded significantly. The excess material sometimes prevented complete consumption of the insert and fusion with the tube section.

FOR ADDITIONAL INFORMATION: *Contact: Director, Technology Transfer Division, P.O. Box 8757, BWI Airport, MD. 21240; (301) 621-0100 Ext. 241*
REFER TO THE NUMBER LISTED AT THE END OF THE ARTICLE

NASA Tech Brief
National Aeronautics and Space Administration

Lead Scales for X-Radiographs

Indentations are made by typing on lead tape.

Marshall Space Flight Center, Alabama

Lead scales for inclusion in x-radiographs as length and position references can be created by repeatedly imprinting a character like upper-case I, L, or V, or lower-case L into lead tape with a typewriter. The character pitch of the typewriter serves as a length reference for the scale. The thinning of the tape caused by the impacts of the type shows up dark in the radiograph.

The typed lead-tape scales are more accurate and convenient to use than are the hand-cut sawtooth shapes or manually stamped scales that were often used on radiographs of weld defects and the like. Other information can also be typed on the lead tape for inclusion in the radiograph for purposes of identification or explanation. The typewriter ribbon should not be used for typing on the lead tape.

This work was done by Richard K. Burley and James F. Adams of Rockwell International Corp. for **Marshall Space Flight Center.** *No further documentation is available.*
MFS-29247/TN

FOR ADDITIONAL INFORMATION: *Contact: Director, Technology Transfer Division, P.O. Box 8757, BWI Airport, MD. 21240; (301) 621-0100 Ext. 241*
REFER TO THE NUMBER LISTED AT THE END OF THE ARTICLE

NASA Tech Brief
National Aeronautics and Space Administration

Linear Anomaly in Welded 2219-T87 Aluminum Alloy

Microdensitometry can be used to distinguish between cracks and harmless anomalies in radiographs.

A study of the causes and significance of two types of linear anomalies (also referred to as weld-radiograph enigmas) that sometimes appear in radiographs of welds is described in a preliminary report. The anomalies are manifested as light or dark linear features parallel to the weld line in a radiograph of a weld. Dark anomalies can be mistaken for weld cracks. The study was undertaken because the anomalies were observed in welds in 2219-T87 aluminum alloy, the alloy used to make the Space Shuttle external tank.

A variety of causes of the anomalies were identified. These include the thermal distribution and the flow of liquid metal during welding; the development of microstructure, second-phase particles, and porosity during solidification; and the pattern of residual stresses after the weld has cooled. The absorption and diffraction of x rays by internal and external weld features also contribute to the anomalies.

The report contains diagrams and descriptions of phenomena that occur during the welding process. It includes microdensitometer traces from x-radiographs of actual welds and from computer simulations based on the calculation of x-ray transmission through assumed weld structures.

The report concludes that the anomalies are not unique to the 2219-T87 aluminum alloy and cites literature references for similar features in other alloys. Microdensitometer traces across suspect features show promise for distinguishing between linear anomalies and cracks: the anomaly images are less dense than crack images, the image-density difference for an anomaly being about 0.1 and that for a crack about 0.5.

This work was done by Wartan A. Jemian of Auburn University for **Marshall Space Flight Center**. *Further information may be found in NASA CR-178745 [N86-22685/NSP], [A03] "On the Determination of Linear Anomaly in the Macrostructure of VPPA Welded 2219-787 Aluminum Alloy — Preliminary Report."*

Copies may be purchased from the National Technical Information Service, Springfield, Virginia 22161, MFS-27152 /TN

FOR ADDITIONAL INFORMATION: *Contact: Director, Technology Transfer Division, P.O. Box 8757, BWI Airport, MD. 21240; (301) 621-0100 Ext. 241*
REFER TO THE NUMBER LISTED AT THE END OF THE ARTICLE

NASA Tech Brief
National Aeronautics and Space Administration
Lyndon B. Johnson Space Center, Houston, Texas

Making Double-Bevel End Cuts on Tubes

A fixture for a power saw saves time, eliminates waste, and ensures precision.

With the aid of a new fixture, tubing sections can be cut so that they mate precisely at orthogonal joints, such as those at the corners of protective railings, for example. The fixture orients the end of a section at the correct angle for two sequential cuts by a power hacksaw or bandsaw. It eliminates cut-and-try methods, thereby saving time and labor and reducing waste.

The fixture is made from a notched, generally L-shaped plate. A tube rests in a notch in one leg of the fixture, secured by a roller chain that is pulled tightly around the tube section by a thumb screw (see figure). With one end of the tube in the fixture and the other end in a clamp on the power saw, the tube is leveled, and the first cut is made. The tube and fixture are rotated 90° and releveled, and the second cut is made. The tube end is then beveled so that it will mate precisely for welding with two mutually perpendicular tubes cut similarly.

This work was done by Joseph R. Cardenas and Harvey L. Berg of Rockwell International Corp. for **Johnson Space Center**. *MSC-21135 /TN*

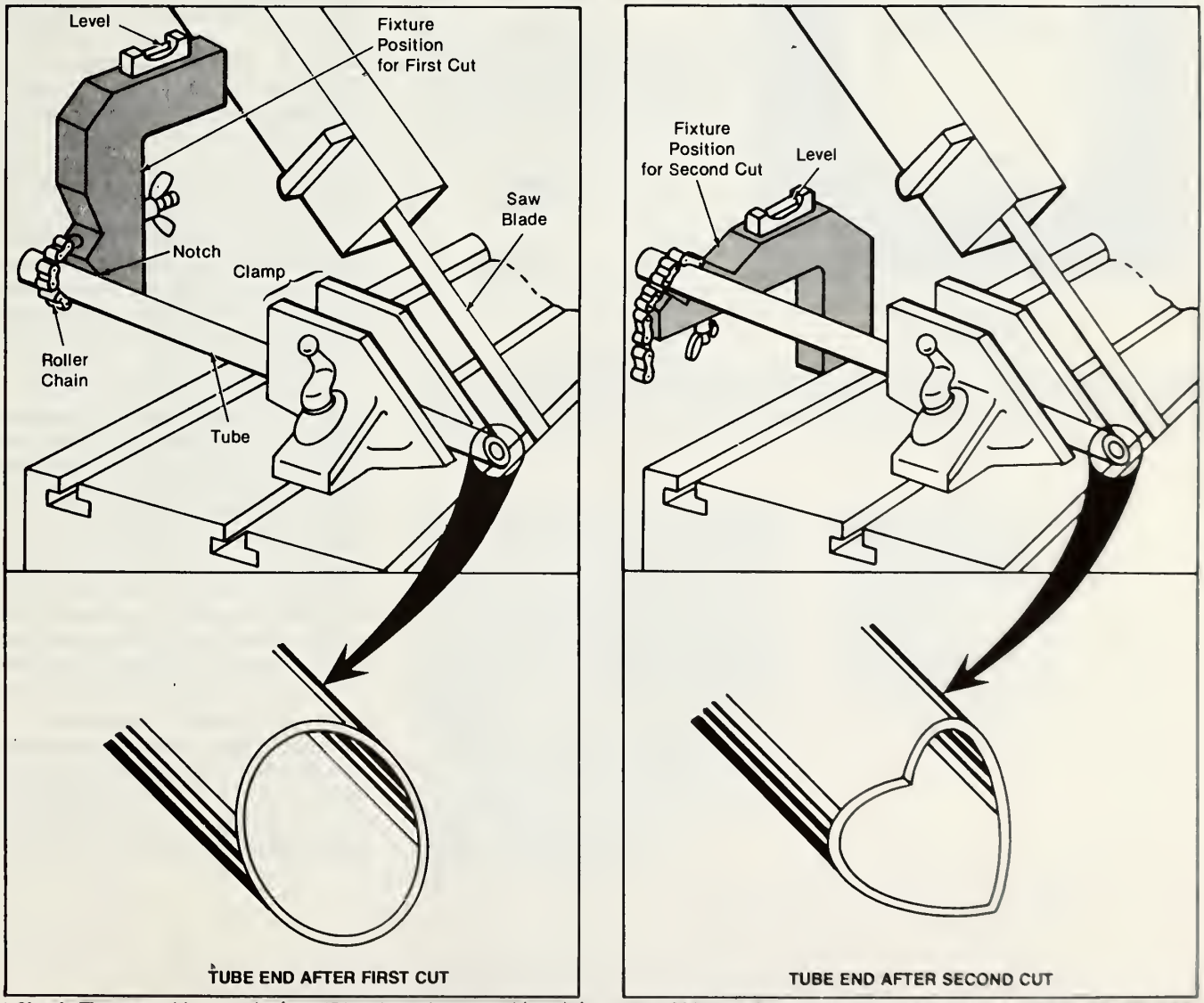

A **Simple Fixture** positions a tube for a 45° end cut, then repositions it for a cut at 90° to the first cut. A roller chain holds the tube in place for both cuts.

FOR ADDITIONAL INFORMATION: *Contact: Director, Technology Transfer Division, P.O. Box 8757, BWI Airport, MD. 21240; (301) 621-0100 Ext. 241*
REFER TO THE NUMBER LISTED AT THE END OF THE ARTICLE

NASA Tech Brief
National Aeronautics and Space Administration

Licensing Opportunity

Pressure-Localizing Inserts for Bagging Laminations

These devices can compress composite laminates to conform to tight inside corners of the molds.

Ames Research Center, Moffett Field, California

The proposed use of a pressure-localizing insert would allow composite laminates to be compacted into tight corners by conventional pressure- or vacuum-bagging techniques. Because of this manufacturing technique, a larger selection of part shapes would become amenable to lamination.

In conventional bagging, a uniform pressure is applied to all areas of the part; consequently, the laminates often fail to conform to tight inside curves or corners. One technique for avoiding this problem is the use of a staggered array of laminas, with expansion joints between adjacent pieces in the same layer (see Figure 1). However, the applied pressure load often produces enough friction to prevent the laminas from slipping into the corners, with the result that corner voids remain between the mold and the laminate.

In the proposed technique, the staggered laminas would be bridged by an insert that localizes the applied pressure at the tight corners (see Figure 2). Consisting of a rigid bar connecting rubber or silicone "rope" pieces that conform to the corners, the insert would provide high compaction force to the corners, while allowing the laminas to slip into the corners. Following compaction of the tight corners, these inserts could be removed to allow conventional compaction to complete the lamination.

A modification of this technique would require only a single bagging operation. The insert would include a flexible connecting bar. The insert would deliver localized pressures to begin corner compaction at a relatively low bagging pressure. However, at the customary bagging pressure of 50 psi (3.4×10^5 N/m^2), the connecting bar would yield so that its entire length would press on the laminas.

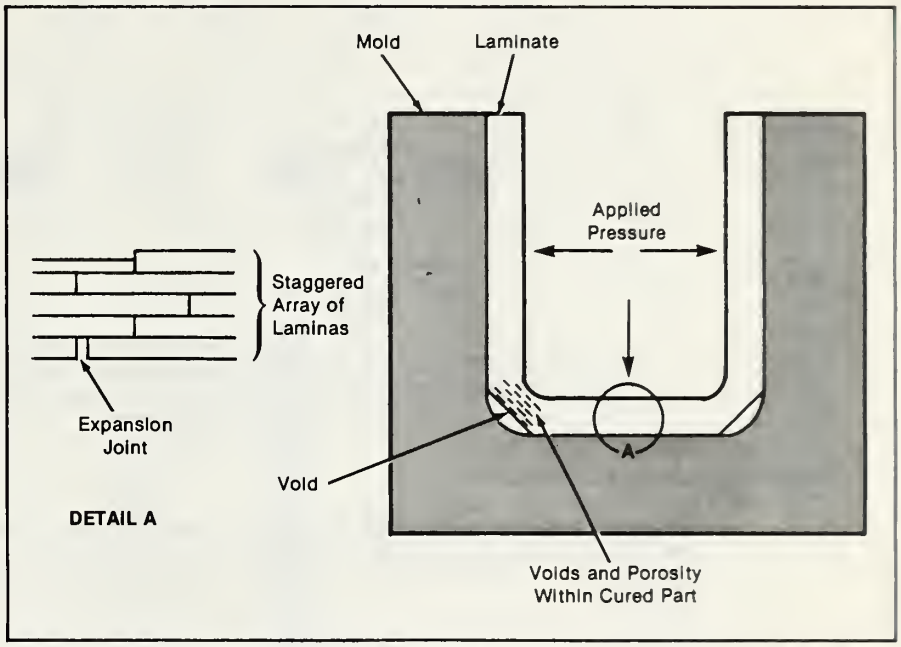

Figure 1. During **Conventional Bagging** the applied pressure can give rise to friction that prevents the laminate from slipping into tight corners, leaving voids between the mold and the laminate.

This work was done by Dave Schmaling and Donald Carter of United Technologies Corp. for **Ames Research Center.** *No further documentation is available.*

Inquiries concerning rights for the commercial use of this invention should be addressed to the Patent Counsel, Ames Research Center
Refer to ARC-11673/TN

Ames Research Ctr.
Moffett Field, CA 94035
Technology Utilization Officer: Laurance Milov
Mail Code 223-3
(415) 694-6370
Patent Counsel: Darrell G. Brekke
Mail Code 200-11
(415) 694-5104

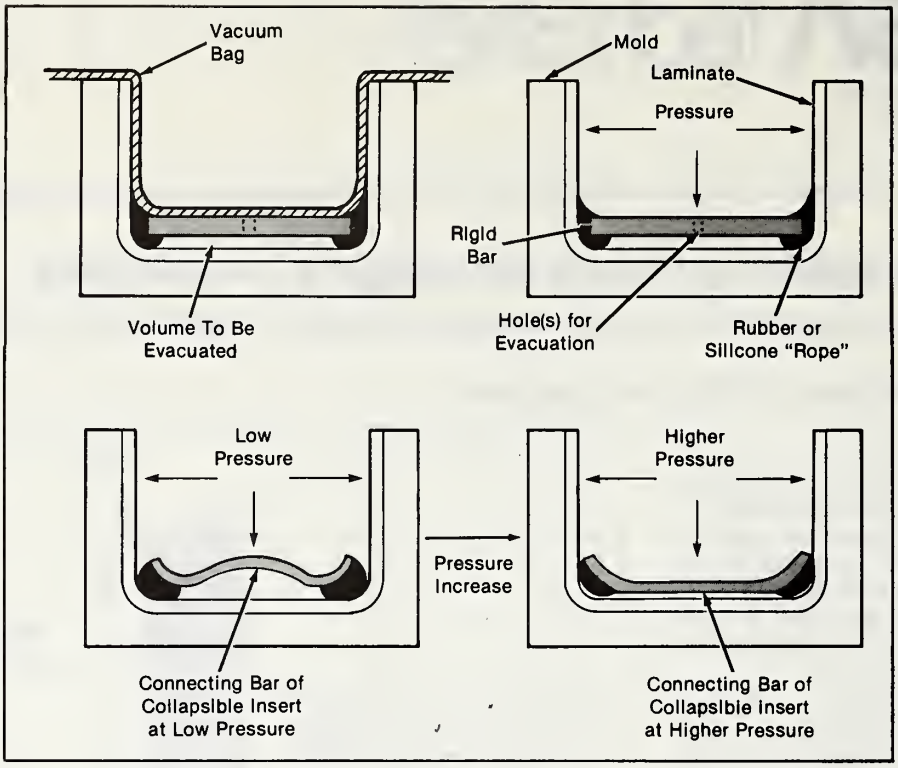

Figure 2. **Localized Pressure** might insure conformity of the mold and the laminate in tight corners. A rigid insert (above) would require a second bagging step. Only one bagging step would be required if the insert is collapsible (below).

FOR ADDITIONAL INFORMATION: *Contact: Director, Technology Transfer Division, P.O. Box 8757, BWI Airport, MD. 21240; (301) 621-0100 Ext. 241*

REFER TO THE NUMBER LISTED AT THE END OF THE ARTICLE

NASA Tech Brief
National Aeronautics and Space Administration

Licensing Opportunity

Preset Electrodes for Electrical-Discharge Machining

Time-consuming loading and setting are eliminated.

Marshall Space Flight Center, Alabama

A new electrode holder for electrical-discharge machining (EDM) provides for the repeatable loading and setting of many electrodes. With the previous holder, each time an electrode was replaced, it had to be carefully set with respect to a master part.

The new holder is a rotating-index tool carrying six, eight, or possibly more electrodes (see figure). Before use, all of the electrodes are set with the aid of a ring that surrounds the tool, and are locked in position with screws.

When an electrode is to be replaced, the EDM operator pulls a spring-loaded pin on the tool so that it can be rotated about a center pin. A fresh electrode is thus rotated into position against the workpiece.

This work was done by Bill E. Coker of Rockwell International Corp. for **Marshall Space Flight Center**.

Inquiries concerning rights for the commercial use of this invention should be addressed to the Patent Counsel, Marshall Space Flight Center
Refer to MFS-29198/TN

George C. Marshall Space Flight Center
Marshall Space Flight Center, AL 35812
Technology Utilization Officer: Ismail Akbay
Code AT01
(205) 544-2223
Patent Counsel:
Leon D. Wofford, Jr.
Mail Code CC01
(205) 544-0024

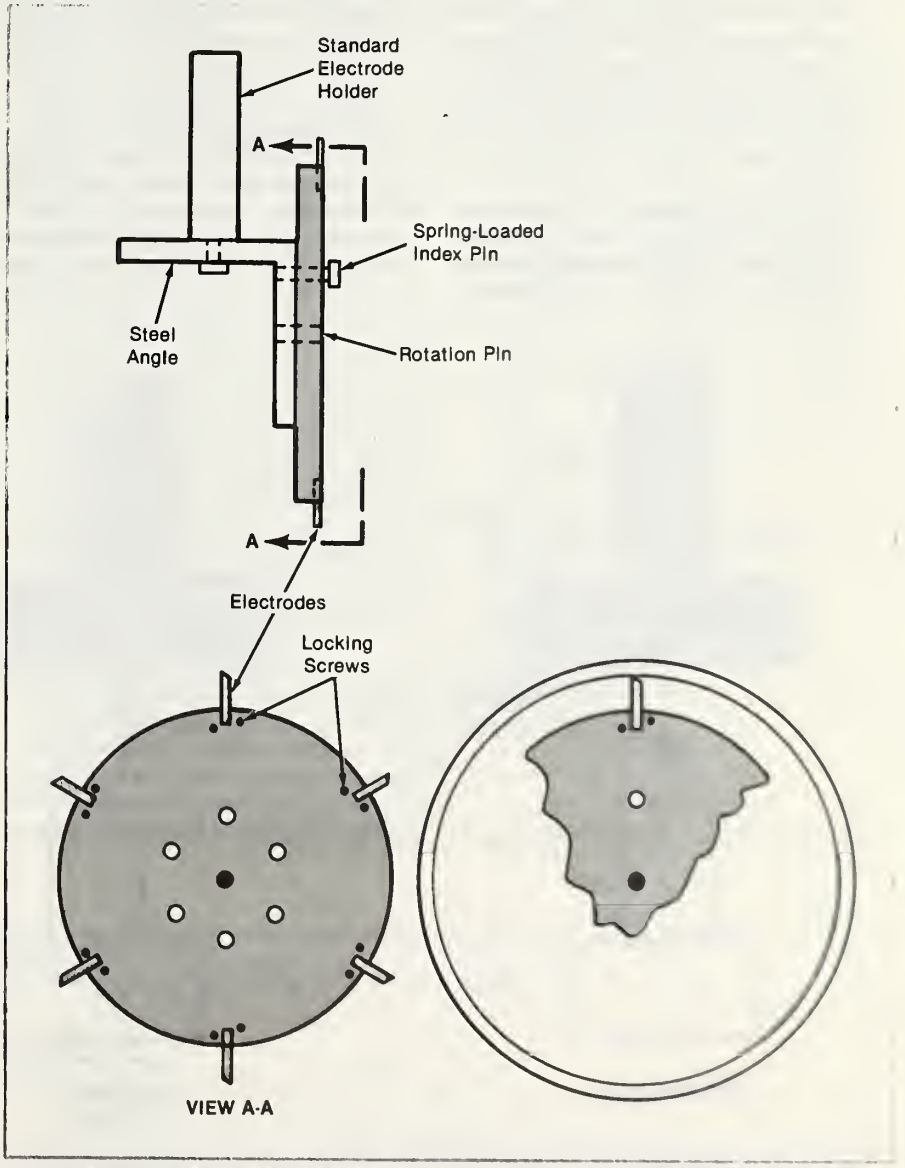

Any One of Six Electrodes on a Disk can be rotated into position for electrical-discharge machining. All the electrodes are set by contact with a ring.

NASA Tech Brief
National Aeronautics and Space Administration

Single-Axis Acoustic Levitator With Rotation Control

Rotation-control equipment is simplified.

NASA's Jet Propulsion Laboratory, Pasadena, California

An acoustic levitator with rotation control handles liquid and solid specimens as dense as steel in both low gravity and normal Earth gravity. Unlike conventional acoustic levitators that rotate samples in a controlled manner, this one does not require three acoustic drivers in a chamber of square cross section nor does it depend on the maintenance of a precise phase relationship between the two acoustic drivers associated with the two axes of the square.

The new levitator is of the single-axis type. A circularly symmetrical acoustic driver excites a standing acoustic wave under a circularly symmetrical reflector, which is wider than the driver. The specimen is suspended at a point between the driver and the reflector. Operating at a frequency above 10 kHz, the levitator can handle specimens ranging in size from 8 mm to 0.1 mm. The exact resonance frequency of the chamber is adjusted to accommodate the size of the specimen.

When the driver and reflector are coaxial, the levitating acoustic field exerts no torque on the specimen. When the reflector is moved aside, however, (see figure) the specimen translates with the reflector into the off-axis region of the airflow field induced by the acoustic driver. In this region, the flow exerts a torque about a rotation axis perpendicular to the driver axis and to the direction of offset. Thus, by offsetting the reflector in a chosen direction, the specimen can be made to rotate about any axis in a plane perpendicular to the axis of the driver. The torque, and therefore the speed of rotation, can be adjusted by the choice of the offset distance or of the acoustic pressure. In experiments, solid spheres have been rotated as fast as 50 revolutions per second.

This work was done by E. H. Trinh and E. E. Olli of Caltech for **NASA's Jet Propulsion Laboratory.**

NPO-16924/TN

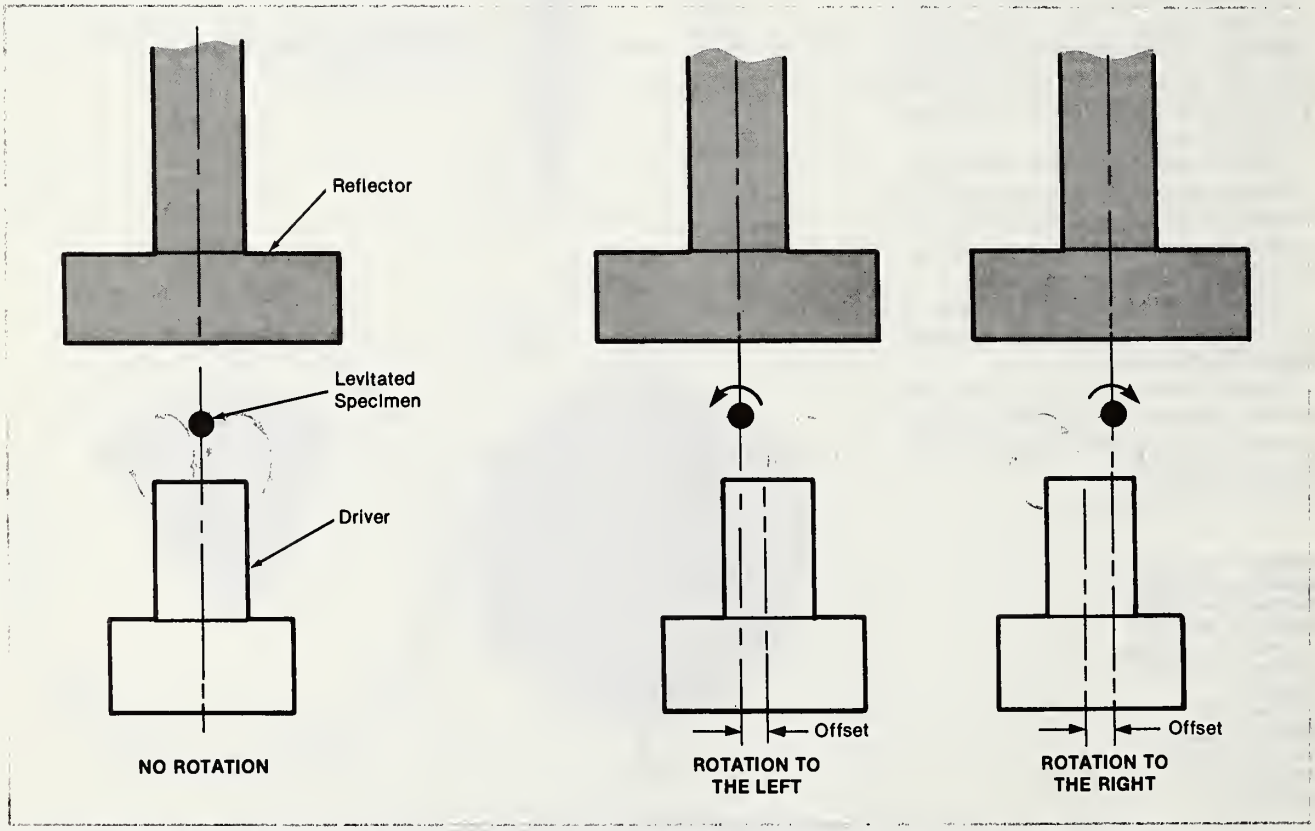

The **Acoustic Reflector Can Be Translated** perpendicularly to the axis of the acoustic driver to move the specimen to different parts of the levitating acoustic field. When the reflector and driver are not coaxial, the acoustic field makes the specimen rotate.

FOR ADDITIONAL INFORMATION: *Contact: Director, Technology Transfer Division, P.O. Box 8757, BWI Airport, MD. 21240; (301) 621-0100 Ext. 241*
REFER TO THE NUMBER LISTED AT THE END OF THE ARTICLE

NASA Tech Brief
National Aeronautics and Space Administration

Computer Software

Assessing the Reliability of NDE

A computer program assesses the ability of inspection techniques to find structural flaws.

A versatile FORTRAN computer algorithm has been developed for calculating and plotting the reliability of a nondestructive evaluation (NDE) technique for the inspection of flaws. The algorithm was developed specifically to determine the reliability of radiographic and ultrasonic methods for the detection of critical flaws in structural ceramic materials. Reliability is displayed in the form of a plot of the probability of detection (at a selected confidence level) versus the flaw size.

NDE methods are used in such applications as diagnostic medicine, quality control in industrial production, and the prediction of failure in structural components. In the latter application, sensitive, reliable NDE techniques are needed to (1) detect flaws and reject parts containing critical flaws or concentrated flaw populations and (2) aid in the optimization of processes by identifying the stages of fabrication during which flaws are introduced.

The reliability of an NDE inspection technique is a quantitative measure of the ability of that technique to detect flaws of a specific type and size in a particular material. In experiments to determine reliability, specially prepared specimens containing a known number of accurately characterized flaws are inspected. Data are gathered on the number and size of flaws detected. Applying binomial-distribution statistical theory to these data, reliability is then calculated in terms of the probabilities of detection at specific confidence levels for various flaw sizes. This calculation requires great computational effort.

This new FORTRAN program calculates and plots the reliability of flaw inspection by NDE. The program was written for a Digital PDP 11/45 minicomputer interfaced with Control/Grinnell 274 image processor. Its task file requires 64 kilobytes (125 blocks) of memory.

Initially, flaw-inspection data are entered into the computer and stored in files. These data are arranged in intervals using the options of equal flaw-size interval, overlapping flaw-size interval, or optimized probability methods. The user selects the interval sizes and method of data grouping, and a record of the number and size of flaws examined and detected per interval is stored. The probability of detection is then calculated over the range of flaw-size data using any preselected confidence level.

Two types of plots displaying quantitative flaw-detectability results are generated on a video monitor by use of the image-processor software routines. One plot shows the number of flaws examined and detected versus the flaw size or flaw size/part thickness. The second plot shows the probability of detection (at the selected confidence level) versus the flaw size or flaw size/part thickness.

An application of the technique includes the determination of the reliability of an NDE inspection technique for detecting such critical flaws as voids, cracks, foreign impurity particles, and delaminations in metal, ceramic, polymeric, and composite structural components. Industrial interests might include developers of NDE inspection equipment who wish to evaluate the reliability of the equipment for flaw detection and producers and users of structural components who use NDE methods to detect flaws deemed critical to component integrity.

This program was written by Don J. Roth of **Lewis Research Center**.

LEW-14286 /TN

FOR ADDITIONAL INFORMATION *CONTACT:*

COSMIC®
112 Barrow Hall
University of Georgia
Athens, GA 30602
(404) 542-3265

FOR ADDITIONAL INFORMATION: *Contact: Director, Technology Transfer Division, P.O. Box 8757, BWI Airport, MD. 21240; (301) 621-0100 Ext. 241*
REFER TO THE NUMBER LISTED AT THE END OF THE ARTICLE

Materials

304 Rapidly Solidified Magnesium-Base and Titanium-Base Alloys

305 Development of a Primer/Topcoat and Flexible Primer for Aluminum

306 Nickel Aluminides-New Superalloys for the Future (Licensing Opportunity)

307 ZZX-4200 High-Temperature Thermal Insulation Structures (Licensing Opportunity)

308 Amorphous Insulator Films with Controllable Properties — These films have potential for optical, electronic, magnetic, and mechanical applications.

309 Bismaleimide Copolymer Matrix Resins — Bismaleimide copolymers yield strong graphite composites. (Licensing Opportunity)

310 Determining Directions of Ultrasound in Solids — Ultrasound shadows are cast by grooves.

311 Fatigue Lives of Materials Cut be Lasers — Laser machining may help to balance high-speed rotating machinery.

312 Fluidized-Bed Cleaning of Silicon Particles — Metallic impurities are removed by acids.

313 Mixing Valve for Protein-Crystal Growth — A multichamber unit combines reactants as necessary. (Licensing Opportunity)

314 Protective Coatings for Spacecraft Polymers — Thin films of metal-oxide/polymer are applied by ion-beam sputtering. (Licensing Opportunity)

315 Radiation Resistances fo Dielectric Liquids — Although data are sparse for some liquids, polyphenyls appear to be particularly stable.

316 Thermomechanical Properties Indicate Degree of Epoxy Cure — The glass-transition temperature and the density increase as the reaction proceeds.

317 Tribological Properties of Structural Ceramics — Studies of wear and lubrication promote longer component lives.

Other Items of Interest

298 Linear Anomaly in Welded 2219-T87 Aluminum Alloy — Microdensitometry can be used to distinguish between cracks and harmless anomalies in radiographs.

U.S. Air Force
Technology Note

Rapidly Solidified Magnesium-Base and Titanium-Base Alloys

Progress in the development of magnesium-base titanium-base alloys using rapid-solidification processes is described in a review article prepared by researchers from the University of Sheffield, Lockheed, General Electric, and the Air Force Materials Laboratory. Information described in this review was obtained from 87 publications or reports of research in progress and provides an excellent picture of the present status of these very promising new materials.

A variety of processes have been used to produce rapidly solidified magnesium-base alloys. Improvements in both fabricability and properties have resulted. Among the objectives of these studies have been a reduction in hot-shortness, improved resistance to stress-corrosion cracking, introduction of superplastic behavior, increased compressive yield strength, and improved toughness. Corrosion resistance can also be considerably enhanced by means of rapid solidification.

Titanium alloys are also amenable to rapid-solidification processing, despite the high reactivity of molten titanium with most container materials. Most studies of rapidly solidified titanium-base alloys appear to have concentrated on the introduction of alloying elements exhibiting relatively low solid solubility. Attractive properties result from the ability to produce uniform, fine dispersions by addition of elements such as Y, B, C, and Si. Appreciable benefits have also been reported to result from the beta-grain refinement possible by rapid-solidification processing.

FOR ADDITIONAL INFORMATION: "The Current Status of Rapid Solidification of Magnesium-Base and Titanium-Base Alloys", The International Journal of Powder Metallurgy, Vol 23:1 Jan 1987, pp13-24

Development of a Primer/Topcoat and Flexible Primer for Aluminum

Two corrosion preventive organic coatings have been developed for use on aluminum and specifically for application on Navy aircraft. They provide two alternatives for improving aircraft paint systems. The first coating can be applied directly to an aluminum substrate and perform as a self-priming topcoat. It consists of a two component, aliphatic polyurethane binder with titanium dioxide, zinc molybdate, zinc phosphate, an organo-zinc salt, and titanium dioxide vesiculated bead pigments. This primer/topcoat meets or exceeds all of the critical performance requirements of the current Navy aircraft paint system. Mil-P-23377 epoxy primer and Mil-C-83286 polyurethane topcoat. It exhibits good adhesion, corrosion inhibition, flexibility, chemical and weather resistance. The use of this coating will reduce: Paint application and removal time and manpower; Aircraft weight; Aircraft downtime; and Volatile organic component (VOC) and chromate emissions. The second coating is a flexible primer which was developed using the above polyurethane binder. It contains strontium chromate zinc chromate, barium chromate, and zinc molybdate corrosion inhibiting pigments. The primer meets or exceeds all of the performance requirements of Mil-P-23377 and has significantly more flexibility. Aluminum specimens coated with the NADC flexible primer remained in 5% salt spray for one year without any corrosion of the aluminum or damage to the coating.

For Additional Information:

A full description of this activity is contained in a backup report which may be purchased from NTIS, Springfield, VA 22161; (703) 487-4650.
NTIS order number: AD-A182 132/1/NAC
Price code: A03
To discuss this effort further, contact:
C.R. Hegedus, Air Vehicle and Crew Systems Technology Directorate
Naval Air Development Center, Warminster, PA18974-5000; (215) 441-1452.

Department of Energy

Technology Application

Oak Ridge National Laboratory

NICKEL ALUMINIDES—NEW SUPERALLOYS FOR THE FUTURE

Nickel aluminides (Ni_3Al and its derivatives containing chromium) are a new class of alloys that have a unique combination of high temperature properties and corrosion resistance. Nickel aluminides are ordered intermetallic compounds of Ni_3Al composition that have increased ductility because of small additions of boron and increased strength because of small additions of zirconium and hafnium. Because of their high aluminum content, these alloys are 10 to 20% lower in density than most commercial nickel-based superalloys. These alloys are simpler in composition, single phase in microstructure, show increase in yield strength with increasing temperature up to 800°C (1472°F) (most alloys show a decrease in yield strength with increasing temperature) (Fig. 1), have excellent oxidation resistance at temperatures up to 1000°C (1832°F), and show excellent corrosion resistance in most aqueous solutions. These alloys can be cold worked to obtain yield strengths over 200 ksi at room temperature. Also, these alloys can be fabricated by powder metallurgy, by electroslag remelting and extrusing, air melting, and near-net-shape casting into sheet, bar, or components. The fine-grained material (cast or powder metallurgy) can also be superplastically formed into near-net shapes. This technology

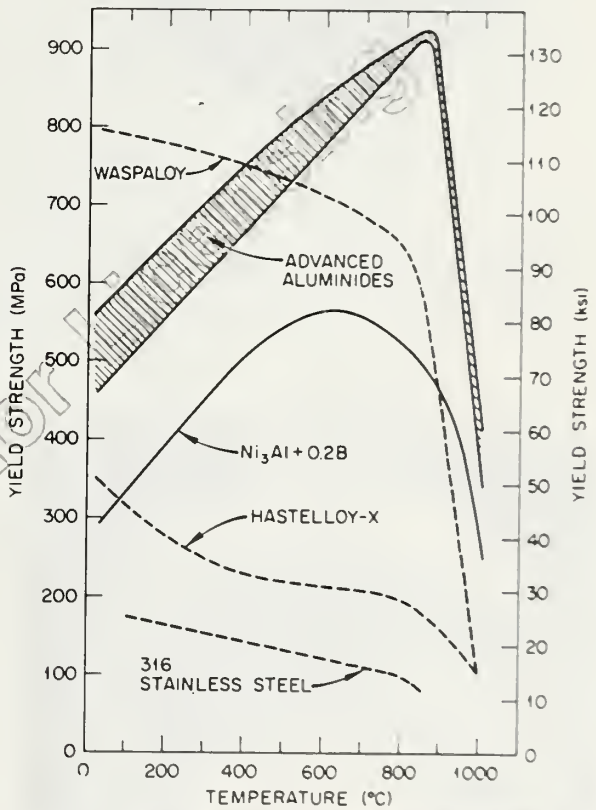

Fig. 1. Yield strength of advanced aluminides compared with other alloys.

was developed at the Oak Ridge National Laboratory and funded by the Department of Energy. Use of this technology in a variety of applications is already being considered and is further encouraged.

Up to 227-kg (500-lb) heats of nickel aluminides have been melted commercially and

Now Available for

processed into a range of shapes by conventional and unconventional techniques. The powder from these materials has been consolidated by extrusion, hot isostatic pressing, isothermal isostatic pressing, and consolidating in glass molds under atmospheric pressure (Fig. 2).

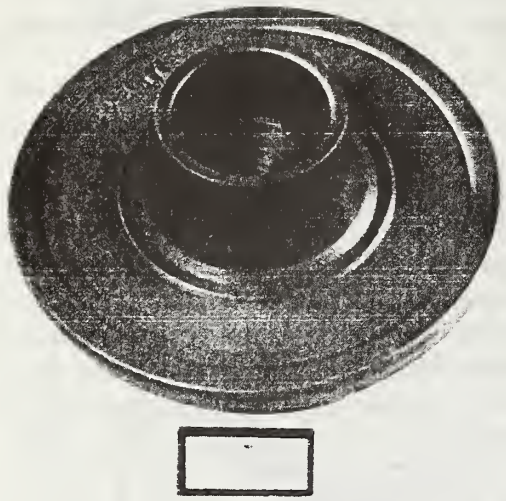

Fig. 2. Prototypic turbine disk fabricated by isothermal forging.

Mechanical properties including tensile, creep, fatigue, and crack growth are under way at room temperature up to 1100°C (2012°F). Sufficient data are available to provide strength values for design evaluation studies. Aqueous corrosion and high temperature oxidation and corrosion data are also available. Wear and machinability studies are currently under way.

Additional information:

Office of Technology Applications
Information Service
Martin Marietta Energy Systems, Inc.
P.O. Box X
Oak Ridge, TN 37831
Telephone: (615) 574-4192; FTS 624-4192

C. T. Liu and V. K. Sikka, "Nickel Aluminides for Structural Use," *Journal of Metals*, **38**, 5, 19-21 (May 1986).

V. K. Sikka, "Processing Technology for Nickel Aluminide," to be published in Proceedings of MRS Fall Meeting, Boston, Mass., December 1-6, 1986.

Department of Energy

Technology Application

Oak Ridge National Laboratory

ZZX-4200 High-Temperature Thermal Insulation Structures

ZZX-4200 high-temperature thermal insulation structures are a family of low-density, molded-fiber insulation shapes that can be used to an operating temperature of 4200°F (2590 K) in vacuum, inert, and oxidizing environments. ZZX-4200 structures are uniquely qualified for use in oxidizing environments at temperatures above 3200°F (2030 K) and are suitable for use as highly efficient thermal insulation in aerospace systems and high-temperature industrial processes. Typical applications include backup insulation for aerospace leading edges and supersonic entry and exit cones, furnace chamber insulation, conformal shape insulation for refractory specialty shapes, low-pressure combustion chambers, heat exchangers, and hot-gas filters.

ZZX-4200 insulation structures are porous composites of zirconia-bonded zirconia fibers that are partially stabilized in the cubic phase with 3 to 5 vol % yttria. Partially stabilized zirconia is a refractory oxide material that melts at 4773°F (2907 K) and has a theoretical density of 349 pcf (5.82 g/cm^3). As produced, ZZX-4200 structures have a bulk density of 55 pcf (0.92 g/cm^3), which increases to a maximum of 75 pcf (1.25 g/cm^3) after extended service above 3500°F (2200 K). Standard insulation shapes (cylinders, frustra, and domes) are manufactured in sizes up to 15 in. (38 cm) in diameter by 15 in. (38 cm) long. Other geometries are designed and produced to meet specific customer requirements.

The thermal efficiency of ZZX-4200 structures is maximized by the technique used to produce the molded shapes. This unique molding

Cross-section of ZZX-4200 insulator for high-temperature research furnace.

technique ensures that the fibers are oriented perpendicular (85°-95°) to the wall thickness of the structure; this orientation reduces heat flow by a factor of 2 compared with that in homogeneous materials and randomly oriented fiber structures.

ZZX-4200 technology will allow development of new classes of research and industrial process furnaces that must operate at temperatures above 3650°F (2285 K) in oxidizing atmospheres. No other fiber insulation structures can be used in oxidizing environments at temperatures in the 3200°F (2035 K) to 4200°F (2590 K) range. The operating limit for conventional ceramic fiber structures is 2800°F (1810 K). Other types of specialty oxide fiber insulation structures cannot be used above 3100°F (1980 K).

Additional information:

Office of Technology Applications
Information Service
Martin Marietta Energy Systems, Inc.
P.O. Box X
Oak Ridge, TN 37831
Telephone: (615) 574-4192; FTS 624-4192

G. E. Wrenn, Jr., et al., *Zirconia-Bonded Zirconia Fiber Insulation Structures*, Y/DV-378, Oak Ridge Y-12 Plant (July 1984).

NASA Tech Brief
National Aeronautics and Space Administration

Amorphous Insulator Films With Controllable Properties

These films have potential for optical, electronic, magnetic, and mechanical applications.

In experiments described in a report, amorphous hydrogenated carbon (a-C:H) films were grown at room temperature by low-frequency plasma deposition, using methane or butane gas. These films have a unique array of useful properties: (a) they adhere to a wide variety of materials (including quartz insulators, semiconductors, and metals); (b) they contain only carbon and hydrogen; (c) they are very smooth and free of pinholes; (d) they are resistant to attack by moisture and chemicals; and (e) they have high electric-breakdown strength and electrical resistivity. Two of the optical properties (refractive index and absorption coefficient) and the hardness of this film can be controlled by the deposition conditions.

In this work, the film thickness of the a-C:H varied from 2 to 30 μin. (0.05 to 0.76 μm), and the deposition time was kept at or below 30 min. The films were smooth [better than 0.1 μin. (0.0025 μm)], uniform (better than ±2 percent), and without an overlayer or interface layer. Some deposition conditions resulted in a-C:H films so hard that they were not easily scratched by a sharp carbide edge.

In an application where the transparency edge (the light frequency or wavelength corresponding to 1 percent absorption) is required to be in the deep ultraviolet [down to a wavelength of 10 μin. (0.25 μm)], another amorphous insulator film can be used; namely, boron nitride (BN). The BN films are generally similar to the a-C:H films. Deposition techniques for BN are different from those for a-C:H. The amorphous a-C:H and BN films are expected to be used for the hermetic sealing and protection of optical, electronic, magnetic, or delicate mechanical systems, and for semiconductor field dielectrics.

This work was done by Samuel A. Alterovitz, Joseph D. Warner, David C. Liu, and John J. Pouch of **Lewis Research Center**. *Further information may be found in NASA TM-87135 [N86-12134/NSP], "Ellipsometric and Optical Study of Some Uncommon Insulator Films on III-V Semiconductors."*

Copies may be purchased from the National Technical Information Service, Springfield, Virginia 22161, [A02]
LEW-14370 /TN

FOR ADDITIONAL INFORMATION: *Contact: Director, Technology Transfer Division, P.O. Box 8757, BWI Airport, MD. 21240; (301) 621-0100 Ext. 241*
REFER TO THE NUMBER LISTED AT THE END OF THE ARTICLE

NASA Tech Brief
National Aeronautics and Space Administration

Licensing Opportunity

Bismaleimide Copolymer Matrix Resins

Bismaleimide copolymers yield strong graphite composites.

Ames Research Center, Moffett Field, California

Graphite composites, prepared from a 1:1 copolymer of two new bismaleimides based on the N,N′-m-phenylene-bis(m-amino-benzamide) structure have mechanical properties superior to those prepared from other bismaleimide-type resins. The new heat-resistant composites could replace metal in some structural applications.

The bismaleimide monomer (BMI-1) and the methyl-substituted monomer (MBMI-1) are prepared by the reaction of N,N′-m-phenylene-bis (m-amino-benzamide) (MMAB) with maleic anhydride or citraconic anhydride in N,N-dimethylformamide (DMF) at room temperature, followed by the elimination of water by use of sodium acetate and acetic anhydride at room temperature (see figure). After 3 to 4 h of stirring, the DMF solutions are poured into water, yielding the solid monomers.

The monomers are collected, washed with water, and dried in vacuum at 60 °C. For BMI-1 the melting point is 235 °C, and the curing temperature is 244 °C. For MBMI-1 the melting point is 147 °C, and the curing temperature is 217 °C. A 1:1 (molar) mixture of BMI-1 and MBMI-1 melts and cures at 142 °C and 213 °C, respectively.

The composite prepregs are prepared by coating graphite cloth with a DMF or DMF/acetone (1:1) solution of the resin, then drying them in a vacuum oven at 100 °C for 1 h. The dried prepreg is stacked and pressed between aluminum plates covered with polytetrafluoroethylene film. The laminate is then cured in a flat-platen press at 200 ° to 240 °C at a pressure of 100 psi (690 kN/m^2) for 5 to 6 h.

These composite mixtures of the two resins exhibit better handling, processing, mechanical, and thermal properties than do the individual resins. The strongest composites are made from a 1:1 copolymer of the two resins; these possess excellent mechanical strength at both ambient and elevated temperatures. They are stronger than composites made of epoxy. They are also stronger than composites made from BMI-2 and MBMI-2 resins (which are similar except that they are formed from the popular methylenedianiline). Even in the case of BMI-2 and MBMI-2, however, copolymers show better properties than do the individual resins.

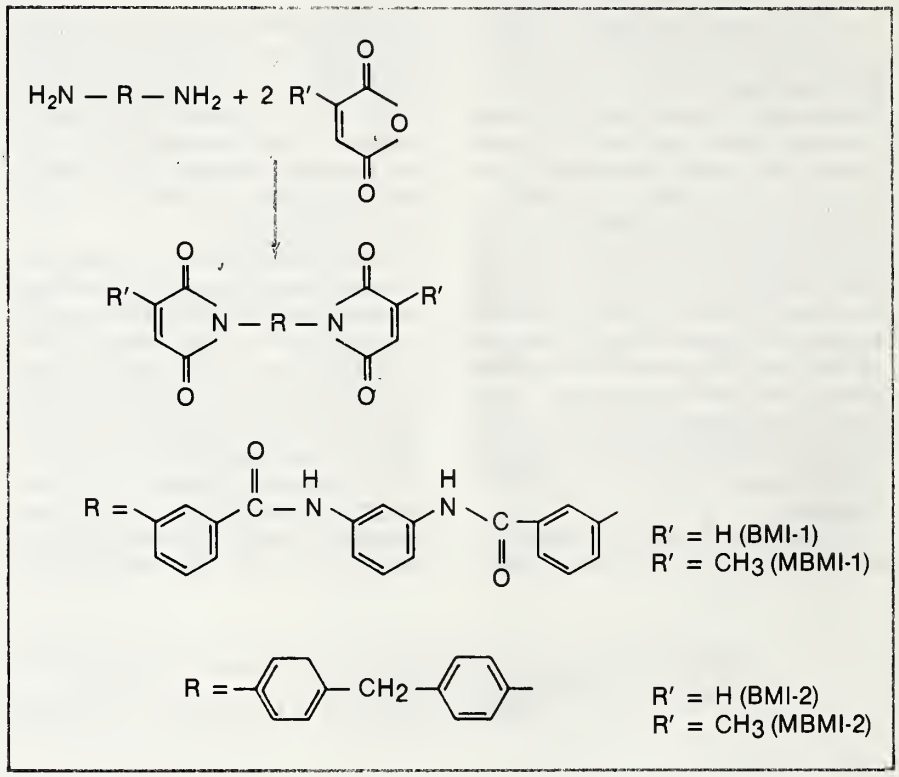

The **Monomers** used to form copolymers with superior mechanical properties are prepared by the reaction of MMAB with maleic or citraconic anhydride.

This work was done by John A. Parker and Alvin H. Heimbuch of the **Ames Research Center** *and Ming-Ta S. Hsu and Timothy S. Chen of HC Chem Research & Service Corp.*

Inquiries concerning rights for the commercial use of this invention should be addressed to the Patent Counsel, Ames Research Center
Refer to ARC-11599 /TN

Ames Research Ctr.
Moffett Field, CA 94035
Technology Utilization Officer: Laurance Milov
Mail Code 223-3
(415) 694-6370
Patent Counsel:
Darrell G. Brekke
Mail Code 200-11
(415) 694-5104

NASA Tech Brief
National Aeronautics and Space Administration

Determining Directions of Ultrasound in Solids

Ultrasound shadows are cast by grooves.

Lewis Research Center, Cleveland, Ohio

Defects or flaws within a structural material can effectively weaken a component or degrade its toughness to the point of catastrophic failure. For example, ceramics being investigated as replacements for metal components in automobile engines exhibit both low toughness and wide variability in strength. This combination of undesirable properties is generally attributed to impurities, voids, or microcracks introduced during processing. Pinpointing the locations of such flaws is important in determining whether a manufactured component is fit for service.

Scanning laser acoustic microscopy (SLAM) uses high-frequency ultrasound in conjunction with a laser to produce acoustic images of specimens on a video monitor. These acoustic images are analogous to optical images. Depths of flaws within opaque specimens can be predicted using a stereoscopic method with SLAM. The accurate determination of flaw depth requires accurate knowledge of the direction at which ultrasound travels within the specimen. This direction can be calculated from Snell's relation if the velocity of ultrasound in the material is known and if the specimen surface is acoustically flat and smooth.

An improved method for determining the direction of ultrasound in materials is the shadow method using SLAM. The shadow method is applicable to a wide range of surface roughnesses. The configuration for the shadow method is shown in the figure. A rectangular groove cut into the surface of a specimen blocks the ultrasound signal from reaching a limited area of the surface. On the video screen, this area shows up as an extremely dark (low-sound-intensity) region compared to adja-

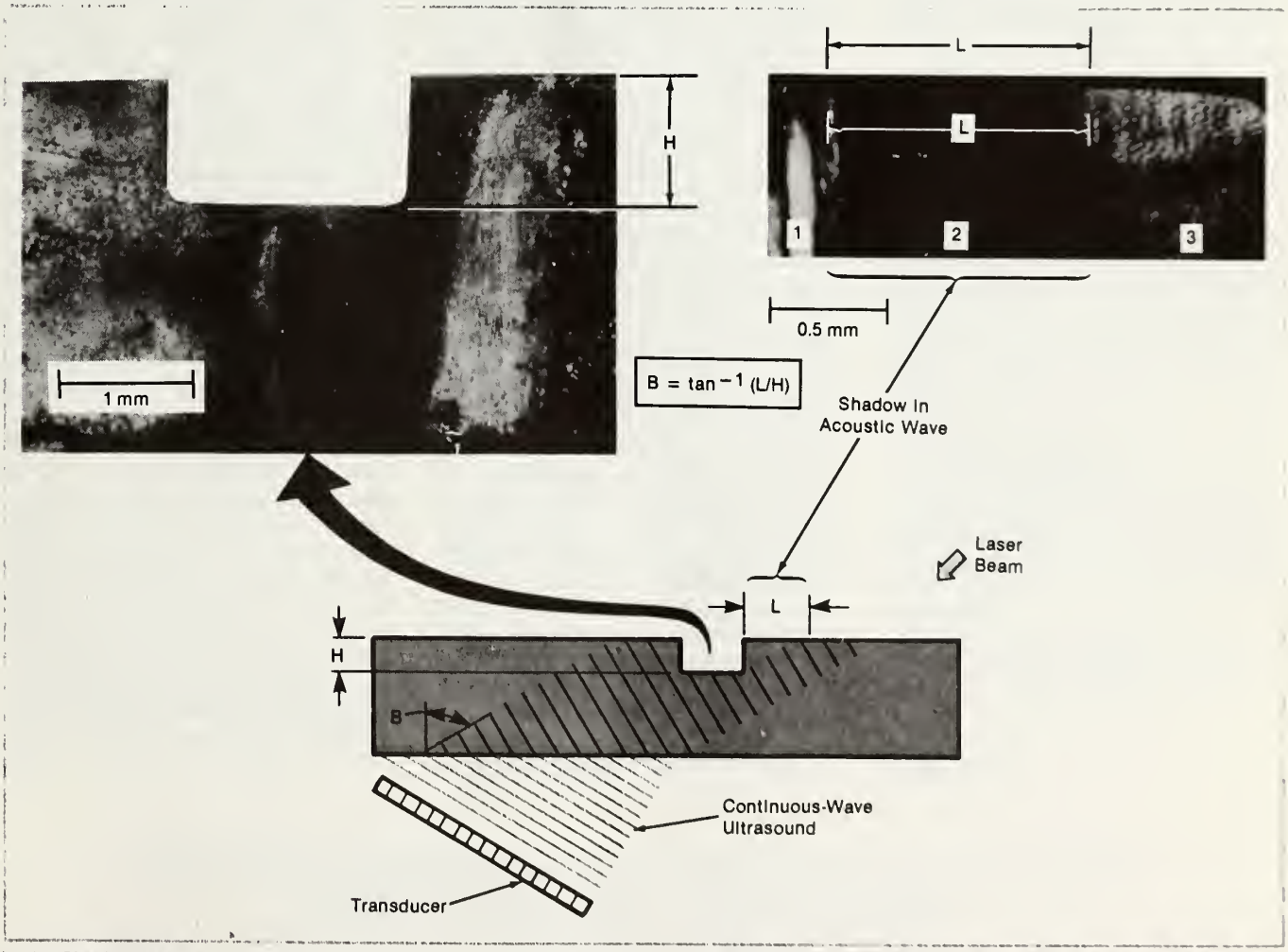

In the **Shadow Method**, the direction of ultrasound is calculated from the dimensions of a groove and the portion of the surface that the groove shields from the ultrasound.

cent areas in the acoustic image and is defined as the shadow region.

The direction of ultrasound, as denoted by the angle B, is determined by the simple trigonometric relationship shown in the figure. Despite the uncertainty in the measurements of the channel height and of the shadow length, the maximum uncertainty is 10 percent for channels approximately 1 mm high with B equal to approximately 25 ° to 45 °. This shadow method has been used to determine the directions of ultrasound accurately in ceramic, glass, and plastic specimens having surface finishes ranging from highly polished to as-fired. From these directions, the stereoscopic method has been used to predict the depths of flaws in these specimens accurately. This method may have a variety of applications in nontraditional quality-control applications.

This work was done by Edward R. Generazio and Don J. Roth of **Lewis Research Center**. *Further information may be found in:*

NASA CP-2383 [N86-22962/NSP], [A16] "Analysis Ultrasonics in Materials Research and Testing" (Reprinted as "Quantitative Flaw Characterization with Scanning Laser Acoustic Microscopy" and NASA TM-88797 [N86-31913/NSP] [A02] "Quantitative Void Characterization in Structural Ceramics Using Scanning Laser Acoustic Microscopy."

Copies may be purchased [prepayment required] from the National Technical Information Service Springfield, VA 22161, Telephone No. (703) 487-4650. Rush orders can be placed for an extra fee by calling (800) 336-4700.

LEW-14473/TN

FOR ADDITIONAL INFORMATION: *Contact: Director, Technology Transfer Division, P.O. Box 8757, BWI Airport, MD. 21240; (301) 621-0100 Ext. 241*

REFER TO THE NUMBER LISTED AT THE END OF THE ARTICLE

NASA Tech Brief
National Aeronautics and Space Administration

Fatigue Lives of Materials Cut by Lasers

Laser machining may help to balance high-speed rotating machinery.

A report describes continuing studies of the fatigue lives of materials cut by lasers. One of the long-term objectives of such studies is the use of laser machining to balance rotors that operate at high speeds. To achieve this objective, it is necessary to know the relationship between the effects of conventional and laser machining on the fatigue lives of the machined materials.

The evolution of rotating machinery has given rise to the need for multiplane and multispeed balancing. Research in balancing at high speeds performed by Lewis Research Center has shown that the exceedingly flexible high-speed shafts employed in advanced machines do not respond adequately to balancing procedures commonly used in the past. Operating above one or more critical speeds, these shafts require a sophisticated approach to balancing if increased reliability is to be achieved. This requirement has an impact on the design of entire machines in that access to the shafts at multiple planes may be necessary for an acceptable balance.

The utlimate success of any balancing procedure depends on the ability to apply balance correlations precisely and in optimum balance planes. The use of laser machining to apply these balance correlations holds promise for solving two problems: accessibility to balance planes in assembled machines and reliance on such labor-intensive balance corrections as hand grinding and bolt-on weights. The removal of material by lasers requires access to balancing areas only along lines of sight, and the process is readily automated.

The use of a laser for the removal of material in the balancing of a rotor has several important advantages. The most important advantage is that the material can be removed in an extremely accurate manner while the machine is operating, thus eliminating the need to stop the rotor to add or remove material after each balancing run. Much time can be saved, especially when working with high-inertia rotors. Another advantage is that many machines can be balanced inside their normal housings without disassembly. Rotors can be balanced accurately on their production supports under actual dynamic conditions. Ports designed into the balancing planes of the machine housings can support lenses or adjustable-focus lens tubes. The lenses would then be in position to converge the laser beam on the surface from which the material is to be removed.

Using this method, rotors could be balanced to a much finer degree than they could from outside the machine, causing a reduction of the dynamic loads and, in turn, a relaxation in the design contraints needed to withstand these loads. There would be a consequent reduction in the time needed to balance each unit and in manufacturing costs. Developments in the technology of laser and multiplane balancing of flexible rotors indicate that influence-coefficient balancing methodology has considerable promise as a practical, cost-effective procedure for the manufacture and overhaul of gas turbines, especially when it is combined with laser machining for the precise removal of metal.

An investigation into the removal of material by lasers showed that laser burns act in a manner typical of mechanical stress raisers, causing a reduction in fatigue strength; the fatigue strength is decreased relative to that of a smooth specimen. Laser-burn zones were studied in four materials: alloy steel 4340, stainless steel 17-4 PH, Inconel* 718, and aluminum alloy 6061-T6. Calculations were made of stress-concentration factors for laser-burn grooves of each material type. A comparison was then made to determine experimentally the fatigue-strength-reduction factors. No attempt was made to optimize the laser cuts to maximize fatigue lives nor to compare the effects of laser machining with those of the more-conventional hand-grinding method of removing material.

To qualify laser machining for eventual use in the balancing of gas-turbine rotors, it will be necessary to determine the reduction in fatigue life due to currently used hand grinding and compare it with the results of an optimized laser-machining procedure.

*Inconel is a registered trademark of the Inco family of companies.

This work was done by Michael R Martin of Mechanical Technology Inc., for **Lewis Research Center**. *Further information may be found in NASA CR-179501 [N87-11158/NSP], "Fatigue Life of Laser Cut Metals."*

Copies may be purchased from the National Technical Information Service, Springfield, Virginia 22161. [A04]

LEW-14532/TN

FOR ADDITIONAL INFORMATION: *Contact: Director, Technology Transfer Division, P.O. Box 8757, BWI Airport, MD. 21240; (301) 621-0100 Ext. 241*
REFER TO THE NUMBER LISTED AT THE END OF THE ARTICLE

NASA Tech Brief
National Aeronautics and Space Administration

Fluidized-Bed Cleaning of Silicon Particles

Metallic impurities are removed by acids.

NASA's Jet Propulsion Laboratory, Pasadena, California

A fluidized-bed chemical cleaning process is developed to remove metallic impurities from small silicon particles. These particles (250 μm in size) are utilized as a seed material in a silane pyrolysis process for production of 1-mm-size silicon. The product silicon (1 mm in size) is used as a raw material for fabrication of solar cells and other semiconductor devices. The principal cleaning step is a wash in a mixture of hydrochloric and nitric acids, which leaches out the metals and carries them away as soluble chlorides. The particles are fluidized by the cleaning solution to assure good mixing and uniform wetting.

Typically, the silicon particles as purchased contain significant impurities and range in size up to 2 mm. These particles are jet-milled down to sizes of 111 to 400 μm, with an average size of about 250 μm. A batch of about 500 g of milled particles is placed in each of three bottles in a fluidized-bed apparatus (see figure), restrained at the bottom by a screen with 50-μm pores and at the top by a screen with 75-μm pores.

A pump forces the cleaning fluid into each bottle through its bottom screen and a distributor that provides a tangential flow for good mixing. The solution passes through and fluidizes the bed of particles, flows out through the top screen, then falls back into the tank and is recirculated by the pump. The tank is usually filled with about 2 gallons (7.6 liters) of solution. All parts in contact with the silicon or cleaning fluid (including the pump) are made of polyethylene and polypropylene.

In the first washing step, the particle beds are flushed with deionized water to remove silicon particles smaller than 75 μm. This is followed by the main 20-minute wash in a mixture of two parts 12N HCl and one part 16N HNO_3, then by a rinse in deionized water. The oxide layer on the silicon particles is then removed by washing for 20 minutes in 48-percent HF. After a final rinse in deionized water, the particles are removed from the fluidized beds, dried in a quartz diffusion furnace at 150 °C under a nitrogen blanket, and sealed in a plastic bag. The concentrations of the principal metallic impurities (Fe, Cr, Ni, Cu, Mn, and Al) are reduced significantly by this cleaning process — in most cases, below the detection limits of spark-source mass spectroscopy (see table).

This work was done by Naresh K. Rohatgi and George C. Hsu of Caltech for **NASA's Jet Propulsion Laboratory.**
NPO-16935 /TN

Impurity Elements	Impurity Levels, Atoms Per Million Atoms of Silicon	
	In Raw Particles	In Cleaned Particles
P	0.2	0.2
Fe	20	≤0.6
Cr	0.05	0.03
Ni	10	<0.5
Cu	0.06	≤0.02
Zn	<0.02	≤0.04
Co	≤0.1	≤0.1
Mn	0.5	≤0.02
Na	≤0.1	≤0.1
Mg	≤1	<1
Al	2	0.05
S	<1	<1
K	≤0.07	<0.1
Ca	0.6	0.1

The Concentrations of Metallic Impurities are reduced by the acid cleaning process.

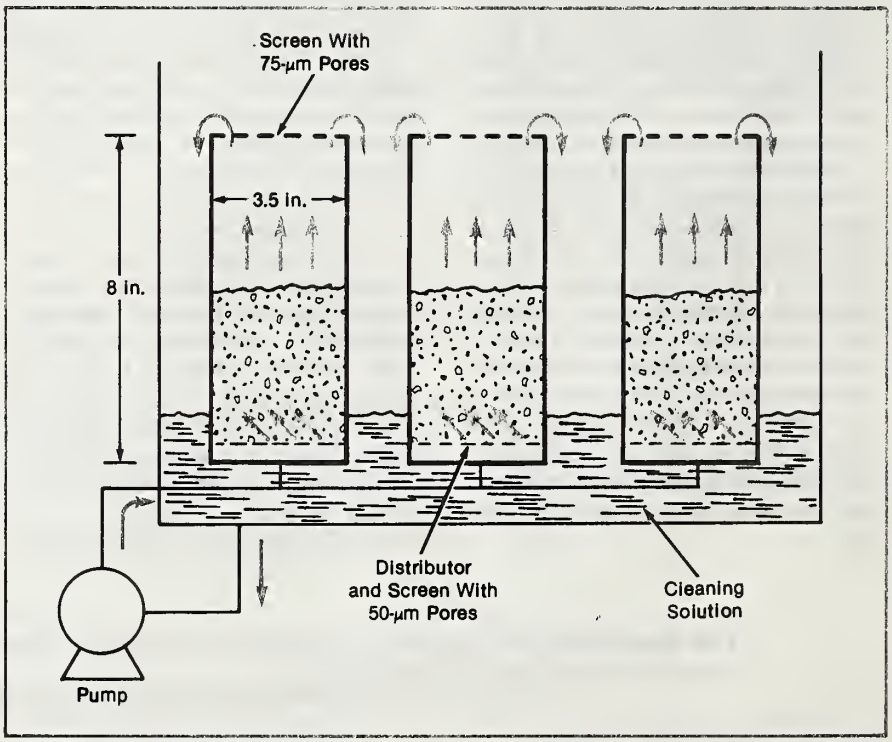

Beds of Silicon Particles are fluidized and washed by recirculating an acid cleaning solution.

FOR ADDITIONAL INFORMATION: *Contact: Director, Technology Transfer Division, P.O. Box 8757, BWI Airport, MD. 21240; (301) 621-0100 Ext. 241*
REFER TO THE NUMBER LISTED AT THE END OF THE ARTICLE

NASA Tech Brief
National Aeronautics and Space Administration
Marshall Space Flight Center, Alabamba

Licensing Opportunity

Mixing Valve for Protein-Crystal Growth

A multichamber unit combines reactants as necessary.

An apparatus for growing protein and other crystals holds reactants in separate chambers, then allows them to combine at the proper time. With a suitable design, a provision can also be made for a quenching agent to join the reactants when it is time to stop the reaction.

The apparatus was developed for protein-growth experiments in microgravity, in which crystal growth is unaffected by convection currents in the reactants. However, for some experiments it may also function in normal Earth gravity. It is compatible with the principal techniques for protein growth — the dialysis, batch, and liquid/liquid diffusion processes.

The apparatus consists of a series of opposed chambers separated by a rotary valve (see Figure 1). Passages inside the valve connect the chambers or isolate them, depending on the rotational position of the valve and its openings. O-rings and linear strips of elastomer on the valve prevent leakage between chambers.

Materials are introduced into the chambers through removable screwcaps at the outside ends of the chambers. Alternatively, material can be fed into a chamber by a syringe needle inserted through a polytetrafluoroethylene-coated silicone-rubber septum in the screwcap. A syringe can also be used to remove air from a chamber.

When the chambers have been filled, but before mixing, the valve passages are perpendicular to the chambers so that the chambers remain isolated. To initiate mixing, the valve is rotated 90°. This aligns the valve passages with the chambers so that the contents of pairs of opposing chambers mingle and the crystal-growth reaction proceeds (see Figure 2). If a quenching agent is to be used to stop the reaction, the valve is rotated an additional 180° to release the agent to the chambers.

The apparatus can easily be automated. It can be enlarged to accommodate more experiments simply by adding modules of chambers. Multiple-step chemical syntheses can be carried out if enough passages are provided in the valve. The apparatus can be made from various chemically inert materials, and its chambers can be designed with capacities ranging from milliliters to liters.

This work was done by Daniel C. Carter and Mary Beth H. Broom of **Marshall Space Flight Center**.

Inquiries concerning rights for the commercial use of this invention should be addressed to the Patent Counsel, Marshall Space Flight Center. Refer to MFS-26047 /TN

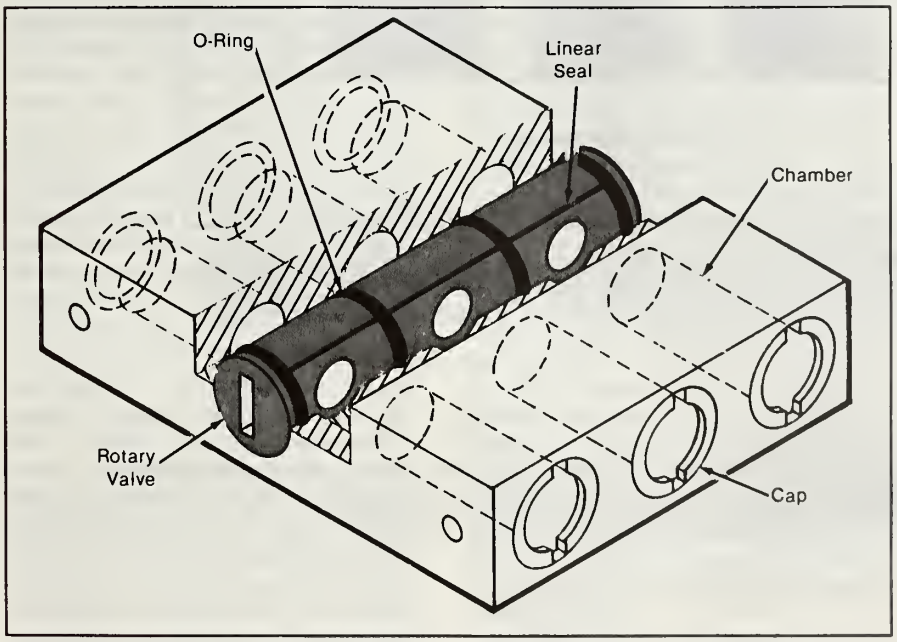

Figure 1. **Openings in a Cylindrical Rotary Valve** connect chambers to each other selectively through internal passages. O-ring and strip seals prevent leakage over the valve surface. Caps on the chambers seal them tightly but are removable for the addition of reactants or withdrawal of reaction products.

George C. Marshall Space Flight Center
Marshall Space Flight Center, AL 35812
Technology Utilization Officer: Ismail Akbay
Code AT01
(205) 544-2223
Patent Counsel:
Leon D. Wofford, Jr.
Mail Code CC01
(205) 544-0024

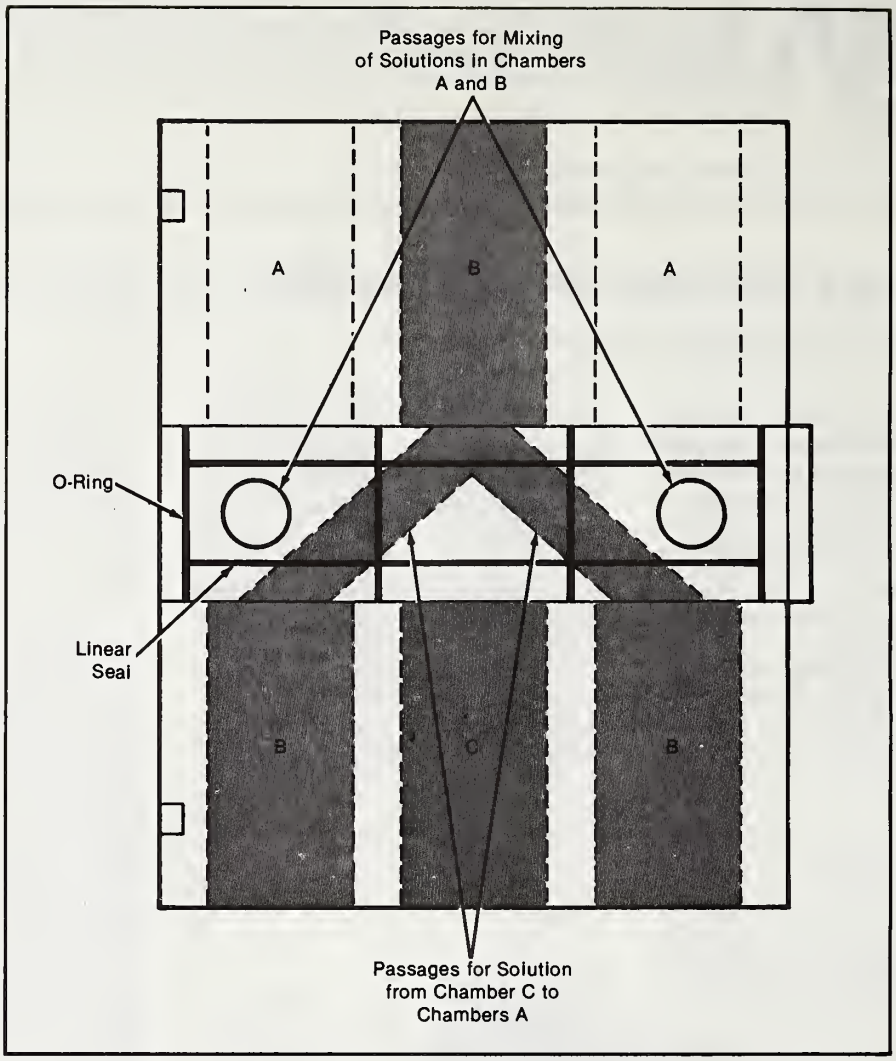

Figure 2. A **Cylindrical Rotary Valve**, shown here in cross section, is 90° from a position in which reactants A and B can mix and react. Rotation of the valve by 180° from the position shown would place it in a position in which the reactant C, a quencher, is released to chambers A.

FOR ADDITIONAL INFORMATION: *Contact: Director, Technology Transfer Division, P.O. Box 8757, BWI Airport, MD. 21240; (301) 621-0100 Ext. 241*

REFER TO THE NUMBER LISTED AT THE END OF THE ARTICLE

NASA Tech Brief
National Aeronautics and Space Administration

Licensing Opportunity

Protective Coatings for Spacecraft Polymers

Thin films of metal-oxide/polymer are applied by ion-beam sputtering.

A report describes experiments in the development of coatings to protect polymers from bombardment by atomic oxygen. Anticipated space systems like the space station, which must operate in low orbits around the Earth for many years, will require materials that are durable in their environment. Early Space Shuttle flights have demonstrated that many materials, such as polyimide (Kapton® or equivalent), carbon coatings, and some paints, are gradually eroded and suffer changes in optical properties when exposed in low orbit. The observed rates of material loss may be sufficiently high to compromise the long-term durability of polymers typically used in solar arrays or thermal blankets in low Earth orbit. The postulated mechanism for the material loss is oxidation by ram impact (at approximately 4.5 eV) of the geosynchronous atomic oxygen, which is the predominant environmental species at altitudes between 180 km (97 nmi) and 650 km (351 nmi).

One approach to prevent oxidation of materials in low Earth orbits is to provide a protective coating over the oxidizable material. In addition to being unaffected by atomic-oxygen bombardment, such a coating should be flexible, thin, lightweight, adherent, tolerant of ultraviolet light, resistant to abrasion, and susceptible to adhesive bonding; it must not alter the optical properties of the substrate if it is to be used for protecting such polymers as polyimide. Finally, oxidation-preventing coatings must be sufficiently elastic to allow the typical flexure and handling required for a specific polymer application.

Oxidation-preventing, flexible coatings consisting predominantly of metal oxide with small amounts of fluoropolymer have been produced by ion-beam sputter co-deposition. The use of mixed metal-oxide and fluoropolymer ingredients results in protective films of increased flexibility, but additional film thickness may be required to assure long-term (>10 yr) protection against oxidation.

The ground-laboratory tests used thin-film-sensing techniques and radio-frequency-plasma ashers to assess thin-film performance. The space-flight test consisted of a 41.17-h exposure of four samples to the ram atomic oxygen in a low orbit around the Earth on Space Shuttle flight STS-8. Characterizations of the sample exposed to space were performed to address two general questions: (1) What are the changes in properties of the protected Kapton® (or equivalent) as a result of the exposure to atomic oxygen in orbit and (2) how effective is the coating in providing long-term durability to the underlying Kapton® (or equivalent)?

Ion-beam sputter-deposited thin films of Al_2O_3, SiO_2, and SiO_2/polytetrafluoroethylene molecular mixtures are effective in preventing oxidation of such underlying materials as Kapton® (or equivalent), as demonstrated in both ground-based-laboratory and flight tests. The addition of small amounts (<15 percent by volume) of codeposited polytetrafluoroethylene to SiO_2 can be used to increase, by a factor of 3, the strain that the film can withstand without fracture.

However the ground-based radio-frequency-plasma ashing tests, in conjunction with the optical detection of the protective films, indicate that the minimum protective film thickness required for permanent protection from oxidation is increased by an order of magnitude (from 50 to 600 Å) if one adds 15 percent polytetrafluoroethylene. The application of protective films of Al_2O_3, SiO_2, and >96 percent SiO_2 with <4 percent polytetrafluoroethylene did not alter the optical properties of Kapton® (or equivalent) over the wavelengths from 0.33 to 50 μm. In addition, no change occurred in optical properties of the protected Kapton® (or equivalent) over the wavelengths from 0.33 to 2.2 μm. Postflight analysis indicates that the three protective coatings remained intact and functional throughout the 41.17-h orbital ram exposure to environmental atomic oxygen.

This work was done by Bruce A. Banks, Michael J. Mirtich, Jr., Sharon K. Rutledge, Henry K. Nahra, and Diane Swec of **Lewis Research Center**.

Further information may be found in NASA TM-87051 [N85-30137] "Ion Beam Sputter-Deposited Thin Film Coatings for Protection of Spacecraft Polymers in Low Earth Orbit."

Copies may be purchased from the National Technical Information Service, Springfield, Virginia 22161, [A02]

This invention has been patented by NASA (U.S. Patent No. 4,560,577). Inquiries concerning nonexclusive or exclusive license for its commercial development should be addressed to the Patent Counsel, Lewis Research Center
Refer to LEW-14384/TN

Lewis Research Center
21000 Brookpark Road
Cleveland, OH 44135
Technology Utilization Officer: Daniel G Soltis
Mail Stop 7-3
(216) 433-5567
Patent Counsel: Gene E. Shook
Mail Code 301-6
(216) 433-5753

NASA Tech Brief
National Aeronautics and Space Administration

Radiation Resistances of Dielectric Liquids

Although data are sparse for some liquids, polyphenyls appear to be particularly stable.

A report presents data on the effects of ionizing radiation on dielectric liquids for high-energy-density, pulsed-power capacitors. The report is based on Jet Propulsion Laboratory test results, a search of NASA and Department of Energy computer files, a survey of the open literature, and contacts with manufacturers and suppliers. The report covers 22 organic liquids, although detailed data were found for only one compound, polydimethyl siloxane. Generic data on the effects of radiation on compounds with similar chemical structures are provided where data on specific compounds are lacking.

Some organic liquids are much more radiation-resistant than others, according to the report; the polyphenyls are particularly stable. For reasons of economy and viscosity, the diphenyls and triphenyls are preferred. When irradiated in a nuclear reactor, these materials lose some hydrogen atoms and gradually polymerize to higher polyphenyls. The polyphenyls become useless as liquid insulators after exposure to a thermal-neutron fluence of 10^{19} neutrons per square centimeter because they polymerize excessively and form solids.

A radiation exposure of 10^7 to 10^8 rads causes observable degradation in organic dielectric liquids. The liquids are less stable than are plastic dielectric films, and the stability of a given liquid depends strongly on the film with which it is combined.

This work was done by Frank L. Bouquet and Robert B. Somoano of Caltech for **NASA's Jet Propulsion Laboratory**. *To obtain a copy of the report, "Radiation Effects Data on Dielectric Liquids for Capacitor Applications," NPO-16891/TN*

FOR ADDITIONAL INFORMATION: *Contact: Director, Technology Transfer Division, P.O. Box 8757, BWI Airport, MD. 21240; (301) 621-0100 Ext. 241*
REFER TO THE NUMBER LISTED AT THE END OF THE ARTICLE

NASA Tech Brief
National Aeronautics and Space Administration

Thermomechanical Properties Indicate Degree of Epoxy Cure

The glass-transition temperature and the density increase as the reaction proceeds.

NASA's Jet Propulsion Laboratory, Pasadena, California

The glass-transition temperature (T_g) and the density of a cured epoxy resin have been found to be related to the extent of the cure. In addition to providing insight into the chemical reactions of curing, these relationships show potential for process monitoring and control in the fabrication of strong, lightweight composite parts.

The material investigated was a commercial epoxy containing tetraglycidyl diaminodiphenyl methane (TGDDM) monomer with diaminodiphenyl sulfone (DDS) hardener. This material is used in nonstoichiometric, epoxy-rich proportions of about 2.1 moles of resin per mole of hardener. Samples of these two components were mixed at 120 °C in an N_2 atmosphere, then poured into aluminum weighing dishes and partially cured in an N_2 atmosphere at various temperatures from 140 to 201 °C and various times from 15 min to 6 h.

The partially cured samples were subjected to differential scanning calorimetry to measure the residual heat of cure, H_R. The total heat of cure, H_T, was also measured on uncured samples. Then the extent of cure, α, of each partially cured sample was determined from

$$\alpha = (H_T - H_R)/H_T$$

The sample densities were measured in an 80-cm density-gradient column filled with K_2CO_3 solution having a density range of 1.21 to 1.3 g/cm^3. The glass-transition temperature was measured in a thermomechanical analyzer: an expansion probe with a contact diameter of 2.54 mm was loaded to 1 g against 2-mm-thick samples of the same diameter. Each sample was

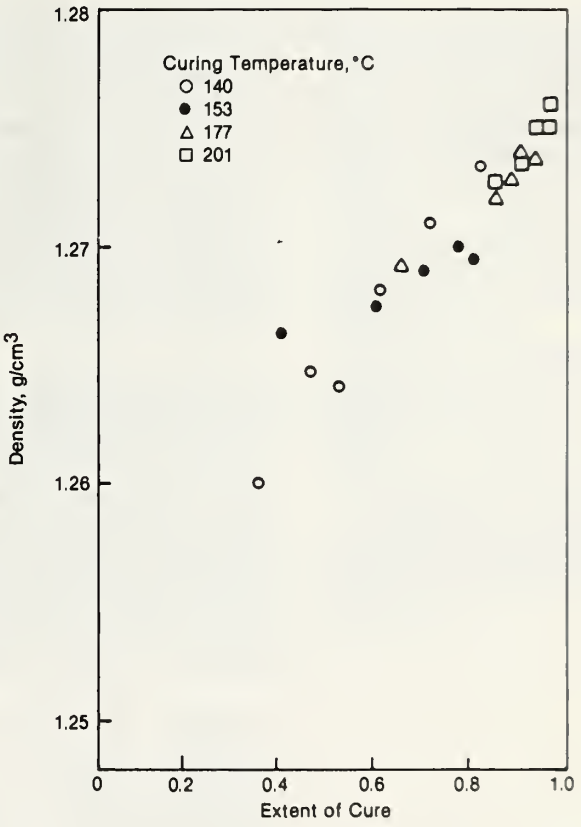

Figure 1. The **Increase of Density With the Extent of Cure** is believed to indicate that the free volume in the resin has been reduced by cross-linking of molecular segments.

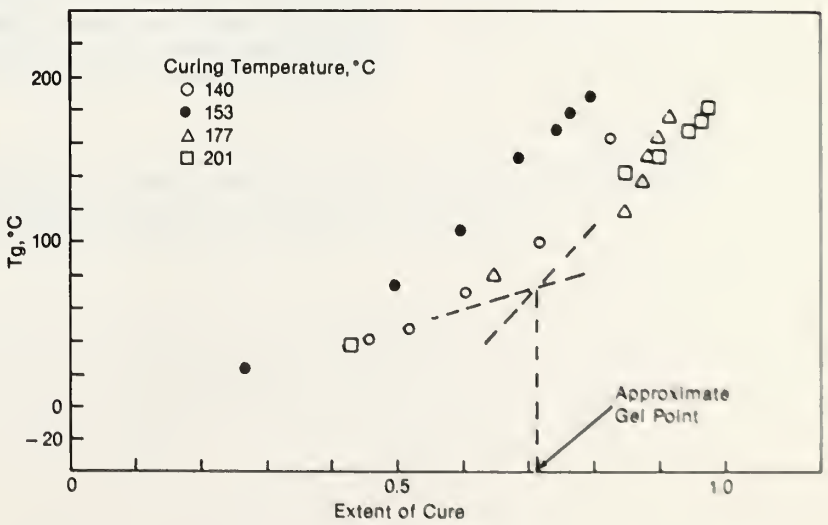

Figure 2. The **Glass-Transition Temperature** increases with the molecular weight below the gel point. Above the gel point, T_g also increases with the degree of cross-linking, making the rate of increase larger. The anomaly of the curve for 153°C is not understood.

heated at 10 °C/min. The glass-transition temperature was taken to be the temperature at which the two tangent lines to the thermal-expansion curves intersected.

As shown in Figure 1, the measurements yielded a linear relationship between the density and the extent of cure; this relationship appears to be independent of the curing temperature. As shown in Figure 2, the glass-transition temperature was found to depend on the extent of cure and to be independent of the curing temperature for three of the four curing temperatures used. At present, the divergence of the data for the 153 °C cure is not understood. Overall, the data seem consistent with a theory of gelation that takes into account the functionalities of the reactants, the degree of cross-linking, and the molecular distribution.

This work was done by Muzaffer Cizmecioglu, Amitava Gupta, and Robert F. Fedors of Caltech for **NASA's Jet Propulsion Laboratory**. *NPO-16903 /TN*

FOR ADDITIONAL INFORMATION: *Contact: Director, Technology Transfer Division, P.O. Box 8757, BWI Airport, MD. 21240; (301) 621-0100 Ext. 241*

REFER TO THE NUMBER LISTED AT THE END OF THE ARTICLE

NASA Tech Brief
National Aeronautics and Space Administration

Tribological Properties of Structural Ceramics

Studies of wear and lubrication promote longer component lives.

A paper discusses the tribological properties of structural ceramics. Tribology is the study of the adhesion, friction, wear, and lubricated behavior of solid materials in contact. The function of tribological research is to bring about a reduction in the adhesion, friction, and wear of mechanical components; to prevent their failure; and to provide long, reliable component life — through the judicious selection of materials, operating parameters, and lubricants.

The paper reviews the adhesion, friction, wear, and lubrication of ceramics; their anisotropic friction and wear behavior; and the effects of surface films and of interactions between ceramics and metals. Analogies with metals are made. Both oxide and nonoxide ceramics, including ceramics used as high temperature lubricants, are discussed.

Mechanical systems like bearings, gears, and seals are examples of components amenable to tribology. Whenever there is relative motion between two or more solid surfaces in contact, tribology is involved. Such mundane activities as shaving involve both friction and corrosive wear, and considerable tribological research has gone into increasing blade life and reducing friction and shaving discomfort. With more complex tribological systems such as gyroscope bearings and instrumentation gears, attention must be directed to many elements.

With a notable amount of research effort already having been put into fundamental studies of the tribological behavior of metals, attention is focused on ceramics because of their increasing potential as components in mechanical systems. Tribological studies have been conducted to gain increased understanding of those physical and chemical properties of ceramic parts that will affect their behavior when they are in contact with parts either of the same material or of other ceramics or metals.

Whereas metals readily deform plastically, ceramics, while having high strength, are normally brittle and fracture with little or no evidence of plastic flow. However, plastic flow has been observed in the surface layers of a number of ceramics, at the interface between two ceramics in contact under load and relative motion. Plastic flow has been observed with magnesium oxide, aluminum oxide, and silicon carbide, under relatively modest conditions of rubbing contact.

Factors like dislocations, vacancies, stacking faults, and crystal structure, which influence the mechanical behavior of materials when plastic flow occurs, also influence the friction and wear behavior of ceramics. Comparisons can be made between the anisotropic friction behaviors of ceramics and of metals. Surface films such as adsorbates markedly influence the adhesion, friction and wear behavior of ceramics. Further, with ceramics and other ionic solids, the presence of such surface films as water and surface-active organics can influence adhesion, friction, and wear by altering the amount of plastic deformation that will occur during sliding or rubbing.

Ceramic compositions can be used both as coatings and in composites for the high-temperature lubrication of both alloys and ceramics.

This work was done by Donald H. Buckley and Kazuhisa Miyoshi of **Lewis Research Center**. *Further information may be found in NASA TM-87105 [N86-10341/NSP], "Tribological Properties of Structural Ceramics."*

Copies may be purchased from the National Technical Information Service, Springfield, Virginia 22161, [A06]
LEW-14387/TN

FOR ADDITIONAL INFORMATION: *Contact: Director, Technology Transfer Division, P.O. Box 8757, BWI Airport, MD. 21240; (301) 621-0100 Ext. 241*
REFER TO THE NUMBER LISTED AT THE END OF THE ARTICLE

Medicine & Biology

318 Baron Studies in Bone Hardening

319 Dual-Energy X-Radiography with Gadolinium Filter — The image resolution would be increased, and the cost would be reduced.

Testing & Instrumentation

320 High Selectivity-Sensitivity Determination of PAH-DNA Adducts and Metabolites Using Fluorescence Line Narrowing Spectrometry

321 Bacterium, Listeria Monocytogenes, Now can be Detected Accurately

United States Department of Agriculture

Research Technology
Agricultural Research Service

Boron Studies in Bone Hardening

Boron, an element long known for softening water, may play an important role in hardening bones, Agricultural Research Service scientists report.

A 6-month study indicates that boron, not even considered an essential nutrient for people and animals, may be a key to preventing osteoporosis, say nutritionist Forrest H. Nielsen and anatomist Curtiss D. Hunt at ARS' Grand Forks, North Dakota, Human Nutrition Research Center.

They believe the results of the study—the first to look at the nutritional effects of boron in humans—"will generate a lot of interest in the element."

In the study, 12 postmenopausal women consumed a very low boron diet (0.25 milligrams per day) for 17 weeks then were given a daily 3-mg supplement—representing the boron intake from a well-balanced diet—for 7 more weeks.

Within 8 days after the supplement was introduced, they lost 40 percent less calcium, one-third less magnesium, and slightly less phosphorus through the urine. In fact, their calcium and magnesium losses were lower than prestudy levels, when they were on their normal diets.

"These elements are important in maintaining the integrity of bone," says Nielsen, who is director of the Center.

Each day the women took the 3-mg boron supplement they retained an average of 52 mg more calcium. "That's a gram of calcium every 20 days. The body contains roughly 1,100 grams of calcium, so over a period of several years, that's a significant savings in calcium," Nielsen says.

"Boron has a remarkable effect on indicators that the body is conserving calcium or preventing bone demineralization," he says. "But we really became excited when we saw its effect on steroid hormones."

Blood levels of the most active form of estrogen—estradiol 17B—doubled to "levels found in women on estrogen replacement therapy," he says, noting that they were also 50 percent higher than prestudy levels. "And blood levels of testosterone—the precursor of estradiol—more than doubled.

"These steroid hormones are thought to be very important for maintaining bone and calcium status," says Nielsen. "In fact, estrogen replacement is currently the only proven treatment for osteoporosis."

Hunt says he suspects that "the body needs boron to synthesize estrogen, vitamin D, and other steroid hormones. And it may also protect these hormones against rapid breakdown." In his studies on chickens, for example, boron helped the animals overcome low vitamin D levels that stunted their bone growth.

Hunt believes boron is involved in adding the hydroxyl (hydrogen-oxygen) groups that steroids need to be biologically active. "But," he says, "there is no experimental evidence to support this hypothesis yet."

He and Nielsen will be taking a closer look at the thesis in two more human studies scheduled to begin early in 1988.

Nielsen says that their boron research began 6 years ago when they found that boron improved the growth of chickens whose diets were deficient in vitamin D.

The subtlety of boron's function in the body has probably kept it from being "discovered" until now, says Nielsen. "If you don't need it to overcome certain inadequacies, you don't know it's missing. You have to put a little stress on the hormone system before you start seeing the effects."

The element was recognized as essential for plants in the 1920's, he says, "but plant scientists still don't know how it functions."

Since boron isn't considered essential for people, there is no recommended intake and no boron supplement on the market. Nielsen says the supplement of sodium borate used in the study was specially prepared based on the amount of boron a person would get from a well-balanced diet containing fruits and vegetables. He says the average boron intake is about 1.5 mg—or half the experimental dose—"but average means a lot of people get less and a lot get more."

Hunt cautioned that large doses of boron can be toxic, even lethal. The lowest reported lethal dose of boric acid is about 45 grams (1.6 ounces) for an adult and only 2 grams (0.07 ounce) for an infant.

People can get ample boron—up to 4 or 5 mg per day—by eating plenty of fruit—especially apples, pears, and grapes—nuts, leafy vegetables, and legumes. These foods have the highest levels of the element as well as many essential vitamins and minerals, Hunt says.

Hunt and coworkers analyzed various foods for their boron content. (See box to right.)

Nielsen points out that "Seventh Day Adventists, who are vegetarians, have a much lower occurrence of osteoporosis than Americans as a whole; but Eskimos, who eat almost no fruits or vegetables, have a very high incidence of bone demineralization."

Osteoporosis affects as many as 15 to 20 million older Americans, predominantly women, according to a 1984 conference sponsored by the National Institutes of Health. Each year, osteoporosis contributes to about 1.3 million fractures (primarily in the hip, spine, and wrist) in people 45 years old and over. This costs an estimated $3.8 billion annually.

Calcium supplement sales are at an all-time high as women try to prevent bone loss, but little evidence exists to support the claim that adequate calcium alone prevents the loss of bone. According to Mark Hegsted, professor emeritus of nutrition at Harvard University, "osteoporosis looks like a dietary problem but not a calcium problem."

Nielsen says, "We've only scratched the surface with our research. If boron is involved in adding the hydrogen-oxygen group that steroid hormones need to be biologically active, it may be important in preventing a lot of other diseases of unknown cause—including some forms of arthritis."

Nielsen and Hunt reported findings from the human study in the November 1987 issue of *The FASEB Journal*, a new publication of the Federation of American Societies of Experimental Biology.

Boron Content in a Serving of Various Foods[1]

Apple sauce, bottled	0.279
Grape juice, bottled	.202
Apple juice, bottled	.188
Peaches, canned	.187
Broccoli, frozen	
flowers	.185
stalks	.089
Cherries, frozen	.147
Pears, canned	.122
Carrots, canned	.075
Green beans, frozen	.046
Orange juice, frozen	.041
Lettuce, iceberg	.039
Noodles	
egg	.037
spaghetti	.006
Cornflakes, fortified	.031
Bread, white enriched	.020
Ice cream, vanilla	.019
Potatoes, canned	.017
Chicken breast, ground	.005
Coffee, freeze dried	.005
Rice, Minute	.003
Milk, 2%	.002
Beef, ground round	ND[2]
Cheese, cheddar or cream	ND
Eggs, frozen	ND
Sugar, granulated	ND

[1] Milligrams boron per 100 milliliters (3 1/3 fluid ounces or 0.42 cup) or 100 grams (3 2/3 ounces, dry weight).

[2] ND - nondetectable

Source: Curtiss D. Hunt, USDA Agricultural Research Service

FOR FURTHER INFORMATION

To discuss this effort further, contact:

Dr. Forrest H. Nielsen
USDA-ARS Grand Forks Human Nutrition Research Center
P.O. Box 7166 University Station
Grand Forks, ND 58202
(701) 795-8353

NASA Tech Brief
National Aeronautics and Space Administration
NASA's Jet Propulsion Laboratory. Pasadena, California

Dual-Energy X-Radiography With Gadolinium Filter

The image resolution would be increased, and the cost would be reduced.

In a proposed dual-energy x-ray imaging system, the continuous bremsstrahlung spectrum from an x-ray tube would be filtered by a foil of nonradioactive gadolinium or another rare-earth metal to form a two-peaked energy spectrum. After passing through the patient or object under examination, the filtered radiation would be detected by an array of energy-discriminating, photon-counting detectors (see figure). The detector outputs would be processed to form the x-ray image for each peak and possibly an enhanced image based on the data taken at both peaks.

Dual-energy x-radiography exploits the variation of x-ray attenuation with energy. By forming images at different energies and therefore different attenuations, one can enhance the radiographic contrast between different tissues. For example, dual-energy imaging has been used to reduce the effects of variable soft-tissue and fat content when measuring the density of bone. Prior methods of forming dual-energy spectra include alternately applying two voltages to the x-ray tube, filtering one bremsstrahlung spectrum with two different materials, using back-to-back detectors, and irradiating the patient with 45- and 100-keV x rays from a radioactive Gd^{153} source.

The latter method is often preferred because the photon energies of Gd^{153} are optimal for quantitative bone-mineral determination. However, to be sufficiently intense, a Gd^{153} source has to be large enough (typically forming a focal spot with an area of 5 mm^2) to limit image resolution seriously. Futhermore, the radioactive decay of the source necessitates annual replacement at a cost of about $10,000 to $20,000.

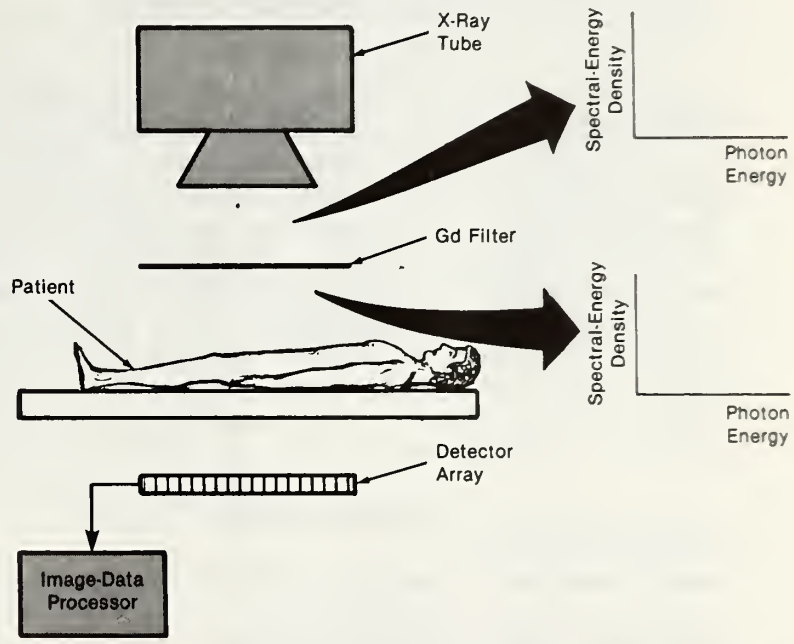

The **Gadolinium Foil** acts as a "K-edge" filter, which absorbs photons strongly in the middle portion of the spectrum above the K-edge energy. When illuminated with the continuous spectrum from an x-ray tube, the foil therefore produces a double-peaked spectrum. The images formed at the two peaks reveal more than does a single image.

Because the new system would use an x-ray tube with a source only 1/20 as large, it could achieve higher resolution. The radiation intensity available from the tube is 50 times that from a typical Gd^{153} source. When the continuous x-ray-tube spectrum is filtered by the nonradioactive gadolinium foil, the output spectrum has two peaks separated by 40 keV and nearly identical to the Gd^{153} peaks. The radiation dose to the patient would be about the same as with Gd^{153}. The x-ray image would be formed on a linear array of 15 to 24 detector elements etched 2 mm apart onto a single crystal of highly pure germanium. The detector array would be moved across the scene in a line-scanning mode.

This work was done by Brian Rutt of the University of California at San Francisco for **NASA's Jet Propulsion Laboratory**.
NPO-16773 /TN

FOR ADDITIONAL INFORMATION: *Contact: Director, Technology Transfer Division, P.O. Box 8757, BWI Airport, MD 21240; (301) 621-0100 Ext. 241*
REFER TO THE NUMBER LISTED AT THE END OF THIS ARTICLE

Department of Energy

Technology Application

Ames Laboratory

High Selectivity - Sensitivity Determination of PAH-DNA Adducts and Metabolites Using Fluorescence Line Narrowing Spectrometry

Carcinogenesis and mutagenesis produced by genotoxic agents is triggered by chemical attack of nucleic acids by chemical agents. From the points of view of body burden assessment and an adequate understanding of mechanistic carcinogenesis, new highly sensitive and selective and practical analytical techniques are required for the analysis of intact DNA (nucleic acid) - carcinogen adducts. A new technique, fluorescence line narrowing spectrometry, has been shown to possess the above desired attributes. This spectrometry is unique in its capabilities. It is the only technique in existence that permits high sensitivity and selectivity analysis of nucleic acid (DNA) damage from carcinogens and mutagens through the utilization of intact nucleic acid adducts. Currently, it is being applied to nucleic acid samples from animals exposed to carcinogens.

FOR ADDITIONAL INFORMATION:
Daniel E. Williams
Ames Laboratory, Associate Director for Planning
and Technology Application
119 Office and Laboratory Building
Iowa State University
Ames, Iowa 50011
(515) 294-2635
Refer to AL-87-05/TN.

United States Department of Agriculture

Research Technology
Agricultural Research Service

Bacterium, Listeria Monocytogenes, Now can be Detected Accurately

More accurate detection of a bacterium that causes food poisoning is now possible. Scientists have developed a method for distinguishing between healthy and injured cells of Listeria monocytogenes, a bacterium that causes the food-poisoning disease listeriosis. The bacterium, which can grow in meats and dairy products, is killed by heating during cooking or pasteurization. But improper heating only injures the organism, which can then repair itself and multiply. Current tests sometimes fail to pinpoint these injured cells; the new test detects them and lets industry and regulatory agencies know the true level of contamination. In 1985, L. monocytogenes killed 47 people who ate tainted cheese in California. On September 1, USDA's Food Safety and Inspection Service officially began monitoring the organism in cooked, ready-to-eat meat and poultry.

FOR ADDITIONAL INFORMATION:
Dr. James L. Smith/Robert L. Buchanan
Microbial Food Safety, Eastern Regional
Research Center
Philadelphia, PA
(215) 233-6620

Natural Resources Technology & Engineering

322 Ventilated Cutting Drum Reduces Longwall Dust

Software

323 Estimating Geophysical Parameters from Gravity Data — Features of planets are extracted from Doppler spacecraft-tracking measurements

Technology News

From the Bureau of Mines, United States Department of the Interior

Ventilated Cutting Drum Reduces Longwall Dust

Objective

Reduce respirable dust concentrations generated by longwall shearing machines.

Approach

Integrate water-powered dust collectors into the cutting drum to capture and remove the airborne dust before it is released into the primary airstream.

How It Works

The ventilated drum is designed to reduce the amount of airborne dust generated during cutting. This is achieved by drawing dust-laden air from the cutting zone through twelve water-powered "dust capture" tubes built into the shell of the shearer drum (see illustration). High-pressure water, up to 1,500 psig, is released from a spray ring manifold located on the face side of the drum. These sprays act as a fan, and by momentum transfer-induce a total airflow of 3,500 cfm from the face side of the drum. The 33 pressure sprays act as scrubbers, removing 90 to 95 pct of the respirable dust from the air drawn through the tubes. At the gob side of the drum a deflector plate, attached to the cowl arm, deflects the water spray away from the operator.

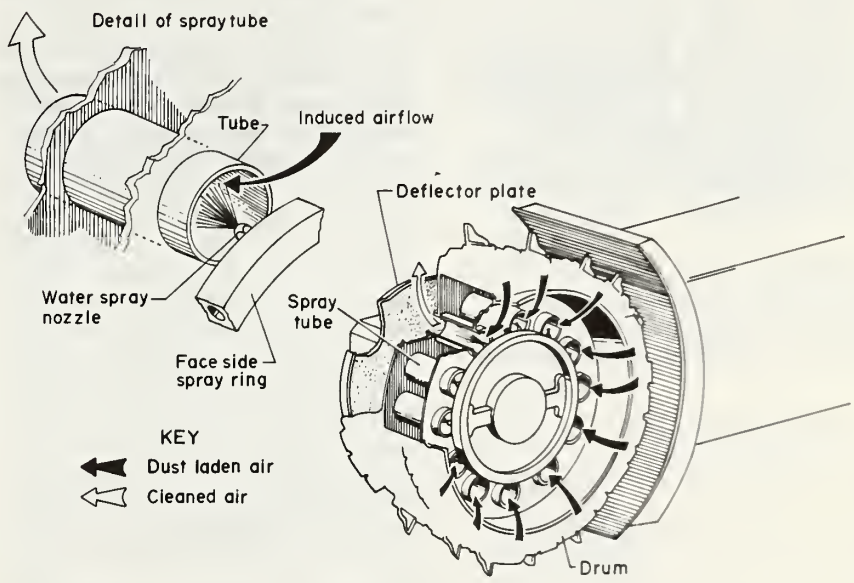

Cutaway view of components and airflow paths of the ventilated drum.

To date, more than 50 ventilated drums have been installed in the United Kingdom where the drum was initially developed. Tests carried out on fixed-height and single-ended ranging drum shearers have shown reductions in respirable dust of 60 to 80% as compared with conventional wet cutting. However, only limited testing had been conducted on double-ended ranging-arm shearers. The baseline condition was conventional wet cutting also using 33 high pressure bit sprays per drum for a total flow of 60 gpm. The Bureau of Mines has recently filled in this research gap by completing tests evaluating the use of the ventilated drums on double-drum shearers.

Test Results

The first evaluation of the ventilation drum in the United States was conducted at the Plateau Mine near Price, Utah. Two ventilated drums were installed on an Eichkoff EDW 300 double-drum shearer. High pressure water, 1,500 psig, at a flow rate of 25 gpm was delivered to the spray tubes in each drum

from a remote pump. Total flow to shearer was 85 gpm which included the low pressure sprays on the drum plus external and cooling sprays. Three weeks of extensive underground testing showed that mechanical durability of all components was excellent. Respirable dust reductions were good to excellent with reductions of: 40% at the operator's position, 55% at the tailgate, and 20% in the intake (this reduction in intake dust was due to increased total water flow). In addition, the ventilated drum proved to be one of the most effective spray type devices for controlling shearer-generated dust levels at the shield men and tailgate positions.

Acceptance of the ventilated drum by face crew and company was unanimous. Plateau intends to order a second set of ventilated drums based on the marked improvement in dust control. A ventilated drum costs approximately $5,000 more than a standard drum. High pressure pumps, piping or tubing required for operation of the drum add an additional $30,000 to $40,000.

Patent Status

International patents for several items used in the design of the ventilated drum are held by British Coal. Inquiries may be addressed to the Headquarters Technical Department, Ashby Road, Stanhope Bretby, Burton-on-Trent, U.K. DE15 0QE.

For More Information

Additional information can be obtained by contacting the technical project officer, Edward F. Divers, at the Bureau of Mines, Pittsburgh Research Center, P.O. Box 18070, Pittsburgh PA 15236; telephone (412) 675-6825. *Technology News* issues 112, 113, 118, 150, 155, 245, and 246 contain additional information on water application for longwall double-drum shearers, including the Bureau's shearer clearer system. Free single copies can be obtained by writing to the Bureau of Mines, Branch of Technology Transfer, 2401 E Street N.W., Washington, D.C. 20241 or by calling (202) 634-1224.

NASA Tech Brief
National Aeronautics and Space Administration

Computer Software

Estimating Geophysical Parameters From Gravity Data

Features of planets are extracted from Doppler spacecraft- tracking measurements.

The ORBSIM program was developed for the accurate extraction of parameters of geophysical models from Doppler-radio-tracking data acquired from orbiting planetary spacecraft. The model of the proposed planetary structure is used in a numerical integration along simulated trajectories of the spacecraft around the primary body.

Using line-of-sight (LOS) Doppler residuals, ORBSIM applies fast and efficient modeling and optimization procedures that avoid the traditional complex dynamic reduction of data. ORBSIM produces such quantitative geophysical results as size, depth, and mass. ORBSIM has been used extensively to investigate topographic features on the Moon, Mars, and Venus. The program has proved particularly suitable for modeling gravitational anomalies and concentrations of mass.

The basic observable quantity for spacecraft-based gravity data is the Doppler frequency shift of a transponded radio signal. The derivative of this signal with respect to time carries information regarding the gravity field acting on the spacecraft in the LOS direction (the LOS direction being the path between the spacecraft and the receiving station — either Earth or another satellite). Many dynamic factors are taken into account, such as the rotation of the Earth, solar radiation, acceleration from planetary bodies, and adjustments of the location and time of the tracking station.

The actual trajectories of the spacecraft are simulated by the use of least-squares fits to conic motions. The theoretical Doppler readings from the simulated orbits are compared to actual Doppler observations, and another least-squares adjustment is made.

ORBSIM has three modes of operation: (1) trajectory simulation, (2) optimization, and (3) gravity modeling. In all cases, an initial gravity model of curved and/or flat disks, harmonics, and/or a force table are required input.

ORBSIM is written in FORTRAN 77 for batch execution and has been implemented on a DEC VAX 11/780 computer operating under VMS. The program was released in 1985.

This program was written by William L. Sjogren of Caltech and Ravenel N. Wimberly of Sterling Software for **NASA's Jet Propulsion Laboratory**.

NPO-16671 /TN

FOR ADDITIONAL INFORMATION *CONTACT:*

COSMIC®
112 Barrow Hall
University of Georgia
Athens, GA 30602
(404) 542-3265

Physical Sciences

324 Ternary Rare Earth-Lanthanide Sulfide

325 Approximate Simulation of Turbulence — Computed spectra resemble van Karman spectra of frequencies of interest.

326 Coating a Hydrogran-Maser Chamber with CF_4 — Sprayed gas forms a smooth frozen surface.

327 Experiments in Boundary-Layer Turbulence — Motion in the layer is highly three-dimensional.

328 Growing II/VI Semiconductors with Double Decantation — A concept for growing single crystals combines sheet solidification with controlled cooling.

Testing & Instrumentation

329 Low-Level Particle Beam Monitor and Current Meter

330 Micropolarimeter for High Performance Liquid Chromatography (Licensing Opportunity)

331 Concentrating Trace Gases at Low Pressures — An open adsorption tube enables the measurement of gases at parts-per-trillion-by-volume concentrations. (Licensing Opportunity)

332 High-Rydberg Xenon Submillimeter-Wave Detector — The use of reactive alkali metals is avoided. (Licensing Opportunity)

333 Measuring Contact Thermal Conductances at Low Temperatures — An apparatus applies controlled force to metal samples at controlled heat flows. (Licensing Opportunity)

334 Fiber-Optic Temperature Sensor — A remote thermometer should be small, lightweight, and immune to electrical noise.

335 Measuring Electrostatic Discharge — A variety of materials can be tested together under controlled conditions. (Licensing Opportunity)

336 Measuring Gases with Laser-Induced Fluorescence — The temperature, density, and pressure are measured simultaneously in supersonic, turbulent flow. (Licensing Opportunity)

337 Measuring Viscosities of Gases at Atmospheric Pressure — A thermal mass flowmeter provides a capillary section for differential-pressure measurement. (Licensing Opportunity)

Other Items of Interest

320 High Selectivity-Sensitivity Determination of PAH-DNA Adducts and Metabolites Using Fluorescence Line Narrowing Spectrometry

Department of Energy

Technology Application

Ames Laboratory

Ternary Rare Earth-Lanthanide Sulfide

A new ternary rare earth sulfur compound has been prepared which has the formula $La_{(3-x)}M_{(x)}S_{(4)}$ where M is one or more elements selected from the group of Eu, Sm and Yb and X = 0.15 to 0.8. The invention provides a new lanthanum rare earth sulfide for application as a new thermoelectric material which is stable at high temperature and has good high temperature thermoelectric properties. These new materials have higher figures of merit than the existing Si-Ge thermoelectrics used in isotopic electrical generators for deep space missions at the current operational temperatures and they can be used at higher temperatures and thus improve the efficiency in converting thermal to electrical energy.

FOR ADDITIONAL INFORMATION
Daniel E. Williams
Ames Laboratory, Associate Director for Planning
and Technology Application
119 Office and Laboratory Building
Iowa State University
Ames, Iowa 50011
(515) 294-2635
Refer to assessment AL-87-03/TN

NASA Tech Brief
National Aeronautics and Space Administration

Approximate Simulation of Turbulence

Computed spectra resemble von Kármán spectra of frequencies of interest.

Marshall Space Flight Center, Alabama

A numerical technique yields simulated atmospheric-turbulence spectra that closely approximate von Kármán spectra within the frequency ranges of interest for aircraft response. The technique uses approximate spectra that are especially suitable for computation in that they represent stable systems and roll off as f^{-2} (where f = frequency) at high frequencies outside the range of interest.

Real atmospheric turbulence tends to follow the von Kármán model, with spectral density proportional to $f^{-5/3}$. A simulated turbulence signal can be generated by a system like that of Figure 1, provided that the transfer function of the filter gives the required $f^{-5/3}$ dependence. For purposes of numerical simulation of the instantaneous turbulence signal, the filter transfer function is replaced by its corresponding differential equation, which is then approximated by a finite-time-step difference equation. As a result, the turbulence at the present time step is expressed as a function of the present input noise and the turbulence and input noise at the previous time steps.

Because it is computationally more efficient to simulate a rational rather than an irrational spectrum, the transfer function $(1+S)^{-5/6}$ that represents the exact $f^{-5/3}$ spectral dependence is approximated by the rational expression. For the longitudinal turbulence, this is $(1+S)^{-5/6} \approx [60 + 52S + (91/12)S^2]/[60 + 102S + (561/12)S^2 + (935/216)S^3]$, where S is the Laplace-transform complex frequency. Because all the poles of this function lie in the left half of the complex S plane, the system that it represents is unconditionally stable.

Figure 1. **Monte Carlo Simulation of Turbulence** can be done with digital or analog equipment by passing Gaussian white noise through a filter that has a transfer function corresponding to the turbulence spectrum.

The transfer function for transverse turbulence is obtained by multiplying the longitudinal transfer function by $[1 + (8/3)^{1/2}S]/[1 + S]$. This function also represents a stable system. In both the longitudinal and transverse cases, the spectral density is found by multiplying the transfer functions by their complex conjugates.

Longitudinal turbulence and transverse turbulence have been simulated by difference equations based on these transfer functions, using a sampling frequency of 5 Hz, an aircraft speed of 100 m/s, a turbulence length scale of 500 m, and a root-mean square turbulent velocity of 1 m/s. As shown in Figure 2, the spectra of the simulated turbulence closely approximate the corresponding von Kármán spectra. In fact, the statistical scatter is greater than the difference between the simulated and von Kármán spectra.

This work was done by C. W. Campbell of the American Institute of Aeronautics and Astronautics for **Marshall Space Flight Center.** *MFS-28172/TN*

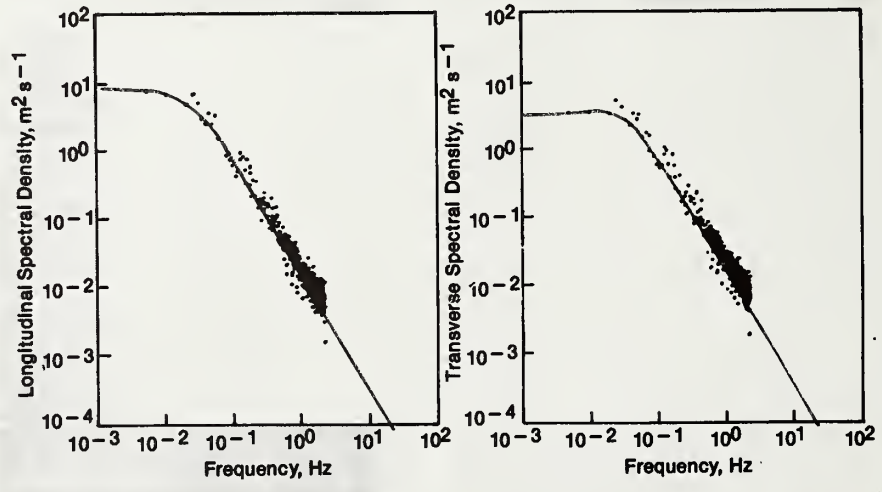
Longitudinal Spectral Density, m² s⁻¹
Transverse Spectral Density, m² s⁻¹
10² 10¹ 10⁰ 10⁻¹ 10⁻² 10⁻³ 10⁻⁴
10⁻³ 10⁻² 10⁻¹ 10⁰ 10¹ 10²
Frequency, Hz
Frequency, Hz

Figure 2. **Spectra of Simulated Turbulence** (dots) are plotted with the corresponding von Kármán spectra (lines).

FOR ADDITIONAL INFORMATION: *Contact: Director, Technology Transfer Division, P.O. Box 8757, BWI Airport, MD. 21240; (301) 621-0100 Ext. 241*
REFER TO THE NUMBER LISTED AT THE END OF THE ARTICLE

NASA Tech Brief
National Aeronautics and Space Administration

Coating a Hydrogran-Maser Chamber With CF_4

Sprayed gas forms a smooth frozen surface.

NASA's Jet Propulsion Laboratory, Pasadena, California

A coating of carbon tetrafluoride (CF_4) has been formed on the interior surface of an atomic-hydrogen maser by allowing CF_4 gas to freeze on the surface. The new coating enables the maser to oscillate down to 26 K; the most effective previous coating, a fluorinated ethylene/polypropylene (FEP) copolymer allowed oscillation down to about 50 K.

The key to maintaining maser stability while lowering the operating temperature is to find a surface coating that reflects hydrogen atoms without disturbing the phase of the oscillating magnetic dipole moment of the hyperfine interaction between the electron and proton in each atom. The CF_4 coating performs this function better than does FEP because CF_4 is a tetrahedral molecule with no polymer end groups to harbor impurities and because the surface formed is smoother.

The CF_4 gas is sprayed into the cooled, evacuated chamber using a pair of opposed nozzles, one on each side of the maser septum (see figure). Pulses of electric current are passed through the nozzles to heat them enough to prevent the gas from condensing and freezing in them. The coating obtained with the nozzles is more uniform than the one that results from simply introducing the gas via the existing hydrogen-beam collimator.

Since the electronic structure of the bound fluorine atom is similar to that of the inert gas neon, the use of the latter gas as a maser-chamber coating has been proposed. It should be possible to hold neon in place at a reasonably low vapor pressure of 10^{-5} torr (about 10^{-3} Pa) at a temperature of about 10 K.

This work was done by Robert F. C. Vessot and Edward Mattison of the Smithsonian Institution for **NASA's Jet Propulsion Laboratory.**

NPO-16380 and NPO-16381 /TN

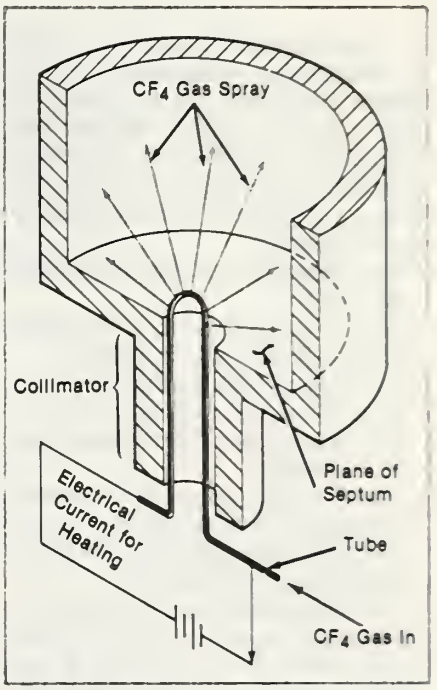

The Coating Nozzle used to spray the CF into half of the TE_{111}-mode maser chamber is formed from 0.020-inch (0.5-mm) diameter nonmagnetic metal tubing. The nozzle for each half is placed on one side of the septum in the chamber. Several small holes are drilled on the outside of the bend to distribute the gas evenly. The nozzle is electrically insulated from ground and thermally isolated, except for contact with the septum.

FOR ADDITIONAL INFORMATION: *Contact: Director, Technology Transfer Division, P.O. Box 8757, BWI Airport, MD. 21240; (301) 621-0100 Ext. 241*
REFER TO THE NUMBER LISTED AT THE END OF THE ARTICLE

NASA Tech Brief
National Aeronautics and Space Administration

Experiments in Boundary-Layer Turbulence

Motion in the layer is highly three-dimensional.

A report describes experimental studies of the disturbances induced by weak freestream turbulence in a pre-transitional Blasius boundary layer. The report asks and partially answers some fundamental questions concerning these large-amplitude, low-frequency disturbances, including the following:

- What causes the low-frequency mode of the layer?
- Does the low-frequency mode excite Tollmien-Schlichting (T-S) waves?
- Does the low-frequency mode render existing T-S waves oblique, preventing them from remaining two-dimensional for maximum growth?
- Are T-S waves important in the transition from laminar to turbulent flow, or does the ingested turbulence cause sufficient mixing to ensure transition?

The experiments were performed in a wind-tunnel test section of 0.6 by 0.6 m cross section and 2.5 m long, at freestream speeds up to 19.8 m/s. Upstream of the test section, six turbulence-damping screens 1.8 m square and a 3:1-by-3:1 contraction section provided a freestream turbulence level of 0.07, measured at frequencies above 0.3 Hz. The test model was a flat glass plate 1.8 m long and 6.5 mm thick, with a semi-elliptical leading edge, oriented horizontally and lengthwise in the test section. Attached to the plate was a small earphone to generate T-S waves on the underside.

The freestream turbulence in the test section could be increased deliberately by installing a comb of vertical rods of either 6.35 or 4.8 mm diameter, or a comb of 4.8 mm horizontal rods. All flow measurements were taken on the underside of the plate. A three-axis translation stage under computer control carried hot-wire anemometers or anemometer arrays. Notable among the sensors was an eight-wire rake for simultaneous observation at eight stations across the flow at 1.25-cm intervals. The flow was visualized by oil emitted from the surface of an electrically heated 0.07-mm wire. A timing circuit controlled both the heating of the wire and a flashlamp for photography.

For grid-produced freestream turbulence near 0.15 percent and a lateral scale similar to that of the pre-transitional Blasius-layer thickness, the following conclusions were reached:

- The root-mean-square fluctuation amplitude in the layer grew to more than 6.0 percent.
- The motion was highly three-dimensional, with a lateral scale similar to that of the freestream.
- The large-amplitude disturbances altered the mean velocity within the profile by about 1.5 percent.
- Evidence of streamwise vorticity was found.
- At the highest Reynolds numbers tested (1.6×10^6), the naturally occurring T-S waves were weak in comparison with the large-amplitude background motion.
- Forced T-S waves were strongly amplitude- and phase-modulated by the large-amplitude motion, but the time-average amplitude was not greatly different in the absence of the grid.
- With the finer grid, sharp velocity gradients appeared locally and randomly. With the coarser grid, there arose turbulent spots wider than the coherence scale of the background motion.

This work was done by James M. Kendall, Jr., of Caltech for **NASA's Jet Propulsion Laboratory**. *To obtain a copy of the report, "Experimental Study of Disturbances Produced in a Pre-Transitional Laminar Boundary Layer by Weak Freestream Turbulence,"*

NPO-16754/TN

FOR ADDITIONAL INFORMATION: *Contact: Director, Technology Transfer Division, P.O. Box 8757, BWI Airport, MD. 21240; (301) 621-0100 Ext. 241*
REFER TO THE NUMBER LISTED AT THE END OF THE ARTICLE

NASA Tech Brief
National Aeronautics and Space Administration

Growing II/VI Semiconductors With Double Decantation

A concept for growing single crystals combines sheet solidification with controlled cooling.

NASA's Jet Propulsion Laboratory, Pasadena, California

A proposed crystal-growth method for II/VI semiconductor compounds would cool a newly solidified crystal gradually and nearly isothermally so that few defects are formed. At the same time, the method would obtain the maximum amount of crystal from the minimum amount of melt.

Only a small amount of a II/VI melt is usable for crystal growth. In growing a binary crystal, impurities build up in the melt, and so the crystal must be withdrawn well before the melt is used up. A ternary crystal must similarly be withdrawn because the composition of the melt changes as solidification proceeds. In the new technique, the crystalline material would be solidified in a sheet so that as much of the melt as possible would be utilized before the impurity content rises excessively or the composition changes too much. In addition, the crystal would be cooled in a liquid that would remove heat gradually and evenly at a controlled rate. Thermal stresses and the consequent defects induced by uneven cooling would thus be reduced.

In one version of the proposed technique, the molten semiconductor would be contained by baffles in a horizontally oriented vessel (see figure). A layer of molten encapsulant having a freezing temperature much lower than that of the semiconductor would float on top of the semiconductor melt.

A seed crystal would be introduced into the melt, just below the layer of encapsulant. The crystal would grow in a horizontal sheet along the semiconductor/encapsulant interface. When the crystal reaches its optimum size, the vessel would be tilted to raise the crystal into the encapsulant. The melt would run through a pair of end baffles into the space at the lower end of the vessel. When the vessel is returned to its horizontal position, much of the melt would remain in the end space, and the balance of the melt would form a shallow layer on the bottom of the growth chamber. The crystal would remain immersed in the molten encapsulant. The vessel would then be cooled at a controlled rate to just above the melting point of the encapsulating liquid. During this cooling, the molten semiconductor would turn to a solid.

The vessel would then be tilted in the opposite direction to pour much of encapsulant into the unfilled space at the other end. The vessel would be cooled further, and the encapsulant would solidify. The crystal would undergo a final cooling to room temperature in the gas that fills the upper part of the vessel.

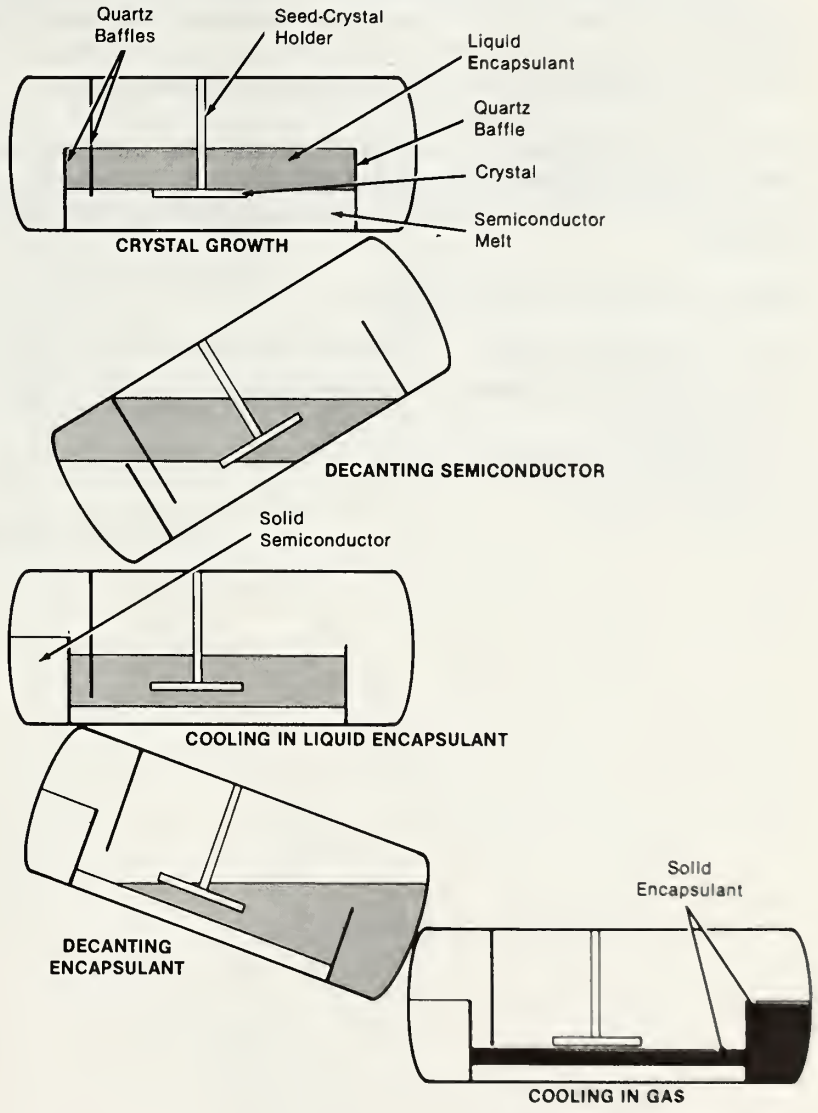

Double Decantation causes a sheet crystal to cool first in a liquid, then in a gas. The vessel is tilted to pour off molten semiconductor material. A second tilt, in the opposite direction, pours off the encapsulant.

This work was done by Andrew D. Morrison of Caltech for **NASA's Jet Propulsion Laboratory**
NPO-16808/TN

FOR ADDITIONAL INFORMATION: *Contact: Director, Technology Transfer Division, P.O. Box 8757, BWI Airport, MD. 21240; (301) 621-0100 Ext. 241*
REFER TO THE NUMBER LISTED AT THE END OF THE ARTICLE

Oak Ridge Associated Universities

Low Level Particle Beam Monitor and Current Meter

A new device measures the profile of particle beams with intensities as low as 1.8pA and uses this information to calculate the total beam intensity. This method provides a continuous, non-destructive measurement of beam intensity. The most innovative features of this design are the current meter and a circuit used to compensate for changing capacitance noise.

This device provides a method of measuring particle beams of lower intensity than is possible using existing equipment by compensating for changing capacitance noise. It also provides a non-destructive means for measuring beam intensity.

For Additional Information:

Dr. Kennon Carter
Oak Ridge Associated Universities
P.O. Box 117
Oak Ridge, TN 37831-0117
(615) 576-2642

Department of Energy

Technology Application

Ames Laboratory

Micropolarimeter for High Performance Liquid Chromatography

A new apparatus provides a sensitive detection method for optically active molecules. Such molecules usually are also biologically active. The novel design of optics and electronics is its key. As little as one microliter of a sample containing one nanogram can be measured. Its sensitivity is 1000 times better than the best commercial instruments.

FOR ADDITIONAL INFORMATION:
Daniel E. Williams
Ames Laboratory, Associate Director for Planning
and Technology Application
119 Office and Laboratory Building
Iowa State University
Ames, Iowa 50011
(515) 294-2635
Refer to patent 4,498,774/TN

NASA Tech Brief
National Aeronautics and Space Administration

Licensing Opportunity

Concentrating Trace Gases at Low Pressures

An open adsorption tube enables the measurement of gases at parts-per-trillion-by-volume concentrations.

Ames Research Center, Moffett Field, California

Trace constituents of low-pressure air are collected and concentrated for analysis by a multistage open-tube trap. The trap was developed for collecting samples at high altitudes, at pressure as low as about 6.6 kPa, but can also be used on the ground to collect samples from gas flows at pressures of up to 27 kPa (about one-quarter of 1 atmosphere).

Ordinarily, traps consist of tubes densely packed with adsorbent particles and often cryogenically cooled. As a gas flows through these tubes, constituents are adsorbed by the particles. The adsorbed constituents are later released as enriched samples for analysis. At pressures below about 100 kPa, adsorbent particles impede the flow of the gas and thereby increase the sampling time.

The trap described therefore employs an open tube. It consists of a coil of stainless-steel tubing with each loop, or stage, partly immersed in liquid nitrogen (see figure). After the tube has been evacuated and cooled, a measured volume of low-pressure gas flows through the tube. The trace constituents are adsorbed on the cryogenically cooled tube wall. The open tube allows a flow rate more than an order of magnitude greater than that of a packed tube for gas samples of about 13 kPa. After the enrichment of the sample, the six-part valve is rotated part way to isolate the trace constituents in the trap.

Next, the liquid-nitrogen bath is replaced by a water bath at 50 °C. As the coils warm up to the temperature of the water, the concentrated trace constituents are desorbed. The six-port valve is further rotated to admit a flow of helium gas to the tube. The flow carries the trace constituents to a gas chromatograph for quantitative analysis.

In a demonstration of the multistage open-tube trap, samples containing 200 to 2,500 parts per trillion by volume of ethane and of ethene were enriched. The trapping efficiency (the ratio of the found concentration to the known concentration of a trace constituent) was 100 ± 4 percent. Total immersion of the coils in the cryogen results in an efficiency of 85 ± 8 percent under similar conditions.

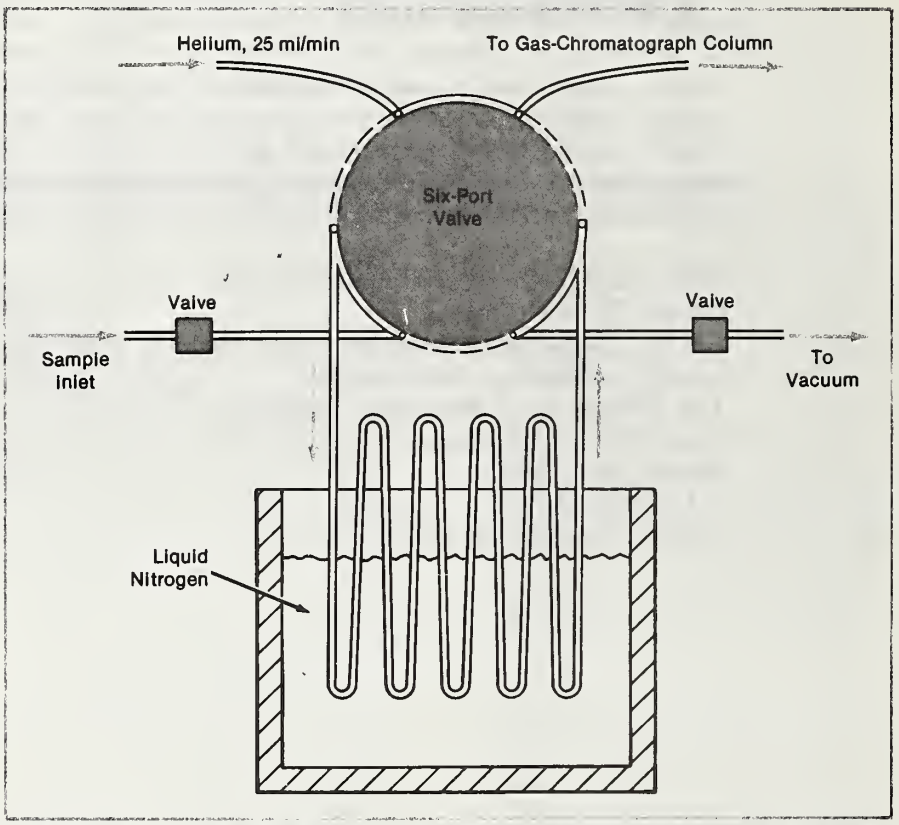

An **Open Tube Traps Trace Materials** in a flowing gas. A variety of configurations is possible; the tube may consist of a single long coil instead of several short ones, and the tube may be made of materials other than stainless steel. The partial immersion of the coil in the cryogen results in 100% trapping rather than a typical 85% for total immersion.

This work was done by James F. Vedder of **Ames Research Center**, *Dean O'Hara of San Jose State University Foundation, and Tuyen Vo of San Jose State University.*

Inquiries concerning rights for the commercial use of this invention should be addressed to the Patent Counsel. Ames Research Center Refer to ARC-11671. /TN

Ames Research Ctr.
Moffett Field, CA 94035
Technology Utilization Officer: Laurance Milov
Mail Code 223-3
(415) 694-6370
Patent Counsel:
Darrell G. Brekke
Mail Code 200-11
(415) 694-5104

NASA Tech Brief
National Aeronautics and Space Administration

Licensing Opportunity

High-Rydberg Xenon Submillimeter-Wave Detector

The use of reactive alkali metals is avoided.

NASA's Jet Propulsion Laboratory, Pasadena, California

A proposed detector for infrared and submillimeter-wavelength radiation would use excited xenon atoms as Rydberg sensors instead of the customary beams of sodium, potassium, or cesium. The chemically inert xenon is easily stored in (and released from) pressurized containers, whereas beams of the dangerously reactive alkali metals must be generated in cumbersome, unreliable ovens. The xenon-based detector has potential for infrared astronomy and for the Earth-orbiter detection of terrestrial radiation sources.

The Rydberg-sensor concept is based on the excitation of one of the electrons in each detector atom to a high energy state. In the xenon-based detector, the excitation would be performed in two stages (see figure). First, one of the six electrons in the highest level, (5p), of each ground-state xenon atom would be raised to the 6s level by radiation from a xenon resonance lamp. Next, a tunable laser emitting light of about 400 nm would raise the electron to an np (n>6) energy level.

The excited xenon atoms would absorb infrared radiation, causing the already twice-excited electron to be excited to the (n + 1)d level. The frequency of the absorbed infrared radiation would correspond to the energy spacing between the np and (n + 1)d levels, which would depend on the value of n and hence on the wavelength of the laser light used to excite the electron to the np level; alternatively, the wavelength sensitivity of the device could be tuned by shifting a given (n + 1)d level via the Stark effect. In either case, the atoms in the (n + 1)d level would be field ionized; the intensity of the incident infrared radiation would be determined by counting the resulting positive xenon ions using a microchannel-plate detector and standard particle-counting circuitry.

As in the case of other infrared detectors, this device would have to be cooled to very low temperatures to reduce interfering black-body radiation from the device walls. In terms of the noise-equivalent power, the device is expected to be competitive with, or even to exceed, bolometers, point-contact Josephson junctions, and Schottky diodes.

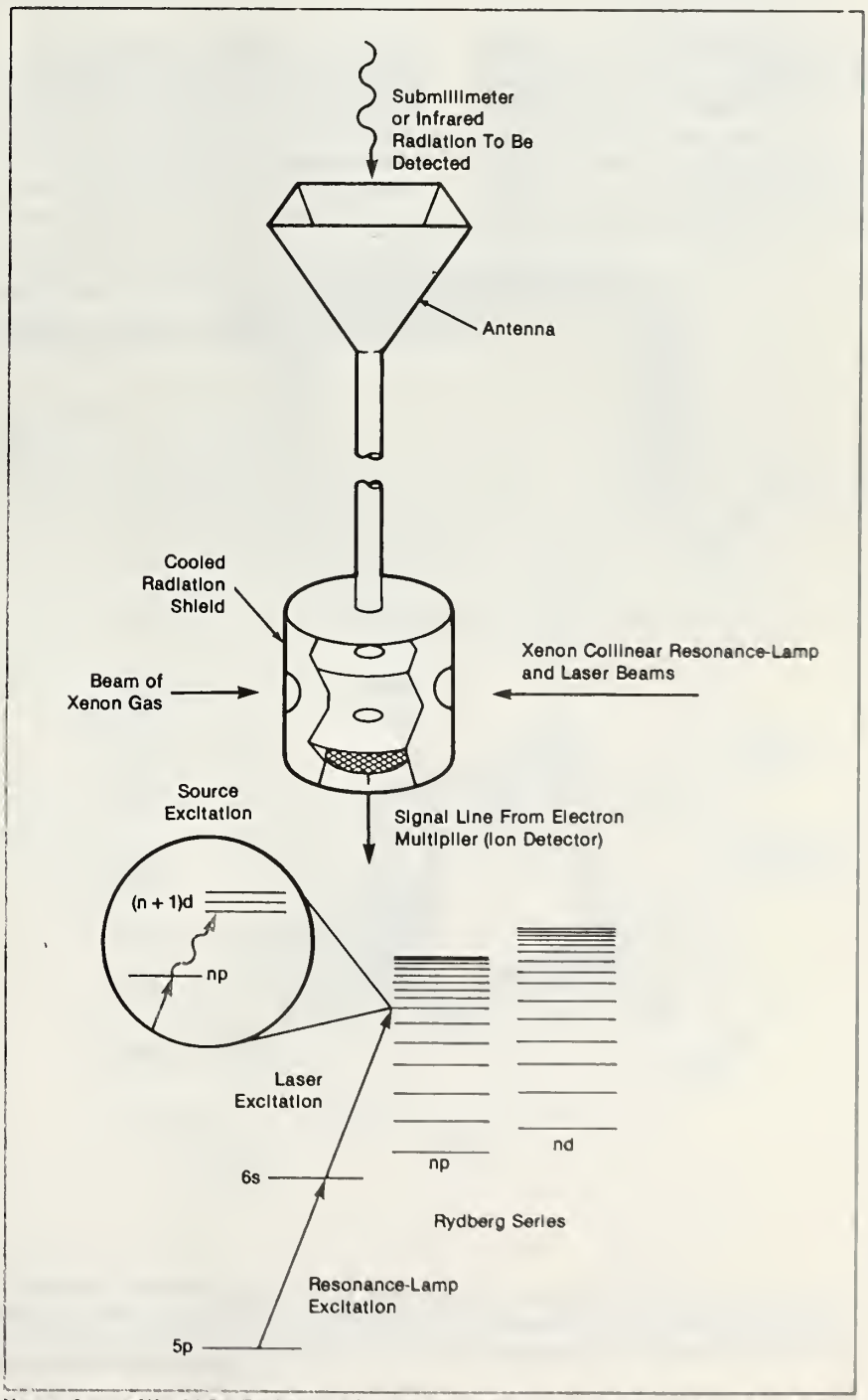

Xenon Atoms Would Be Excited to high energy states in two stages. The doubly excited atoms, which are sensitive to photons in the submillimeter wavelength range, would be further excited by these photons, then ionized and counted.

This work was done by Ara Chutjian of Caltech for **NASA's Jet Propulsion Laboratory.**

Inquiries concerning rights for the commercial use of this invention should be addressed to the Patent Counsel, NASA's Jet Propulsion Laboratory Refer to NPO-16372/TN

Jet Propulsion Lab.
4800 Oak Grove Drive
Pasadena CA 91109

Technology Utilization Mgr.: Norman L. Chalfin
Mail Stop 156-211
(818) 354-2240

NASA Resident Technology Utilization Officer: Gordon S. Chapman
Mail Stop 180-801
(818) 354-4849

Patent Counsel: Paul F. McCaul
Mail Code 180-801
(818) 354-2734

FOR ADDITIONAL INFORMATION: *Contact: Director, Technology Transfer Division, P.O. Box 8757, BWI Airport, MD. 21240; (301) 621-0100 Ext. 241*
REFER TO THE NUMBER LISTED AT THE END OF THE ARTICLE

NASA Tech Brief
National Aeronautics and Space Administration

Licensing Opportunity

Measuring Contact Thermal Conductances at Low Temperatures

An apparatus applies controlled force to metal samples at controlled heat flows.

Ames Research Center, Moffett Field, California

An instrument measures the thermal conductance of pressed contacts in liquid helium. The instrument makes its measurements automatically as a function of the force on pairs of brass samples having various surface finishes. The instrument was developed as part of an effort to determine the heat-transfer characteristics of bolted joints on cryogenically cooled focal planes in infrared equipment.

A rocker arm presses a pair of samples together in a fixture. A small gear motor applies force to an end of the rocker arm through a wire extending through a stain-

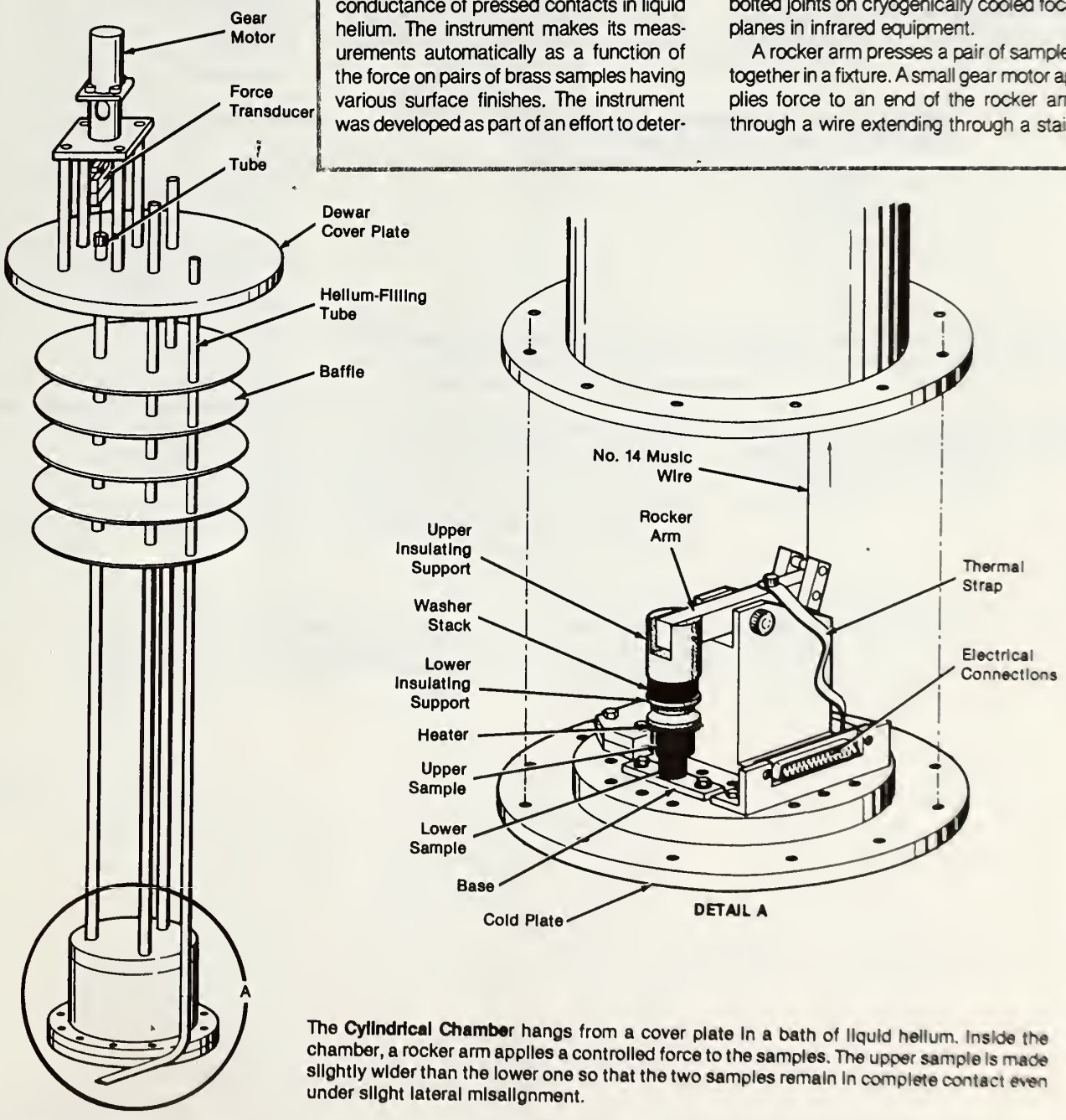

The **Cylindrical Chamber** hangs from a cover plate in a bath of liquid helium. Inside the chamber, a rocker arm applies a controlled force to the samples. The upper sample is made slightly wider than the lower one so that the two samples remain in complete contact even under slight lateral misalignment.

less-steel tube into the vacuum cylinder, which is immersed in liquid helium. A second tube carries electrical wiring into the cylinder, and a third is used to evacuate the cylinder.

Heat flows from a small electrical heating disk through the upper and lower samples into the base of the fixture. A force transducer calibrated from 0 to 1,100 N measures the force on the sample pair. Germanium resistance thermometers in the upper insulating support, the upper sample, the lower sample, and the base measure the local temperatures.

The thermal-conductance data are obtained by measuring the upper and lower sample temperatures while the heater power is varied between 0.1 and 10 mW. After the temperatures reach equilibrium (45 seconds to 2.5 minutes) for a given heat load, the data are recorded. The force is raised to the next value, the system is allowed to equilibrate, and the data are logged. The procedure is repeated for other heater powers and for other values of surface roughness.

The sequence is completely automated, under the control of a calculator that controls temperatures, heat loads, and applied forces. The temperature can be set at 1.5 to 6.5 K. The force on the contacts can be set at values up to 700 N. The samples tested had surface roughness ranging from 0.1 to 1.6 μm rms.

The measurements showed that the conductance of a joint increases asymptotically with increasing force and varies with the absolute temperature according to a simple power-law equation. For any given force, the conductance peaks at a surface roughness of about 0.4 μm.

This work was done by Louis J. Salerno, Peter Kittel, and Walter Brooks of **Ames Research Center**; *Alan L. Spivak of Trans-Bay Electronics, Inc.; and William G. Marks, Jr., of Lockheed Missiles and Space Co.*

Inquiries concerning rights for the commercial use of this invention should be addressed to the Patent Counsel, Ames Research Center. Refer to ARC-11693/TN

Ames Research Ctr.
Moffett Field, CA 94035
Technology Utilization Officer: Laurance Milov
Mail Code 223-3
(415) 694-6370
Patent Counsel: Darrell G. Brekke
Mail Code 200-11
(415) 694-5104

FOR ADDITIONAL INFORMATION: *Contact: Director, Technology Transfer Division, P.O. Box 8757, BWI Airport, MD. 21240; (301) 621-0100 Ext. 241*
REFER TO THE NUMBER LISTED AT THE END OF THE ARTICLE

NASA Tech Brief
National Aeronautics and Space Administration

Fiber-Optic Temperature Sensor

A remote thermometer would be small, lightweight, and immune to electrical noise.

Marshall Space Flight Center, Alabama

A proposed sensor would measure temperatures over a wide range — from those of cryogenic liquids to those of burning gases. Made in part of optical fibers, the sensor would be lighter in weight than a thermocouple and immune to electromagnetic interference. Unlike some other fiber-optic temperature sensors, the new device would not respond to temperatures elsewhere than at its sensing tip.

The probe consists of the polished tip of a fiber and a small mirror mounted on it (see figure). The fiber carries light from a laser to the tip. The inside surface of the fiber end reflects part of the light back into the fiber. The mirror reflects the remaining light transmitted through the tip back into the fiber.

The two reflected light beams interfere. The intensity of the light returning through the fiber therefore varies with the phase difference between the reflected beams, which in turn varies with the distance between the fiber end and the mirror surface. The gap changes with temperature as a result of the thermal expansion and contraction of the probe.

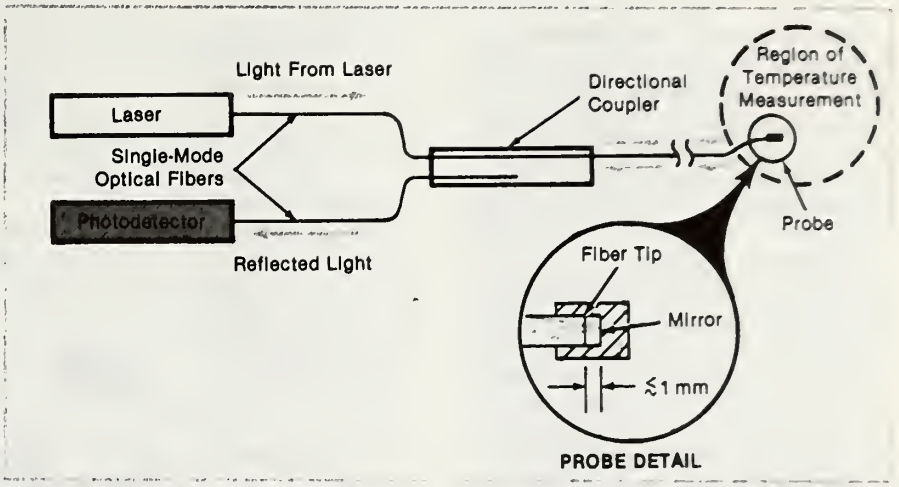

The Thermal Expansion and Contraction of the distance between fiber end and the mirror would alter the interference between the light reflected from those two surfaces, thereby giving an interferometric indication of temperatures.

A directional coupler extracts part of the returned light from the fiber, feeding it into a second fiber. A photodetector converts the extracted light into an electrical signal indicative of the probe temperature.

This work was done by Jonathan M. Maram of Rockwell International Corp. for **Marshall Space Flight Center**. *No further documentation is available.*
MFS-29164 /TN

FOR ADDITIONAL INFORMATION: *Contact: Director, Technology Transfer Division, P.O. Box 8757, BWI Airport, MD. 21240; (301) 621-0100 Ext. 241*
REFER TO THE NUMBER LISTED AT THE END OF THE ARTICLE

NASA Tech Brief
National Aeronautics and Space Administration

Licensing Opportunity

Measuring Electrostatic Discharge

A variety of materials can be tested together under controlled conditions.

Lyndon B. Johnson Space Center, Houston, Texas

An apparatus measures the electrostatic-discharge properties of several materials at once. It allows the samples to be charged either by friction or by exposure to a corona. By testing several samples simultaneously, the apparatus eliminates errors introduced by variations among test conditions.

The samples are placed on a turntable and rotated beneath a charging arm and a diametrically opposed noncontacting voltmeter probe (see figure). Positioned 6 millimeters above the turntable, the probe registers the voltage on each sample as it passes. The voltmeter output is displayed on a fast-responding chart recorder.

When the corona-charging arm is selected, it is extended to the radius of the samples; the pointed electrode of the arm is held 15 millimeters above the surface of the samples. When frictional charging is required, the corona arm is retracted and the frictional, or tribocharging, arm is extended; the abrasive tip of this arm is held against the surfaces of the samples.

As the turntable rotates, the samples are repeatedly charged by the selected arm. After about 150 seconds at a turntable speed of 8 radians per second, the charges on the samples build up to equilibrium levels. At this point, charging is stopped, and the voltmeter readings are started. The readings thus indicate the rates at which various materials dissipate the charge imposed on them.

The apparatus has been used to measure the electrical-discharge characteristics of paints. The measurements showed that the maximum charge on a sample increases with the sample thickness and decreases with the discharge rate of the sample material. The charge-versus-time curve for each paint is fit approximately by a sum of two exponentials, indicating that several discharge mechanisms operate simultaneously.

Electrostatic properties of materials can be compared under identical, controlled conditions with the apparatus. The results of such comparisons are immediately available. In addition, samples can be compared with reference materials also on the turntable — for example, with polytetrafluoroethylene, which holds a charge for a long time, or with antistatic polyethylene film ("pink poly"), which loses a charge within 5 seconds.

Generally, the corona arm is preferable to the tribocharging arm. It gives more-consistent results from measurement to measurement, is more sensitive to variations in material composition, and is nondestructive.

This work was done by William C. Smith of Lockheed Engineering and Management Services Co. for **Johnson Space Center.** *MSC-21094 /TN*

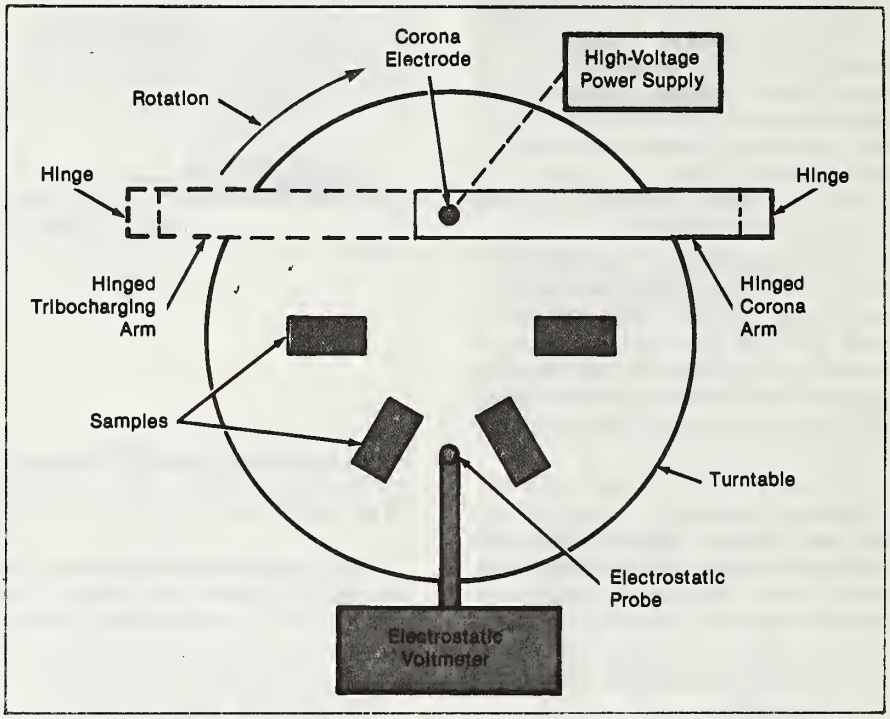

Samples Are Spaced so that they pass at intervals under either of two retractable arms. The samples are 2 inches (5 centimeters) wide along the circular path. The arm tips and the voltmeter probe are 6 inches (15 centimeters) from the turntable center. The servocontrolled turntable speed is constant within 0.1 percent.

Inquiries concerning rights for the commercial use of this invention should be addressed to the Patent Counsel, Johnson Space Center

Lyndon B. Johnson Space Center
Houston, TX 77058
Technology Utilization Officer: Dean C. Glenn
Mail Code EA4
(713) 483-3809
Patent Counsel: Edward K. Fein
Mail Code AL3
(713) 483-4871

FOR ADDITIONAL INFORMATION: *Contact: Director, Technology Transfer Division, P.O. Box 8757, BWI Airport, MD. 21240; (301) 621-0100 Ext. 241*
REFER TO THE NUMBER LISTED AT THE END OF THE ARTICLE

NASA Tech Brief
National Aeronautics and Space Administration

Licensing Opportunity

Measuring Gases With Laser-Induced Fluorescence

The temperature, density, and pressure are measured simultaneously in supersonic, turbulent flow.

Ames Research Center, Moffett Field, California

The temperature, density, and pressure at a selected point in a low-temperature, turbulent gaseous flow are measured simultaneously by pulsed laser-induced fluorescence (LIF). The measurements are made with spatial and temporal resolution comparable to those obtained with modern laser-anemometer techniques used for research on turbulent boundary layers. These LIF measurements are unique in that they are nonintrusive and constitute the first alternative means of measuring turbulent fluctuations in temperature and density that can be compared with conventional hot-wire-anemometer data.

The LIF technique involves seeding a bulk nitrogen flow with a low concentration (up to 100 parts per million) of nitric oxide (NO) and relies on the ultraviolet fluorescence following single-photon excitation of two rotational/vibrational electronic transitions in the NO gamma band. The test section of the small wind tunnel used for these experiments is a rectangular mach-2 nozzle with a 25- by 64-mm exit, followed by a slightly diverging channel, 762 mm in length from the nozzle throat to the optical ports.

The optical arrangement is illustrated in the figure. The laser beam is admitted through either of two 50-mm-diameter quartz windows on opposite sides of the channel. Fluorescence is observed through a similar window on a third side of the channel. The volume observed is spatially limited by the collection optics and field-stop arrangement to a 1-mm segment of the laser beam centered on its focal point.

Two grating-tuned dye lasers are simultaneously pumped by the third-harmonic output of a Nd/YAG laser at a repetition rate of 10 Hz. The portion of the 354.7-nm pump beam directed to the second dye laser is optically delayed, giving a temporal separation of 125 ns between dye-laser pulses. The beams of both dye lasers are doubled in frequency, and each second harmonic is tuned to one of the NO transitions.

The two beams are combined collinearly, focused by a common lens of 500-mm focal length and partitioned into the wind-tunnel and reference paths. The reference path contains the same gas as does the wind tunnel, but the gas does not flow and is maintained at a known temperature and pressure. The focal-spot sizes were less than 0.5 mm.

The broad-band fluorescences from the wind tunnel and the reference cell were collected by nearly identical f/1 fused-silica optics and nominally filtered with ultraviolet-transmitting shortwave-pass filters. The fluorescence waveforms from each source were detected by solar-blind photomultipliers sensitive to the spectral range from 225 to 330 nm

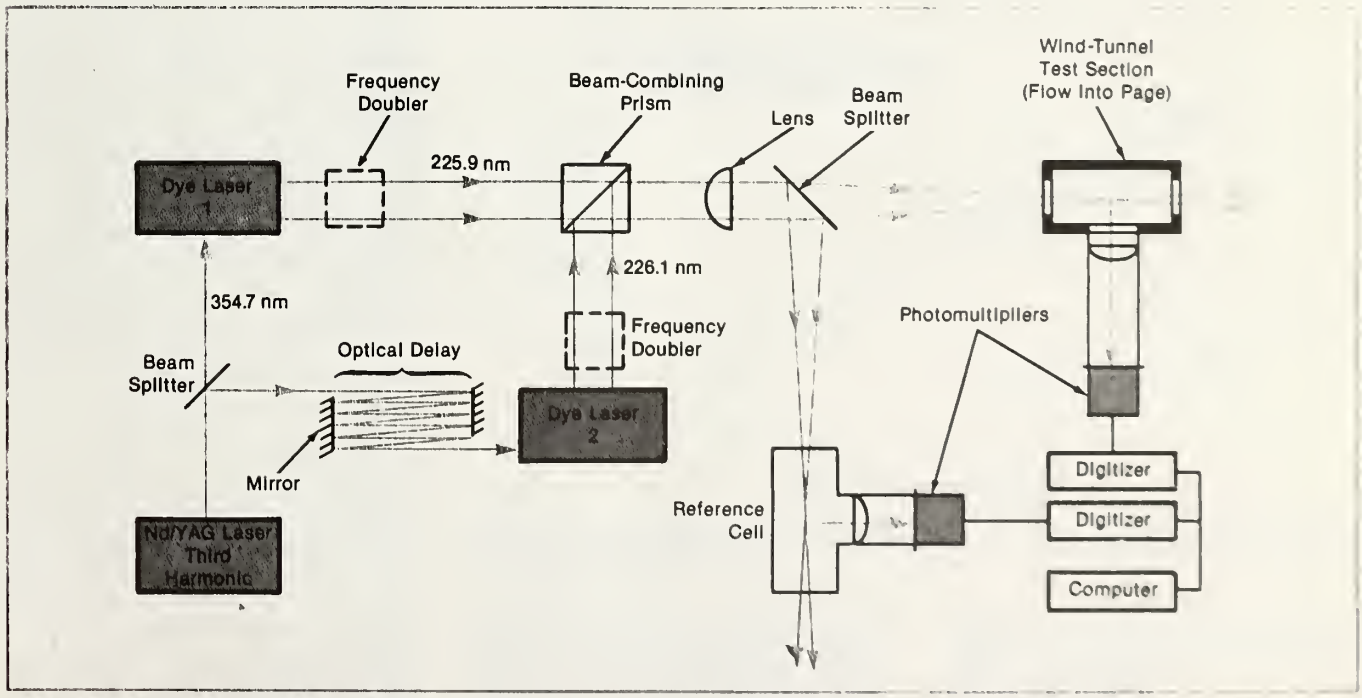

Laser Beams Focused to Small Spots in the wind tunnel and reference cell induce fluorescence in nitric oxide, a small amount of which is mixed with the main gas flow. The fluorescence radiation depends on the main-gas temperature, pressure, and density and is measured to deduce these quantities.

and recorded by transient digitizers interfaced to a computer.

The computer deconvolved the double-pulse waveforms to separate the contributions from each excitation, integrated to obtain the relative fluorescence energy associated with each excitation, and compared wind-tunnel with reference values to obtain normalized wind-tunnel data.

The ratio of fluorescence energies from both transitions is related to the rotational temperature of the ground-state NO molecule, with account taken of the effects of collisional quenching and transition spectral broadening. The rotational temperature, in turn, is assumed to be closely coupled to the kinetic temperature of the gas mixture. The density and pressure are obtained from the measured temperature, together with the combined use of the fluorescence energy from one excitation and the equation of state for the gas mixture.

This work was done by Robert L. McKenzie of **Ames Research Center and** *Kenneth P. Gross of Polyatomics Research Institute and Pamela Logan of Stanford University.*

Inquiries concerning rights for the commercial use of this invention should be addressed to the Patent Counsel, Ames Research Center
Refer to ARC-11678/TN

Ames Research Ctr.
Moffett Field, CA 94035
Technology Utilization Officer: Laurance Milov
Mail Code 223-3
(415) 694-6370
Patent Counsel:
Darrell G. Brekke
Mail Code 200-11
(415) 694-5104

FOR ADDITIONAL INFORMATION: *Contact: Director, Technology Transfer Division, P.O. Box 8757, BWI Airport, MD. 21240; (301) 621-0100 Ext. 241*
REFER TO THE NUMBER LISTED AT THE END OF THE ARTICLE

NASA Tech Brief
National Aeronautics and Space Administration

Licensing Opportunity

Measuring Viscosities of Gases at Atmospheric Pressure

A thermal mass flowmeter provides a capillary section for differential-pressure measurement.

Langley Research Center, Hampton, Virginia

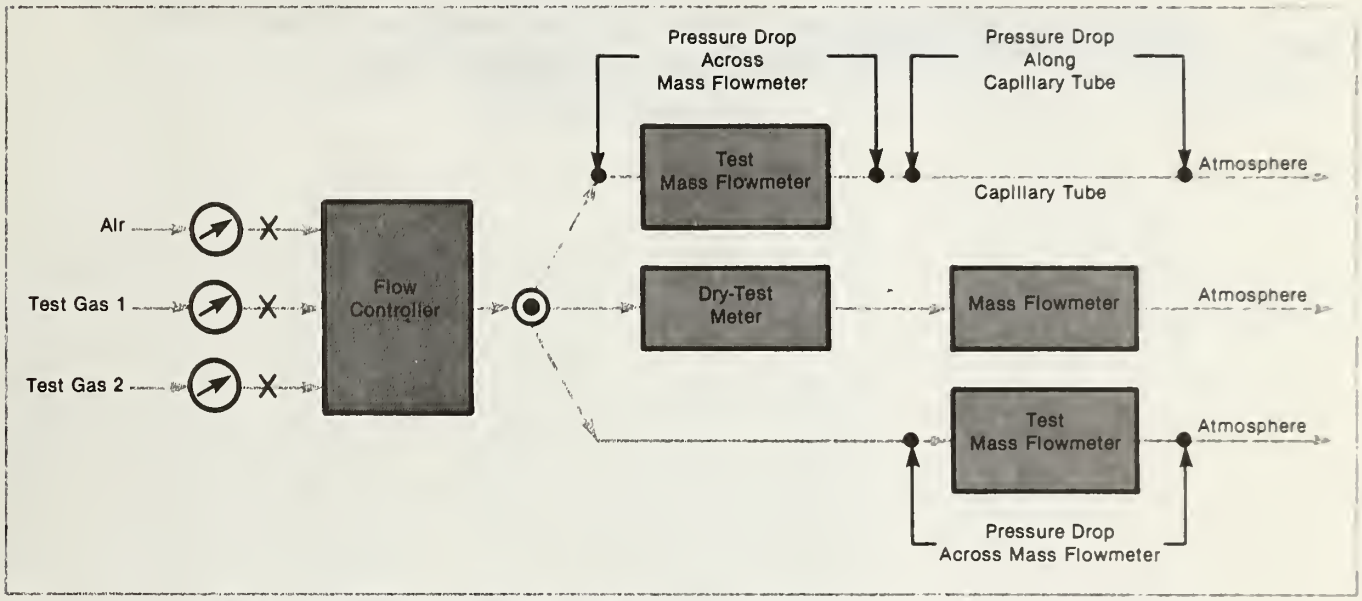

Figure 1. The **Pressure Drop Along the Capillary Section** is measured first in air, then in the test gas.

A variant of the general capillary method for measuring the viscosities of unknown gases is based on the use of a thermal mass-flowmeter section for direct measurement of pressure drops. In this technique, the flowmeter serves a dual role, providing data for determining the volume flow rates and serving as a well-characterized capillary-tube section for the measurement of differential pressures across it.

Coefficients of viscosity of various types of gas mixtures, including simulated natural gas, have been measured at atmospheric pressure and room temperature by the use of this technique. Pressure differences across the capillary-tube section of the thermal mass flowmeter were measured at small, well-defined, volume flow rates in the test gases and in standard air. Care was exercised to ensure that the flow rates for the air and test gas were such as to maintain the laminarity of the gas flows through the capillary section of the flowmeter.

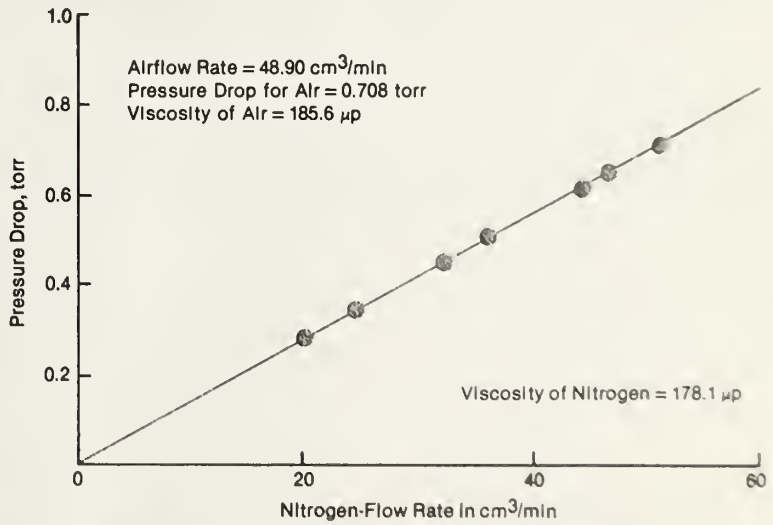

Figure 2. A **Linear Relationship** exists between the flow rates and the pressure drops along the capillary section.

The coefficients of viscosity of the test gases were calculated using the reported value of 185.6 micropoises for the viscosity of dry air at 300 K. The coefficients of viscosity for the test mixtures were also calculated using Wilke's approximation of Chapman-Enskog (C-E) theory. The experimental and calculated values for binary mixtures were in agreement within the reported accuracy of Wilke's approximation of C-E theory, but agreement for multicomponent gases was less satisfactory, presumably because of the limitations of Wilke's approximations of the classical dilute-gas state model.

The new method is simple, sensitive, and adaptable for absolute or relative viscosity measurements of low-pressure

gases. Figure 1 is a diagram of the experimental system. Figure 2 shows the linear correlation between the pressure difference across the capillary-tube section of the thermal mass flowmeter and the flow rate through it. This technique is particularly suited for very complex hydrocarbon mixtures where the limitations of classical theory and compositional errors make theoretical calculations less reliable. The results for pure gases indicate that the technique is accurate to within ±1 percent. In fact, the only limiting factors appear to be the accuracies with which volume flow rates and differential pressures can be measured.

This work was done by Jag J. Singh of **Langley Research Center**, *Gerald H. Mall of Computer Sciences Corp., and Chegini Hoshang of Old Dominion University. Further information may found in NASA TP-2582 [N86-24962/NSP], "Measurement of Viscosity of Gaseous Mixtures at Atmospheric Pressure."*

Copies may be purchased from the National Technical Information Service, Springfield, Virginia 22161, [A02]

Langley Research Ctr.
Hampton, VA 23665
Technology Utilization Officer: John Samos
Mail Stop 139A
(804) 865-3281
Patent Counsel: George F. Helfrich
Mail Code 279
(804) 865-3725

FOR ADDITIONAL INFORMATION: *Contact: Director, Technology Transfer Division, P.O. Box 8757, BWI Airport, MD. 21240; (301) 621-0100 Ext. 241*
REFER TO THE NUMBER LISTED AT THE END OF THE ARTICLE

Transportation & Components

338 Computing Aerodynamics of Propfans — The cost and duration of wind-tunnel tests could be reduced.

339 Engine-Monitoring Algorithm — Allowances are made for erroneous sensor readings.

340 Generating Coordinates for Aerodynamical Calculations — A mathematical method represents an aircraft surface as grids of variable spacing. (Licensing Opportunity)

NASA Tech Brief
National Aeronautics and Space Administration

Computer Software

Computing Aerodynamics of Propfans

The cost and duration of wind-tunnel tests could be reduced.

High-speed turboprops (propfans) have the potential to reduce significantly the fuel consumption of current transport aircraft. The propfans also offer higher installed propulsive efficiency at high subsonic cruise speeds. The integration of the propfan/nacelle with the airframe is the key factor in determining the efficiency of the propfan propulsion system under installed conditions. A computer program was developed to predict the interference of the slipstream of a propfan on a supercritical wing at subsonic speeds. The use of this program could reduce the cost and time involved in the wind-tunnel testing of newly-designed wing/nacelle configurations.

For the computer program, a subsonic-flow panel code was modified to handle the effects of a propeller wake. The effects of the propeller slipstream are increased axial velocity, a new tangential velocity, and a total-pressure rise in the wake of the propeller. Principles based on blade-performance theory, momentum theory, and vortex theory are used to evaluate the slipstream characteristics. The slipstream effects are superimposed on Neumann boundary conditions to predict the installation aerodynamics of the powered propellers mounted on overwing or underwing nacelles integrated with supercritical wings. The inclusion of viscous-flow modeling enhances the accuracy of the prediction.

The input to the program includes the free-stream mach number, the propeller angle of attack, the propeller geometry, the propeller location, the propeller rotation, the thrust coefficient, the root-cutout position of the propeller blade, and the control parameters of the solution technique. The output includes the panel-induced velocities, the pressure increases, the final velocity distribution, and the pressure-coefficient distribution.

This program is written in FORTRAN V for batch execution and has been implemented on a CDC CYBER 800-series computer operating under NOS with a central-memory requirement of approximately 74K (octal) of 60-bit words. The program was developed in 1986.

This program was written by B. Chandrasekaran of Vigyan Research Associates, Inc., for **Langley Research Center**. *LAR-13623 /TN*

FOR ADDITIONAL INFORMATION *CONTACT:*

COSMIC®
112 Barrow Hall
University of Georgia
Athens, GA 30602
(404) 542-3265

NASA Tech Brief
National Aeronautics and Space Administration
Lewis Research Center, Cleveland, Ohio

Engine-Monitoring Algorithm

Allowances are made for erroneous sensor readings.

An algorithm has been developed to increase the reliability of digital electronic control systems for aircraft turbine engines: the algorithm detects, isolates, and accommodates failures or errors in engine sensors, which are typically the least reliable elements of engine-control systems. Heretofore, redundancy of sensors has been used in the effort to increase reliability. In contrast, the developmental algorithm is based on analytical redundancy, which uses a simplified mathematical model of the engine to interrelate the "normal" readings of different sensors: the algorithm determines whether the indication of a given sensor is consistent with those of the other sensors, within prescribed limits.

The inputs to the algorithm include the measured engine inputs $U_m(t)$, where t = time; the fuel flow; nozzle area; compresser-inlet-guide-vane angle; rear-compressor-variable-vane angle; and bleed flow. The inputs to the algorithm also include the measured engine outputs $Z_m(t)$, the fan and compressor speeds, burner and augmentor pressures, and fan-turbine-inlet temperature. The outputs of the algorithm are optimal (that is, as realistic as possible) estimates of the engine outputs, $\hat{Z}(t)$.

The algorithm consists of three elements (see figure): (1) logic for the detection of hard failures; (2) logic for the detection of soft failures; and (3) the accommodation filter, which contains the mathematical engine model and produces the estimates of the engine outputs. Hard failures are large out-of-range readings or bias errors that occur suddenly. These are relatively easy to detect via sudden large differences $Z(t) - \hat{Z}_m(t)$ between the accommodation-filter outputs and the sensor readings.

Soft failures are small bias errors or drift errors that accummulate slowly and are more difficult to detect. The soft-error-detection logic includes one normal-mode- and five failure-mode-hypothesis filters; these filters continuously track the sensor readings, searching for erroneous values. The performance of the algorithm is enhanced by the incorporation of integral action in a Kalman filter to improve the steady-state accuracy in the estimate of the fan-turbine-inlet temperature and by an adaptive error threshold that increases during commanded transients of engine operation to prevent false soft-error alarms.

The algorithm was tested in a computer simulation of the operation of an F100 turbofan engine. The algorithm performed well in tests of soft-error performance at seven operating points for all five sensed outputs. A test on a real engine has been scheduled.

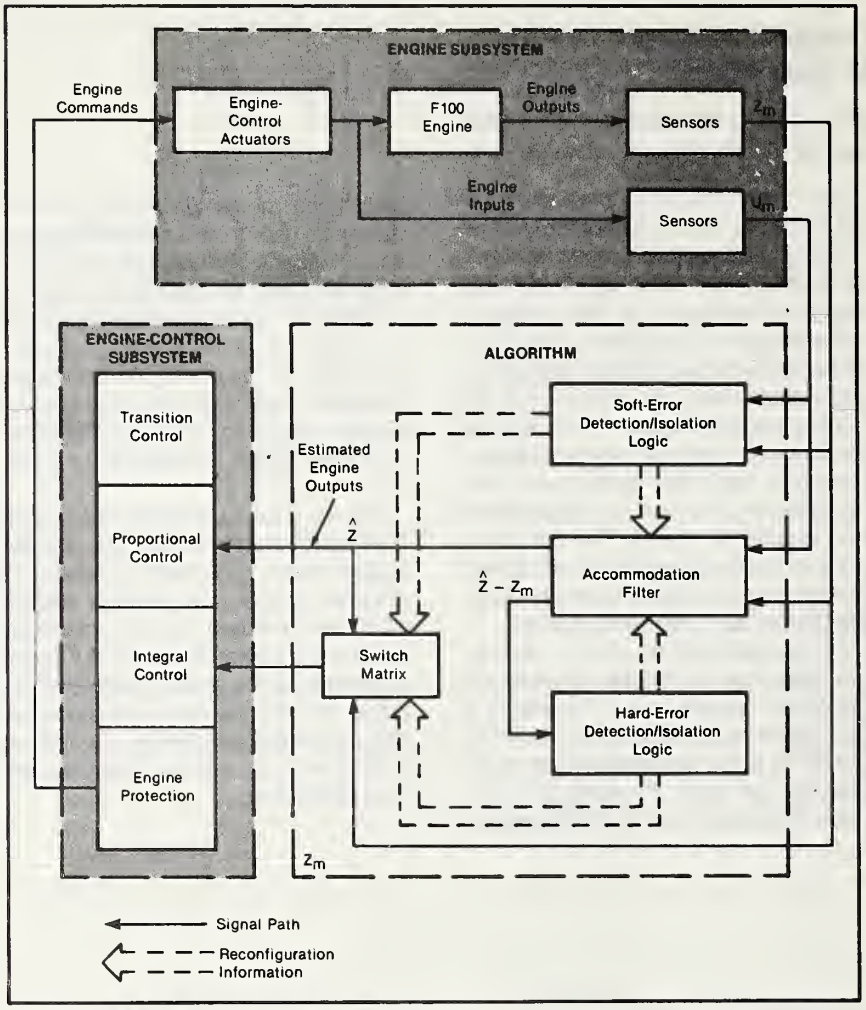

As Part of an Engine-Control System, an algorithm generates engine-output estimates based on measurements of the inputs and outputs and detects failures of the input- and output-measuring sensors.

This work was done by Walter C. Merrill and John C. DeLaat of **Lewis Research Center.** *Further information may be found in NASA TM-87289 [N86-24697/NSP], "A Real-Time Simulation Evaluation of an Advanced Detection, Isolation, and Accommodation Algorithm for Sensor Failures in Turbine Engines."*

Copies may be purchased from the National Technical Information Service, Springfield, Virginia 22161, [A02]
LEW-14514 /TN

FOR ADDITIONAL INFORMATION: *Contact: Director, Technology Transfer Division, P.O. Box 8757, BWI Airport, MD. 21240; (301) 621-0100 Ext. 241*
REFER TO THE NUMBER LISTED AT THE END OF THE ARTICLE

NASA Tech Brief
National Aeronautics and Space Administration
Ames Research Center, Moffett Field, California

Licensing Opportunity

Generating Coordinates for Aerodynamical Calculations

A mathematical method represents an aircraft surface as grids of variable spacing.

An elliptic method generates composite grids about a three-dimensional aircraft body. The realistic grids are useful in mathematical models of aerodynamic flow. A computer can generate the grids with little or no human intervention.

A body-conforming grid is first generated about the entire aircraft by the solution of Poisson's differential equation. This initial grid has relatively coarse spacing, and it covers the entire body. At boundary surfaces, the sizes of grid cells are controlled, and cell skewness is nearly eliminated, by the incorporation of the inhomogeneous Poisson terms, which are found automatically by the program. Certain regions of the grid — those in which high gradients are expected and which map into rectangular solids in the computational domain — are then designated for zonal refinement. Spacing in the zonal grids is reduced by adding points according to a simple algebraic scheme.

When flow-solver results require an adjustment to the size, location, or resolution of the fine zonal grids, the adjustment is usually made without any modification to the coarse grid and with simple changes to the subdivision that produces the zonal grids.

The method has been applied to a wing-and-body configuration based on the F-16 fighter airplane. The fuselage, including the canopy, the strakes, and the shelf aft of the main wing, has been fully modeled, as have been the main wing and the horizontal tail (see figure). The ventral inlet was faired over, and the vertical tail, the ventral fins, and the missile rails on the wing tips were deleted. A tapering sting of circular cross section was added to the rear.

The Poisson grid equations, including the side-condition equations that determine the inhomogeneous terms, were solved by a point-successive over-relaxation technique, which was chosen for its ease of programming and its flexibility with respect to boundary conditions. One hundred iterations, at about 1 second of central-processing-unit time per iteration, were required to generate the 37,000-point coarse global mesh.

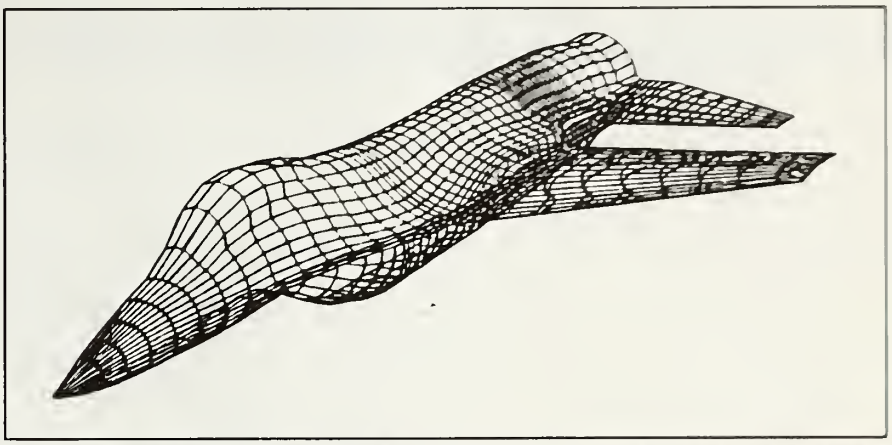

Grid Lines on the Surface of the Wing and Body vary in spacing, depending on level of detail needed to model airflow accurately in the region. The grid intervals for a zone might be unchanged in one direction, halved in the second orthogonal direction, and reduced to much finer spacing in the third direction.

The coarse global grid was divided into 16 zones. The degree to which the coarse grid intervals were subdivided varied from no change at all to intervals as small as a thousandth that of a coarse grid layer; such small intervals are needed for the simulation of viscosity. A total of 300,000 points were used in the zones. The computer time to generate the zonal grids was insignificant.

Eventually, as grids become more realistic and complex, the entire flow field will have to be divided into several regions, with a coarse grid generated in each region. The ability of the new method to control the behavior of grids at boundary surfaces will make it easier to patch such regional grids together.

This work was done by Reese L. Sorenson of **Ames Research Center**. *Further information may be found in NASA TM-88240 [N86-31527/NSP], "Elliptic Generation of Composite Three-Dimensional Grids About Realistic Aircraft."*

Copies may be purchased from the National Technical Information Service, Springfield, Virginia 22161.

Inquiries concerning rights for the commercial use of this invention should be addressed to the Patent Counsel, Ames Research Center
Refer to ARC-11732 /TN

Ames Research Ctr.
Moffett Field, CA 94035
Technology Utilization Officer: Laurance Milov
Mail Code 223-3
(415) 694-6370
Patent Counsel:
Darrell G. Brekke
Mail Code 200-11
(415) 694-5104

FOR ADDITIONAL INFORMATION: *Contact: Director, Technology Transfer Division, P.O. Box 8757, BWI Airport, MD. 21240; (301) 621-0100 Ext. 241*
REFER TO THE NUMBER LISTED AT THE END OF THE ARTICLE

NTIS Order Form

NTIS Telephone Numbers

To Order Reports
(703) 487-4650

For Subscription Questions
(703) 487-4630

Other Information
(703) 487-4600

Editorial Questions
(703) 487-4805

Postage:
NTIS uses First Class Delivery, or equivalent service, on all shipping. For information about one day RUSH ordering, call (703) 487-4600.

NTIS PRICE CODE SCHEDULE *

This schedule gives the current values to the price codes cited in those Tech Notes having a backup report available from NTIS.

Microfiche	
A01	$6.95
Paper copy	
A02	9.95
A03	12.50
A04 through A05	14.95
A06 through A09	19.95
A10 through A13	25.95
A14 through A17	32.95
A18 through A21	38.95
A22 through A25	44.95
A99	Call for price

Customers in Canada, United States, and Mexico use this schedule. Other addresses should write for the price listing, number PR-360-4.

Prices effective January 1, 1988

Use this form ONLY to order reports designated as available from NTIS

MAIL ORDER TO: National Technical Information Service
U.S. DEPARTMENT OF COMMERCE
5265 Port Royal Road
Springfield, VA 22161

Send me the reports I have selected on this form. I have placed order numbers in appropriate blanks and have indicated the quantity. IF ADDRESS LABEL

Last Name: .....

Title: .....

Company/Organization: .....

Address: .....

.....

City/State/Zip: .....

Telephone Number: .....

METHOD OF PAYMENT

☐ Check enclosed payable to NTIS for $ .....

☐ Charge to my NTIS Deposit Account, No: .....

☐ Purchase order number: .....

Charge to: ☐ American Express ☐ VISA ☐ MasterCard

Card Number: .....

Expation date: .....

Signature: .....
(Required to validate order)

NTIS ORDER NUMBER (Use only for backup reports stated as available from NTIS)

NTIS Order Number	*Price**	*Quantity*	*Total Price*
.....	.....	.....	.....
.....	.....	.....	.....
.....	.....	.....	.....
.....	.....	.....	.....
.....	.....	.....	.....
	Shipping and handling fee		$3.00
	Total		.....

NTIS Order Form

NTIS Telephone Numbers

To Order Reports
(703) 487-4650

For Subscription Questions
(703) 487-4630

Other Information
(703) 487-4600

Editorial Questions
(703) 487-4805

Postage:
NTIS uses First Class Delivery, or equivalent service, on all shipping. For information about one day RUSH ordering, call (703) 487-4600.

NTIS PRICE CODE SCHEDULE *

This schedule gives the current values to the price codes cited in those Tech Notes having a backup report available from NTIS.

Microfiche	
A01	$6.95
Paper copy	
A02	9.95
A03	12.50
A04 through A05	14.95
A06 through A09	19.95
A10 through A13	25.95
A14 through A17	32.95
A18 through A21	38.95
A22 through A25	44.95
A99	Call for price

Customers in Canada, United States, and Mexico use this schedule. Other addresses should write for the price listing, number PR-360-4.

Prices effective January 1, 1988

Use this form ONLY to order reports designated as available from NTIS

MAIL ORDER TO: National Technical Information Service
U.S. DEPARTMENT OF COMMERCE
5265 Port Royal Road
Springfield, VA 22161

Send me the reports I have selected on this form. I have placed order numbers in appropriate blanks and have indicated the quantity. IF ADDRESS LABEL

Last Name: .....

Title: .....

Company/Organization: .....

Address: .....

.....

City/State/Zip: .....

Telephone Number: .....

METHOD OF PAYMENT

☐ Check enclosed payable to NTIS for $ .....

☐ Charge to my NTIS Deposit Account, No: ....-.....

☐ Purchase order number: .....

Charge to: ☐ American Express ☐ VISA ☐ MasterCard

Card Number: .....

Expation date: .....

Signature: .....
(Required to validate order)

NTIS ORDER NUMBER (Use only for backup reports stated as available from NTIS)

NTIS Order Number	*Price**	*Quantity*	*Total Price*
.....	.....	.....	.....
.....	.....	.....	.....
.....	.....	.....	.....
.....	.....	.....	.....
.....	.....	.....	.....
		Shipping and handling fee	$3.00
		Total	.....

- Agriculture & Food
- Computers
- Electrotechnology
- Energy
- Engineering
- Environmental Science & Technology
- Manufacturing, Machinery, & Tools
- Materials
- Medicine & Biology
- Natural Resources Technology & Engineering
- Physical Sciences
- Transportation & Components

Route To:

PENN STATE UNIVERSITY LIBRARIES
A000072009956

EPARTMENT OF COMMERCE
ial Technical Information Service
eld, Va. 22161

L BUSINESS
or Private Use, $300

[OF COMMERCE

Stimulating America's Progress
1913-1988

AN EQUAL OPPORTUNITY EMPLOYER

BULK RATE
POSTAGE & FEES PAID
NTIS
Permit No. G-292